

Response to CO₂ Storage of Danish Reservoir- and Cap-rocks

Summary of Results from the EFP-project AQUA-DK

Claus Kjøller, Rikke Weibel, Lars H. Nielsen, Troels Laier,
Peter Frykman & Niels Springer



Response to CO₂ Storage of Danish Reservoir- and Cap-rocks

Summary of Results from the EFP-project AQUA-DK

Claus Kjøller, Rikke Weibel, Lars H. Nielsen, Troels Laier,
Peter Frykman & Niels Springer

Dansk Resumé

Denne rapport sammenfatter resultaterne af forskningsprojektet "Geologisk lagring af CO₂ i den danske undergrund: Vurdering af segl- og reservoir-bjergarternes respons på CO₂ lagring (AQUA-DK)". Hovedformålet med projektet har været at identificere reservoirbjergarter og segl (cap-rocks), der er egnede i forbindelse med lagring af CO₂ i Danmark samt at undersøge mulige CO₂-mineral reaktioner i disse bjergarter. Derudover har formålet været at vurdere "seglkapaciteten" for de egnede danske cap-rocks. Undersøgelsen blev derfor gennemført med ønsket om i fremtiden at kunne kvalificere forudsigelser om integriteten af danske reservoirer og cap-rocks i forbindelse med eventuel CO₂-lagring i Danmark.

Den eksisterende viden om potentielle danske reservoirer og cap-rocks er, som en del af projektet, opdateret, især med hensyn til dannelseshistorie, udbredelse, dybde og petrografisk og mineralogisk sammensætning. Med hensyn til CO₂-lagring er de mest lovende reservoirer: Bunter Sandsten Formationen (Nedre Trias), Skagerrak Formationen (Trias), Gassum Formationen (Øvre Trias-Nedre Jura) og Haldager Sand Formationen (Mellem Jura). De vigtigste cap-rocks er muddersten fra Fjerritslev og Børglum Formationerne.

For at kunne gennemføre laboratorieforsøg med kernemateriale under reservoirbetingelser, blev der foretaget en vurdering af den kemiske sammensætning af porevæsker fra lokaliteter, hvor der er udtaget kernemateriale. Ved projektets start var formationsvandets kemi kun kendt med rimelig sikkerhed for Stenlille reservoir og cap-rock, hvor der tidligere er foretaget prøve-pumpninger. For kernemateriale fra de øvrige lokaliteter blev test-data fra et større antal boringer, der kunne give information om formationsvandets kemi, gennemgået med henblik på at korrigere for mulige fejlkilder som f.eks. boremudderfiltrat og rest efter syrestimulering. På basis heraf konstrueredes en dybde relation for forskellige kemiske parametre i formationsvandet og herudfra blev en tilnærmet formationskemi beregnet for de relevante lokaliteter og geologiske lag, hvorfra kernematerialet til laboratorieforsøgene stammede.

Laboratorieforsøg med CO₂ eksponering af udvalgte prøver af de potentielle reservoirer og cap-rocks blev gennemført i en periode på op til 14 måneder. Eksperimenterne blev udført under reservoirbetingelser (20 MPa og 70°C) og med anvendelse af syntetiske porevæsker med en kemisk sammensætning tilnærmet *in situ* sammensætningen i hver formation. I løbet af forsøgsperioden på 14 måneder blev der udtaget prøver af porevæsken med regelmæssige mellemrum, og bjergartsprøver blev udtaget efter henholdsvis 7 og 14 måneder. Petrografisk og mineralogisk analyse af hver bjergartsprøve blev udført både før og efter forsøgene ved brug af mikroskopi (med både transmitteret og reflekteret lys), skanning elektronmikroskopi (SEM) og røtgendiffraktion (XRD).

Generelt viser den petrografiske og mineralogiske analyse, at karbonatminerallerne er de mineraler, der er mest udsat for ændringer, når bjergartsprøverne udsættes for CO₂. Karbonatopløsning synes således at kunne forklare størstedelen af ændringerne i porevæskernes kemiske sammensætning under forsøgene. Når forskellige karbonatmineraller er til stede i en prøve, sker der generelt opløsning af kalcit før dolomit, og siderit før ankerit. Med hensyn til silikatminerallerne i både reservoir- og cap-rock prøver har det ved den petrografiske analyse ikke været muligt at påvise en øget grad af opløsning, som følge af CO₂-eksponeringen, men muligheden kan ikke udelukkes. Således viser feldspat kornene tydelige tegn på opløsning både før og efter eksperimenterne, hvorfor øget opløsning i forbindelse med CO₂ forsøgene hverken kan påvises

eller afvises. Da de fleste lerminerale udgøres af små, fine krystaller er det ikke muligt ud fra den petrografiske analyse at vurdere, om der er sket opløsning af disse under eksperimenterne. Det mest grovkornede lermineral er kaolinit, der umiddelbart ikke viser nogen tegn på opløsning.

Geokemisk modellering af "batch" eksperimenterne blev udført ved hjælp af modelkoden PHREEQC. Modelleringen blev foretaget for at supplere den petrografiske og mineralogiske analyse samt for at kalibrere modellerne med henblik på fremskrivning af resultaterne i et længere tidsperspektiv (1000 år). Generelt støtter resultaterne af modelkalibreringen den petrografiske og mineralogiske tolkning. Således simulerer modellerne typisk opløsning af karbonater. Dog ses der i flere modeller genudfældning af små mængder karbonat mod slutningen af eksperimenterne på grund af en svagt stigende pH, som er forårsaget af opløsning af lerminerale ("mixed-layer" illit/smectit, illite/chlorit eller chlorit). Den supplerende viden opnået ved modelkalibreringen tyder således på, at også små mængder af lerminerale samt K-feldspat opløses i løbet af forsøgsperioden på 14 måneder.

De kalibrerede modeller har dannet grundlag for simuleringer af langvarig CO₂-eksponering (1000 år) af reservoirer og cap-rocks. Mulige mineral-CO₂ interaktioner er på baggrund af simuleringerne vurderet for et REV (repræsentativt elementarvolumen) for hver formation. Generelt viser prognosemodellerne, at store mineralogiske ændringer kan finde sted som følge af CO₂-eksponering over længere perioder. Således er et typisk resultat, at "mixed-layer" illit/smectit er helt opløst og erstattet af glimmer (K-mica), ren illit og/eller kaolinit efter 1000 års CO₂-eksponering. Tilsvarende er den generelle tendens, at der i løbet af perioden på 1000 år sker opløsning af K-feldspat. Undtagelsen er cap-rock modellerne, hvor der sker udfældning af K-feldspat på lang sigt. På grund af opløsning af lerminerale og feldspat ses en generel stigning i pH, som medfører, at der samlet set sker udfældning af små mængder karbonatminerale i simuleringsperioden på 1000 år.

Overvejelser om opskalering af geokemiske modeller er gennemført på grundlag af en simpel 2D model opstillet med TOUGHREACT. Resultaterne viser, at valget af modellens rumlige diskretisering kan have en stor indflydelse på fremskrivninger baseret på modellering. Dette gælder eksempelvis med hensyn til mængden af CO₂, der bindes ved mineraludfældning.

Sammenfattende indikerer modelberegningerne, at der på lang sigt kan ske både opløsning og udfældning af minerale ved CO₂ lagring i de undersøgte formationer. Den samlede virkning på porøsiteten af formationerne synes at være meget begrænset for reservoirformationerne, mens der for cap-rocks er en tendens til en lille reduktion af porøsiteten på lang sigt. Modelleringen illustrerer endvidere, at de forskellige porevæsker, der er anvendt samt den varierende mineral-sammensætning i de undersøgte formationer samlet set resulterer i at væsentligt forskellige mængder CO₂ bindes ved opløsning i porevæsken og ved mineraludfældning. Dette afhænger i høj grad af den mineralogiske sammensætning af den formation, hvor man ønsker at lagre CO₂ og understreger betydningen af at gennemføre "site specifikke" undersøgelser i fremtiden.

Endelig er der som en selvstændig del af projektet udført en evaluering af "forseglingsevnen" af de potentielle cap-rocks. Evalueringen omfatter bestemmelse af kapillartrykskurver (ved kviksølvinjektion), mineralogisk karakterisering og dynamiske flow eksperimenter. Baseret på evalueringen vurderes det, at "forseglingsevnen" med hensyn til CO₂ af de undersøgte cap-rocks (Børglum og Fjerritslev Formationen) er fremragende.

English Summary

This report summarises the results of the research project "Geologisk lagring af CO₂ i den danske undergrund: Vurdering af segl- og reservoir-bjergarternes respons på CO₂ lagring (AQUA-DK)". The main objective of the research project has been to identify reservoir rocks and cap-rocks suitable to CO₂ storage in Denmark and investigate possible CO₂ –mineral reactions in these rocks. Furthermore, the objective has been to evaluate the seal capacity of the suitable Danish cap-rocks. Thus, the study was carried out with the aim to constrain predictions regarding the integrity of Danish reservoir rocks and cap-rocks in a possible future Danish CO₂ geological storage scenario.

The literature about potential Danish reservoirs and cap-rocks was reviewed and the existing knowledge was updated, especially with respect to the formation history, distribution, depth, and petrographic and mineralogical composition of the reservoir rocks and cap-rocks. The most promising reservoir rocks for CO₂ storage are the Lower Triassic Bunter Sandstone Formation, the Triassic Skagerrak Formation, the Upper Triassic-lowermost Jurassic Gassum Formation and the Middle Jurassic Haldager Sand Formation while the most important cap-rocks are the mudstones of the Fjerritslev and the Børglum Formations.

In order to establish the best possible knowledge prior to reservoir condition laboratory experiments with core material from the various geological formations, the pore fluid compositions of core sampling locations were evaluated. Initially, the pore fluid chemistry of the Stenlille reservoir and cap-rock was the only reasonably well known chemistry due to existing data from previous pump tests in the Stenlille area. With regard to the other sampling locations, test-data from a number of different wells were used to correct for errors caused by mud filtrate, acid treatment of boreholes, etc. Based on the corrected dataset, a chemistry-depth relation was established for various chemical parameters in the pore fluid, and subsequently the approximate chemical composition of the pore fluid was estimated for each sample location and geologic formation.

CO₂ exposure laboratory experiments with selected samples of the identified potential reservoir rocks and cap-rocks were carried out during a period of up to 14 months. The experiments were carried out at reservoir conditions (20 MPa and 70°C) using the suggested pore fluid compositions. Pore fluid samples were taken for chemical analysis at regular intervals during the 14 months period and rock samples were taken after 7 and 14 months, respectively. Petrographical and mineralogical analysis of each formation prior to and after the experiments was performed by the use of transmitted light (and reflected light) microscopy, scanning electron microscopy (SEM) and X-ray diffraction (XRD).

In general, the petrographical and mineralogical analysis show that the carbonate minerals seem to be the minerals most exposed to changes when the selected rock samples are exposed to CO₂. Carbonate dissolution seems to account for most of the changes in the pore fluids during the experiments. When various carbonate minerals are present in one sample, the relative dissolution succession is calcite prior to dolomite, and siderite prior to ankerite. With regard to the silicate minerals, it has not been possible to verify by petrographical analysis whether detrital feldspar and authigenic analcime show increased degrees of dissolution after the CO₂ experiments, but the possibility cannot be ruled out. The fragile nature of most clay minerals makes it impossible by petrographical analysis to evaluate if they have been exposed

to dissolution. The most coarse-grained clay mineral is kaolinite, which shows no signs of dissolution.

Geochemical modelling of the batch experiments was carried out using the modelling code PHREEQC. The modelling was carried out in order to provide additional information to the petrographical and mineralogical analysis as well as with the purpose of calibrating the models for predictive calculations. In general, the findings of the model calibration support the results of the petrographical and mineralogical analysis. Thus, distinct initial dissolution of carbonates is observed in most models. At later time steps some carbonates may reprecipitate due to slightly increasing pH caused by dissolution of clay minerals (mixed-layer illite/smectite or illite/chlorite, and if present chlorite). Thus, in addition to the results of the petrographical and mineralogical analysis, the forward modelling of the laboratory experiments suggests that small amounts of clay minerals (mixed-layer illite/smectite or illite/chlorite, and if present chlorite) as well as K-feldspar are dissolved during the 14 months experimental period.

The calibrated models formed the basis for predictive simulations of long term (1000 years) exposure of the reservoir rocks and cap-rocks to CO₂. Possible mineral-CO₂ interactions were modelled for a REV (representative elementary volume) of each formation. In general, the predictive modelling suggests that large mineral changes can take place as the result of the CO₂ exposure over long periods. Thus, the typical result is that mixed-layer illite/smectite is totally dissolved and replaced by K-mica (or pure illite) and/or kaolinite at the end of the 1000 years simulation period. Also, overall dissolution of K-feldspar is most commonly seen, except in the models for the cap-rock formations where precipitation of K-feldspar is taking place. Due to the dissolution of clay minerals and feldspar a general increase in pH causes a small overall precipitation of carbonate minerals in the 1000 years simulation period.

Considerations regarding upscaling of geochemical models were based on a simple 2D model set up using TOUGHREACT. The results show that the choice of model discretisation may have a huge impact on the predictions based on the modelling, e.g. regarding the amount of CO₂ sequestered by mineral reactions.

In summary, based on the modelling both mineral dissolution and precipitation are predicted to take place. The overall effect on porosity seems to be negligible for the reservoir formations while for the cap-rocks the tendency is towards a slightly decreasing porosity. The predictive modelling illustrates that the various pore fluids and mineral assemblages present gives reason to quite different amounts of overall carbon sequestration by dissolution in the fluid and precipitation of carbonate minerals. This highlights the importance of carrying out site specific studies in the future.

Finally, an evaluation of the cap-rock sealing capacity of cap-rocks relevant for Danish reservoirs suitable for CO₂ storage was performed. The evaluation included mercury injection analysis, mineral characterization and dynamic flow experiments. Based on the the evaluation, the CO₂ sealing capacity quality of the investigated cap-rocks (Børglum and Fjerritslev Formation) is excellent.

Content

1.	Introduction	2
2.	The Danish reservoir- and cap-rocks	6
3.	Porewater chemistry in the Danish saline aquifers	11
3.1	Background	11
3.2	Methodology	11
3.3	Summary of results.....	14
3.4	Origin of saline formation waters in the Danish Sub basin.....	14
4.	CO₂ exposure and rock response in the laboratory	17
4.1	Methodology	17
4.2	Evolution in water chemistry during experiments.....	20
4.3	Petrographic evidence from CO ₂ experiments.....	22
5.	Geochemical modelling	26
6.	Cap-rock sealing properties	42
7.	Overall evaluation of reservoir and cap-rock response to CO₂ storage	47
8.	References	48

APPENDICES:

Appendix 1: Petrographical analysis

Appendix 2: Results of BET- and CEC-analyses

Appendix 3: Results of XRD analyses

Appendix 4: Selected results of chemical analysis and forward modelling

Appendix 5: Selected results of 1000 years of predictive modelling

ENCLOSURE:

CD-ROM with papers, reports, and presentations of the AQUA-DK project

1. Introduction

This report summarises the results of the AQUA-DK research project “Geologisk lagring af CO₂ i den danske undergrund: Vurdering af segl- og reservoir-bjergarternes respons på CO₂ lagring (AQUA-DK)”. GEUS and the project group acknowledge the financial support by DONG Energy, Vattenfall and the Danish EFP-programme funded by the Danish Energy Agency.

Background

The growing concern of global warming caused by large CO₂ emission to the atmosphere owing to combustion of fossil fuels has increased the focus on geological storage of CO₂ as a possible mitigation measure for reducing the emission to the atmosphere. This approach has amplified the need for a better understanding of the distribution and composition of the subsurface reservoirs, the capacity of the sealing cap-rocks, and the occurrence of suitable geological structures for CO₂ storage.

Previous geological mapping conducted by GEUS has indicated that potential reservoirs, cap-rocks and structures are present in the Norwegian-Danish Basin including the Danish onshore subsurface. Preliminary estimations of the CO₂ storage potential have indicated a large potential in the many gentle, four-way dip closures in the Mesozoic succession formed by movements of Zechstein salts. However, the detailed mineralogical composition of the reservoir- and cap-rocks and their possible response to CO₂ storage was poorly understood. Hence, GEUS approached DONG Energy and Vattenfall in 2007 with a proposal for a laboratory and modelling study designed to investigate the geochemical response of the potential reservoir rocks and cap-rocks to CO₂ storage in order to constrain predictions of mineral-CO₂ reactions prior to geological storage. With the support from DONG Energy and Vattenfall, GEUS submitted a research application to the EFP-programme and after positive reviews, the project was approved early 2008. This report summarises the results of the project.

Objectives

With the aim to constrain predictions regarding the integrity of Danish reservoir rocks suitable to CO₂ storage and their cap-rocks, the *overall objectives* of the research project are:

- To study and predict possible mineral-CO₂ interactions of Danish reservoir rocks suitable to CO₂ storage and their cap-rocks.
- To evaluate the cap-rock seal capacity of potential cap-rocks.

Content of the summary report

The overall objective of the project is achieved through a number of tasks carried out as part of the project, including:

- An update of the existing knowledge about potential reservoirs and cap-rocks and their formation history, distribution, depth, and petrographic and mineralogical composition.
- An evaluation of pore fluid composition from existing chemical data in order to establish the best possible knowledge about reservoir conditions prior to experiments.
- CO₂ exposure laboratory experiments of up to 14 months with selected reservoir rocks and cap-rocks and petrographical and mineralogical analysis prior to and after the experiments.
- Geochemical modelling of the experimental results and predictions regarding the possible long-term CO₂-mineral interactions.
- Considerations regarding upscaling of small scale geochemical results to larger scale models.
- An evaluation of the cap-rock sealing capacity of cap-rocks relevant for Danish reservoirs suitable for CO₂ storage.

The present report summarises the results of each of these tasks in the following chapters. Detailed results related to specific parts of the project are enclosed in appendices 1-5. In addition, a CD-ROM is enclosed with all relevant papers, posters, reports, and presentations given as part of the project in the period January 2008 – December 2010. The content of the CD-ROM is specified below:

Papers and conference proceedings:

- /1/ Kjøller, C., Weibel, R., Bateman, K., Laier, T., Nielsen, L.H., Frykman, P. & Springer, N., 2010. Geochemical impacts of CO₂ storage in saline aquifers with various mineralogy – results from laboratory experiments and reactive geochemical modelling. Energy Procedia, In press.
- /2/ Weibel, R., Kjøller, C., Bateman, K., Nielsen, L.H., Frykman, P. Springer, N. & Laier, T., 2010. Mineral changes in CO₂ experiments – Examples from Danish onshore saline aquifers. Energy Procedia, In press.

Reports:

- /3/ Bateman, K. and Purser, G., 2010. Geological storage of CO₂ in the Danish Underground: Evaluation of the Response of the Reservoir and Cap Rocks to CO₂. British Geological Survey External Report, CR/10/153. 27 pp.
- /4/ Kjøller, C., Weibel, R., Nielsen, L.H., Laier, T., Frykman, P., Springer, N., 2010. Response to CO₂ storage of Danish reservoir- and cap-rocks. Summary of results from the EFP-project AQUA-DK. GEUS report 2010/106. 50 pp.
- /5/ Laier, T., 2008. Chemistry of Danish saline formation waters relevant for core fluid experiments. Fluid chemistry data for lab experiments related to CO₂ storage in deep aquifers. GEUS Report 2008/48. 10 pp.
- /6/ Springer, N., Lorentzen H., Fries, K. and Lindgren, H., 2010. Caprock seal capacity evaluation of the Fjerritslev and Børglum formations. Contribution to the EFP-project AQUA-DK. GEUS Report 2010/112. 20 pp.

- /7/ Weibel, R., Olivarius, M., Nielsen, L.H., Abbramovitz, T., and Kjøller, C., 2010. Petrography and diagenesis of the Triassic and Jurassic sandstones, eastern part of the Norwegian-Danish Basin. Contributions to the EFP-project AQUA-DK. GEUS Report 2010/114. 77 pp.

Posters:

- /8/ Kjøller, C., Weibel, R., Bateman, K., Laier, T., Nielsen, L.H., Frykman, P. & Springer, N., 2010. Geochemical impacts of CO₂ storage in saline aquifers with various mineralogy – results from laboratory experiments and reactive geochemical modelling. Presented at the GHGT10 Conference. September 19-23, 2010, Amsterdam.
- /9/ Laier, T. and Øbro, H., 2009, Gaining public confidence in CO₂ storage. Presented at the IARU International Scientific Congress on Climate Change, Copenhagen, Denmark, 10 – 12 March 2009
- /10/ Weibel, R., Kjøller, C., Bateman, K., Nielsen, L.H., Frykman, P. Springer, N. & Laier, T., 2010. Mineral changes in CO₂ experiments – Examples from Danish onshore saline aquifers. Presented at the GHGT10 Conference. September 19-23, 2010, Amsterdam.

Presentations (external meetings):

- /11/ Kjøller, C.: AQUA-DK. Geochemical response to CO₂ storage. Presented at the GeoCapacity Conference, October 22, 2009, Copenhagen.
- /12/ Nielsen, L.H., Springer, N., Larsen, F., Weibel, R.: Geological storage of CO₂ in the Danish underground: Evaluation of the response of the reservoir rocks and cap rocks on the CO₂ storage. Presented at external workshop at the British Geological Survey – CO₂ Workshop GEUS/BGS – 2008, Nottingham.

Presentations (project meetings):

Project meeting December 11, 2008 at GEUS:

- /13/ Nielsen, L.H.: Indledning og strategi: projektets tilblivelse, ide og CO₂ i DK.
- /14/ Weibel, R.: Status for de eksperimentelle forsøg ved BGS og karakterisering af reservoirbjergarterne.
- /15/ Laier, T.: Hvad ved vi om porevandskemien ?
- /16/ Kjøller, C.: Kemisk modellering – hvorfor og hvordan?
- /17/ Springer, N.: Caprock, hvorfor og hvordan?
- /18/ Laier, T.: CO₂ baggrundsmåling før lagring, hvorfor, hvordan? – CO₂ niveauer i aktive områder og ved Ketzin forsøgs lager.

Project meeting January 25, 2010 at GEUS:

- /19/ Weibel, R.: Bjergarter og reservoirer, der indgår i projektet - et overblik.
- /20/ Kjøller, C.: Foreløbige resultater - fokus på vandkemi og modellering.
- /21/ Weibel, R.: Foreløbige resultater - fokus på petrografisk analyse.
- /22/ Springer, N.: Status for arbejdet med cap-rock analyse.
- /23/ Frykman, P.: Overvejelser om opskalering.

Project meeting December 9, 2010 at GEUS:

- /24/ Nielsen, L.H.: Valg af reservoirer og cap-rock til projektet
- /25/ Laier, T.: Porevandskemi i dybe danske reservoirer - resultater og udfordringer
- /26/ Weibel, R.: Resultater af laboratorieeksperimenter
- /27/ Kjøller, C.: Modellering og fremskrivning
- /28/ Frykman, P.: Overvejelser omkring opskalering af modeller
- /29/ Springer, N.: Resultater af cap-rock analyser

2. The Danish reservoir- and cap-rocks

The Danish part of the Norwegian-Danish Basin consists of a rift-succession formed in Late Carboniferous–Early Permian times overlain by a thick post-rift succession formed during Late Permian–Mesozoic times. The rift-succession mainly comprises wedges of alluvial conglomerates and sandstones, and lacustrine mudstones formed in grabens and half-grabens. Although these Rootliegendes coarse-grained clastics may be potential reservoirs in some areas, the main interest has been focused toward the Mesozoic succession which is better known and occurs in the depth window relevant to CO₂ storage of 0.8–3 km (Holloway et al. 2002) in large parts of the onshore area.

The Mesozoic succession is up to 9 km thick and comprises sandstones, mudstones, evaporates and carbonates deposited in a wide range of environments (Bertelsen 1980; Nielsen & Japsen 1991; Michelsen et al. 2003; Nielsen 2003). Reservoirs potentially suitable for CO₂ storage and fine-grained rocks with sufficient sealing capacity are found at several stratigraphic levels. The most important among the potential reservoirs are the Lower Triassic Bunter Sandstone Formation, the Triassic Skagerrak Formation, the Upper Triassic-lowermost Jurassic Gassum Formation and the Middle Jurassic Haldager Sand Formation (Figure 2.1).

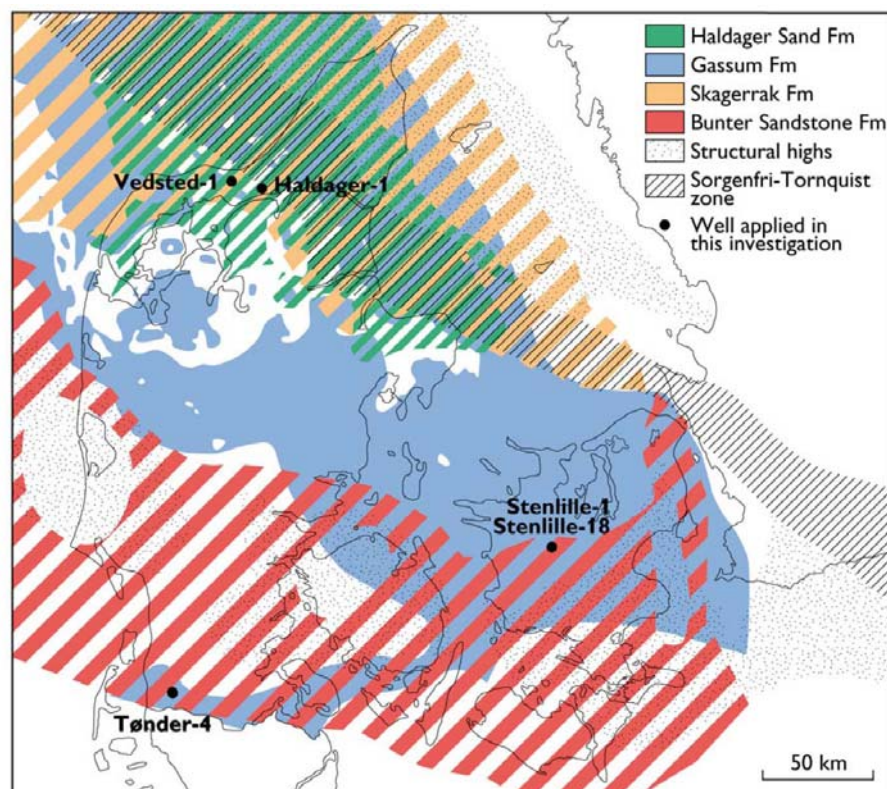


Figure 2.1. Map of Denmark showing the regional potential for CO₂ storage in the Triassic-Jurassic formations. The distribution of formations is shown for intervals thicker than 25 m and in the depth interval 800 m to 3000 m. From Weibel et al. (2010).

The Bunter Sandstone Formation, with up to four regional sandstone units of fluvial and aeolian origin, and interbedded with thick mudstones, is present onshore Denmark in the North German Basin south of the Ringkøbing-Fyn High. The formation thins on the high and may be absent in places, but thickens northwards to more than 900 m in central parts of the Danish Basin (Nielsen & Japsen 1991; Michelsen & Clausen 2002). Closer toward the northern and eastern margin of the basin the Bunter Sandstone Formation is contemporaneous with the poorly-moderately sorted, alluvial subarkosic-arkosic sandstones and mudstones of the Skagerrak Formation (Figure 2.2), which encompasses an up to 2–3 km thick, heterogeneous basin margin succession formed during the Early–Late Triassic (Bertelsen 1980; Nielsen 2003). Both the Bunter Sandstone Formation and the Skagerrak Formation contain mudstones that may act as cap-rocks for the interbedded sandstones, although their sealing capacity is poorly known.

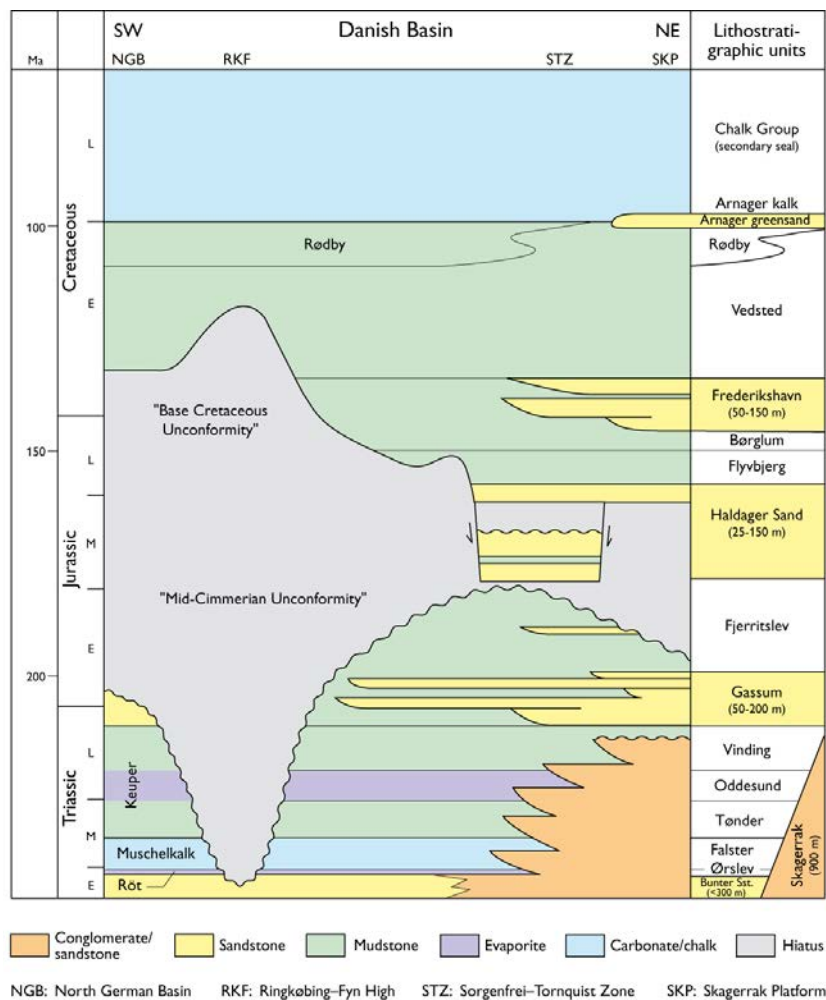


Figure 2.2. Stratigraphic scheme showing the Triassic-Jurassic-Cretaceous stratigraphy relevant to geological CO₂ storage in Denmark. From Mathiesen et al. (2009).

The Gassum Formation is present in most of the Danish area as a 50–300 m thick succession of fluvial and marine sandstones interbedded with marine, lagoonal and lacustrine mudstones reflecting repeated fluctuations in sea-level during deposition (Nielsen 2003). The formation is overlain by thick, uniform marine mudstones (the Fjerritslev Formation, Figure 2.2) with large lateral continuity forming a highly competent cap-rock unit probably making the Gassum Formation one of the most promising reservoirs for CO₂ storage in the Danish subsurface. The source area of the Gassum sand probably comprised reworked Bunter Sandstones in the south-eastern part of the basin, whereas more heterogeneous bedrock to the north and east supplied the sand to the northern and central parts of the basin causing a variable petrography of the formation.

The Haldager Sand Formation, dominated by marine and fluvial greywacke sandstones is mainly present in the fault-bounded Sorgenfrei-Tornquist Zone where it locally attain up to 200 m in thickness; outside this zone it wedges out rapidly toward the southwest and northeast (Nielsen 2003). On the Skagerrak-Kattegat Platform and in the Sorgenfrei-Tornquist Zone, the Haldager Sand Formation is overlain by interbedded marine sandstones and mudstones of the Flyvbjerg Formation and marine mudstones of the Børglum Formation. Toward southwest and west the Flyvbjerg Formation wedges out and the Haldager Sand Formation is in places directly overlain by marine mudstones of the Børglum Formation, which has a large caprock potential.

The Bunter Sandstone, Skagerrak, Gassum and Haldager Sand Formations therefore constitute the principal reservoirs suitable for CO₂ storage, and the Fjerritslev and Børglum Formations constitute the principal cap-rocks. Cores are available from these formations as they have been the target for previous hydrocarbon exploration activities. Thus, a number of core samples were selected with the strategy to cover the variable petrographical composition of the potential cap-rock and reservoir formations. With regard to the potential reservoir formations, primary variations related to source areas and depositional environments and secondary alterations caused by diverse diagenetic development related to different burial depths in the basin was specially emphasised. Secondary alterations were also studied in relation to the lithology of the embracing formations. This strategy was followed in order to obtain the best possible overview of the potential chemical reactions in the reservoirs which subsequently may be the target of further in-depths studies.

The results of the detailed petrographical and mineralogical analysis of the potential reservoir formations are presented in Weibel et al. (2010) and summarised in the following sections.

Bunter Sandstone Formation

The sandstones of the Bunter Sandstone Formation consist mainly of arkoses and subarkoses (Weibel and Friis 2004) according to the classification of McBride (1963). The framework grains are dominated by quartz with subordinate feldspar. K-feldspar is more common than plagioclase, and plagioclase seems to be more intensively altered and dissolved than K-feldspar. Some samples contain numerous ooids, carbonate clasts or clay intraclasts – “rip-up” clasts from overbank strata. The detrital grains are variably altered showing replacement by authigenic phases, dissolution, oxidation and reduction. The

volumetrically important authigenic phases in the Bunter Sandstone Formation are carbonates (calcite and dolomite), anhydrite and clay minerals (illite, chlorite, mixed-layer illite/smectite, mixed-layer smectite/chlorite). Dolomite, calcite and anhydrite may occur as pore-filling cement. Authigenic calcite also occurs as overgrowths on ooids or other carbonate rock fragments and dolomite occurs as rhombohedral-shaped single crystals commonly in clay intraclasts. Common subordinate authigenic minerals are analcime, feldspar overgrowths, quartz overgrowths, barite, red coatings of primarily hematite, anatase and other authigenic opaque minerals (Weibel and Friis, 2004). Analcime is present in most samples and occurs as perfect, outer crystal shapes, whereas the internal parts frequently have irregular dissolution voids. Since dissolution is generally not observed on the surface of anhydrite crystals, the porosity is mainly uncemented primary porosity.

Skagerrak Formation

The sandstones and conglomerates of the Skagerrak Formation are arkoses, lithic arkoses and subarkoses (Weibel 1998) according to the classification of McBride (1963). The framework grains are quartz with relatively high content of feldspar and few rock fragments. The feldspar group is completely dominated by K-feldspar, though rare plagioclase grains have been identified. Alteration of feldspar grains includes sericitisation, clay mineral or carbonate replacement and dissolution. Furthermore, a relatively high content of altered grains are probably altered feldspar grains, besides altered rock fragments. The rock fragments are mainly igneous and rare metamorphic, but in specific areas volcanic rock fragments occur. Clay intraclasts which probably are rip-up clasts from overbank deposits occur in high abundance in few samples. Mica occurs in small amounts in most samples. Mica shows sign of oxidation, reduction (only in reduction spots) and expansion due to precipitation of authigenic phases between their cleavage planes. Transparent and opaque heavy minerals are common accessory minerals, though they may be abundant in specific samples containing heavy mineral lamina. The alteration of opaque minerals include among other leucoxene replacement of ilmenite and hematization of magnetite, (Weibel 1999; Weibel & Friis 2007). The dominating porosity reducing cements in the Skagerrak Formation are carbonates and clays. The clays are dominated by smectite in the shallow wells, whereas mixed-layer illite/smectite and illite becomes more abundant with increased burial depth (Weibel 1999). Kaolin dominates the clay mineral assemblage in the reduction spots and reduced areas, but is rare in the red host. The carbonate cement is typically dolomite, which occurs either as rhombohedral-shaped crystals, commonly with distinct growth zones, or as pore filling cement, commonly replacing other mineral phases. Occasionally the pore filling carbonate cement is calcite or ankerite cement instead of dolomite. The red colouration originates in the shallow wells (< 2100 m) from goethite needles, which is pseudo-morphously transformed into hematite needles in the deeper wells (>2700 m) (Weibel 1999; Weibel & Groberty 1999). Additionally, hematite occurs as replacement of mica and amphiboles, syntaxial overgrowth on detrital hematite and as pore filling crystals. Of minor volumetrically importance are quartz overgrowths, feldspar overgrowths and anatase. Anhydrite is a rare late authigenic phase and corrosive to all other mineral phases.

Gassum Formation

The sandstones of the Gassum Formation are mainly subarkoses and arkoses (Friis 1987) according to the classification by McBride (1963). The framework grains are dominated by quartz and subordinate feldspars and rock fragments. The feldspar abundance varies across the basin and feldspar is relatively more abundant in the northwestern part than in the eastern part. K-feldspar is more common than albite and Ca-rich plagioclase has not been observed. Alteration of feldspar grains include partly dissolution, replacement by kaolinite or carbonate, incipient albitisation in the deep wells. Mica, present in all samples, show varying degree of alteration from expansion along cleavage planes caused by precipitation of authigenic minerals to compaction along stylolites in the deepest wells. Transparent and opaque heavy minerals occur as accessory minerals. The opaque minerals are dominated by leucosene altered ilmenite, and the transparent minerals characterized by rutile, zircon and tourmaline. The porosity reduction is mainly due to compaction in wells of burial depths down to 1500 m (Friis 1987). Changes in the porosity are mainly the result of limited amounts of authigenic phases as siderite, pyrite and calcite besides generation of secondary porosity by feldspar dissolution. In deep wells (below 1500 m), the porosity reduction is caused in particular by quartz diagenesis and locally by ankerite and kaolinite. Volumetrically, minor authigenic phases include illite, chlorite, albite.

Haldager Sand Formation

The sandstones of the Haldager Sand Formation are characteristically quartz arenites with subordinate subarkoses. Quartz dominates the framework grains. K-feldspar is more common than plagioclase, the latter being extremely rare in the deepest wells. Rock fragments are of plutonic, metamorphic or sedimentary origin. Organic matter is abundant in some samples, and occasional root or soil horizons have been reported (Nielsen and Friis 1984). Mica is commonly concentrated in the same samples as the organic matter. A typical completely kaolinised mica is found in most samples of the Haldager Sand Formation. The authigenic phases is similar to those of the Gassum Formation, however their abundance is typically lower. Early quartz and kaolinite occur randomly distributed in the fluvio-deltaic sandstones, whereas calcite cement may be important in the marine deposits (Nielsen and Friis 1984). Siderite, pyrite, iron-oxide/hydroxides and anatase are common minor authigenic phases.

3. Porewater chemistry in the Danish saline aquifers

3.1 Background

For the performance of laboratory tests in order to simulate the effect of CO₂ injection into geological formations information on the initial formation water chemistry was needed. Core material representing reservoir rock as well as cap rock was selected among the drill cores available at GEUS (Table 3.1). The first task to perform was therefore to provide information on formation water chemistry for the geological formations at the locations listed in Table 3.1 as accurately as possible.

The most reliable data on formation water chemistry can be obtained from pumping tests. However, such tests have only been performed for a limited number of wells. Therefore, it was necessary to extrapolate from a limited number of data available for on-shore Denmark using the general knowledge on evolution of subsurface formation waters obtained from more thoroughly studied basins published in the literature. The second task for the present project on CO₂ sequestration was therefore to provide a more general understanding on the evolution of formation waters in order to be able to make better prediction concerning formation water chemistry in the future.

Table 3.1. List of core samples for laboratory tests

	Formation	Depth, m	Geol. period	Stage	Well
Reservoir	1. Gassum Fm	1662	U Triassic	Raethian	Stenlille-18
Reservoir	2. Gassum Fm	2009	U Triassic	Raethian	Vedsted-1
Reservoir	3. Haldager Sand Fm	1150	M Jurassic	Aalenian-Oxfordian	Vedsted-1
Cap rock	4. Børglum Fm	1041	U Jurassic	Kimmeridgian-Volgian	Haldager-1
Cap rock	5. Fjerritslev Fm	1500	L Jurassic	Hettangian-Toarcian	Stenlille-1
Reservoir	6. Bunter Sandstone Fm	1662	L Triassic		Tønder-4
Reservoir	7. Skagerrak Fm (possib.)	2064	M/U Triassic		Vedsted-1

3.2 Methodology

Almost one hundred deep (> 500 m) wells have been drilled on-shore Denmark. However, reliable formation water chemistry data were only obtained from relatively few of these wells. Until 1978, wells were mostly drilled for oil exploration purposes, and only few tests were performed since no commercial quantities of oil had been encountered. After 1978, drilling activities relating to geothermal energy, natural gas underground storage and nuclear high level waste storage greatly enhanced our knowledge on formation water chemistry. Samples of formation water were obtained by different techniques: 1) production tests, 2) air-lift testing and 3) pore-water extraction from cores using a centrifuge. All available formation chemistry data for the Danish on-shore area are summarised in Figure 3.1.

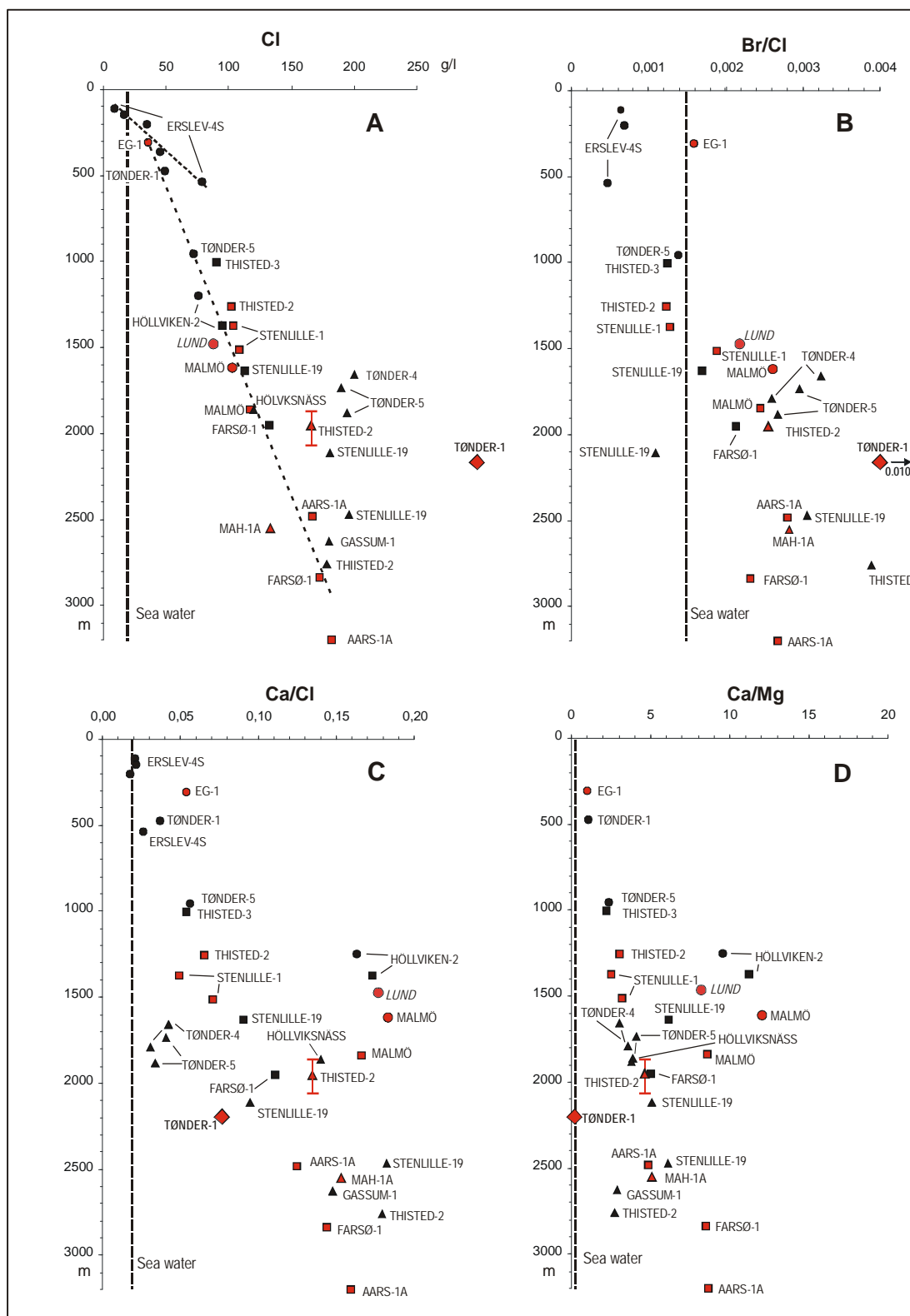


Figure 3.1. Chemistry of formation waters in the Danish sub basin. Triangles = Triassic, squares = Jurassic and circles = Cretaceous-Tertiary. Ion-ratios are in mole units. Red indicate most reliable data, usually from well tests lasting more than one day. Well locations are indicated in Figure 3.2.

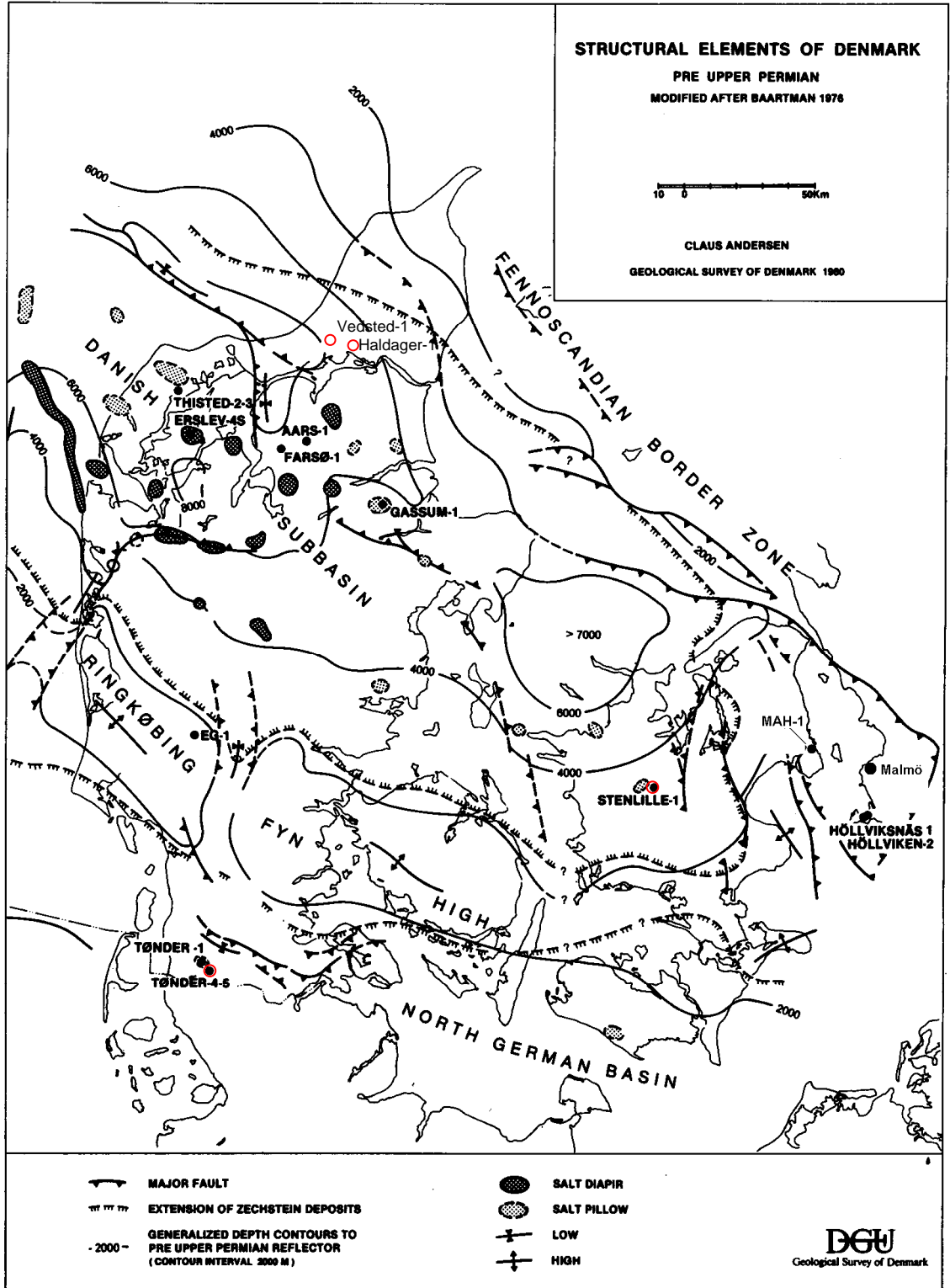


Figure 3.2. Location map indicating the position of wells from which data on formation water chemistry have been obtained. Red circles indicate position of wells from which cores samples have been selected.

3.3 Summary of results

The suggested formation water chemistry of the formations from which cores were selected for test experiments (Table 3.1) is shown in Table 3.2. The data in Table 3.2 were selected from the GEUS data set based on the assumptions presented by Laier (2008). The fluid chemical composition listed in Table 3.2 was recommended for the test experiments that were performed at BGS (cf. Chapter 4).

Table 3.2. Suggested fluid chemistry for rock- fluid test experiments

Test No.	1	2	3	4	5	6	7	
Formation	Gassum	Gassum	Haldager	Børglum	Fjerritslev	BunterSSt	Skagerrak	
Well	Stenlille-18	Vedsted-1	Vedsted-1	Haldager-1	Stenlille-1	Tønder-4	Vedsted-1	
Depth, m	1662	2009	1150	1041	1500	1662	2064	
pH	6.2	6.6	-	6.4	6.4		6.6	
Cl ⁻	113	166	132	102	90	103	200	166
SO ₄ ²⁻	0.015	0.29	0.05	0.01	0.05	0.015	0.5	0.29
Br ⁻	0.44	0.98	-	0.29	0.3	0.31	1.5	0.98
HCO ₃ ⁻	0.08	0.03	-	0.043		0.061		0.03
Na	59	70	63	55	46	58	115	70
Ca	11.5	23.5	16	7.5	8.11	5.7	9.5	23.5
Mg	1.6	3.34	2.1	1.50	1.55	1.40	1.9	3.34
K	1.1	1.88	0.35	0.25	0.24	0.29	1.7	1.88
Sr	0.66	0.62	0.6	0.38	0.5	0.6		0.62
Fe	0.06	0.03	-	0.04		0.03		0.03
	<i>Stenille-19</i>	<i>Thisted-2</i>	<i>Farsø-1</i>	<i>Thisted-2</i>	<i>Haldager-1</i>	<i>Stenille-1</i>	<i>Tønder-4</i>	<i>Thisted-2</i>
	<i>Gassum</i>	<i>Skagerrak</i>	<i>Haldag.</i>	<i>Gassum</i>	<i>DST#3</i>	<i>Fjerritslev</i>	<i>BunterSSt</i>	<i>Skagerrak</i>

Concentrations are given in g/L. Chemistry data were based on well information shown in italics.

3.4 Origin of saline formation waters in the Danish Sub basin

The salinity of formation waters increases gradually with depth approaching saturation with respect to halite (sodium chloride) at approximately 3000 m (Figure 3.1A). Close to salt diapirs, salinity gradients are steeper with respect to depth as is seen for the Erslev and Tønder-4, and -5 wells (Figures 3.1A and 3.2). The high salinity of subsurface water is most likely related to the massive Zechstein salt deposits, while the gradual increase in salinity with depth may be due to diffusion of ions in solution (Figure 3.1A). However, increase in salinity due to hyper-filtration through semi-permeable geological clay membranes may also play a role. Triassic evaporites are also present in some areas. The relatively high bromide to chloride ratios of most formation waters indicate that dissolution of salt is not the primary source, since halite has a lower bromide to chloride ratio compared to sea water, compare Figures 3.3 and 3.1B. The source is more likely the residual brines left after the precipitation of the Zechstein salts. Such brines have been encountered in some cases when penetrating the Zechstein deposits (Dinesen, 1961), exemplified by the Tønder-1 brine (Figure 3.1).

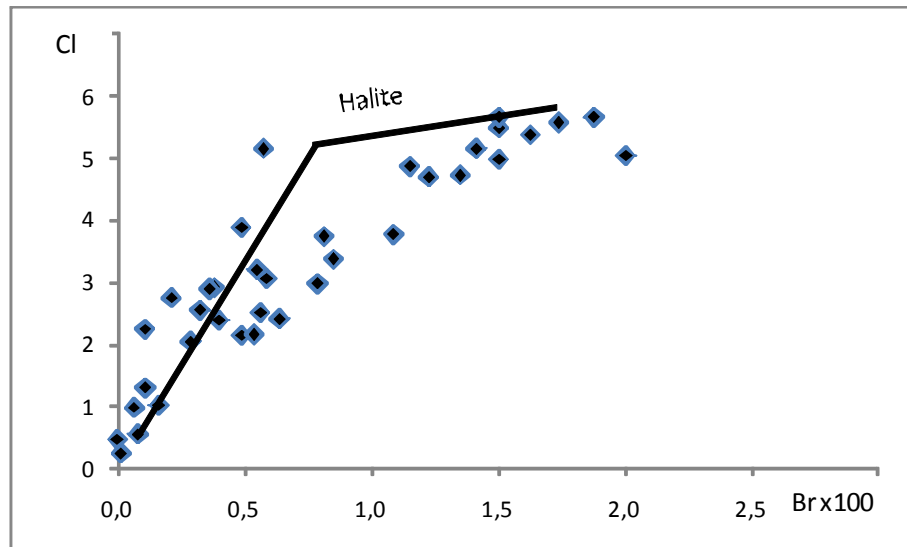
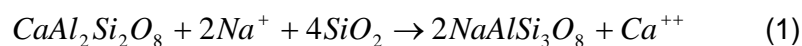


Figure 3.3. Chloride vs. bromide (molar concentration) for Danish subsurface waters. The solid line indicates the Cl/Br relationship in sea water during evaporation. Bromide increases relative to chloride in solution when halite starts to precipitate.

The Zechstein brine had a very high bromide content $7,8 \times 10^{-2}$ M (6200 mg/L) and a Br/Cl ratio of 0.01 (not shown in Figure 3.3), which indicate a very high degree of evaporation, almost to the point where carnalit starts to precipitate.

A stable isotopic ratio of the water itself indicates that most formation waters are mixtures of evaporated sea water and meteoric water (Figure 3.4). The more shallow water from the Erslev well above the Mors salt diapir is of meteoric origin (Figure 3.4). The low Br/Cl ratio in the Erslev water (Figure 3.1B) indicates that salinity originates from salt dissolved by water percolating from the surface.

Assuming the Tønder-1 brine to be one possible end-member for the mixtures of waters that presently occupies the subsurface, it is obvious that some reactions must have taken place in addition to dilution. The concentration of calcium relative to magnesium and sodium has increased considerably (Figures 3.1C-D). This is probably due to dolomitisation and diagenesis of plagioclase, whereby anorthite reacts to form albite, releasing calcium into solution (eq. 1).



The degree of diagenesis depends on both temperature and time, and this could explain why the calcium concentration increases relative to salinity with depth since the temperature of the formation increases with depth.

Although most of the dissolved salt probably derives from evaporated sea water a certain proportion of salt could derive from dissolution of halite. The distinctly higher Ca/Cl ratio (Figure 3.1C) observed outside the Zechstein deposit area (Figure 3.2) may be explained by the lack of salt deposits.

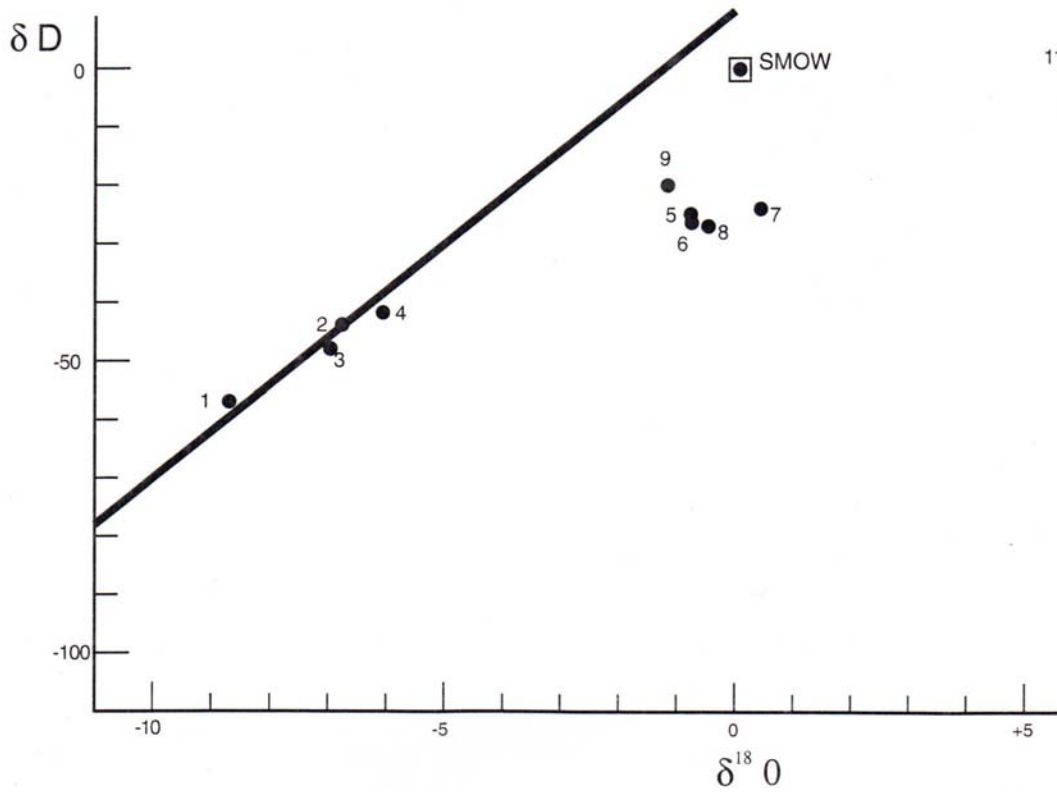


Figure 3.4. Stable isotopic ratio $\delta D/\delta^{18}O$ of some Danish formation waters. The solid line indicate GMWL (global meteoric water line). SMOW denotes standard mean ocean water. Data points 1-4 represent water samples from Erslev, data 5-9 represent Triassic water mostly from the Gassum formation. 11 represent Zechstein evaporated seawater (Løgumkloster-1 well)

4. CO₂ exposure and rock response in the laboratory

In order to form the basis for both the petrographical analysis of possible CO₂-mineral interactions and for calibration of the geochemical models used to carry out long term predictions, a series of CO₂ exposure batch experiments were conducted in the laboratory. The laboratory experiments included samples from all the identified potential reservoir formations (Bunter Formation, Haldager Formation, Skagerrak Formation and Gassum Formation) as well as samples from the potential cap-rock formations Fjerritslev Formation and Børglum Formation.

In addition, a column experiment using crushed material of the Gassum Formation – Stenlille 18 well was also carried out. However, the petrographical analysis showed that the sediment from the Stenlille 18 well unfortunately was contaminated by drilling mud and therefore no further interpretation of the column experiments was attempted. Thus the following sections include only descriptions and results from the batch experiments. Further information about the column experiment can be found in Bateman and Purser (2010) (reference /3/ on the attached CD-ROM).

4.1 Methodology

Experimental set up

The batch experiments were conducted at the British Geological Survey (BGS) (Bateman and Purser 2010). Reservoir rock plugs of 1 inch diameter were placed in pressure vessels at 70°C and 20 MPa, and immersed in a synthetic pore fluid mimicking the true porewater chemical composition of the reservoir formations (cf. Chapter 3 and Laier 2008). With regard to the cap-rock experiments, crushed samples were used instead of plugs in order to speed up the CO₂-mineral reactions. CO₂ saturated synthetic pore fluids were injected at the beginning of the experiments, and the CO₂ pressure was kept constant at 20 MPa during the entire experiment.

Parallel experiments were conducted with N₂ gas and degassed pore fluid instead of CO₂. This was done to be able to distinguish between effects of CO₂ exposure and effects of chemical disequilibrium between the mineral assemblage present and the synthetic brine used in the experiments. Fluid samples were taken after 1, 2, 3, 7, 9, 11, and 14 months, and rock samples were available after 7 and 14 months.

It should be noted that by experience such experiments are quite complex and several risks of errors exists. Some of the possible and experienced uncertainties during the experiment are:

- A too small initial amount of pore fluid in the batch or difficulties with fluid sampling, resulting in:
 - insufficient amount of fluid to carry out reliable fluid sampling after 14 months in some of the experiments
 - plug dried out during experiment (salt precipitation)
- Risk of small leaks in pressure vessels during the experiment, resulting in:
 - overall increased ionic concentration due to evaporation
 - possible oxidation in at least one batch
- Evaporation of fluid samples prior to chemical measurements, resulting in:
 - overall increased ionic concentration due to evaporation
- Problems related to concentration measurements of the highly saline fluids:
 - In order to carry out analyses of the fluid samples, they have to be diluted several thousands times. Though dilution is carried out as a thorough gravimetric dilution, some uncertainty is related to this procedure.
 - Cleaning of the instrument (plasma-optical emission spectroscopy (ICP-OES)). Working with the high salinity samples requires special attendance to the cleaning procedure of the ICP-OES instrument between analysis runs. Insufficient cleaning may result in erroneous measurements.

Chemical analyses

The fluid composition was analysed for major (Na, K, Ca, Mg) and some minor elements (Si, Al, Fe, Mn, Sr, Ba, Co, Ni, Cu, Zn, Cr, Mo, Cd, P, Pb, V, Li, B, As, Se and total S) using inductive coupled plasma - optical emission spectroscopy (ICP-OES), and for major and some minor anions (F^- , Br^- , Cl^- , SO_4^{2-} , NO_3^- , HPO_4^{2-}) using ion chromatography (IC). Analysis of HCO_3^- was performed by titration against sulphuric acid on cooled depressurised samples. Measurements of pH were made on cooled, depressurised samples using an Orion® 900A pH meter.

Petrographical and mineralogical analyses

Petrography was evaluated from transmitted light and reflected light microscopy of polished thin sections. Modal compositions of the sandstones were obtained by point counting minimum 300 points in each thin section, which were stained for K-feldspar. Supplementary studies of crystal morphologies, dissolution features and paragenetic relationships were performed on gold coated rock chips mounted on stubs and on carbon coated thin sections using a Phillips XL 40 scanning electron microscope (SEM). The scanning electron microscope was equipped with a secondary electron detector (SE), back-scatter detector (BSE); and with a Thermo Nanotrace 30 mm² detector surface window and a Pioneer Voyager 2.7

10 mm² window Si(Li) detector energy dispersive X-ray analysis (EDX) system. The electron beam was generated by a tungsten filament operating at 17 kV and 50-70 μ A.

Uncertainties during the petrographical investigations include:

- Heterogeneities of the samples
- Infiltrated drilling mud
- Partly dissolved grains and authigenic phases exist prior to the experiment. It is not possible to evaluate if the degree of dissolution is increased.
- Dissolution of clay minerals cannot be identified by SEM
- SEM investigations of the bottom part of the plugs to avoid the dried out samples
- SEM investigation of the outer rim of the plug, as the internal part showed remarkably less alterations

X-ray diffraction

The clay fraction samples were separated by sieving and gravitational settling and prepared as smear slides. Bulk samples were mounted with random orientation. Samples were scanned on an automated Philips© PW 3710 X-ray diffractometer with automatic divergence slit, using graphite monochromated CuK α radiation. The clay specimens were scanned air-dried; ethylene glycolated at 60°C; and after heating at 500°C for one hour. Criteria for identification of clay minerals can be found in Weibel (1999). Quantification of major mineral phases was done by Rietveld analysis of x-ray diffractograms of bulk-rock samples analysed at University of Copenhagen (KU), though semi-quantitative on samples analysed at University of Aarhus (AU) by application of corrections factors determined for the diffractometer. Clay minerals were evaluated semi-quantitative.

Cation exchange capacity (CEC)

Selected clay fractions were analysed for cation ion exchange capacity. Cation exchange capacity (CEC) was determined by exchange with sodium at pH 8.2, washing out of excess sodium chloride and exchange of sodium by ammonium. Exchanged sodium was determined by Atomic Absorption Spectrophotometry (AAS).

Specific surface area (BET)

The specific surface area was analysed for all clay fractions. Before measuring the N₂-BET specific surface area, the samples were outgassed at high vacuum at 20°C. Subsequently, the specific surface was determined by nitrogen adsorption at liquid nitrogen temperature in a Micromeritics Accusorb instrument by application of the BET equation (Brunauer et al. 1938).

4.2 Evolution in water chemistry during experiments

The general trends in the pore fluid chemical evolution during the batch experiments are illustrated for selected chemical parameters in Figure 4.1, showing the results from the batch experiments with plug samples from the Gassum Formation (Vedsted-1 well).

As a response to the pressurisation with CO₂, the batches exposed to a constant CO₂ pressure show a rapid decrease in pH and increase in HCO₃⁻ content. Following the fast decrease in pH and increase in HCO₃⁻ content, both values level off at fairly constant values during the remaining part of the experiment. Thus, initially a fast dissolution of CO₂ in the pore fluid takes place followed by a period with equilibrium between the CO₂ content in the pore fluid and the gas phase. In comparison, the N₂ experiments have relatively constant pH and a HCO₃⁻ content below detection limit during the entire experiment.

Similar to the fast evolution in parameters related to the aqueous carbonate system (pH and HCO₃⁻), a fast increase in concentration of most major cations is observed during the first month of the experiments (cf. Ca, Mg, and K in Figure 4.1). This probably illustrates that though the initial composition of the synthetic pore fluid was chosen carefully, some degree of disequilibrium exists at the beginning of the experiments. Apparently, the pore fluid composition approaches equilibrium fast in the initial period (i.e. the first month) of the experiments, followed by a period with slower overall mineral reactions as indicated by the less pronounced increase in ion concentrations during the remaining part of the experiments. Discarding the increase in concentration during the first month, the most pronounced concentration increases during the 14 months experiments are seen for K, not only for the Gassum Formation (Vedsted 1 well) as illustrated in Figure 4.1, but also for other experiments (see Appendix 4 for specific experiments).

Whether the overall increase in major ion composition during the experiments is a result of mineral reactions taking place is uncertain since in several experiments an increase in the pore fluid Cl⁻ concentration is also seen, suggesting that some uncertainties are related to the experimental set-up as already discussed.

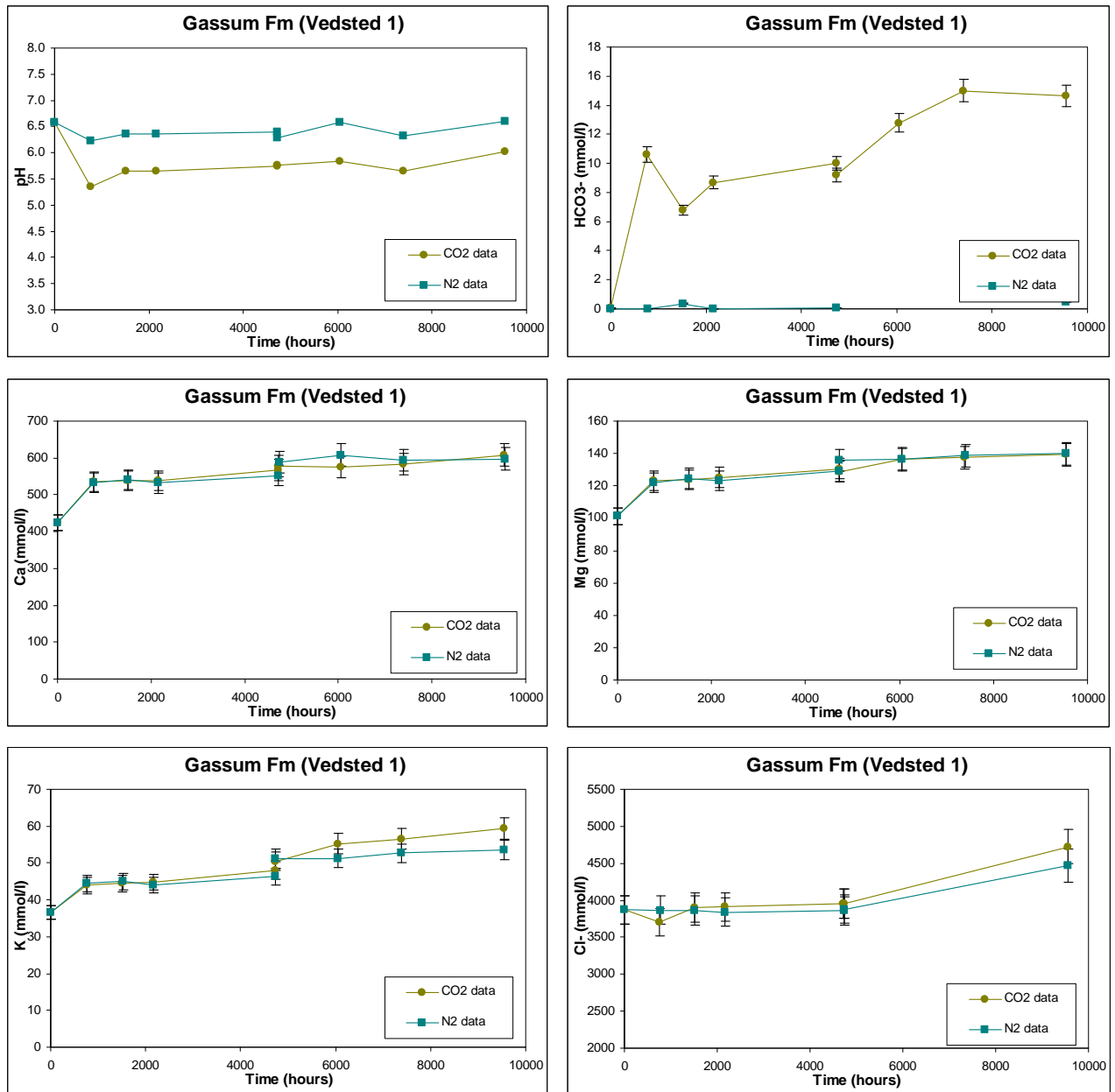


Figure 4.1. Evolution in selected fluid chemical parameters during batch experiments with plug samples from the Gassum Formation (Vedsted-1 well).

Significant differences are hard to detect for most major ions when comparing the results from the CO₂ and N₂ batch experiments. This indicates that, within the timeframe of the experiments (14 months), the mineral dissolution caused by CO₂ is not possible to distinguish from the dissolution caused by the initial disequilibrium between synthetic pore fluid and the mineral assemblage present in the rock sample – at least not when considering the evolution of the major ions in the pore fluid. However, the results of the experiments with crushed cap-rock suggest a fairly more pronounced dissolution of minerals indicated by elevated Ca (Fjerritslev Formation, Appendix 4), Mg (Børglum Formation, Appendix 4), and K concentrations (both cap-rock formations, Appendix 4) in the CO₂ pressurised experiments as compared to the N₂ pressurised experiments. In addition, the evolution in some

minor ions such as Fe and Mn also indicates that CO₂-mineral reactions take place in the CO₂ pressurised experiments (cf. Figure 4.2)

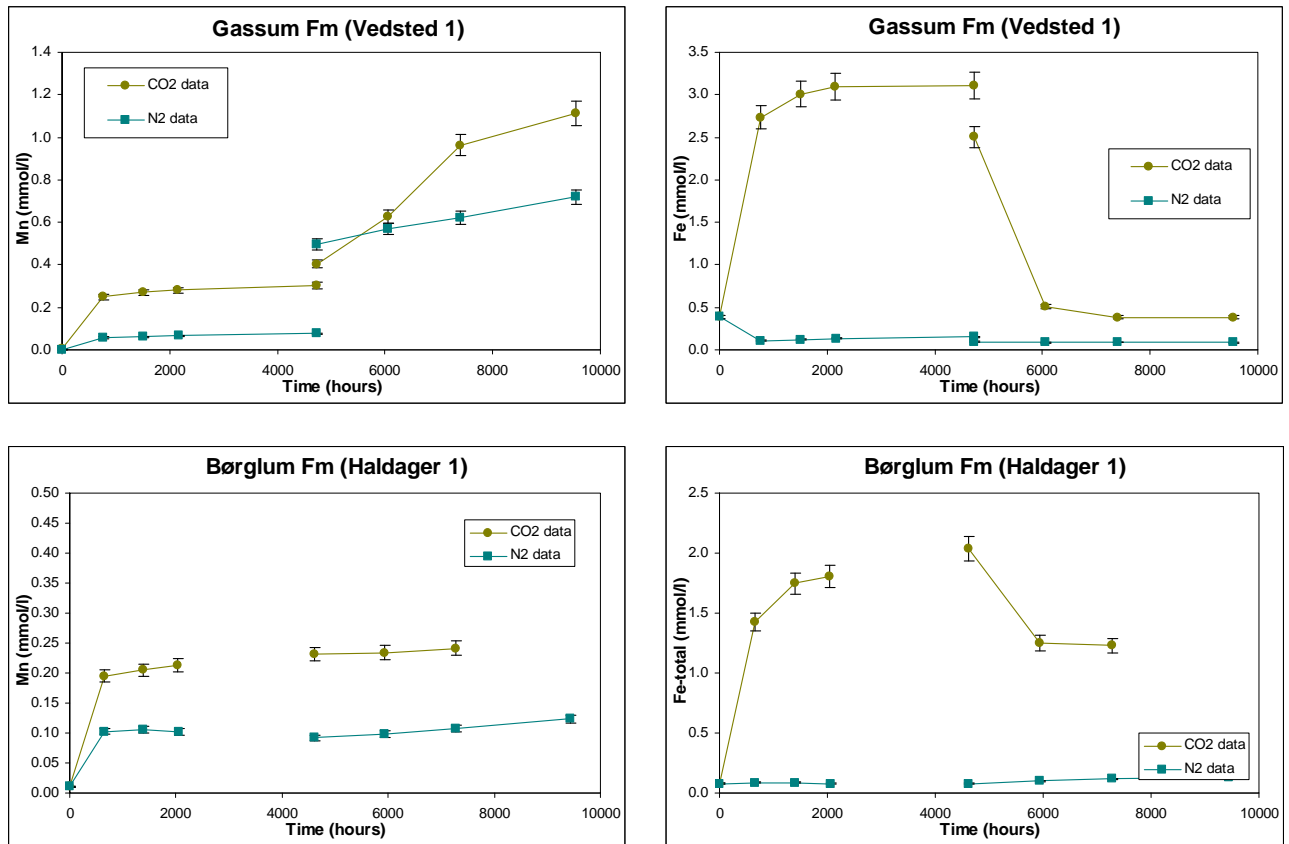


Figure 4.2. Evolution in Mn and Fe-tot concentrations during batch experiments with rock samples from the Gassum Formation (Vedsted-1 well) and Børglum Formation (Haldager-1 well), respectively.

The evolution in pore fluid pH, HCO₃⁻, Ca, Mg, K, Na, Cl⁻, Mn, Fe, and total-S is presented in Appendix 4 for each experiment. Si and Al concentrations are not shown since given the difficulties with carrying out chemical analysis on highly saline water, the concentration of these two species is below detection limit in all samples measured.

4.3 Petrographic evidence from CO₂ experiments

The advantage of applying sandstone plugs in the experiments rather than crushed samples is documented by the fact, that more decisive conclusions on the mineral alterations can be made. It has been important to investigate the rim of the plug rather than the core, as even in the 14 months experiments, the reaction front has not penetrated the plugs completely. The cap-rock samples had to be crushed as their low permeability would slow the reactions too much within the duration of the experiments. However, identification of mineral alteration is inhibited by the intense treatment as well as the fine-grained nature of the cap-rocks.

The following sections describe the findings of the petrographical analysis for each geological formation.

Bunter Sandstone Formation

The Bunter Sandstone Formation shows corrosion of calcite rhombs after 7 months of CO₂ experiment and clear signs of calcite cement dissolution after 14 months of experiments. Possibly also some corrosion features on dolomite rhombs are present (Figures 1, 2, 3 and 4 in Appendix 1). Pore fluid changes with slightly increased Ca and Mg in the CO₂ exposed batches as compared to the N₂ exposed samples during the experiments also indicate calcite and dolomite dissolution in the CO₂ experiment (Appendix 4). The Bunter Sandstone Formation contains partly dissolved feldspars and authigenic analcime with internal dissolution voids prior to the experiments. It is not possible to verify an increased degree of dissolution during the experiment, but it cannot be excluded. Dissolution of anhydrite in both the CO₂ and the N₂ experiments show that this is related to a sulphate subsaturated initial synthetic pore fluid rather than the CO₂ exposure. Increasing sulphur in both CO₂ and the N₂ experiments suggests anhydrite dissolution.

Skagerrak Formation

The Skagerrak Formation shows clear signs of ankerite dissolution both after 7 and 14 months of CO₂ experiment (Figures 6 and 8 in Appendix 1). Pore fluid changes with slightly increased Fe and Mn concentrations (Appendix 4) also support the dissolution of ankerite. The Skagerrak Formation contains abundant partly dissolved feldspars, though authigenic albite shows no sign of corrosion (Figures 5 and 7 in Appendix 1). Increased dissolution of detrital K-feldspar is indicated from pore fluid changes during CO₂ experiment, but an increased degree of dissolution cannot be petrographically verified. Pyrite appears to be unaltered, though the pore fluid changes indicate a small increase in sulphur content.

Gassum Formation

The Gassum Formation (Vedsted-1 well) shows clear signs of dissolution of ankerite after 7 and 14 months of CO₂ experiment (Figures 10 and 12 in Appendix 1). Siderite rhombs are partly dissolved in both the CO₂ and the N₂ experiments (Figure 12 in Appendix 1). The siderite dissolution features in the N₂ experiments are of a peculiar character, which may be due to problems during thin section preparation. Partly dissolution of both detrital K-feldspar and plagioclase is common both prior to the experiments and after, whereas authigenic albite show no corrosion features (Figures 9 and 11 in Appendix 1). Pore fluid changes with increasing amounts of Mg, Ca, Fe and Mn in the CO₂ experiments also suggest dissolution of ankerite and siderite (Appendix 4). However, a decrease in Fe concentration during the last part of the CO₂ experiments may be caused by precipitation of iron-oxide/hydroxides, as the plug is the only sample, which has a completely reddish colour at the end of the CO₂ experiment. The oxidation of iron and of iron-oxide/hydroxide precipitation may be due to a leak in the pressure vessel during the experiment though this has not been verified.

The results from the experiments studying the Gassum Formation from the Stenlille-18 well has been de-emphasised due to the fact that these contain infiltrated drilling mud, which

complicates the comparison of alterations in the solid rock samples with pore fluid changes during the experiments. Partly dissolution of both detrital K-feldspar and plagioclase prior to and after the experiments are common (Figures 13 and 15 in Appendix 1). Siderite and calcite rhombs are common constituent in the Gassum Formation in the Stenlille-18 well (Figure 14 in Appendix 1). The increase in Fe, Mn and possibly Ca and Mg in the CO₂ experiments supports the dissolution of siderite and calcite. Euhedral pyrite occurs with etched surfaces after 7 months of experiment, whereas changes in the pyrite framboids are difficult to recognise (Figures 13 and 16 in Appendix 1). Pore fluid changes show increase in sulphur content in both CO₂ and the N₂ experiments, and is therefore assumed to originate from barite (in drilling mud) dissolution rather than pyrite corrosion.

Haldager Sand Formation

The Haldager Sand Formation contains abundant framboids of pyrite with an alteration rim both prior to experiments and after the CO₂ and the N₂ experiments (Figures 17, 18, 19 and 20 in Appendix 1). This alteration is either due to oxidation or due to partly dissolution; though an increased degree of dissolution after the CO₂ experiments cannot be verified. The dissolution of pyrite may be related to disequilibrium between mineral composition and synthetic pore fluid at the beginning of the experiments. Thus, Euhedral pyrite with internal circular cavities, possibly from dissolution of an earlier authigenic phase such as pyrrhotite, was first considered to have formed during the CO₂ experiment (Figure 18 in Appendix 1). But this phenomenon, though extremely rare, also occurs in other samples of the Haldager Sand Formation. In addition, the geochemical modelling does not support the hypothesis that pyrite dissolution should take place during the experiments. Pore fluid change during the experiments, however, suggests that a Fe and Mn containing phase is dissolved as a consequence of the exposure to CO₂. Siderite, found in several other samples of the Haldager Sand Formation, seems to be the most likely mineral, though it has not been found in the samples used for the experiments. Quartz overgrowths (Figure 17 in Appendix 1) occur with specific features (quartz mountains after Weibel et al. 2010), which is related to the authigenic growth and not a dissolution phenomenon, which it could resemble.

Børglum and Fjerritslev Formations

Evaluation of the cap-rock samples is extremely difficult as they are dominated by clay minerals where the degree of alteration cannot be verified even by the scanning electron microscope. The Fjerritslev Formation contains only small amounts of calcite, dolomite and siderite rhombs, most of which show signs of incipient dissolution (Figure 21 in Appendix 1). XRD analyses indicate higher calcite contents in both N₂ batch experiments compared to the CO₂ experiments (Appendix 3). Furthermore, the pore fluid changes indicate dissolution of calcite, due to liberation of Ca and a small degree Fe and Mn during the CO₂ experiments.

In the Børglum Formation, dolomite appears with dissolution features after the CO₂ experiments (Figures 23 and 24 in Appendix 1). The synthetic pore fluid may have been undersaturated with sulphate, as the starting pore fluid in the Børglum Formation experiments contained no sulphate, whereas the total sulphur content increased substantially during both experiment. Consequently, the dissolution of sulphur containing mineral(s) must have

taken place. Pyrite is the only sulphur containing mineral identified in the samples applied for the experiments, but its dissolution alone cannot account for the large increase in sulphur. This statement is qualified by the geochemical modelling. Gypsum and halite are quite common minerals in the core samples prior to cleaning with methanol and in case the cleaning has not been sufficient, dispersed gypsum may have been present, as shown by the XRD results (Appendix 3).

General findings from the petrographical analysis

To summarise, the carbonate minerals seem to be the minerals most exposed to changes during the experiments (Table 4.1) and carbonate dissolution seems to account for most of the changes in the pore fluids during the experiments. When various carbonate minerals are present in one sample, the relative dissolution succession is calcite prior to dolomite, and siderite prior to ankerite.

With regard the silicate minerals, it has not been possible to verify by petrographical analysis whether detrital feldspar and authigenic analcime show increased degrees of dissolution after the CO₂ experiments, but the possibility cannot be ruled out. The fragile nature of most clay minerals makes it impossible by petrographical analysis to evaluate if they have been exposed to dissolution. The most coarse-grained clay mineral is kaolinite, which shows no signs of dissolution. The possible dissolution of primary silicates and clay minerals will be further treated in Chapter 5 below.

Table 4.1. Mineralogical changes during CO₂ exposure as identified by petrographical analysis.

Formation	Changes due to CO ₂ exposure	Artefacts
Bunter Sandstone	Calcite dissolution Dolomite corrosion possible	Anhydrite dissolution
Skagerrak	Ankerite dissolution Incipient K-feldspar dissolution possible	
Gassum, Vedsted-1	Siderite dissolution Ankerite dissolution	Oxidation and precipitation of iron-oxide/hydroxides
Gassum, Stenlille-1	Siderite dissolution? Calcite dissolution?	Drilling mud reactions
Haldager Sand	None identified	Dissolution of pyrite doubtful
Fjerritslev	Calcite dissolution	
Børglum	Dolomite dissolution	Dissolution of gypsum possible

5. Geochemical modelling

Geochemical modelling has been carried out with the following three purposes:

- To provide additional information to the petrographical interpretation of the laboratory experiments
- To evaluate possible long term CO₂-mineral interactions and their possible effects on reservoir and cap-rock properties
- To consider uncertainties related to the upscaling of small scale geochemical models to larger scale geochemical models

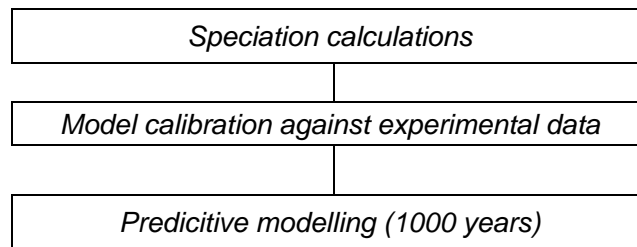
The geochemical modelling was carried out mainly by application of the geochemical modelling software PHREEQC (Parkhurst and Appelo 1999). However, for the upscaling considerations TOUGHREACT (Xu et al. 2004) was used. The advantage of using PHREEQC is that it is a widely used geochemical modelling code designed for 1D calculations as performed in the present study, while TOUGHREACT is specially designed for modelling CO₂-mineral reactions in 2- or 3D systems as is done in the upscaling exercise.

As the case is for the experimental data, some uncertainties are also related to the geochemical modelling of highly saline systems with CO₂-mineral interaction:

- Uncertainties already described for the experimental dataset – most important in relation to modelling are the uncertainties related to the difficulties with analysis of aqueous concentrations in highly saline water, since this may affect the results the geochemical model is calibrated against.
- Uncertainties related to the geochemical database and the model software used in the calculation. Recently, Dethlefsen et al. (2010) described that significantly different results may be obtained by the application of different geochemical databases to the same geochemical problem, whereas the software chosen had minor implications on the final results. In the present case, we have chosen to use the standard PHREEQC database which is normally considered valid for ionic strengths of up to ~0.7 (seawater) – and for NaCl dominated systems somewhat higher (Parkhurst and Appelo 1999). In highly saline waters such as the pore fluids used in the present study, it would be more correct to use alternative formulations of the aqueous model such as the Pitzer formalism (Pitzer 1973). However, valid data for Si and Al are not available for this formulation. Due to this fact and because the pore fluids in the present study are NaCl dominated, it was decided to use the standard PHREEQC database, since it has been important to be able to evaluate possible silicate and clay mineral dissolution and precipitation. The database used for the TOUGHREACT calculations in 2D of Xu et al. 2006 is specially designed for CO₂-mineral interactions in highly saline waters. However, this database is not practically applicable for the 1D PHREEQC calculations necessary to describe the laboratory batch experiments.
- Uncertainties related to heterogeneity of the rocks. The model assumes a homogeneous rock based on petrographical analysis of a relatively small sample volume.

Modelling protocol

The modelling protocol used is sketched below in figure 5.1



Upscaling

Figure 5.1. Modelling protocol used in the AQUA-DK geochemical modelling

Thus, first speciation calculations were carried out using the chemical analysis from the batch experiments. The speciation calculations were performed in order to determine which minerals may dissolve and precipitate in the experiments from a thermodynamic point of view. Second, the model was calibrated against the experimental data by adjusting mineral and kinetic input parameters for each batch experiment. Finally, predictions regarding possible long term effects were evaluated on the basis of forward modelling using the calibrated models for each of the relevant reservoir- and cap-rock formations. As indicated, the upscaling exercise was carried out as a separate modelling exercise not related to the laboratory experiments.

Speciation calculations

The speciation calculations were carried out using all available data from the laboratory experiments. Basically, the exercise comprises the calculation of the saturation state of various minerals that may dissolve or precipitate during the experiments. As mentioned, Si and Al concentrations were generally below the detection limit. Hence, in order to evaluate saturation state of the pore fluid with respect to silicates and clay minerals, the concentration of Si and Al was estimated. The Si concentration was estimated by assuming equilibrium with chalcedony in accordance with findings from other studies (e.g. Azaroual et al. 2004). The Al concentration was estimated assuming equilibrium with kaolinite, as kaolinite is the most abundant clay mineral in most of the rock samples investigated – the Bunter Sandstone sample being the exception though trace amounts of kaolinite is still present in this rock sample.

As shown in figure 5.2, there are large differences in the saturation indices calculated for the N₂ and CO₂ pressurised samples, respectively. Calcite and dolomite of the Gassum and Bunter samples show distinct super-saturation in the CO₂ pressurised samples, suggesting that only precipitation can take place in these samples, while in the corresponding N₂ pressurised samples, the calculated saturation indices suggest equilibrium with calcite and dolomite after 3 months of reaction.

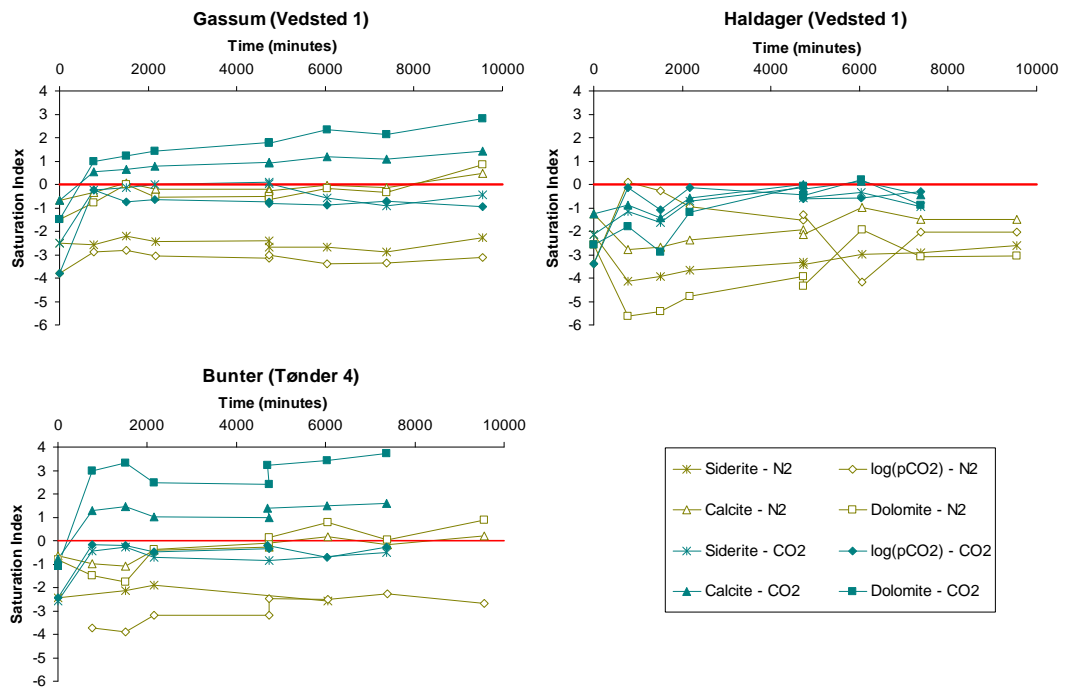


Figure 5.2. Evolution in saturation index of the porewater in the batch experiments with rock samples from the Gassum Formation (Vedsted-1 well), the Haldager Formation, and the Bunter Formation. Calculated on the basis of measured pore water chemistry, assuming chalcedony and kaolinite equilibrium (see text for further details).

The super-saturation calculated for the CO₂ pressurised samples does not correspond well with the observations from the petrographical analyses that dissolution of carbonate minerals take place in these samples. This is because the saturation indices shown in figure 5.2 are calculated on the basis of the measured fluid chemical composition at laboratory conditions, i.e. on the basis of pH measurements of depressurised and cooled samples where degassing of CO₂ has taken place. Thus, in order to try to reflect the true saturation state of the samples, the measured chemical composition of the pore water was corrected by back calculation to experimental conditions (Figure 5.3).

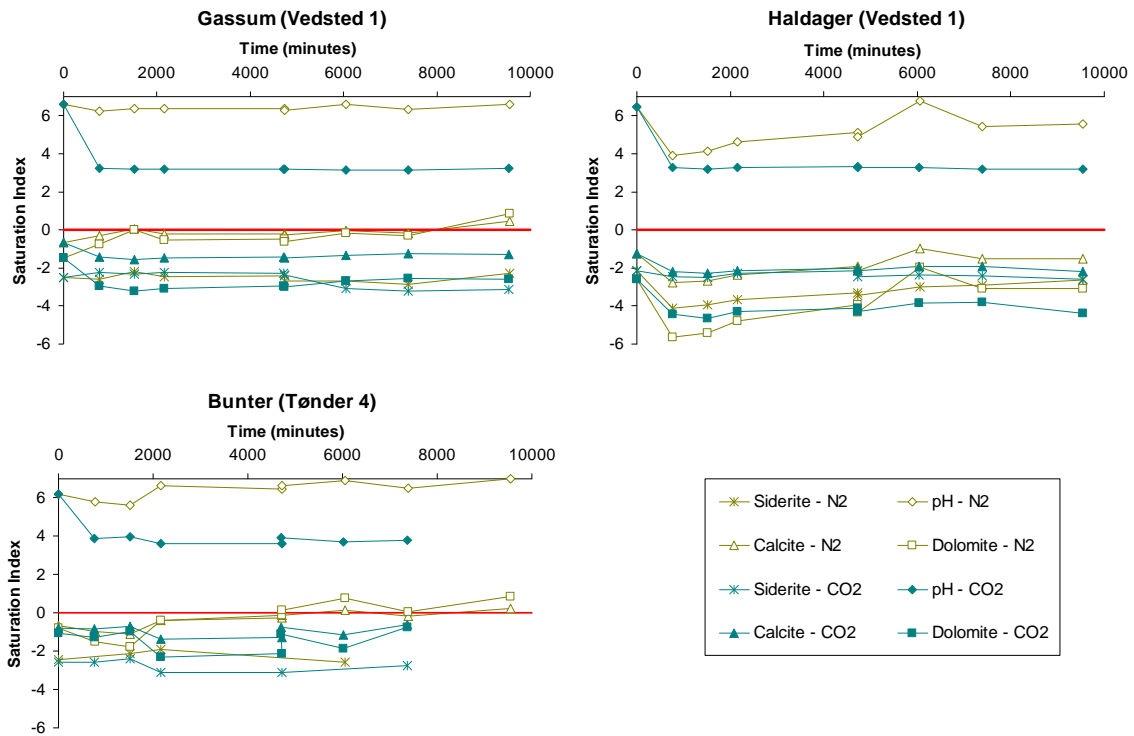


Figure 5.3. Evolution in saturation index of the pore fluid in the same batch experiments as shown in Figure 5.2. CO₂ related data are calculated on the basis of measured main porewater chemistry, assuming a CO₂ partial pressure of 9.8 MPa, and chalcedony and kaolinite equilibrium. N₂ related data are calculated on the basis of measured main porewater chemistry (See text for further details).

The back calculated dataset corresponds much better with the remaining observations of the study. E.g., the sub-saturation with respect to calcite and dolomite shown in figure 5.3 for the CO₂ pressurised samples of the Bunter Sandstone Formation corresponds well with the increased Ca concentrations and the visible dissolution of calcite in these samples.

The limitation of using the back calculation method in the present case is that equilibrium with chalcedony and kaolinite is assumed in order to be able to evaluate the saturation state with respect to silicate and clay minerals. In reality, this is probably not true as also indicated by the predictive modelling. However, for the purpose of evaluating possibilities of mineral dissolution and precipitation as an input to forward modelling, this approach seems the most reasonable considering the lack of Si and Al data.

In general, the results of the speciation calculations show that in all experiments dissolution of carbonates, primary silicates, and clay minerals is possible.

Further details regarding the speciation calculations are available in Kjøller et al. (2010).

Forward modelling of laboratory experiments

Forward modelling of the laboratory experiments was carried out in order to provide supplementary information relevant to the interpretation of the laboratory experimental results and to calibrate the models for subsequent long term predictions. Preliminary kinetic modelling showed that relative to the time step used in the models and the duration of the ex-

periments, carbonate equilibrium was approached fast. Hence, calcite equilibrium was imposed in all models (except for the Bunter Sandstone model) while in case of numerical instability of the model also ankerite and/or siderite equilibrium was imposed in some cases. All other mineral dissolution/precipitation reactions were modelled as kinetically controlled reactions. Further details are provided in Appendix 4.

The input for the forward models was:

- Chemical composition of the various pore fluids based on the chemical analysis prior to experiments
- Mineral composition of each rock sample derived from point counting of thin sections (reservoir rock samples) and Rietveld analysis of X-ray diffractograms (cap-rock samples)
- Reactive mineral specific surface areas partly based on a geometric analysis based on a combination of shape and morphology obtained from scanning electron microscope and quantified amounts obtained from thin sections; and partly on values from Cantucci et al. (2009)
- Rate constants and kinetic expressions as compiled by Palandri and Kharaka (2004)

Calibration of the models was mainly carried out by adjusting the reactive mineral specific surface area by up to an order of magnitude. Calibration by adjustment of the specific surface area is a common procedure in similar modelling studies (e.g. Cantucci et al. 2009; Wigand et al. 2008). The specific surface area adjustment was especially done for the mixed-layer illite in the model in order to create reasonable fits to the evolution in K concentration during the experiments. Furthermore, adjustment of the siderite/dolomite/ankerite contents of Fe and Mn was used to calibrate the model to provide reasonable fits to the evolution in Fe and Mn concentration during the experiments. Calibration was carried out as a trial and error process, and the final input for the formation specific models is provided in Appendix 4 together with the final model fits of the CO₂ pressurised experiments. Overall, the calibrated models provide reasonable fits to the experimental data taking into account the previously described uncertainties. It should be noted that SiO₂ mineral reactions were modelled using the equilibrium constant of chalcedony and rate constants and activation energy of quartz dissolution (Palandri and Kharaka 2004). This is in line with other modelling studies (e.g. Andre et al. 2007), and therefore SiO₂ minerals are referred to as chalcedony/quartz in the following, though chalcedony has not been identified in the petrographical analysis. Test runs applying the equilibrium constant of quartz instead did not show remarkably different results.

Following the model calibration, modelling of both N₂- and CO₂-pressurised experiments was carried out in order to check whether differences between these two experimental setups were possible to simulate. Figure 5.4 illustrates the results for the evolution in Ca and Mg concentration in the experiments using crushed Børglum Formation sample. As shown, the model simulates quite well both the overall concentration level and the more pronounced difference between N₂ and CO₂ experiments in the Mg concentration evolution as compared to the Ca evolution.

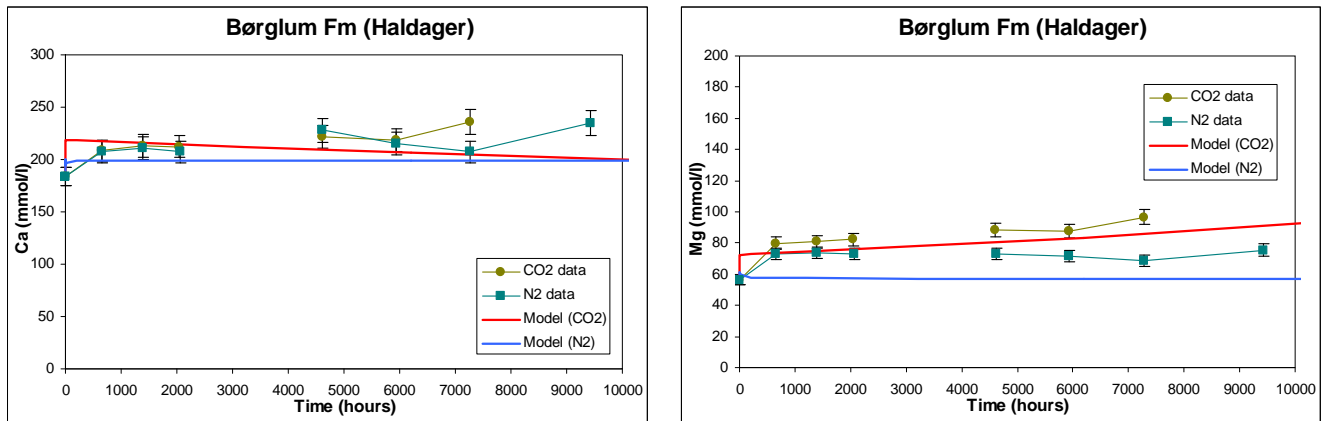


Figure 5.4. Example showing simulation results of two different models simulating the N_2 - and CO_2 -pressurised experiments with the Børglum Formation samples, respectively.

In the following, specific findings related to each geologic formation are summarised.

Bunter Sandstone Formation

With regard to the carbonate minerals present in the model, calcite dissolves fast in the initial phase of the experiment while dolomite (mM scale) precipitates during the entire experiment. This is only in fairly good agreement with the findings from the petrographical analysis, showing dissolution of calcite and possible dissolution of dolomite, but no precipitation of dolomite. The discrepancy between model and petrographical analysis with respect to the dolomite behaviour may be because the model uses kinetic parameters for precipitation that are similar to the parameters for dissolution of dolomite (Palandri and Kharaka 2004). Often, precipitation of minerals is somewhat slower than dissolution and – probably more important - requires somewhat higher activation energy. Thus, the model may overestimate the precipitation of certain minerals (such as dolomite in the present case) – at least during the period of time covered by the experiments. However, for the calibration purpose of the model, a reasonable fit is obtained for the Mg concentration, and the precipitation of small amounts of dolomite does not seem to have any adverse effect on the model results.

With regard to the silicates and clay minerals, the model suggests dissolution of mixed-layer illite/smectite and K-feldspar, and overall precipitation of K-mica (in the model similar to pure illite), albite, kaolinite, and chalcedony/quartz. Except for the dissolution of illite being in mM-scale, the amount of minerals dissolving or precipitating is 0.1 mM or below. Thus, though dissolution and precipitation takes place already in the initial phase of the experiments, the amount of mineral involved in the CO_2 - mineral reaction is rather low. Hence, the accelerated dissolution of e.g. K-feldspar and mixed layer illite/smectite has not been possible to distinguish in the petrographical analysis.

Anhydrite dissolves in agreement with the petrographical analysis while fluorite and goethite are hardly affected by the CO_2 exposure.

Skagerrak Formation

Overall dissolution of the dolomite and ankerite initially present takes place at mM scale, though ankerite precipitation is occurring in the last phase of the simulation due to slightly increasing pH caused by the dissolution of silicates and clay minerals. Calcite precipitation was allowed to occur and takes place at mM scale during the entire simulation period. As for the Bunter Sandstone model, calcite precipitation may be overestimated in the laboratory experiment model but is not considered to have any major impact on the long term predictions. Thus overall, the results correlate reasonably well with the petrographic evidence showing ankerite dissolution.

With regard to the silicates and clay minerals, the model suggests dissolution of mixed-layer illite/smectite, K-feldspar, and albite and overall precipitation of K-mica, kaolinite, and chalcedony/quartz. All mineral reactions are in mM-scale. Thus, dissolution and precipitation of these minerals take place already in the initial phase of the experiments. However, the amount of mineral involved in the CO₂- mineral reaction is rather low, which is in good agreement with the petrographical analysis where enhanced silicate dissolution was not possible to identify.

Gassum Formation

The simulation of the Gassum Formation (Vedsted-1) experiments show total dissolution of the dolomite present and initial dissolution but overall precipitation of siderite/ankerite and calcite. Compared to the petrographical analysis, the model may overestimate slightly the precipitation of the siderite/ankerite which may be due to the true mixed carbonate having different thermodynamical properties than provided in the database used. However, the model simulates quite well the evolution in the pore fluid chemical composition (cf. Appendix 4) and on the long term carbonate precipitation is believed to take place due to the slightly increasing pH caused by mixed-layer illite/smectite dissolution. K-mica, K-feldspar, albite, kaolinite and chalcedony/quartz show overall precipitation (mM to 10 mM scale) during the simulation period.

Due to the absence of dolomite in the model of the Gassum Formation (Stenlille-18) experiments, the calcite and siderite present in the model dissolve. This is in good agreement with the suggestions from the petrographical analysis. In addition, intensive dissolution of mixed-layer illite/smectite (10 mM scale) and much less pronounced dissolution of K-feldspar and albite takes place (0.01 mM scale). Finally, precipitation of kaolinite and chalcedony/quartz take place.

Haldager Sand Formation

As discussed previously in chapter 4, the modelling suggests that only very small amounts (0.01 mM scale) of pyrite are dissolved as a consequence of the CO₂ exposure. A small amount of Mn-containing siderite was included in the model in order to account for the observed increases in Mn- and Fe-concentration. This is in good agreement with the petrographical analysis. Other dissolving minerals in the model are illite, K-feldspar and albite while K-mica, kaolinite and chalcedony/quartz show overall precipitation (all minerals mentioned at the mM scale) during the simulation period.

Børglum and Fjerritslev Formations

In agreement with the suggestions of the mineralogical analysis, the model predicts that as a result of the CO₂ exposure, dissolution of calcite should take place in the experiments conducted with Fjerritslev Formation samples. Likewise, initial dissolution of dolomite is simulated in the Børglum Formation experiments though precipitation of dolomite occurs towards the end of the simulation period due to the slightly increasing pH caused by dissolution of mixed-layer illite/smectite and chlorite. In the model, the dolomite used contains traces of Fe. When dolomite starts to precipitate, the Fe concentration therefore decreases concomitantly. This is in good agreement with the evolution in the pore fluid Fe concentration (cf. Appendix 4), suggesting that dolomite precipitation in the long term is probably occurring but may not be visible in the mineralogical analysis. Likewise, the increase in sulphur content in the Børglum Formation experiments is simulated well by including traces of gypsum in the model (cf. Appendix 4).

In the models of the cap-rock formations, all other silicate and clay minerals present show overall precipitation during the simulation period.

General findings of the model calibration

In general, the findings of the model calibration support the results of the petrographical analysis. Thus, distinct initial dissolution of carbonates is observed in most models. At later time steps some carbonates may reprecipitate due to slightly increasing pH caused by dissolution of clay minerals (mixed-layer illite/smectite or illite/chlorite, and if present chlorite).

The general findings of the calibration of the geochemical models are summarised in Table 5.1 which is developed from Table 4.1.

Table 5.1. Mineralogical changes (for silicates only dissolution features are included) during CO₂ exposure as identified by petrographical/mineralogical analysis (in black) supplemented by findings from the calibration of the geochemical models (in grey).

Formation	Changes due to CO₂ exposure	Artefacts
Bunter Sandstone	Calcite dissolution Dolomite corrosion possible (Long term dolomite precipitation) Illite dissolution K-feldspar dissolution	Anhydrite dissolution
Skagerrak	Ankerite dissolution (initially) Incipient K-feldspar dissolution possible Dolomite dissolution (Long term calcite + ankerite precipitation) Illite dissolution K-feldspar dissolution	
Gassum, Vedsted-1	Siderite dissolution (initially) Ankerite dissolution Dolomite dissolution (Long term calcite + siderite precipitation) Illite dissolution	Oxidation and precipitation of iron-oxide/hydroxides
Gassum, Stenlille-1	Siderite dissolution? - Yes Calcite dissolution? – Yes Illite dissolution K-feldspar dissolution Albite dissolution	Drilling mud reactions
Haldager Sand	None identified Siderite dissolution Illite dissolution K-feldspar dissolution Albite dissolution	Dissolution of pyrite doubtful
Fjerritslev	Calcite dissolution Illite dissolution Chlorite dissolution	
Børglum	Dolomite dissolution Illite dissolution Chlorite dissolution	Dissolution of gypsum possible

Predictive modelling

For the predictive modelling, the modelling concept of modelling a representative elementary volume (REV) of an aquifer was adapted from Gaus et al. (2005) (cf. Figure 5.5).

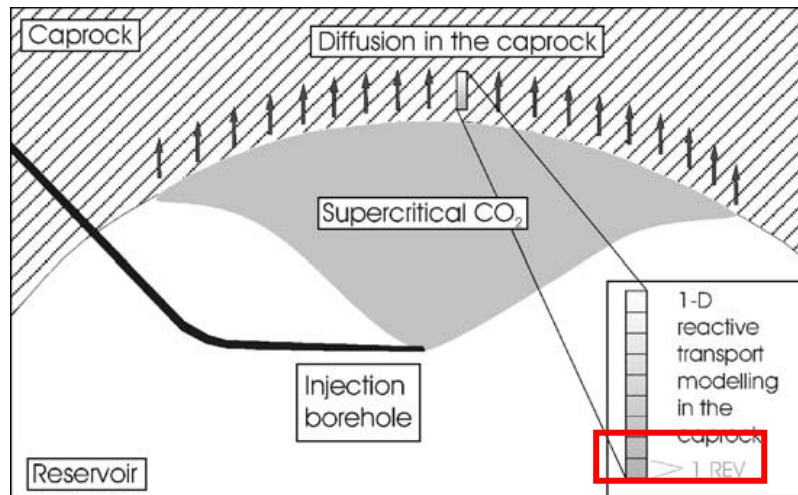


Figure 5.5. Conceptual sketch showing a representative elementary volume (REV) used for the predictive modelling. In the figure, the REV is illustrated as part of a reactive transport model of a cap-rock. In the present study a batch model is used assuming stationary transport conditions in the REV. From Gaus et al. (2005).

In practice, the model comprises a part of the simulated reservoir or cap-rock that contains 1 litre of pore fluid and a mineral assemblage similar to the assemblage used in the calibration of each laboratory experiment. The amount of minerals initially present in the REV is based on an initial porosity of 27% as estimated on the basis of CCAL data of the various reservoir rocks. With regard to the cap-rocks, the true porosity is apparently somewhat lower. However, a porosity of 27% was used for all simulations in order to be able to compare the long term effects of CO₂-mineral reactions only. All other input parameters were similar to the calibrated models of the laboratory experiments, and minerals allowed to precipitate as secondary minerals were the minerals already present in each geological formation. Additionally, calcite was allowed to precipitate in formations where this carbonate mineral is not present initially.

Conceptually, the long term models simulate the CO₂-mineral reactions at a CO₂ partial pressure of 20 MPa (fugacity of 9.8 MPa) at the interface between pore fluid and gas phase of either the reservoir or cap-rock (cf. Figure 5.6).

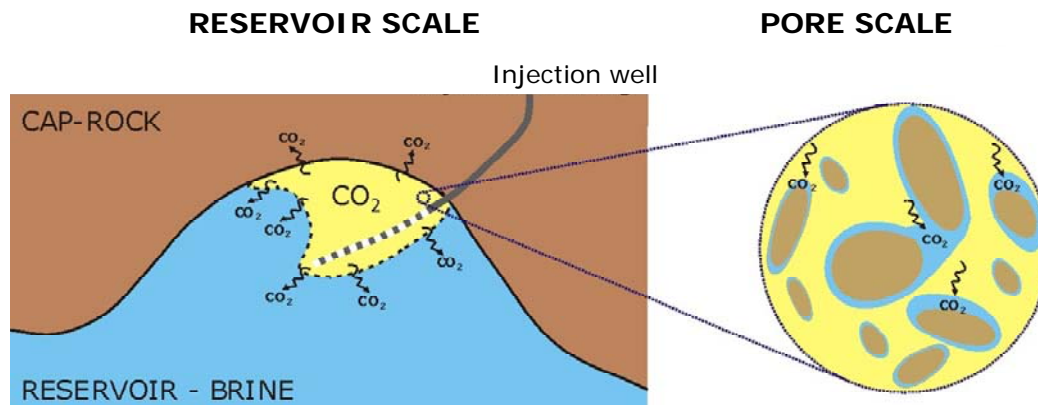


Figure 5.6. Conceptual sketch showing the part of the storage reservoir simulated by the long term batch models in the study

Selected results from the long term modelling are compiled in Appendix 5 for each geological formation. Below in table 5.2, the overall mineral reactions taking place during the 1000 years simulation period are expressed as mineral specific contributions to the porosity change.

Table 5.2. Mineral specific porosity changes as simulated by the predictive REV model with 1000 years of CO₂ exposure to each geological formation. Negative values indicate loss of porosity due to precipitation and positive values indicate increase in porosity due to dissolution.

Formation	Gassum Fm	Gassum Fm	Skagerrak Fm	Haldager Fm	Bunter Fm	Fjerritslev Fm	Børglum Fm
Well	Vedsted 1	Stenlille 18	Vedsted 1	Vedsted 1	Tønder 4	Stenlille 1	Haldager 1
Mineral contribution to por. change							
Calcite	0.000	-0.003	-0.003	-0.002	0.000	0.023	-0.004
Dolomite	-0.009	-	-0.004	-	-0.005	-0.044	0.000
Siderite	0.000	0.000	-	0.000	-	0.000	-
Ankerite	-	-	0.000	-	-	-	-
Illite/smectite	0.054	0.017	0.015	0.019	0.035	0.165	0.148
Ca-mont.	-	-	-	-	-	0.003	0.039
Kaolinite	-0.030	-0.019	0.042	0.023	0.003	-0.120	-0.139
Chlorite	-	-	-	-	-	0.019	-0.007
K-mica	-0.065	-	-0.107	-0.068	-0.110	-	-
Albite	0.087	0.004	0.049	0.005	0.086	-	0.032
K-feldspar	0.021	0.005	0.072	0.065	0.087	-0.060	-0.061
Chalc./quartz	-0.059	-0.007	-0.056	-0.033	-0.083	-0.010	-0.025

As indicated by the results in table 5.2, the 1000 years exposure of the geological formations to CO₂ in general causes overall precipitation of carbonate minerals suggesting some degree of mineral sequestration of CO₂ over time. However, with regard to the Fjerritslev and Børglum cap-rock formations, both dissolution and precipitation of carbonate minerals take place. Thus, for the Fjerritslev Formation, the calcite present dissolves and precipitation of dolomite occurs causing an overall decrease in porosity of 0.021 when only taking the carbonate minerals into account. For the Børglum Formation where calcite is not present initially, dolomite is almost unaffected and precipitation of calcite occurs on the long term. Overall, this causes a slight decrease in porosity when considering the carbonate minerals only. The difference between the results for the two cap-rock formations illustrate

the importance of carrying out site specific studies if CO₂-mineral changes over long periods are to be evaluated.

With regard to the silicates and clay minerals, the predictions for all geological formations suggest that the mixed-layer illite/smectite is totally dissolved and replaced by K-mica (or pure illite) and/or kaolinite. However, in some cases (Skagerrak, Haldager, and Bunter Formations) kaolinite is also dissolved. Overall dissolution of K-feldspar is most commonly seen, except in the models for the cap-rock formations where precipitation of K-feldspar is taking place. Finally, chalcedony/quartz precipitation is observed for all geological formations after simulating 1000 years of CO₂ exposure.

In summary, the predictive modelling suggests that large mineral changes can take place as the result of the CO₂ exposure over long periods. However, both mineral dissolution and precipitation are predicted to take place, and the overall effect on porosity seems to be negligible for the reservoir formations as illustrated in table 5.3. Table 5.3 also illustrates that the various pore fluids and mineral assemblages present gives reason to quite different amounts of overall carbon sequestration by dissolution in the fluid and precipitation of carbonate minerals. Again, this highlights the importance of carrying out site specific studies.

Table 5.3. Overall porosity changes as simulated by the predictive REV model with 1000 years of CO₂ exposure. Also shown are the calculated amounts of carbon sequestered after 1000 years for each geological formation.

Formation	Gassum Fm	Gassum Fm	Skagerrak Fm	Haldager Fm	Bunter Fm	Fjerritslev Fm	Børglum Fm
Well	Vedsted 1	Stenlille 18	Vedsted 1	Vedsted 1	Tønder 4	Stenlille 1	Haldager 1
Initial porosity (fraction)	0.27	0.27	0.27	0.27	0.27	0.27	0.27
Change in porosity	0.000	-0.003	0.008	0.009	0.014	-0.024	-0.019
CO₂ dissolved (mol/kgw)	2.162	0.905	0.980	1.436	3.388	1.524	2.185
CO₂ precipitated (mol/L)	0.467	0.273	0.463	0.162	0.217	0.165	0.357
Total CO₂ sequestered (mol/L)	2.397	1.111	1.347	1.492	3.163	1.551	2.380

Thus, though it is obvious from the modelling exercise that mineral alterations will take place on the long term in the potential Danish reservoirs for CO₂ storage – the overall effect on the porosity of the reservoirs is low – and even seems to decrease the cap-rock porosity and possibly strengthen the cap rock seal capacity.

Upscaling of heterogeneous systems in geochemical modelling

When simulating brine/mineral reactions in geochemical modelling studies involving injection of CO₂, the heavy computational burden often leads to coarsening of the numerical grid for the model in question. In addition to this, the lack of knowledge about the variability and pattern of heterogeneity in the reactive mineral distribution often leads to the assumption about a fairly homogeneous system for the modelling exercise. These simplifications could present a problem for the predictions carried out on the basis of the geochemical modelling. However, hitherto published material that deals with this subject is scarce, except for a few

studies related to pore scale modelling of geochemical reactions (Li et al., 2006; 2007a,b; 2008).

As the heterogeneous chemical modelling exercise presents the interaction of flow, diffusion, dissolution and reaction rates, it is not an easy task to engage in. Besides quoting two statements from the studies mentioned above, we present a small conceptual study of a model at deca-meter scale, indicating at least some significance of heterogeneity at that scale and at the studied time-scale of 10 years.

Quotation from Li et al. 2007:

- “This work addresses the important but difficult question of scaling mineral dissolution and precipitation reaction kinetics, which is often ignored in fields such as geochemistry, water resources, and contaminant hydrology.”
- “Although scaling of physical processes has been studied for almost three decades, very few studies have examined the scaling issues related to chemical processes, despite their importance in governing the transport and fate of contaminants in subsurface systems.”

Upscaling case study

Inspired by the layered nature of the sequence seen e.g. in the Vedsted-1 well in the lower Gassum Formation (Figure 5.7), a 2D model of 40x10 meter extent was constructed. A heterogeneous mineral distribution was assumed in order to try to reflect an all-sand sequence with varying content of carbonate cement and feldspar. The conceptual heterogeneous model is shown in Figure 5.8.

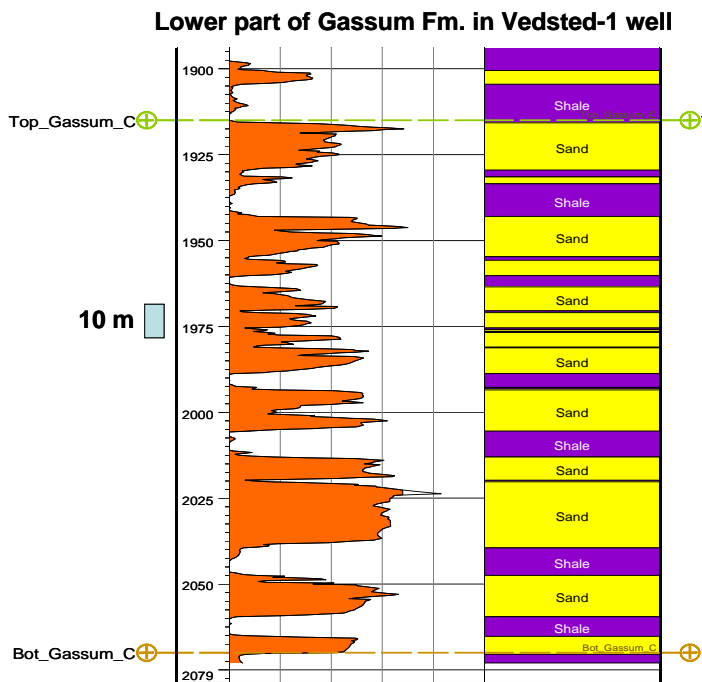


Figure 5.7. Lower part of the Gassum Formation in the Vedsted-1 well with the porosity log and a lithology index for the sandy and shaly lithologies. The variations show up at 5-10 m scale.

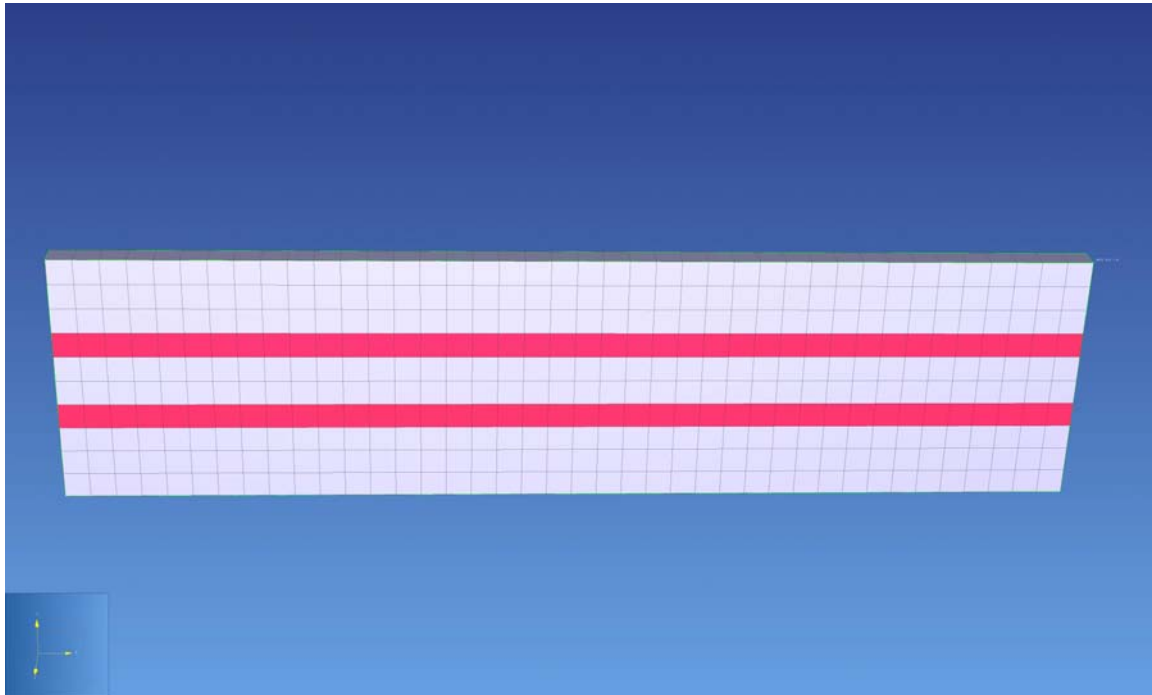


Figure 5.8. Heterogeneous model with layered mineral distribution. 40x10 m 2D vertical section. The red layers contain 5% calcite, 25% albite, and 70% quartz. The grey layer is 100% quartz.

The contrasts for the layers in the heterogeneous model are obviously extreme, but used to enhance the effects we want to illustrate for this example. The model setup is further illustrated for the averaged and homogenised version of the model in Figure 5.9.

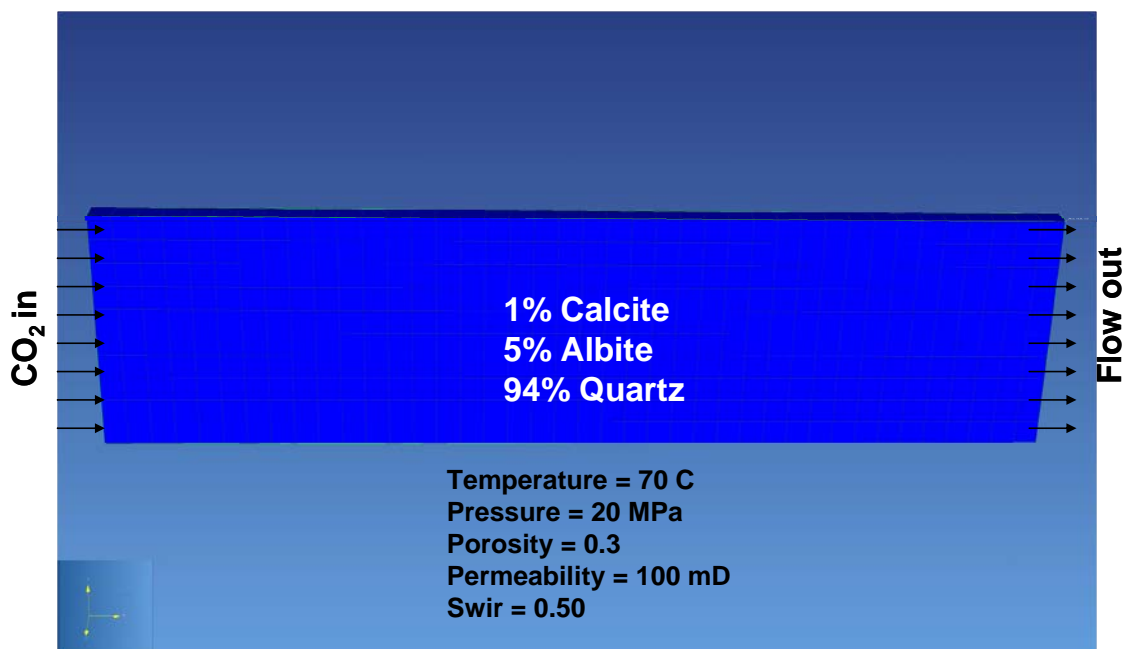


Figure 5.9. Homogeneous model with the mineral composition averaged out for the whole model. The model has the same size and flow conditions as the heterogeneous model in figure 5.8. Also is indicated the modelled injection pattern indicated.

As shown in figures 5.10 and 5.11 by the distribution of pH and the overall dissolution/precipitation of calcite, the two different geochemical distribution models with the same overall content of minerals and same physical flow set up give reason to quite different geochemical footprints in the modelled “reservoir” after only 2.5 years of CO₂ flooding of the 10x40 meter model.

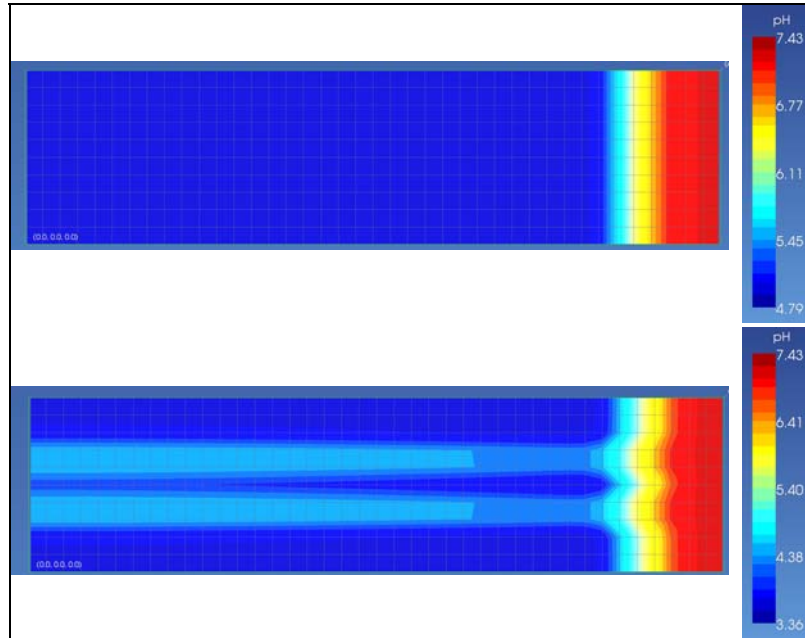


Figure 5.10. pH – after 2.5 years. Note the different endpoints for the scale for the two models.

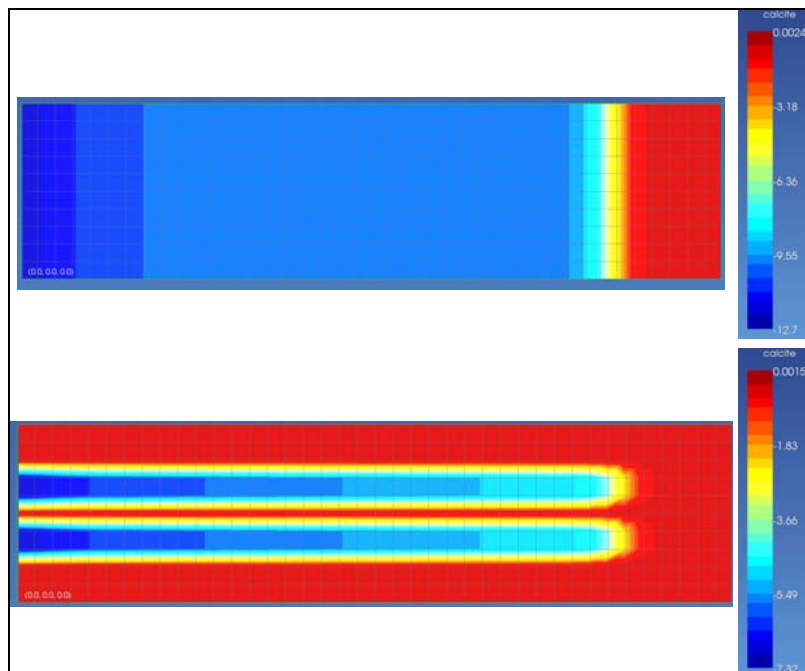


Figure 5.11. Total change in calcite (mol/m^3) – after 2.5 years. Note the different endpoints for the scale for the two models.

Further illustrating the different results of the two models, some selected reactions are plotted in figure 5.12.

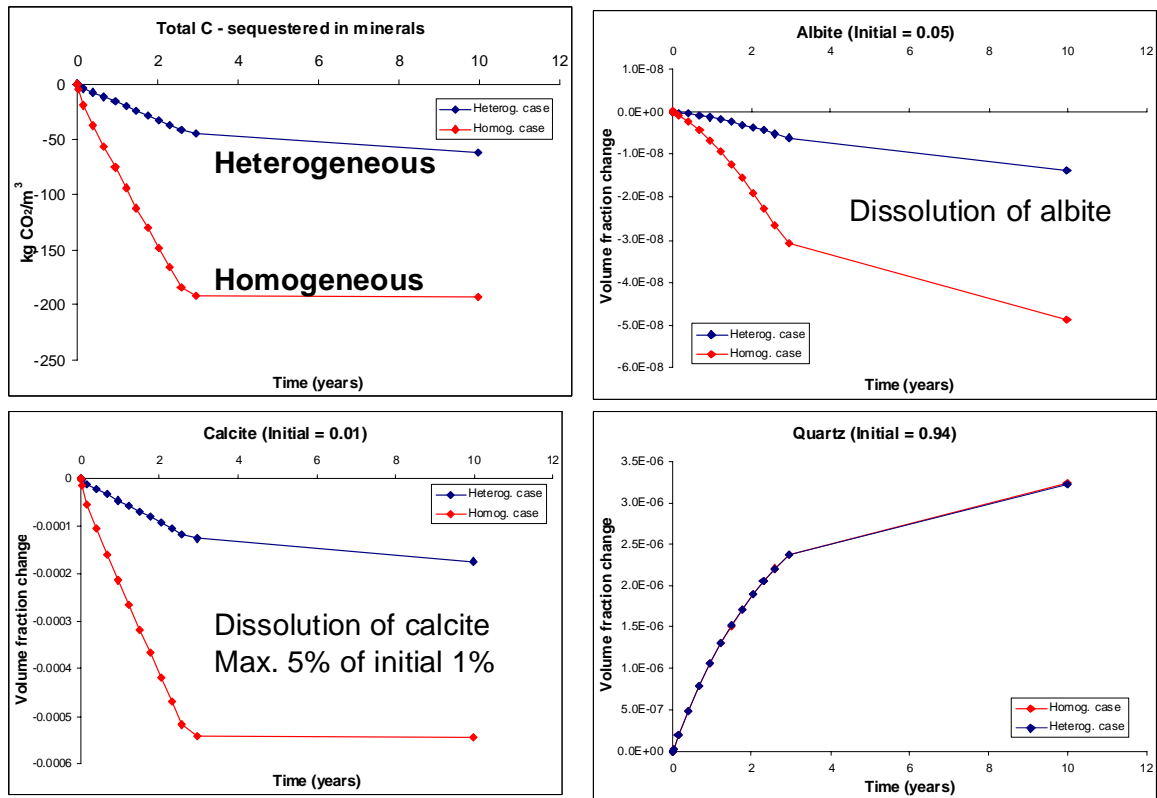


Figure 5.12. Plots of different CO₂-mineral reactions. Over the time period studied, the difference amounts to a factor 3.

Although the system complexity is reduced to 3 minerals and the time-span limited to 10 years, the difference between a heterogeneous and a homogeneous model is significant. During the short term period of 10 years CO₂ injection and/or flow of reactive water, the heterogeneity and spatial pattern influence the chemical reactions and thereby have a potential huge impact on the predictions based on the modelling, e.g. regarding the amount of CO₂ sequestered by mineral reactions. The effects over longer time spans and/or with stationary water are potential subject for further studies in the future.

6. Cap-rock sealing properties

A specific study of cap-rock sealing capacity was carried out to evaluate the quality of potential seal rocks onshore Denmark relative to CO₂ sequestration in geological traps. This was accomplished through mineralogical-petrophysical characterization of potential seals (cap-rocks) of the Børglum and Fjerritslev Formations, i.e. determination of mineralogy, grain and pore size distributions, porosity, permeability and capillary properties.

Sampling

Core material from the two formations was sampled from a number of old onshore wells (table 6.1). The sample material available is generally in a poor condition, i.e. dry, heavily fractured or rubble and drilling of cylindrical plugs for core analysis was seldom possible, except for a preserved core section from the Stenlille-2 well where a fresh plug sample was cut for a reservoir condition test of liquid permeability and threshold pressure (entry pressure) to super-critical CO₂. However, additional samples of dry core material and rubble were taken for characterization studies.

Core analysis

Samples were cleaned for salt and analysed for Helium porosity. Due to the state of the sample material (mainly rubble), very few 1" diameter plugs (from the Fjerritslev Formation wells) could be measured for gas permeability. Results fall in the range 0.015-0.06 mD, but should be treated with caution due to micro cracks often being present in cleaned and dried mudrocks containing smectite and/or mixed layer clay minerals. Mercury injection data for capillary pressure and pore size distribution was measured as well, and seal capacity data are given in table 6.1. The porosity data measured by mercury injection is somewhat lower than the Helium porosity data (not shown) due to the inability of Hg to penetrate the very small pores present in mudrocks, whereas the Helium porosity tends to overestimate the true porosity due to absorption in the clay minerals.

Table 6.1. List of onshore wells included with the cap-rock study. Porosity and seal capacity data read from mercury capillary pressure measurements are given for 10 samples from the Børglum and Fjerritslev Formations; r_{10} and r_{50} denotes the pore throat radius in nano meter where 10% and 50% respectively of the sample pore volume have been filled by injected mercury. The entry pressure in an air-brine system was estimated from the tangent to the plateau in the capillary pressure diagrams.

Well	Sample ID	Formation	MD [m]	Porosity _(Hg) [%]	Entry P _(air-brine) [bar]	Pore radius	
						r_{50} [nm]	r_{10}
Fjerritslev-1	F1-2	Børglum	477.00	20.7	40	21	31
Børglum-1	B8-2		986.03	14.9	35	16	36
Haldager-1	H100-2		1041.20	14.9	30	20	45
Gassum-1	G31-2		1189.90	13.3	75	10	18
Vedsted-1	V6-21	Fjerritslev	1403.40	11.0	60	10	38
	V6-20		1407.10	11.7	75	9	23
	V8-15		1865.40	7.1	110	5	150
	V8-13		1868.60	8.0	95	6	300
Stenlille-1	St-1		1501.33	9.4	65	9	200
Stenlille-2	St-2		1484.70	13.2	75	8	600

Each cap-rock formation has its own characteristic "Hg-fingerprint" (Figure 6.1). The Børglum Formation samples have a sharp entry at a high pressure of ~ 2000 psi in the air/mercury capillary pressure plot and a narrow, uni-modal pore throat size distribution. The Fjerritslev Formation samples are more variable but generally show a gradual entry starting below 100 psi in the air/mercury capillary pressure plot, and have a bi-modal pore throat size distribution; a stable plateau is not reached until filling of ~ 20% of the pore volume representing the largest pore throat radii. The plateau however, is significantly above the Børglum samples in the range 5000-10000 psi.

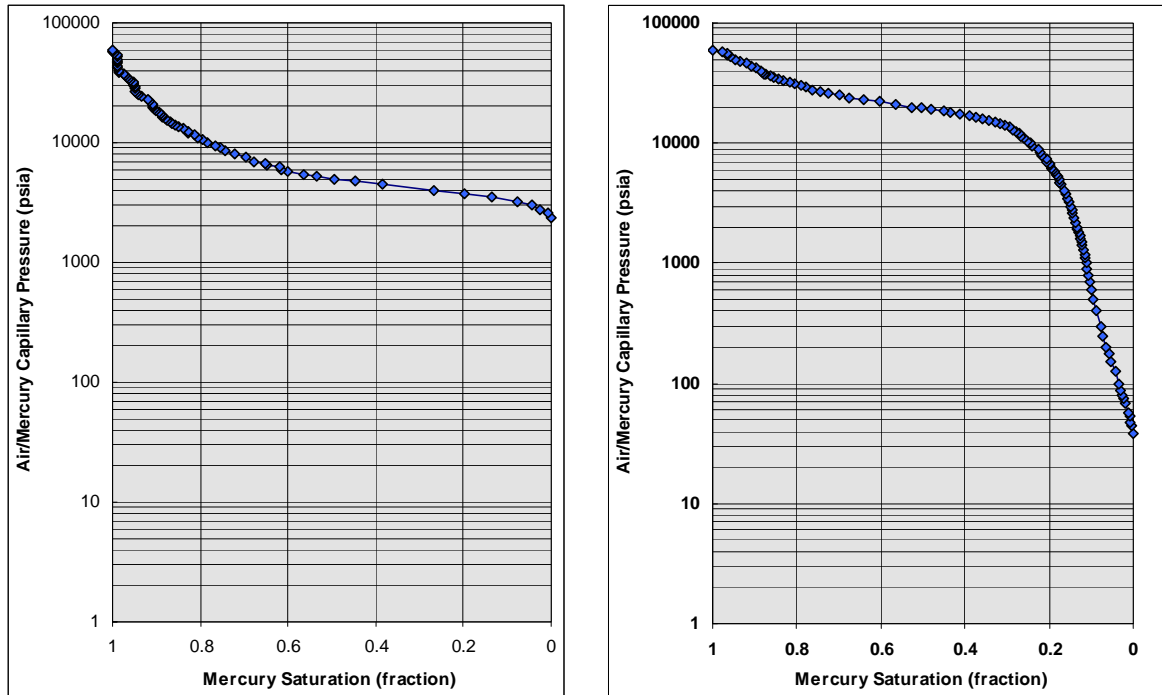


Figure 6.1. Mercury injection diagrams characteristic for the two different pore systems, the Børglum Formation mudstones (left hand side) and the Fjerritslev Formation silty mudstones (right hand side).

Air-mercury capillary pressure diagrams can be converted to any other fluid system if the interfacial tension and contact angle data are known as a function of temperature and pressure. In the cap-rock study, the mercury data was recalculated to an air-brine system at room conditions and the capillary entry pressure estimated by conventional methods (table 6.1).

In the reservoir condition test a fresh state, vertical plug sample from the Stenlille-2 well was tested for liquid permeability and entry pressure to N_2 , CO_2 and super-critical CO_2 ; results are shown below (table 6.2). The observed entry pressure in the N_2 -brine system in the range 70-80 bar is in good agreement with the 75 bar (table 6.1) estimated for an air-brine system based on mercury injection data on a plug trim from the sample used in the reservoir condition study. The observed entries for the CO_2 -brine systems is in fair agreement with estimates calculated from recent interfacial tension data for the CO_2 -brine system as a function of pressure, temperature and salinity (Chalbaud et al., 2006).

Table 6.2. Fluid and capillary pressure data for the Fjerritslev Fm cap-rock at Stenlille, measured at effective stress and reservoir conditions relative to N₂, gas and super-critical CO₂. Net effective stress in the hydrostatic test cell was 105 bar. Pore pressure in the reservoir condition test with super-critical CO₂ was set at 168 bar, entry was observed at an upstream over-pressure of 55-60 bar rel. to the pore pressure.

Sample	Depth	Porosity		Liq. permeability	Entry P _{N2}	Entry P _{CO2}	Entry P _{scCO2}
ID	[m]	room [%]	overburden	[nD]	[bar]	[bar]	[bar]
St-2/1A	1484.70	16.2	13.8	3	70-80	70-72	55-60

Mineralogy

The granulometric analysis showed that hardly any sand-size grains are present in the two formations and that they both contain between 1/3 and 2/3 silt-size grains (figures 6.2 and 6.3). In the sense of Lundegaard & Samuels (1980) they are classified as mudstones (non-laminated) or mudshales (laminated). However, there are distinct differences between the two formations. The Børglum Formation samples are slightly calcareous, contain more quartz and clay size grains - especially fine clay - than seen for the Fjerritslev Formation. This is also reflected in the specific surface area data (N₂BET) of 30-40 m²/g for the Børglum Formation samples vs 25-35 m²/g for the Fjerritslev Formation samples.

The clay mineral identification showed that the Børglum Formation is dominated by illite and kaolinite with smaller amounts of smectite, vermiculite and chlorite; in the fine clay fraction smectite and kaolinite are the dominating minerals. This is in good agreement with the petrographical analysis. In the Fjerritslev Formation more regional variation was observed. Samples from the area around Vedsted are dominated by kaolinite with illite, vermiculite, chlorite and mixed-layers as minor constituents. In samples from Stenlille wells, the dominating clay mineral is smectite, with less kaolinite and minor amounts of illite and chlorite.

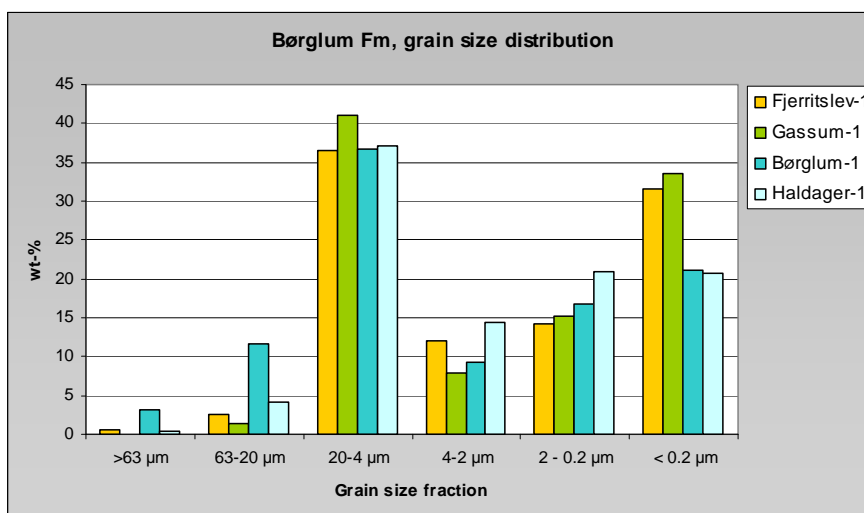


Figure 6.2. Histogram showing the grain size distribution for Børglum Formation mudstones sampled from 4 different wells. Observe the similarity among the samples contrary to the geographical distance between the wells.

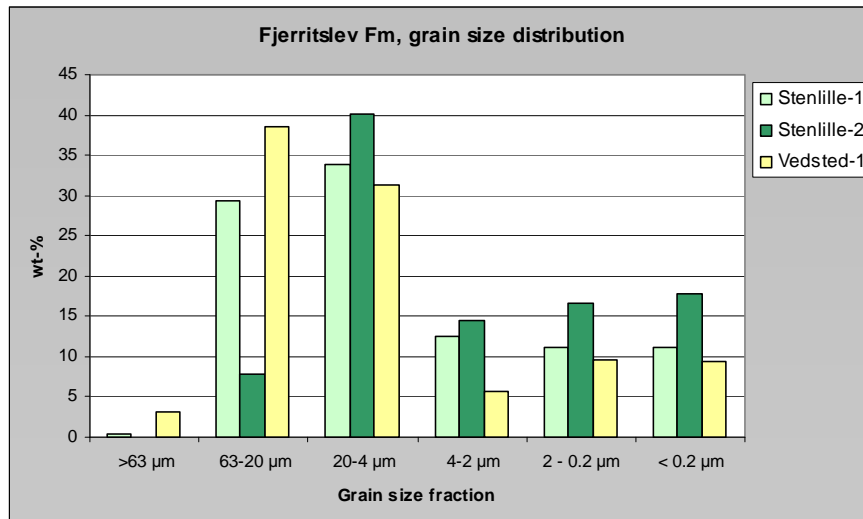


Figure 6.3. Histogram showing the grain size distribution for Fjerritslev Formation mudstones sampled from 3 different wells. Observe the greater variability among the samples, less clay size grains and more coarse silt fraction grains (compared to the Børglum Formation samples).

Conclusions

New and unexpected data from the core analysis and mineralogical characterization has demonstrated that the Børglum Formation has very good sealing properties. Based on the results from the analysis of grain size distribution and mineralogy, and the late entry in the mercury injection diagrams, the Børglum Formation should be expected to be superior to the Fjerritslev Formation as a cap-rock. That is however not the case, mainly because of.

- the porosity of the Fjerritslev Formation is significantly lower than that of the Børglum Formation, i.e. it is a tighter rock
- although an early entry is seen from the mercury injection diagrams, the majority of pore throats are very small in the Fjerritslev Formation, presumably because of a deeper burial and stronger diagenetic imprint on the Fjerritslev Formation.

A nominal seal capacity evaluation has been attempted for two different scenarios 1) the Børglum Formation case with CO₂ storage in 1000 m depth, and 2) the Fjerritslev Formation case (Vedsted, Stenlille) with CO₂ storage in 1500 m depth (table 6.3). Reservoir parameters have been taken from the present study and recent data from the literature on interfacial tension (IFT) and density (ρ) of supercritical CO₂. Allowing for some variation in entry pore throat radius, the results demonstrate that both cap-rock formations will hold a CO₂ column of several hundred meters height, i.e. they have excellent sealing properties. The findings of the reservoir condition test performed on the Stenlille cap-rock can be compared with scenario 2) in the table below if it is assumed that the “effective pore throat radius r ” is approx. 10 nm (nano meter).

Table 6.3. Evaluation of the seal capacity for a hypothetical storage site below a Børglum Formation cap-rock (1000 m depth) and below a Fjerritslev Formation caprock (1500 m depth). Observe that a doubling of the pore throat radius 'r' will halve the height 'H_{max}' of a potential column of supercritical CO₂ that can be safely stored below the cap-rock. It is assumed that the fluid-rock system is waterwet *.

Depth	Pore P	ρ_w (brine)	ρ_{nw} (CO ₂)	IFT	'r' (radius)	P _{ce} (entry P)	H _{max} *
[m]	[MPa]	[kg/m ³]	[kg/m ³]	[mN/m]	[nm]	[MPa]	[m]
1000	10	1085	713	33	10	6.6	1809
					20	3.3	904
1500	17.2	1106	744	30	5	12	3379
					10	6	1690

7. Overall evaluation of reservoir and cap-rock response to CO₂ storage

In brief, the overall conclusions of the project are:

- Potential sandstone reservoirs for CO₂ storage are present on-shore Denmark.
- The extend of the reservoirs and location of potential cap-rocks seem to qualify that geological CO₂ storage is a possibility for reducing CO₂ emmissions in Denmark.
- Though mineral-CO₂ reactions may be expected to occur as a result of CO₂ storage in potential Danish reservoirs, they seem not to prevent that geological CO₂ storage can be carried out.
- Modelling predictions conclude that only minor changes in overall porosity of the reservoir- and cap-rocks will take place as a result of the CO₂-mineral interactions. As regard the cap-rocks, the CO₂-mineral interactions seem to decrease porosity thereby potentially improving the sealing capacity.
- Upscaling to site specific geochemical models should be carried out with care in order to reflect the true geochemical conditions as close as possible.
- The CO₂ sealing capacity quality of the investigated cap-rocks is excellent.

8. References

- API, 1998: API RP 40, Recommended Practice for Core Analysis, second edition, American Petroleum Institute, Washington DC.
- André, L., Audigane, P., Azaroual, M., and Menjot, A., 2007. Numerical modelling of fluid-rock chemical interactions at the supercritical CO₂-liquid interface during CO₂ injection into a carbonate reservoir, the Dogger aquifer (Paris Basin, France). *Energy conversion and management*, 48, 1782-1797.
- Azaroual, M., Durst, P., Czernichowski-Lauriol, I., Olsen, D., Springer, N., Rochelle, C.A., Pearce, K., Bateman, K. & Bircall, D., 2004. Geochemical reactions resulting from CO₂ injection into the Midale formation, Weyburn oilfield; a laboratory experimental and modelling study. *Greenhouse Gas Control Technologies (GHGT7) Conference*, Vancouver, Canada, September 2004, 5 pp.
- Bateman, K. and Purser, G., 2010. Geological storage of CO₂ in the Danish Underground: Evaluation of the Response of the Reservoir and Cap Rocks to CO₂. *British Geological Survey External Report*, CR/10/153. 27 pp.
- Bertelsen, F. 1980: Lithostratigraphy and depositional history of the Danish Triassic. *Danm. Geol. Unders., Ser. B 4*, 59 pp.
- Brunauer S., Emmett P. H. and Teller E. 1938: Adsorption of gases in multi molecular layers. *Journal of American chemical Society* 60, 309-319.
- Cantucci, B, Montegrossi, G., Vaselli, O., Tassi, F., Quattrochi, F., and Perkins, E.H., 2009. Geochemical modelling of CO₂ storage in deep reservoirs: The Weyburn Project (Canada) case study, *Chemical Geology*, 265, 181-197.
- Chalbaud, C., Robin, M. and Egermann, P. 2006: Interfacial tension data and correlations of brine/CO₂ systems under reservoir conditions. Paper SPE 102918 presented at the 2006 SPE Annual Technical Conference and Exhibition held in San Antonio, TX, 24–27 September 2006.
- Dethlefsen, F., Haase, C., Ebert, M., Dahmke, A., 2010. Effects of the variances of input parameters on water-mineral interactions during CO₂ sequestration modelling. *Energy Procedia*, 00, 000-000, In press.
- Dinesen, B. 1961: Salt mineralvand fra Danmarks dybere undergrund. *Danmarks Geologiske Undersøgelse, Serie 4 bd. 4, nr.6*.
- Fine, S. 1986: The diagenesis of the Lower Triassic Bunter Sandstone Formation, Onshore Denmark: *Geological Survey of Denmark*, A 15.
- Friis, H. 1987: Diagenesis of the Gassum Formation Rhaetian-Lower Jurassic, Danish Subbasin. *Geological Survey of Denmark A 18*, 41pp.
- Gaus, I., Azaroual, M., and Czernichowski-Lauriol, I., 2005. Reactive transport modelling of the impact of CO₂ injection on the clayey caprock at Sleipner (NorthSea), *Chemical Geology*, 217, 319-337.
- Holloway, S., Chadwick, A., Lindeberg, E., Czernichowski-Lauriol, I., Arts R., 2002. Best practice manual from SACS- Saline aquifer CO₂ storage project. Appendix A Statoil Research Center, Trondheim, Norway.
- Kjøller, C., Weibel, R., Bateman, K., Laier, T., Nielsen, L.H., Frykman, P. & Springer, N., 2010. Geochemical impacts of CO₂ storage in saline aquifers with various mineralogy – results from laboratory experiments and reactive geochemical modelling. *Energy Procedia*, In press.

- Laier T., 2008. Chemistry of Danish saline formation waters relevant for core fluid experiments- Fluid chemistry data for lab experiments related to CO2 storage on deep aquifers. GEUS report 2008/48.
- Li, L., C. I. Steefel, and L. Yang. 2008. Scale dependence of mineral dissolution kinetics within single pores and fractures." *Geochimica Et Cosmochimica Acta* , 72: 360-377, doi:10.1016/j.gca.2007.10.027.
- Li, L., C. A. Peters, and M. A. Celia. 2007. Applicability of averaged concentrations in determining reaction rates in heterogeneous porous media. *American Journal of Science* . 307: 1146-1166, doi: 10.2475/10.2007.02.
- Li, L., C. A. Peters, and M. A. Celia. 2007. Effects of mineral spatial distributions on reaction rates in porous media. *Water Resources Research*, 43, W01419, doi:10.1029/2005WR004848.
- Li, L., C. A. Peters, and M. A. Celia. 2007. Reply to 'Comments on upscaling geochemical reaction rates using pore-scale network modeling' by Peter C. Lichtner and Qinjun Kang. *Advances in Water Resources* 30: 691-695.
- Li, L., C. A. Peters, and M. A. Celia. 2006. Upscaling geochemical reaction rates using pore-scale network modeling. *Advances in Water Resources* 29: 1351--1370.
- Lundegard, P.D. and Samuels, N.O. 1980: Field classification of fine-grained sedimentary rocks. *J. Sedimentary Petrol.*, **50**, 781-786.
- McBride, E.F., 1963: A classification of common sandstones. *Journal of Sedimentary Petrology* **33**, 664-669.
- Michelsen, O. & Nielsen, L.H., 1991: Well records on the Phanerozoic stratigraphy in the Fennoscandian Border Zone, Denmark. Hans-1, Sæby-1, and Terne-1 wells. *Danm. geol. Unders.*, Ser. A 29, 39 pp.
- Michelsen, O. & Nielsen, L.H., 1993: Structural development of the Fennoscandian Border Zone, offshore Denmark. *Marine and Petroleum Geology* Vol 10 p 124-134.
- Michelsen, O. & Clausen, O.R. 2002. Detailed stratigraphic subdivision and regional correlation of the southern Danish Triassic succession. *Marine and Petroleum Geology* 19, 563-587.
- Michelsen, O., Nielsen, L.H., Johannessen, P., Andsbjerg, J. & Surlyk 2003: Jurassic lithostratigraphy and stratigraphic development onshore and offshore Denmark. In: Ineson, J. R. & Surlyk, F. (eds): *The Jurassic of Denmark and Greenland*. Geological Survey of Denmark and Greenland Bulletin 1, 147–216.
- Nielsen, L.H. 2003: Late Triassic – Jurassic development of the Danish Basin and Fennoscandian Border Zone, Southern Scandinavia. In: Ineson, J. R. & Surlyk, F. (eds): *The Jurassic of Denmark and Greenland*. Geological Survey of Denmark and Greenland Bulletin 1, 459–526.
- Nielsen, B.L. & Friis, H. 1985: Diagenesis of Middle Jurassic Haldager Sand Formation sandstone in the Danish Subbasin, north Jutland. *Bulletin of Geological Society of Denmark* 33, 273-285.
- Nielsen, L.H. & Japsen, P., 1991: Deep wells in Denmark 1935-1990. Lithostratigraphic subdivision. *Danm. geol. Unders.*, Ser. A 31, 179 pp.
- Palandri, J.L., and Kharaka, Y.K., 2004, A compilation of rate parameters of water-mineral interaction kinetics for application to geochemical modeling: U.S. Geological Survey Water-Resources Investigations Report 04-1068

- Parkhurst, D.L. and Appelo, C.A.J., 1999, User's Guide to PHREEQC (Version 2) – A Computer Program for Speciation, Reaction-Path, 1D-Transport, and Inverse Geochemical Calculations, U.S. Geol. Surv., Water Resour. Inv. Rep., 99-4259.
- Pitzer, K.S., 1973. Thermodynamics of electrolytes: I. Theoretical basis and general equations. *J. Phys. Chem.*, **77**, 268–277.
- Weibel, R. 1998: Diagenesis in oxidising and locally reducing conditions – an example from the Triassic Skagerrak Formation, Denmark. *Sedimentary Geology* **121**, 259–276.
- Weibel, R. 1999: Effects of burial on the clay assemblages in the Triassic Skagerrak Formation, Denmark. *Clay Minerals* **34**, 619–635.
- Weibel, R. & Groberty, B. 1999: Pseudomorphous transformation of goethite needles into hematite in sediments of the Triassic Skagerrak Formation, Denmark. *Clay Minerals* **34**, 657–661.
- Weibel, R. & Friis, H. 2004: Opaque minerals as keys for distinguishing oxidising and reducing diagenetic conditions in the Lower Triassic Bunter Sandstone, North German Basin. *Sedimentary Geology* **169**, 129–149.
- Weibel, & Friis, H. 2007: Alteration of opaque heavy minerals as reflection of geochemical conditions in depositional and diagenetic environments. In: Mange, M. A. and Wright, D. T. (eds.) *Heavy minerals in use. Developments in Sedimentology*, Elsevier **58**, 305–333.
- Weibel, R., Olivarius, M., Nielsen, L.H., Abbramovitz, T., and Kjøller, C., 2010. Petrography and diagenesis of the Triassic and Jurassic sandstones, eastern part of the Norwegian-Danish Basin. Contributions to the EFP-project AQUA-DK. GEUS Report 2010/114.
- Wigand, M., Carey, J.W., Schütta, H., Spangenberg, E., and Erzingera, J., 2008. Geochemical effects of CO₂ sequestration in sandstones under simulated insitu conditions of deep saline aquifers. *Applied Geochemistry*, **23**. 2735-2745.
- Xu, T., Sonnenthal, E.L., Spycher, N., Pruess, K., 2004. TOUGH-REACT: a simulation program for non-isothermal multiphase reactive geochemical transport in variably saturated geologic media. *Comput. Geosci.*, **32**, 145–165. doi:10.1016/j.cageo.2005.06.014.

Appendix 1.

Petrographic evaluation

Bunter Sandstone Formation in the Tønder-4 well

Experiment	Prior		CO ₂ (7 mths)	N ₂ (7 mths)	CO ₂ (14 mths)	N ₂ (14 mths)
Method	Thin section	SEM / BSC	SEM / BSC	SEM / BSC	SEM / BSC	SEM / BSC
Depth (m)	1663.27		1663.27	1663.19	1663.24	1663.31
Samples ID	TØ4-Bu166327		1307C	1308N	1297C	1298N
DETRITAL						
Quartz	29.8					
K-feldspar	16.8					
Plagioclase	6.6	Partly dissolution occurs	Partly dissolution occurs			
Mica	5.4					
Intraclasts + allogenic clays	6.2		Dissolution of intraclasts may have occurred			
Sedi. Rock fragments	6.4					
Metamorphic rock fragm.	0.0					
Volcanic rock fragments	0.2					
Plutonic rock fragm.	4.4					
Transparent heavy min.	0.8					
Opaque	3.4					
AUTHIGENIC PHASES						
Quartz	0.0					
Feldspar	0.0	K-feldspar overgrowth show no signs of dissolution	K-feldspar overgrowth show weak signs of dissolution			
Calcite	1.2		Weak dissolution is possible		Clear dissolution	
Dolomite	0.0				Possible weak dissolution	
Siderite	0.0					
Anhydrite	1.4				Clear dissolution	Clear dissolution
Fluorite	2.2					
Barite	0.0					
Analcime	2.2	Clearly internal dissolution voids	Possibly enlarged internal dissolution voids		Enlarged internal dissolution voids cannot be verified	
Red coatings	9.0					
Pyrite	0.0					
Anatase	0.0					
Infiltration clay	0.0					
Smectite	0.0					
Illitic and chloritic clays	3.6					
Kaolin	0.4					
TOTAL	100.0					
		Halite is common	Hallite is common		Hallite is common	Hallite is common

Illustration of the observed changes on Figs 1, 2, 3 and 4.

Bunter Sandstone Formation in the Tønder-4 well

Prior to experiment

CO₂ experiment (7 months)

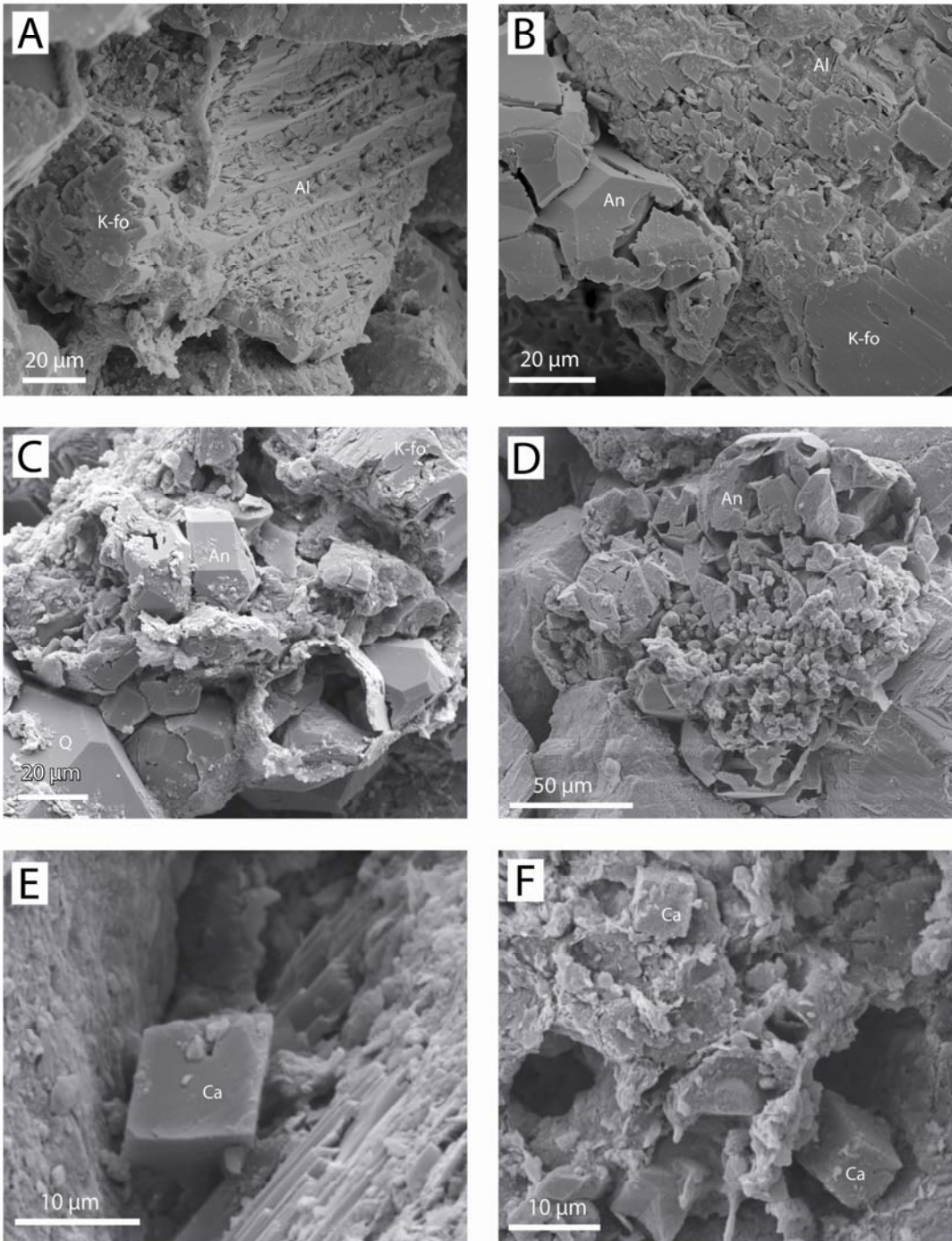


Fig. 1. Bunter Sandstone Formation in the Tønder-4 well, depth 1663.27m, SEM images. A. K-feldspar overgrowth (K-fo) on partly dissolved albite (Al), prior to experiment. B. K-feldspar overgrowth (K-fo) on partly dissolved albite (Al) with no signs of dissolution after CO₂ experiment (7 months). C. Analcime crystals with internal dissolution voids, covered by halite, prior to experiment. D. Analcime crystals with enlarged? dissolution voids, after CO₂ experiment (7 months). E. Calcite rhomb, prior to experiment. F. Calcite rhombs with weak signs of dissolution, after CO₂ experiment (7 months).

Bunter Sandstone Formation in the Tønder-4 well

Prior to experiment

CO₂ experiment (7 months)

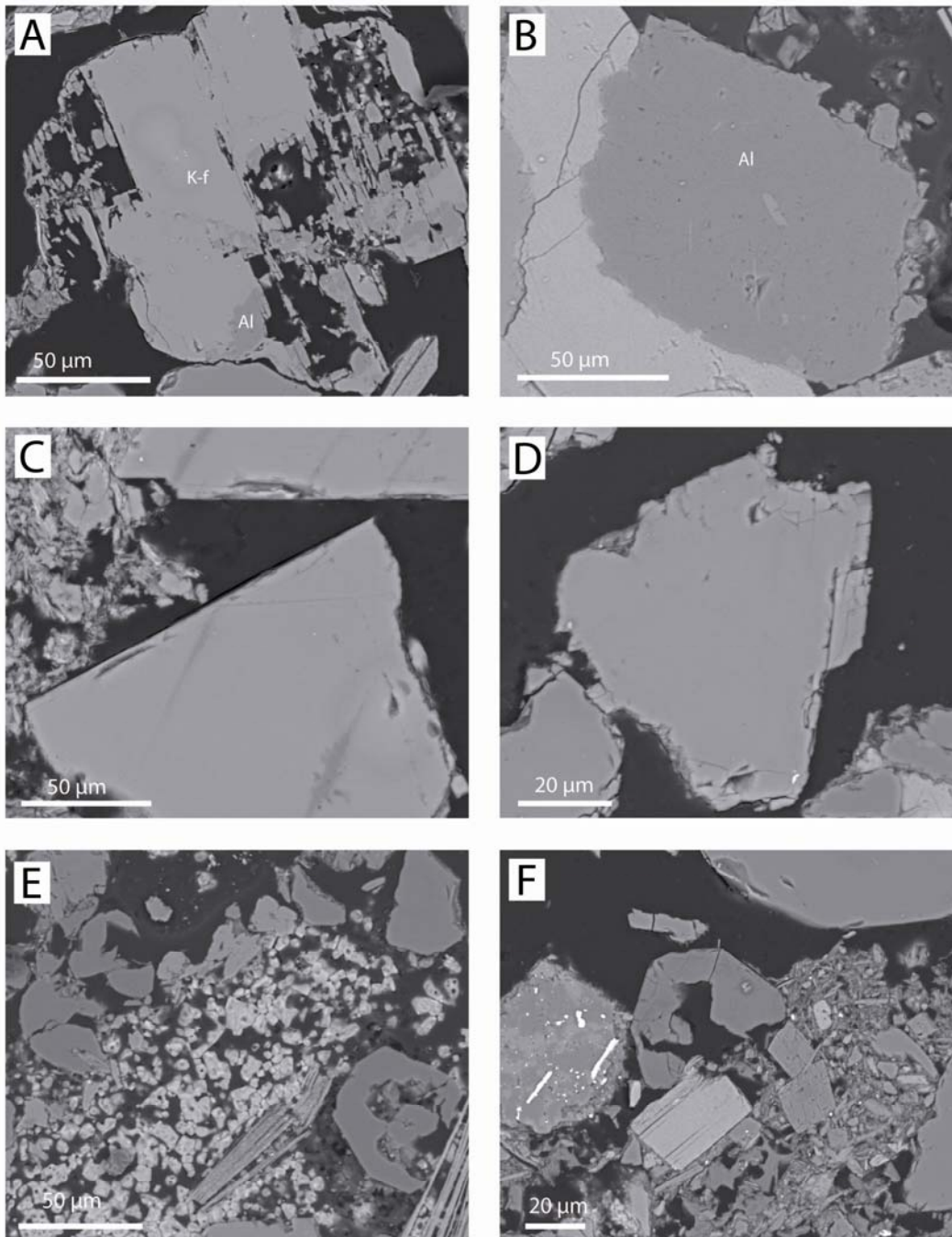


Fig. 2. Bunter Sandstone Formation in the Tønder-4 well, depth 1663.27m, BSC images. A. K-feldspar with albite intergrowth, which are partly dissolved, prior to experiment. B. Albite with no signs of dissolution after CO₂ experiment (7 months). C. K-feldspar overgrowths with no signs of dissolution, prior to experiment. D. K-feldspar overgrowths with weak signs of dissolution, after CO₂ experiment (7 months). E. Analcime with internal dissolution voids, prior to experiment. Note abundant halite cement. F. Analcime with possibly enlarged internal dissolution voids, after CO₂ experiment (7 months).

Bunter Sandstone Formation in the Tønder-4 well

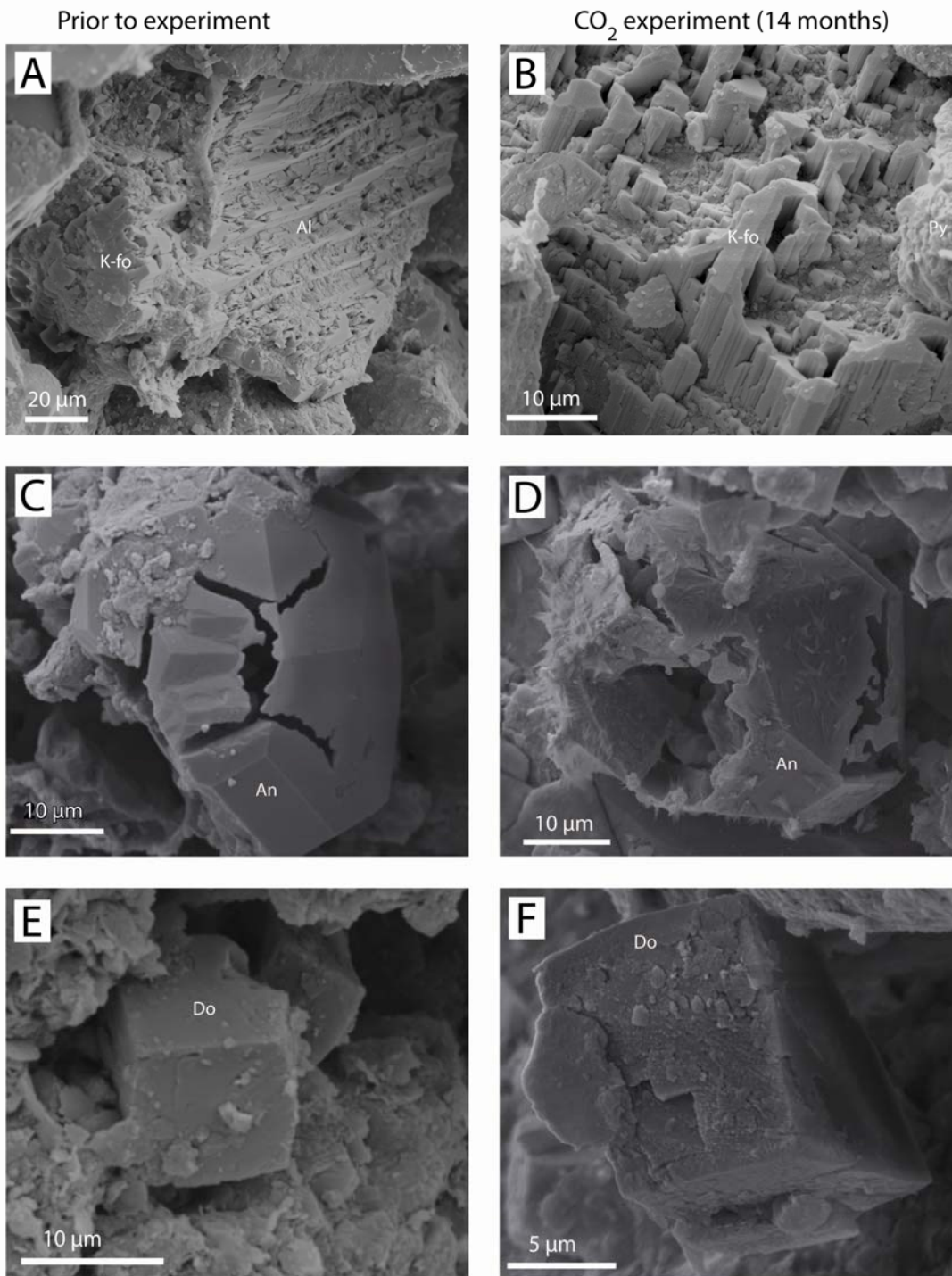


Fig. 3. Bunter Sandstone Formation in the Tønder-4 well, depth 1663.27m, SEM images. A. K-feldspar overgrowth (K-fo) on partly dissolved albite (Al), after N₂ experiment (14 months). B. K-feldspar overgrowth (K-fo) with no signs of dissolution after CO₂ experiment (14 months). C. Analcime crystals with internal dissolution voids, after N₂ experiment (14 months). D. Analcime crystals with enlarged? dissolution voids, after CO₂ experiment (14 months). E. Dolomite rhomb, after N₂ experiment (14 months). F. Dolomite rhomb with signs of corrosion, after CO₂ experiment (14 months).

Bunter Sandstone Formation in the Tønder-4 well

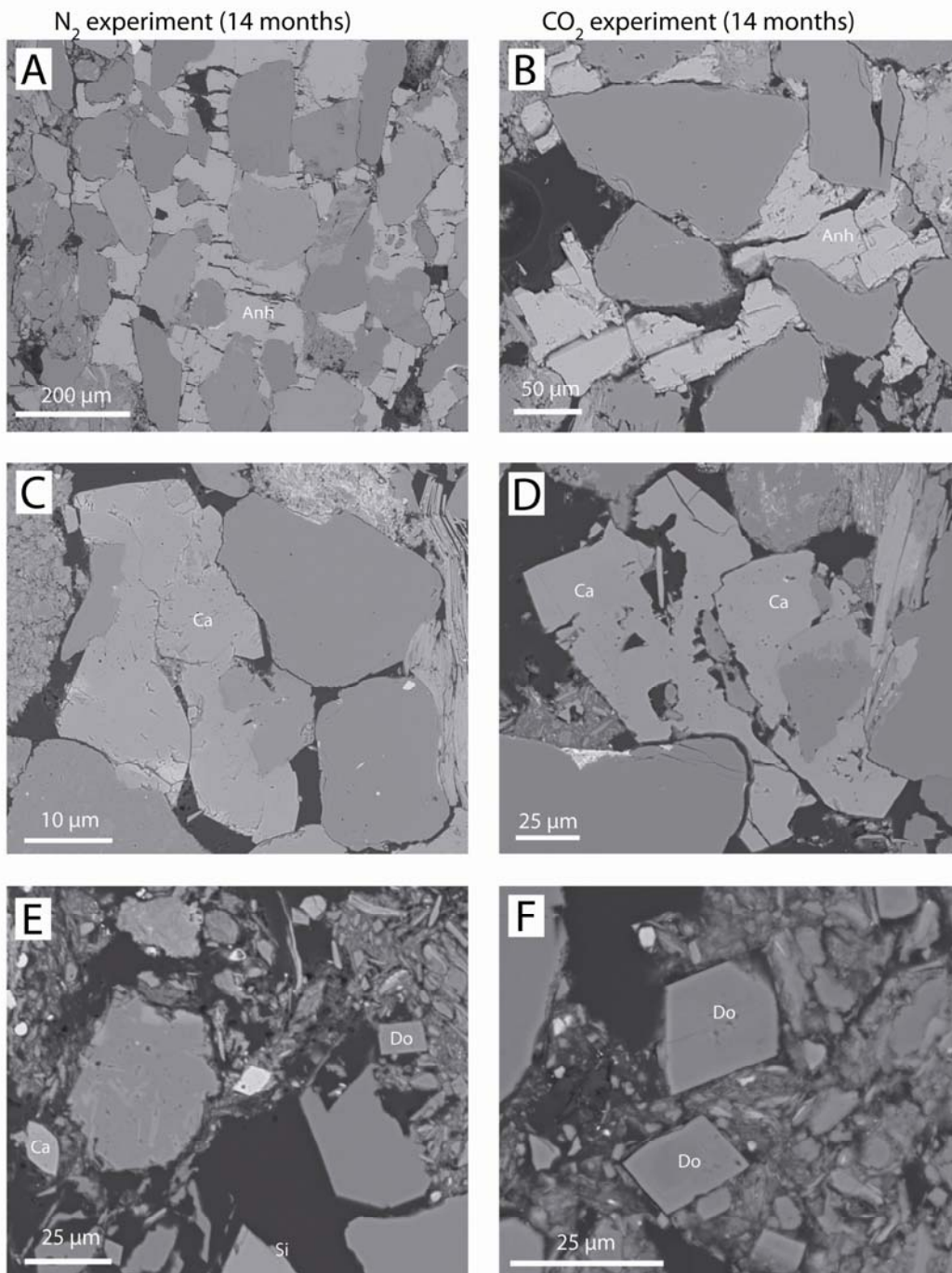


Fig. 4. Bunter Sandstone Formation in the Tønder-4 well, depth 1663.27m, BSC images. A. Pore-filling anhydrite with dissolution along crystallographic weakness zones, after N₂ experiment (14 months). B. Pore-filling anhydrite with dissolution along crystallographic weakness zones, after CO₂ experiment (14 months). C. Calcite cement with no signs of dissolution, after N₂ experiment (14 months). D. Calcite cement with clear sign of dissolution, after CO₂ experiment (14 months). E. Dolomite with no sign of dissolution, after N₂ experiment (14 months). F. Dolomite with no clear sign of dissolution, after CO₂ experiment (14 months).

Skagerrak Formation in the Vedsted-1 well

Experiment	Prior	Prior	CO ₂ (7 mths)	N ₂ (7 mths)	CO ₂ (14 mths)	N ₂ (14 mths)
Method	Thin section	SEM / BSC	SEM / BSC	SEM / BSC	SEM / BSC	SEM / BSC
Depth (m)	2064.87		2064.98	2064.87	2065.00	2064.94
Sample ID	VE1-Sk206487		1311C	1312N	1299C	1300N
DETRITAL						
Quartz	67.2					
K-feldspar	8.4				Intense dissolution	Intense dissolution
Plagioclase	5.6	Intensive dissolution is common	Intensive dissolution is common	Intensive dissolution is common	Intensive dissolution is common	Intensive dissolution is common
Mica	0.4					
Intraclasts + allogenic clays	0					
Sedi. Rock fragments	0.4					
Metamorphic rock fragm.	0					
Volcanic rock fragments	0.2					
Plutonic rock fragm.	0.8					
Transparent heavy min.	0					
Opaque	0.2					
AUTHIGENIC PHASES						
Quartz	5.2					
Feldspar	0		Albite shows no signs of dissolution		Albite shows no signs of dissolution	Albite shows no signs of dissolution
Calcite	0					
Dolomite / ankerite	3.2		Ankerite shows dissolution along crystal faces		Ankerite shows clear dissolution	
Siderite	0					
Anhydrite	0					
Fluorite	0					
Barite	0.6					
Analcime	0					
Red coatings	0					
Pyrite	0		Possibly partly dissolution?			
Anatase	0					
Infiltration clay	0					
Smectite	0					
Illitic and chloritic clays	1.8					
Kaolin	6					
TOTAL	100					
			Halite and a calciumchloride salt occur commonly	Halite and a calciumchloride salt occur commonly		

Illustration of the alterations are shown in Figs 5, 6, 7 and 8.

Skagerrak Formation in the Vedsted-1 well

Prior to experiment / N₂ experiment

CO₂ experiment (7 months)

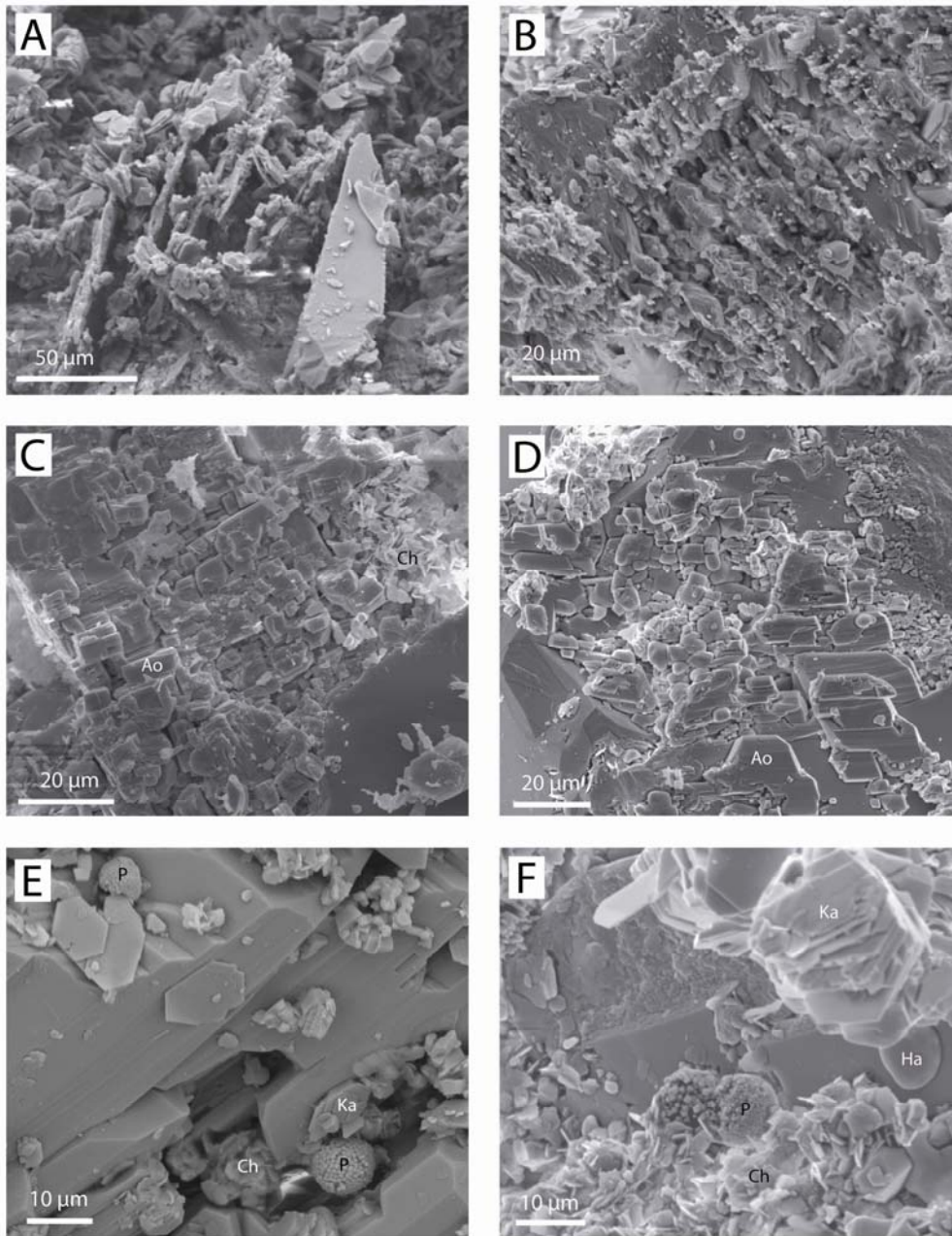


Fig. 5. Skagerrak Formation in the Vedsted-1 well, depth 2064.87m, SEM images. A. Albite lamellae are the only remnants after intensive dissolution of Ca-rich plagioclase, after N₂ experiment (7 months). B. Albite lamellae are the only remnants after Intensive dissolution of Ca-rich plagioclase, after CO₂ experiment (7 months). C. Partly dissolved plagioclase covered by authigenic albite (Ao), prior to experiment. D. Partly dissolved plagioclase covered by unaffected authigenic albite (Ao), after CO₂ experiment (7 months). E. Framboids of pyrite (Py) next to kaolinite (Ka) and chlorite (Ch), after N₂ experiment (7 months). F. Possibly partly dissolved framboids of pyrite (Py) next to kaolinite (Ka), chlorite (Ch) and halite (Ha), after CO₂ experiment (7 months).

Skagerrak Formation in the Vedsted-1 well

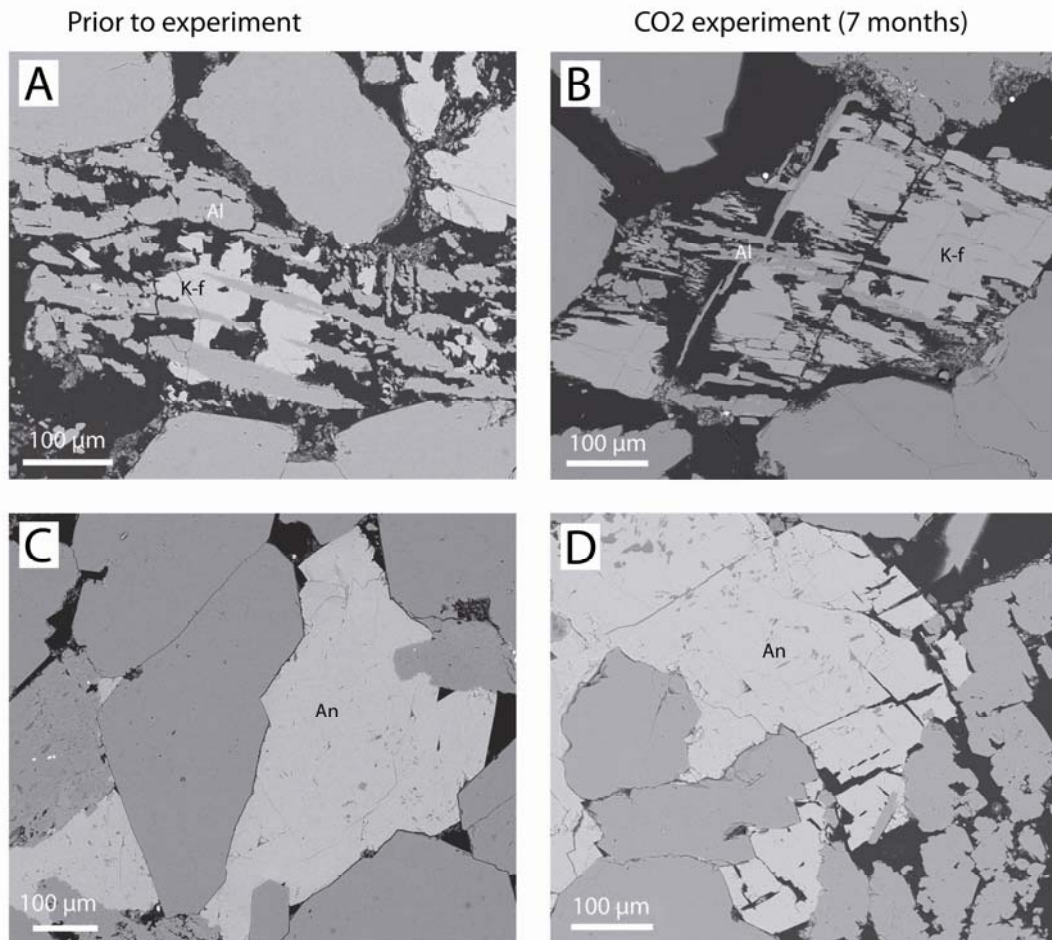


Fig. 6. Skagerrak Formation in the Vedsted-1 well, 2064.87m, BSE images. A. Partly dissolved K-feldspar (K-f) with relatively unaffected alibite lamellae (Al), prior to experiment. B. Partly dissolved K-feldspar (K-f) with relatively unaffected alibite lamellae (Al), after CO₂ experiment (7 months). C. Ankerite cement (An) prior to experiment. D. Ankerite cement (An) with dissolution along crystal faces, after CO₂ experiment (7 months).

Skagerrak Formation in the Vedsted-1 well

N₂ experiment (14 months)

CO₂ experiment (14 months)

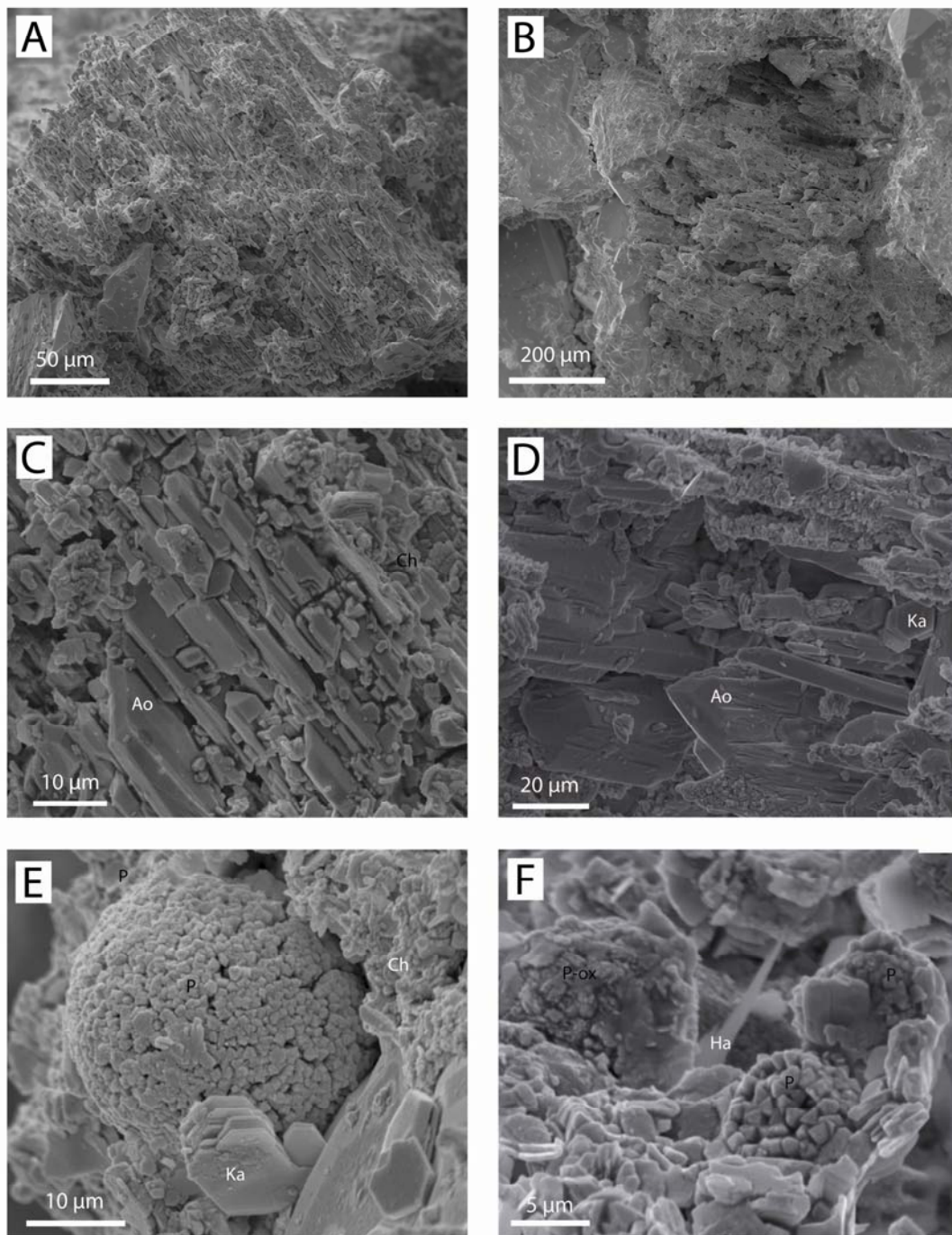


Fig. 7. Skagerrak Formation in the Vedsted-1 well, depth 2064.87m, SEM images. A. Feldspar intensely dissolved, prior to and after N₂ experiment (14 months). B. Feldspar intensely dissolved, after CO₂ experiment (14 months). C. Authigenic albite with no sign of dissolution after N₂ experiment (14 months). D. Authigenic albite with no sign of dissolution, after CO₂ experiment (14 months). E. Framboids of pyrite (Py) next to kaolinite (Ka) and chlorite (Ch), after N₂ experiment (14 months). F. Framboids of pyrite (P), oxidised pyrite (P-ox) and halite (Ha), after CO₂ experiment (14 months).

Skagerrak Formation in the Vedsted-1 well

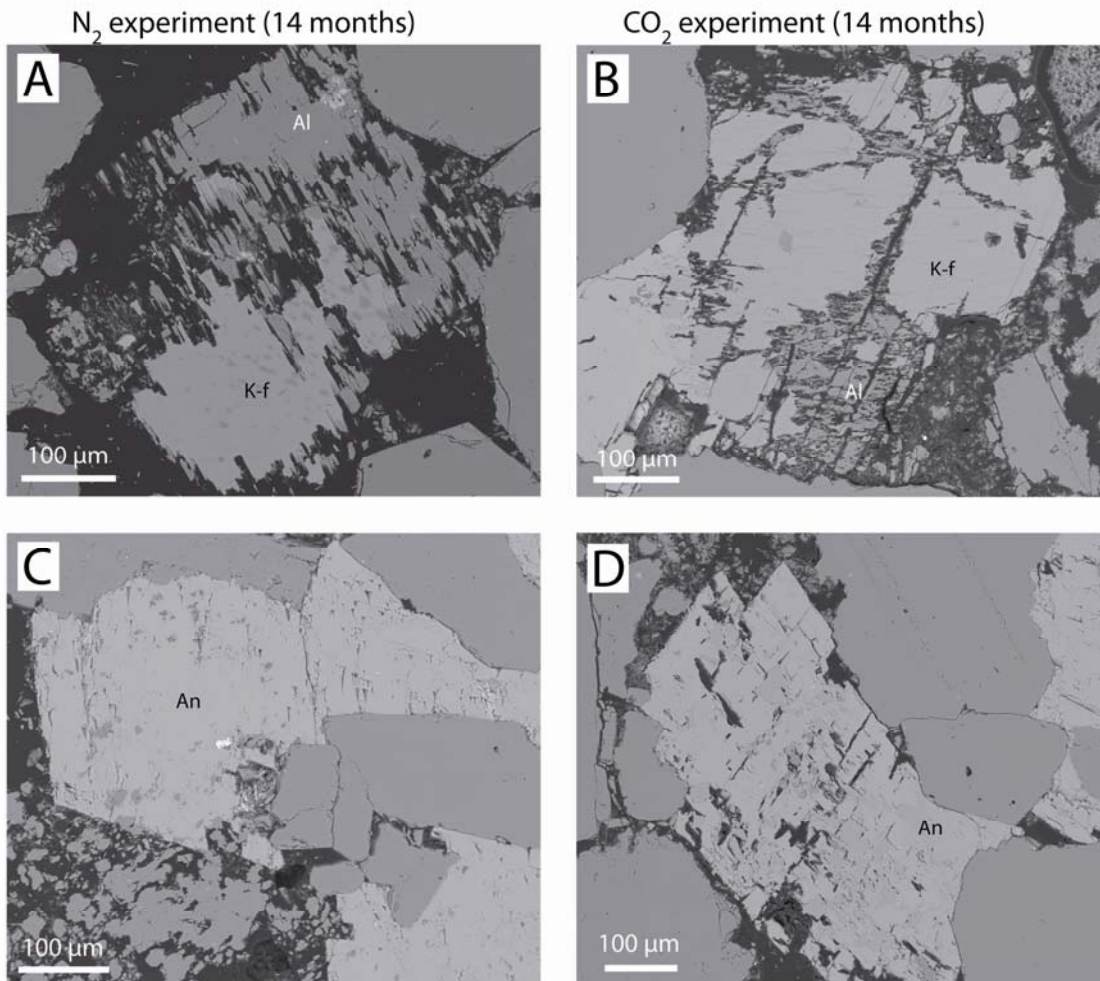


Fig. 8. Skagerrak Formation in the Vedsted-1 well, 2064.87m, BSE images. A. Partly dissolved K-feldspar (K-f) and albite (Al), after N₂ experiment (14 months). B. Partly dissolved K-feldspar (K-f) and alibite (Al), after CO₂ experiment (14 months). C. Ankerite cement (An) with no sign of dissolution, after N₂ experiment (14 months). D. Ankerite cement (An) with dissolution along crystal faces, after CO₂ experiment (14 months).

Gassum Formation in the Vedsted-1 well

Experiment	Prior		CO ₂ (7 months)	N ₂ (7 months)	CO ₂ (14 months)	N ₂ (14 months)
Method	Thin section	SEM / BSC	SEM / BSC	SEM / BSC	SEM / BSC	SEM / BSC
Depth (m)	2010.12		2010.12	2010.09	2010.03	2010.06
Sample ID	VE1-Ga201012		1315C	1316N	1295C	1296N
DETRITAL						
Quartz	59.4					
K-feldspar	6.8	Intense dissolution may occur	Intense dissolution may occur	Intense dissolution may occur	Intense dissolution may occur	Intense dissolution may occur
Plagioclase	9.6	Intense dissolution occurs	Intense dissolution occurs	Intense dissolution occurs	Intense dissolution occurs	Intense dissolution occurs
Mica	1.4					
Intraclasts + allogenic clays	0.2					
Sedi. Rock fragments	1.2					
Metamorphic rock fragm.	0.8					
Volcanic rock fragments	0.0					
Plutonic rock fragm.	2.0					
Transparent heavy min.	0.8					
Opaque	0.4					
AUTHIGENIC PHASES						
Quartz	2.0					
Feldspar	0.0	Albite overgrowths unaffected	Albite overgrowths unaffected		Albite overgrowths unaffected	Albite overgrowths unaffected
Calcite	1.0					
Dolomite / ankerite	2.4		Ankerite shows distinct signs of dissolution		Ankerite shows distinct signs of dissolution	
Siderite	0.4	Unaffected small rhombs	Possibly weakly dissolution of the rhombs		Possibly weakly dissolution of the rhombs	Possibly weakly dissolution of the rhombs
Anhydrite	0.0					
Barite	0.2					
Analcime	0.0					
Red coatings	0.0					
Pyrite	0.6	Occasionally weakly oxidised	Occasionally weakly oxidised			
Anatase	0.8					
Infiltration clay	0.0					
Smectite	0.0					
Illitic and chloritic clays	6.0					
Kaolin	4.0					
TOTAL	100					
				Halite, calcium and magnesium chloride coatings are common		

Illustration of the observed changes on Figs 9, 10, 11 and 12.

Gassum Formation in the Vedsted-1 well

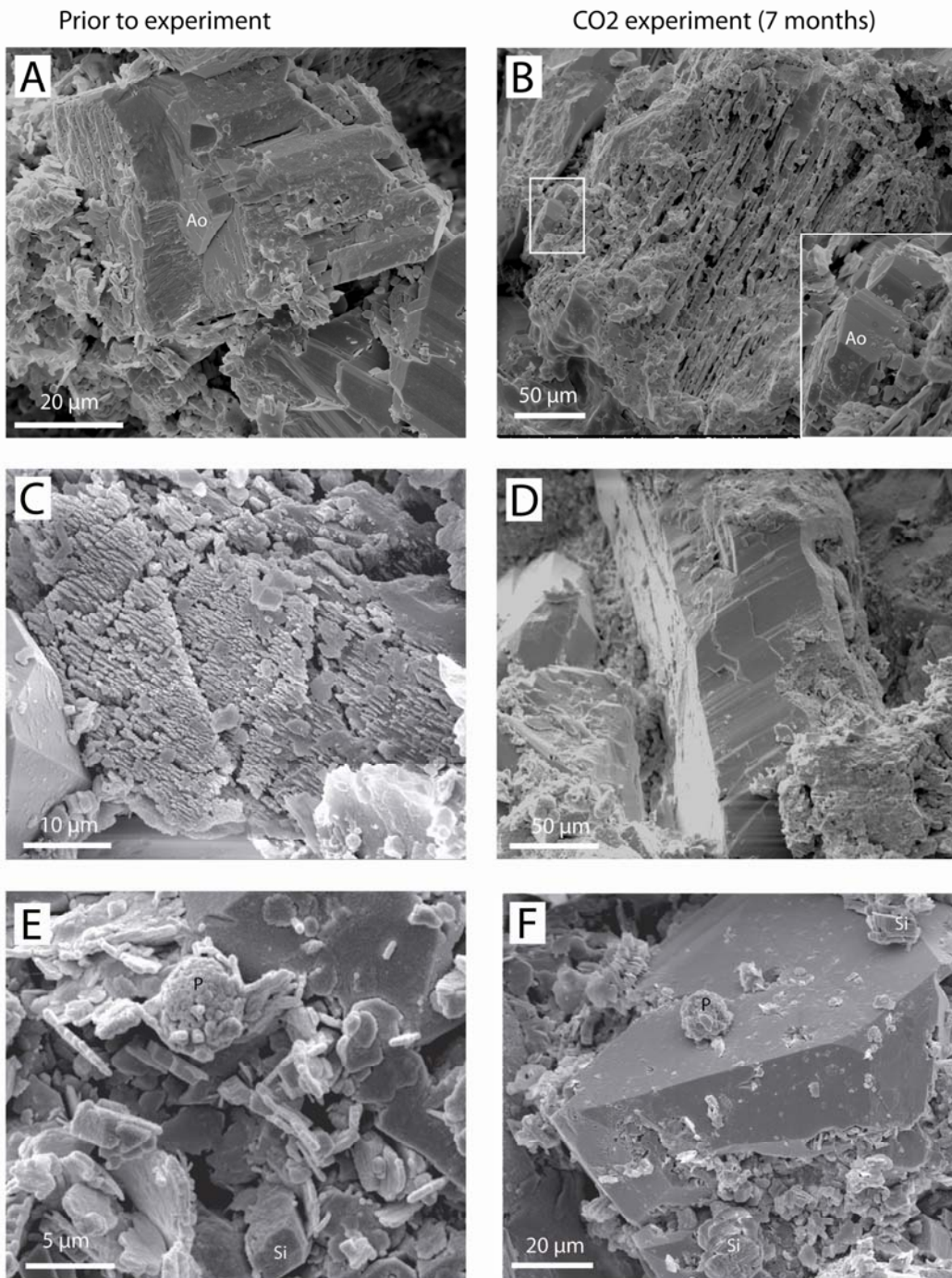


Fig. 9. Gassum Formation in the Vedsted-1 well, depth 2010.1m, SEM images. A. Weakly altered plagioclase with albite overgrowth (Ao) prior to experiment. B. Intensively altered plagioclase with unaffected albite overgrowth (Ao) after CO₂ experiment (7 months). C. Intensively altered K-feldspar prior to experiment (7 months). D. Unaffected K-feldspar overgrowth covering the entire feldspar grain after CO₂ experiment (7 months). E. Weakly oxidised framboids of pyrite (P) and unaffected siderite (Si) prior to experiment. F. Weakly oxidised framboids of pyrite (P) and weakly possibly dissolved siderite (Si) after CO₂ experiment (7 months).

Gassum Formation in the Vedsted-1 well

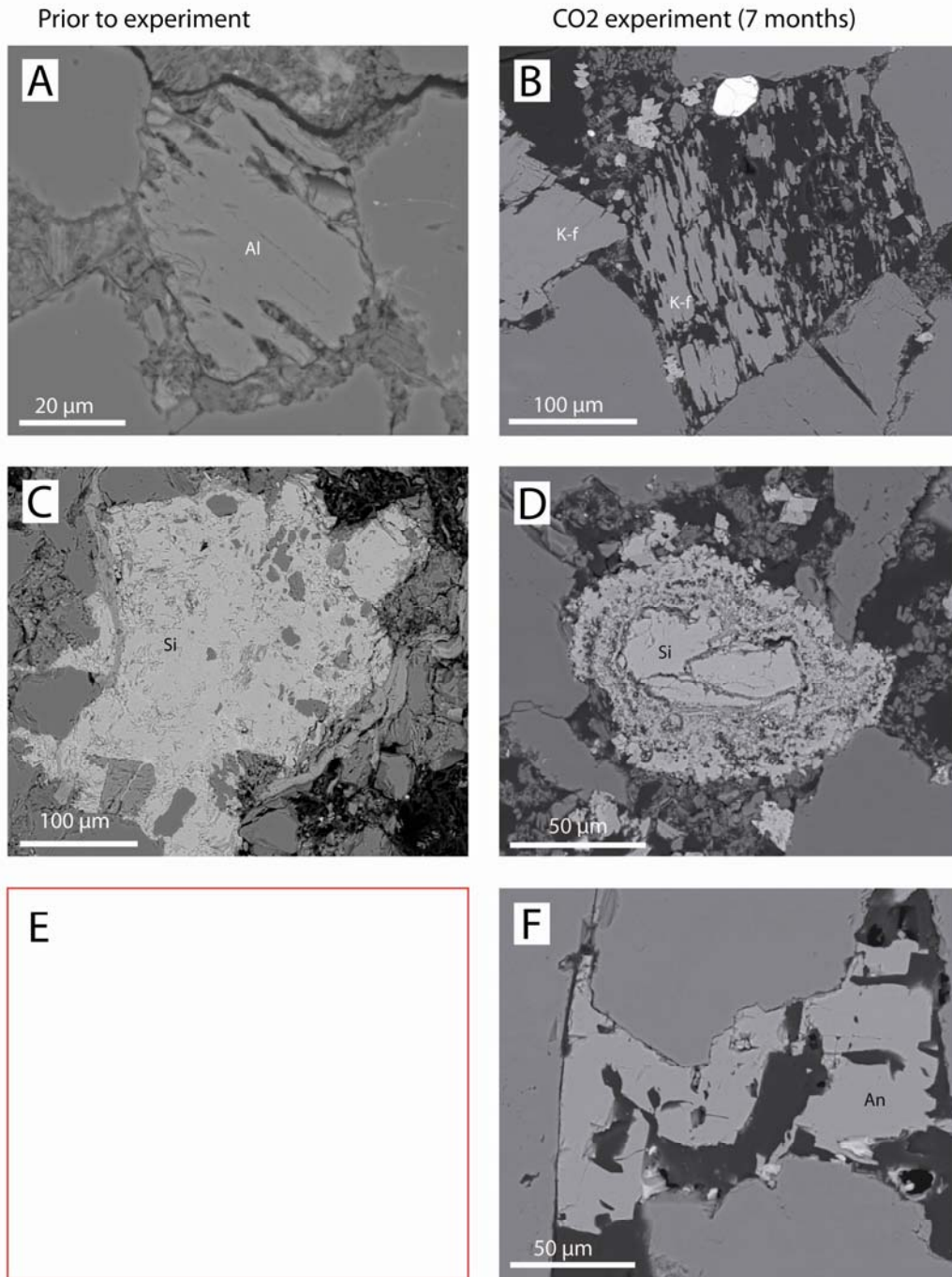


Fig. 10. Gassum Formation in the Vedsted-1 well, depth 2010.1m, BSC images. A. Weakly dissolution of albite lamellae in detrital K-feldspar prior to experiments. B. Intensively dissolved sodium-rich K-feldspar next to an almost unaltered purer K-feldspar after CO₂ experiment (7 months). C. Concretionary siderite cement (Si) prior to experiment. D. Spherulitic siderite showing signs of partly dissolution after CO₂ experiment (7 months). E. No observations. F. Ankerite cement (An) with distinct dissolution phenomenon after CO₂ experiment (7 months).

Gassum Formation in the Vedsted-1 well

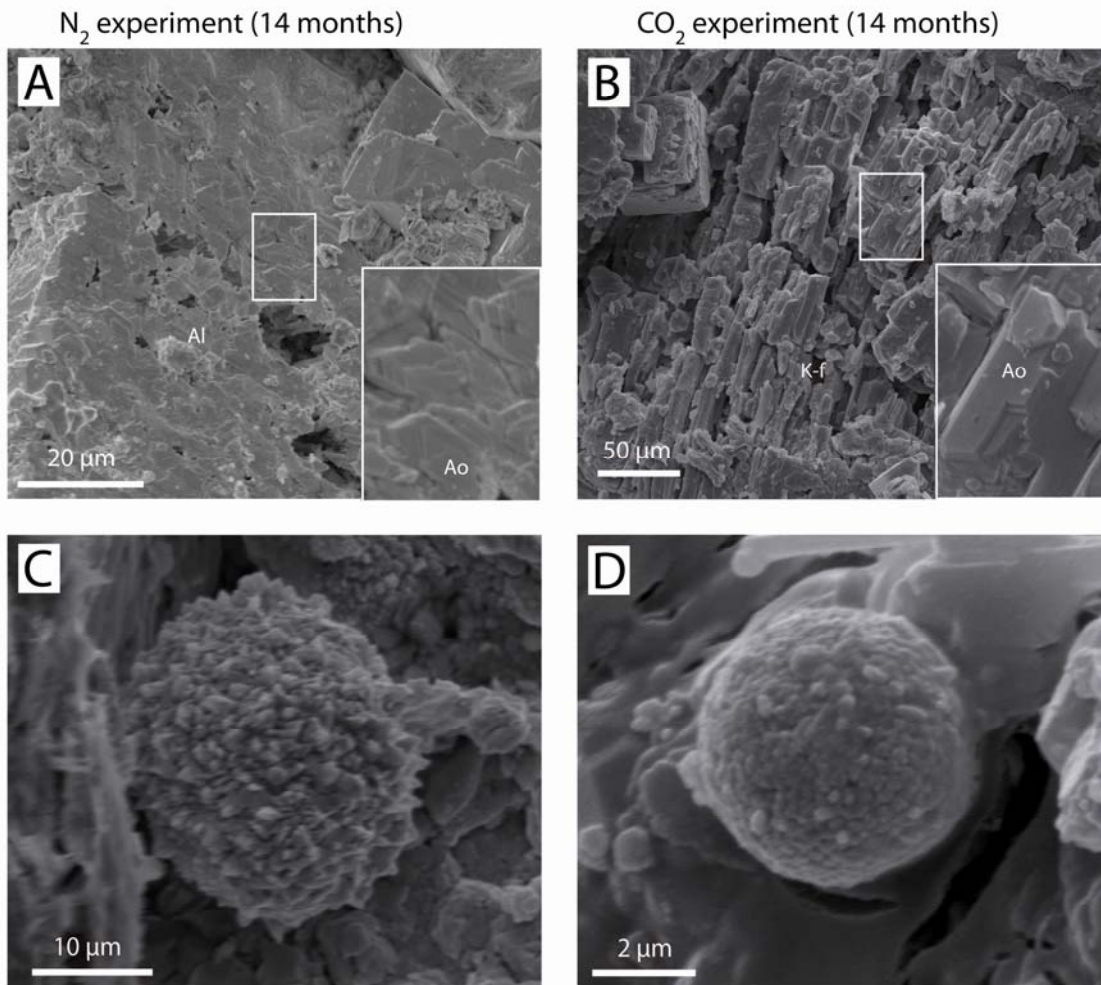


Fig. 11. Gassum Formation in the Vedsted-1 well, depth 2010.1m, SEM images. A. Detrital plagioclase with dissolution grooves and unaffected albite overgrowths (Ao), after N₂ experiment (14 months). B. Intensively altered K-feldspar with unaffected albite overgrowths (Ao) after CO₂ experiment (14 months). C. Weakly oxidised pyrite framboids, after N₂ experiment (14 months). F. Unaffected or weakly oxidised pyriteframboids, after CO₂ experiment (14 months).

Gassum Formation in the Vedsted-1 well

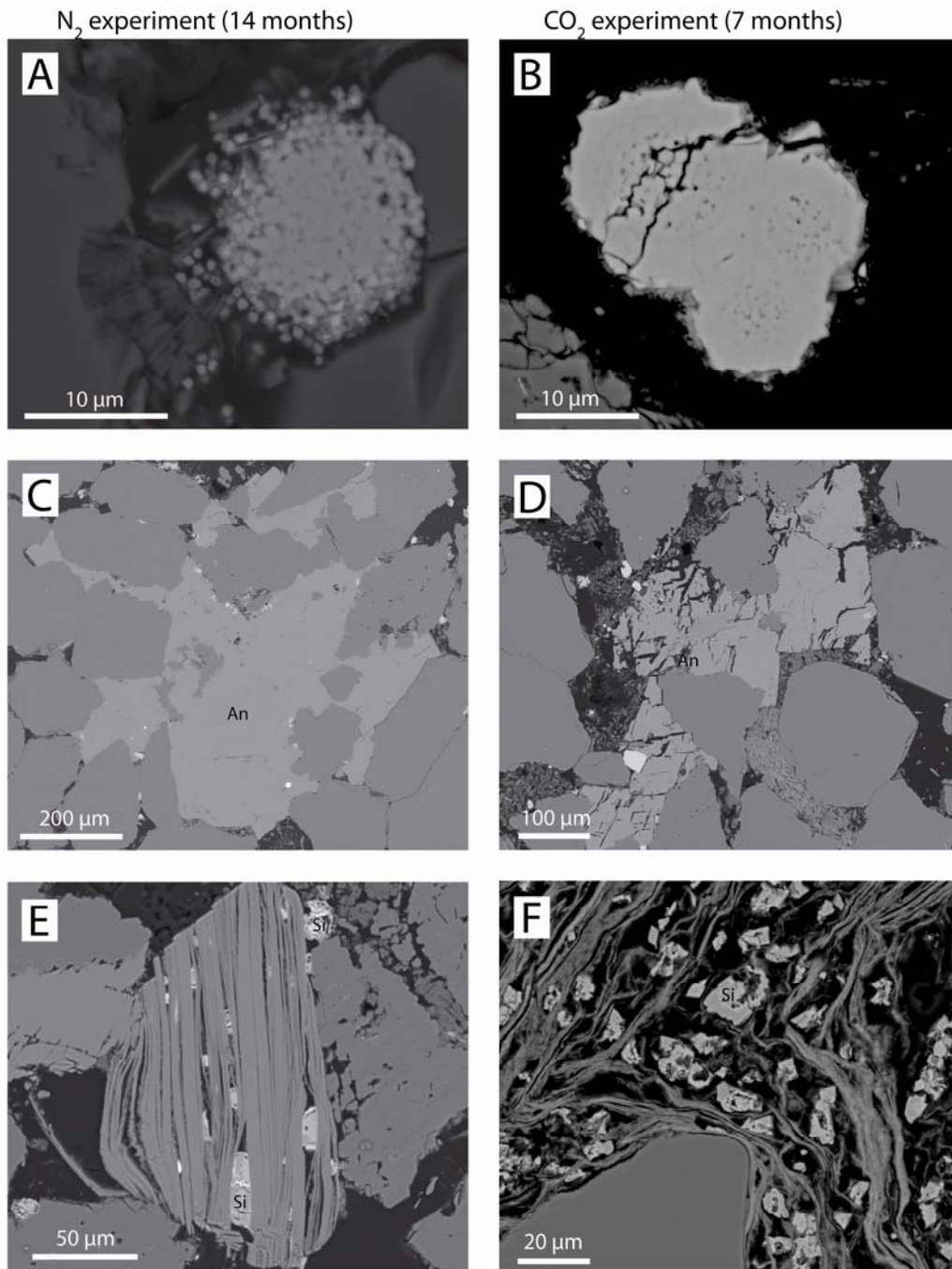


Fig. 12. Gassum Formation in the Vedsted-1 well, depth 2010.1m, BSE images. A. Unaffected pyrite framboid surrounded by kaolin, after N₂ experiment (14 months). B. Unaffected euhedral pyrite enclosing pyrite framboids, after CO₂ experiment (14 months). C. Ankerite cement (An) without any dissolution features, after N₂ experiment (14 months). D. Ankerite cement (An) with distinct dissolution after CO₂ experiment (14 months). E. Siderite rhombs without dissolution inside mica and with special dissolution phenomena outside, after N₂ experiment (14 months). F. Siderite rhombs with typical dissolution, after CO₂ experiment (14 months).

Gassum Formation in the Stenlille-18 well

Experiment	Prior	Prior	CO ₂ (7 months)	N ₂ (7 months)	CO ₂ (14 months)	N ₂ (14 months)
Method	Thin section	SEM / BSC	SEM / BSC	SEM / BSC	SEM / BSC	SEM / BSC
Depth (m)	1663.44		1663.44	1662.40	1662.47	1662.62
Sample ID	ST18-Ga166344		1313C	1314N	1293C	1294N
DETRITAL						
Quartz	84.2					
K-feldspar	0.6	Intense dissolution occurs	Intense dissolution occurs			
Plagioclase	0.8	Intense dissolution occurs	Intense dissolution occurs			
Mica	0.0					
Intraclasts + allogenic clays	9.8					
Sedi. Rock fragments	0.2					
Metamorphic rock fragm.	0.0					
Volcanic rock fragments	0.0					
Plutonic rock fragm.	1.2					
Transparent heavy min.	0.2					
Opaque	0.6					
AUTHIGENIC PHASES	0.0					
Quartz	1.0					
Feldspar	0.0					
Calcite	0.6					
Dolomite	0.0					
Siderite	0.0					
Anhydrite	0.0					
Barite	0.0					
Analcime	0.0					
Red coatings						
Pyrite	0.0		Etched crystal faces may occur			
Anatase	0.0					
Infiltration clay	0.2					
Smectite	0.0					
Illitic and chloritic clays	0.0					
Kaolin	0.6					
TOTAL	100.0					
		Gypsum and calcium oxalate, formed in the cores	Gypsum not identified	Gypsum not identified		
			Halite and salts containing Na, Ca, Cl are common	Halite and salts containing Na, Ca, Cl are common	Problems with salt covering the samples	Problems with salt covering the samples
		Drilling mud consisting of smectite, barite and fluorite is common	Drilling mud is present, the degree of dissolution cannot be estimated	Drilling mud is present, the degree of dissolution cannot be estimated		

Illustration of the observed changes on Figs 13, 14, 15 and 16.

Gassum Formation in Stenlille-18

Prior to experiment / after N₂ experiment

CO₂ experiment (7 months)

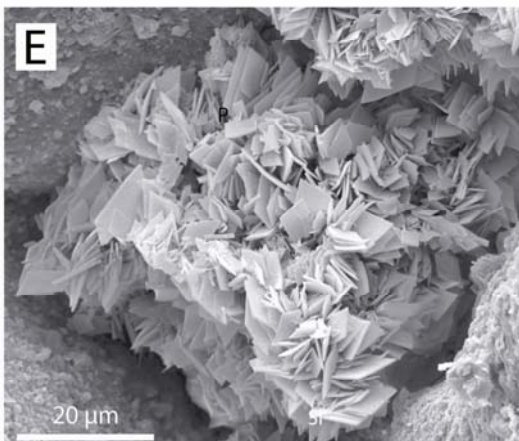
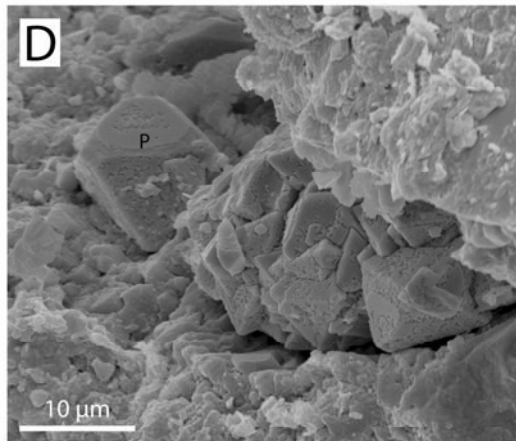
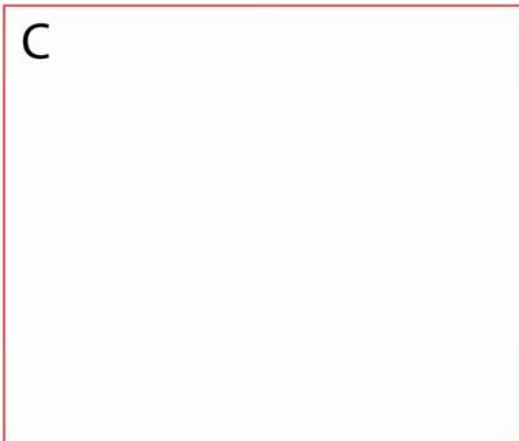
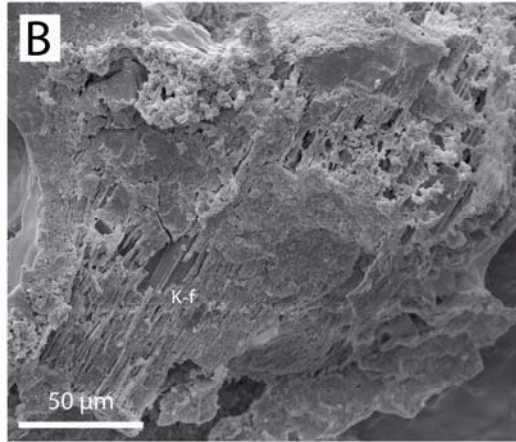
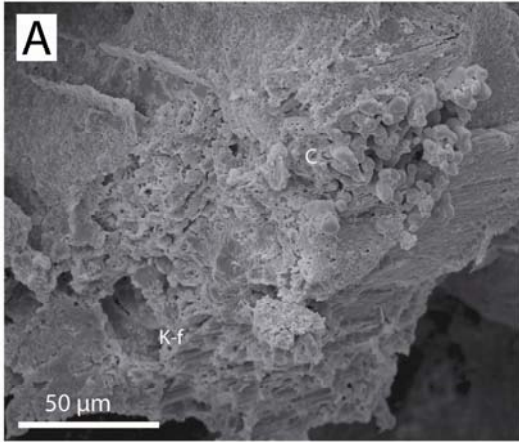


Fig. 13. Gassum Formation in the Stenlille-18 well, depth 1663.44m, SEM images. A. Intensively dissolved K-feldspar (K-f) partly covered by a calcium chloride containing salt (C) after N₂ experiment. B. Intensively dissolved K-feldspar (K-f) after CO₂ experiment (7 months). C. No observations. D. Euhedral pyrite crystals (P) with etched surfaces after CO₂ experiment (7 months). E. Calcium oxalate? precipitated in the samples after the cores were taken, prior to experiment. Gypsum and calcium oxalate has not been identified in the samples after the N₂ and CO₂ experiments (7 months).

Gassum Formation in Stenlille-18

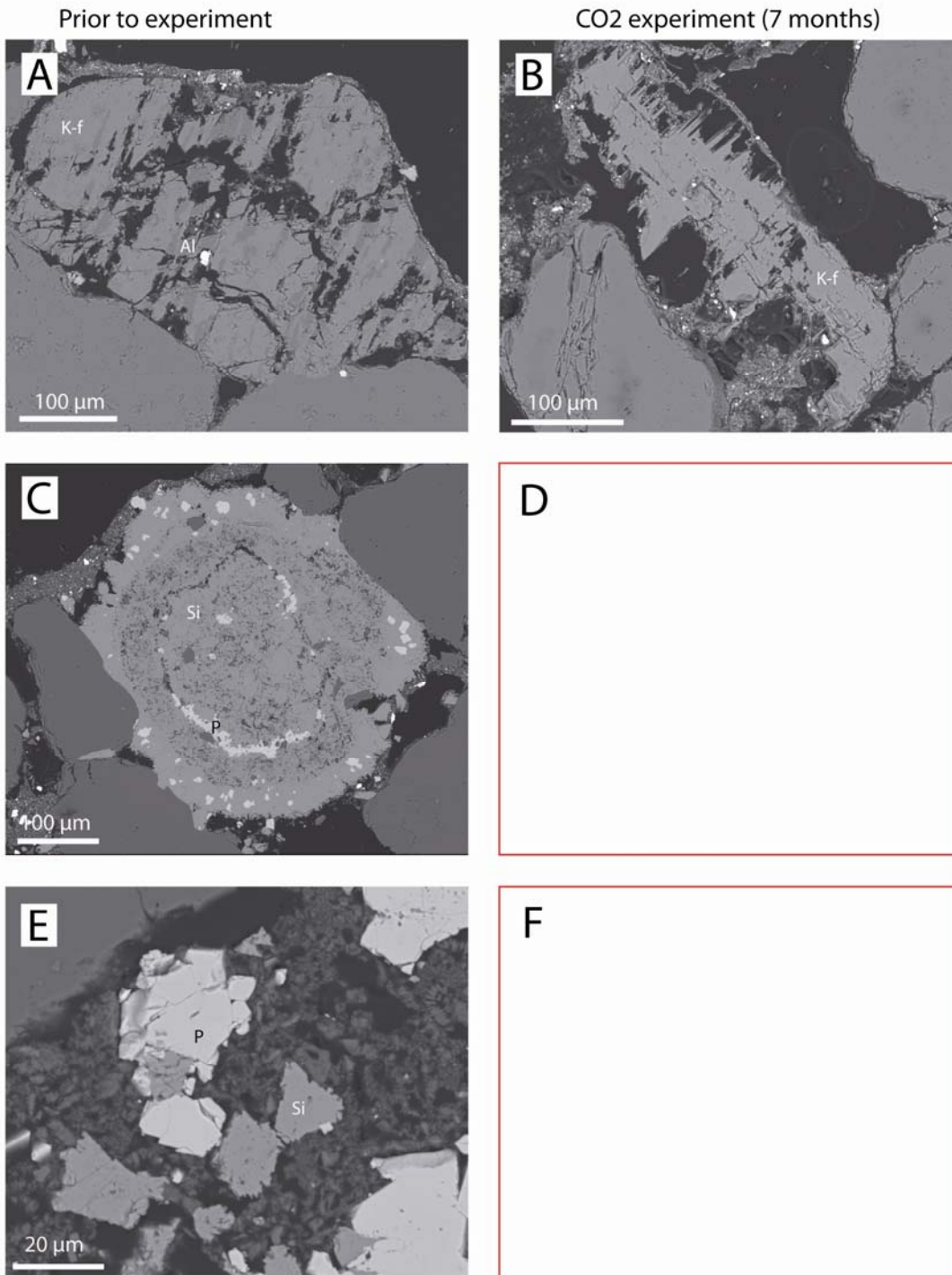
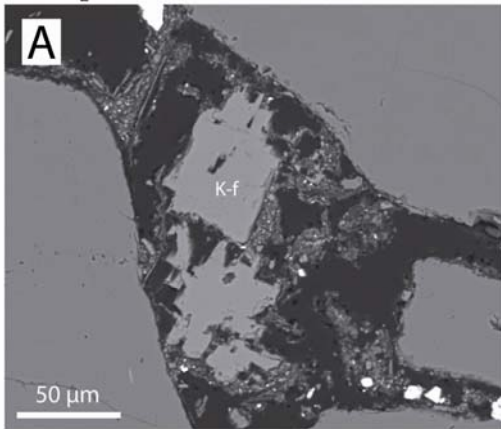


Fig. 14. Gassum Formation in the Stenlille-18 well, depth 1663.44m, BSC images. A. K-feldspar (K-f) with partly dissolved albite lamellae prior to experiment. B. K-feldspar (K-f) partly dissolved after CO₂ experiment (7 months). C. Spherulitic siderite with concentric rings of pyrite (P) prior to experiment. D. No observations. E. Euhedral pyrite (P) and siderite (Si) with an outer rim of tiny crystals. F. No observations. Note the presence of drilling mud (smectite with tiny crystals of barite and fluorite) which may have influenced the experimental results.

Gassum Formation in Stenlille-18

N₂ experiment (14 month)



CO₂ experiment (14 months)

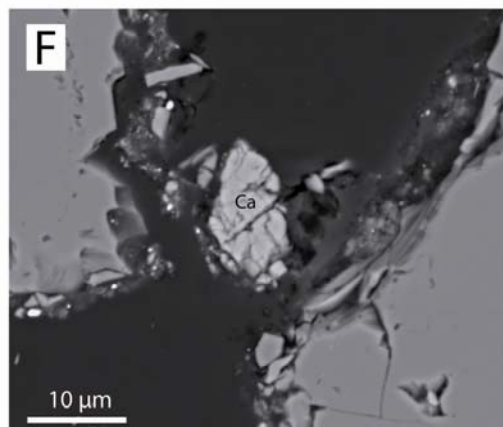
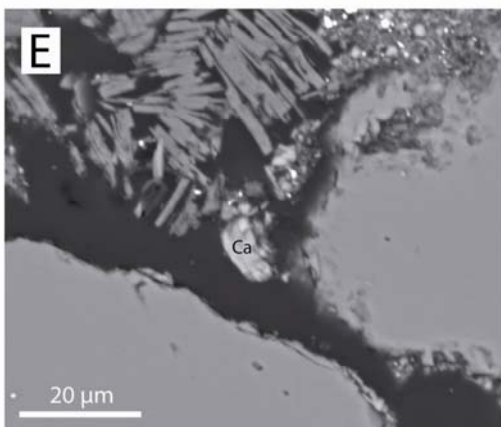
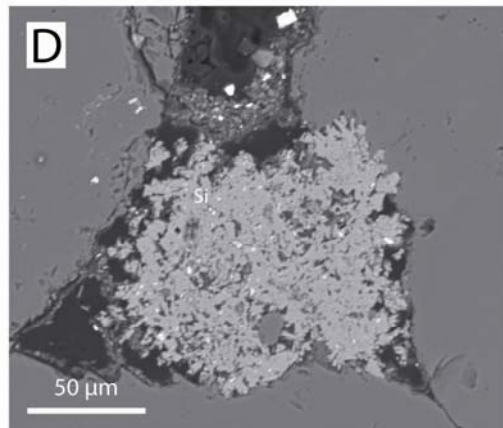
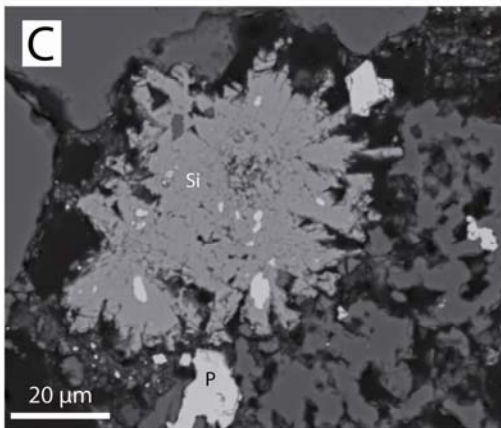
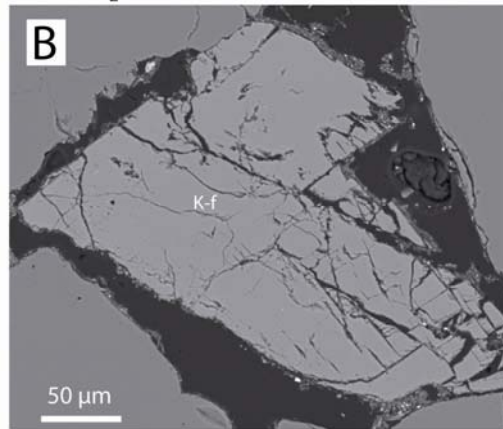
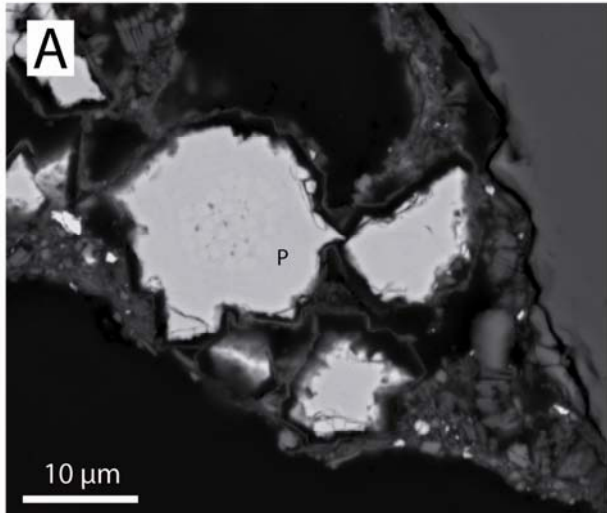


Fig. 15. Gassum Formation in the Stenlille-18 well, depth 1663.44m, BSC images. A. K-feldspar (K-f) with partly dissolved, after N₂ experiment (14 months). B. K-feldspar (K-f) partly dissolved after CO₂ experiment (14 months). C. Spherulitic siderite (Si) enclosing pyrite and followed by pyrite (P) after N₂ experiment (14 months). D. Spherulitic siderite (Si) enclosing pyrite CO₂ experiment (14 months). E. Small calcite rhomb with no clear alteration, after N₂ experiment (14 months). F. Small calcite rhomb with no clear alteration, after CO₂ experiment (14 months). Note the presence of drilling mud (smectite with tiny crystals of barite and fluorite) which may have influenced the experimental results.

Gassum Formation in Stenlille-18

N₂ experiment (14 month)



CO₂ experiment (14 months)

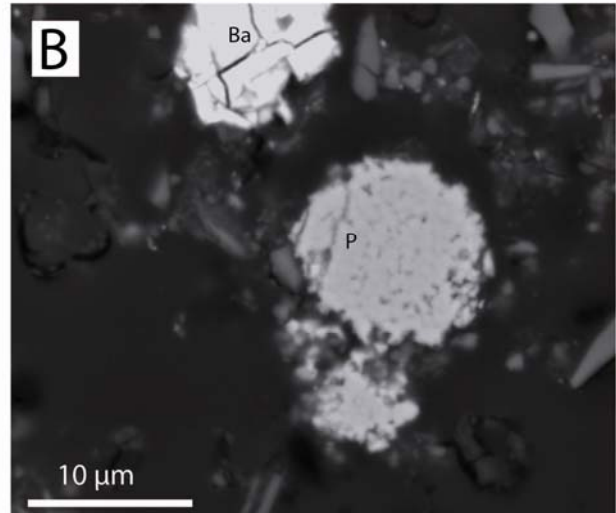


Fig. 16. Gassum Formation in the Stenlille-18 well, depth 1663.44m, BSC images. A. Framboid of pyrite with pyrite overgrowth (P) after N₂ experiment (14 months). B. Framboid of pyrite (P), showing no clear alteration, and barite (Ba) after CO₂ experiment (14 months).

Haldager Sand Formation in the Vedsted-1 well

Experiment	Prior		CO ₂ (7 months)	N ₂ (7 months)	CO ₂ (14 months)	N ₂ (14 months)
Method	Thin section	SEM / BSC	SEM / BSC	SEM / BSC	SEM / BSC	SEM / BSC
Depth (m)	1155.5		1155.50	1155.42	1155.47	1155.44
Sample ID	VE1-Ha115550		1309C	1310N	1301C	1302N
DETRITAL						
Quartz	82.0					
K-feldspar	8.0	Partly dissolution and kaolin replacement of K-feldspar	Partly dissolution and kaolin replacement of K-feldspar		Partly dissolution and kaolin replacement of K-feldspar	Partly dissolution and kaolin replacement of K-feldspar
Plagioclase	0.6					
Mica	0.6					
Intraclasts + allogenic clays	4.4					
Sedi. Rock fragments	0.2					
Metamorphic rock fragm.	0.2					
Volcanic rock fragments	0.0					
Plutonic rock fragm.	0.6					
Transparent heavy min.	0.4					
Opaque	0.2					
AUTHIGENIC PHASES						
Quartz	0.8	Quartz mountains	Quartz mountains	Quartz mountains	Quartz mountains	Quartz mountains
Feldspar	0.0					
Calcite	0.0					
Dolomite / ankerite	0.0					
Siderite	0.0					
Anhydrite	0.0					
Barite	0.0					
Analcime	0.8					
Red coatings	0.0					
Pyrite	0.2	Pyrrhotite in the centre of pyrite framboids	Possibly dissolution of pyrrhotite in the centre of pyrite crystals		Alteration rim on pyrite, possible oxidation or dissolution	Alteration rim on pyrite, possible oxidation or dissolution
Anatase	0.0					
Infiltration clay	0.0					
Smectite	0.0					
Illitic and chloritic clays	0.4					
Kaolin	0.6					
TOTAL	100.0					

Illustration of the observed alterations on Figs 17, 18, 19 and 20.

Haldager Sand Formation in the Vedsted-1

Prior to experiment

CO₂ experiment (7 months)

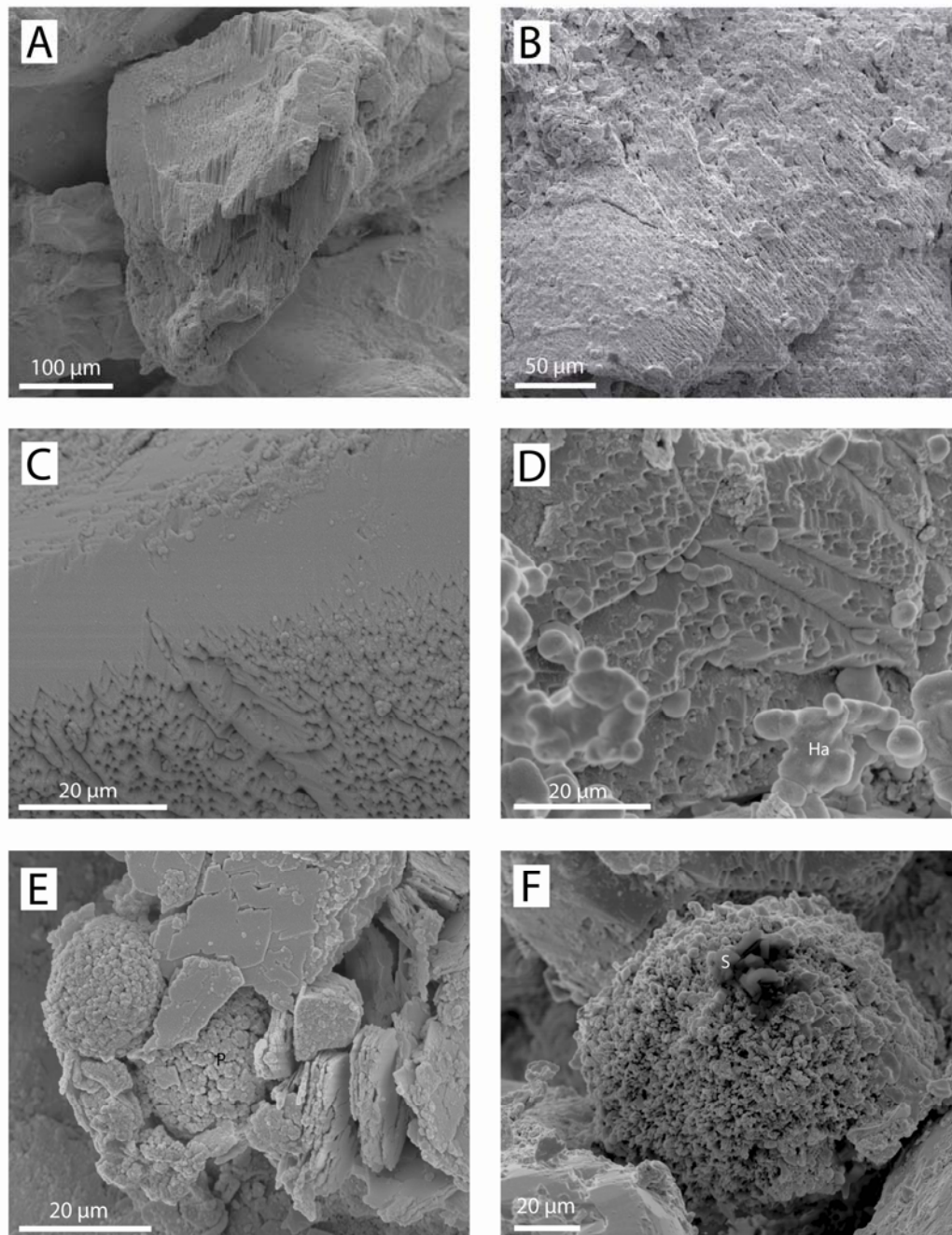


Fig. 17. Haldager Sand Formation in the Vedsted-1 well, depth 1155.5m, SEM images. A. Partly dissolved K-feldspar grain prior to the experiment. B. Partly dissolved K-feldspar grain after CO₂ experiment (7 months). C. Quartz overgrowths (quartz mountains) prior to experiment. D. Quartz overgrowths (quartz mountains) after CO₂ experiment (7 months) partly covered by halite crystals (Ha). E. Oxidised framboids of pyrite prior to experiment. F. Oxidised framboids of pyrite on which sylvite crystals (S) have formed after CO₂ experiment (7 months).

Haldager Sand Formation in the Vedsted-1 well

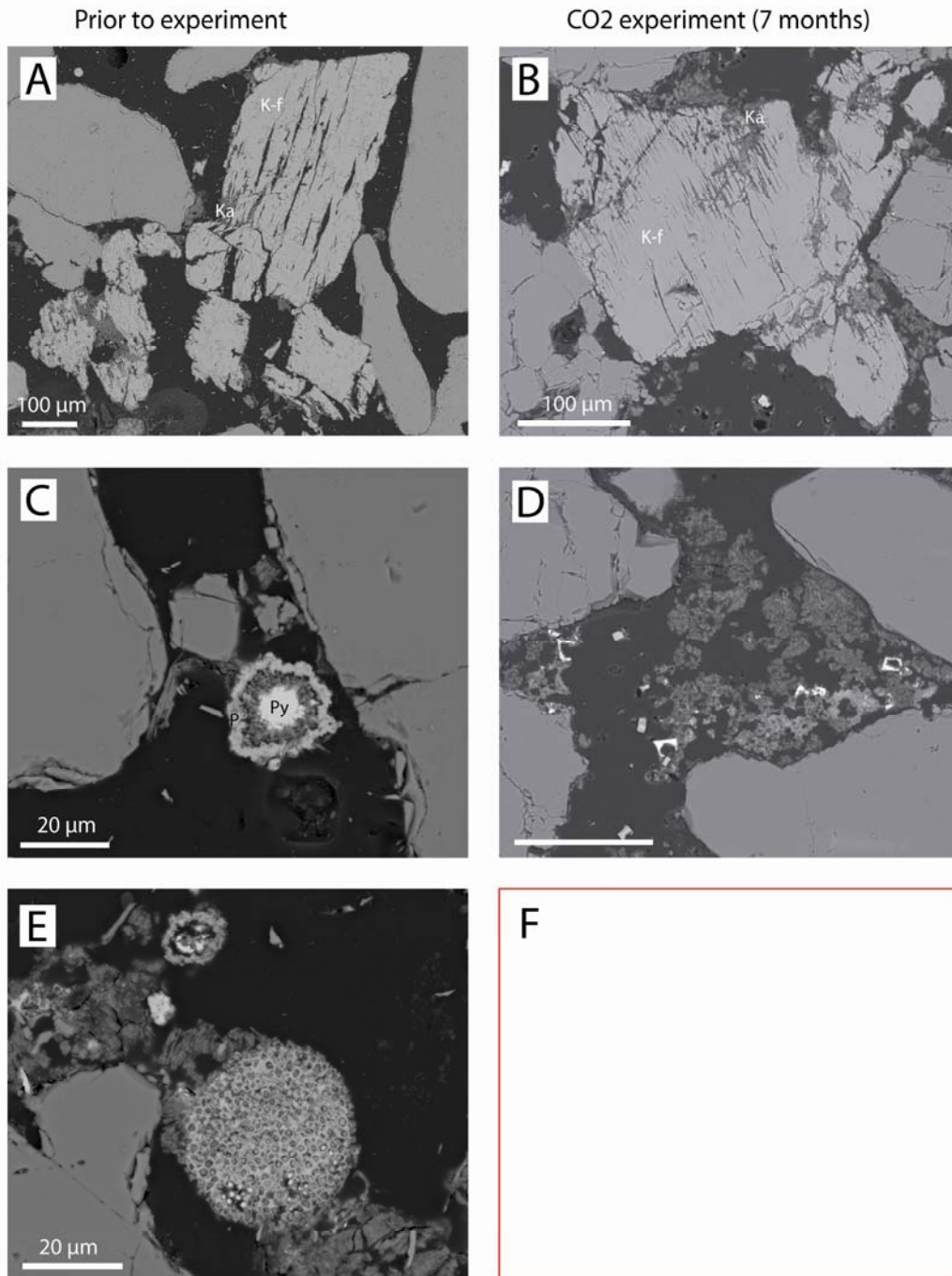


Fig. 18. Haldager Sand Formation in the Vedsted-1 well (depth 1155.5m), BSC images. A. Partly dissolved and kaolin (Ka) replaced K-feldspar grain (K-f) prior to experiment. B. Partly dissolved and kaolin (Ka) replaced K-feldspar grains (K-f) after CO₂ experiment (7 months). C. Framboids consisting of pyrrhotite (Fe₇S₈-FeS) in the centre and pyrite (FeS₂) in the outer rim, prior to experiment. D. Euhedral pyrite with internal circular cavities, possibly from dissolution of an earlier authigenic phase – pyrrhotite?, after CO₂ experiment (7 months). E. Framboid consisting of pyrrhotite (white spots) and pyrite (grey), prior to experiment.

Haldager Sand Formation in the Vedsted-1

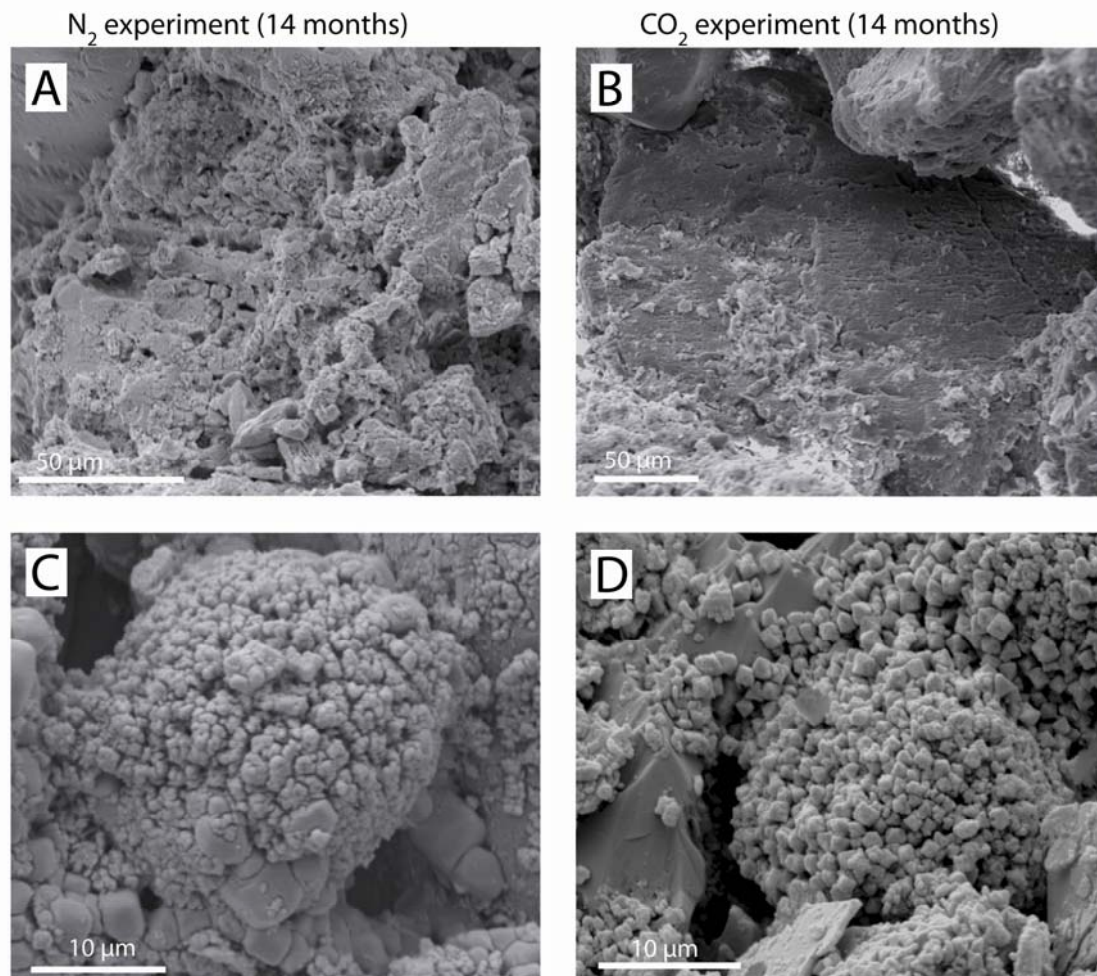


Fig. 19. Haldager Sand Formation in the Vedsted-1 well, depth 1155.5m, SEM images. A. Partly dissolved K-feldspar grain, after N₂ experiment (14 months). B. Partly dissolved K-feldspar grain after CO₂ experiment (14 months). C. Oxidised framboid of pyrite, after N₂ experiment (14 months). D. Oxidised framboid pyrite after CO₂ experiment (14 months).

Haldager Sand Formation in the Vedsted-1 well

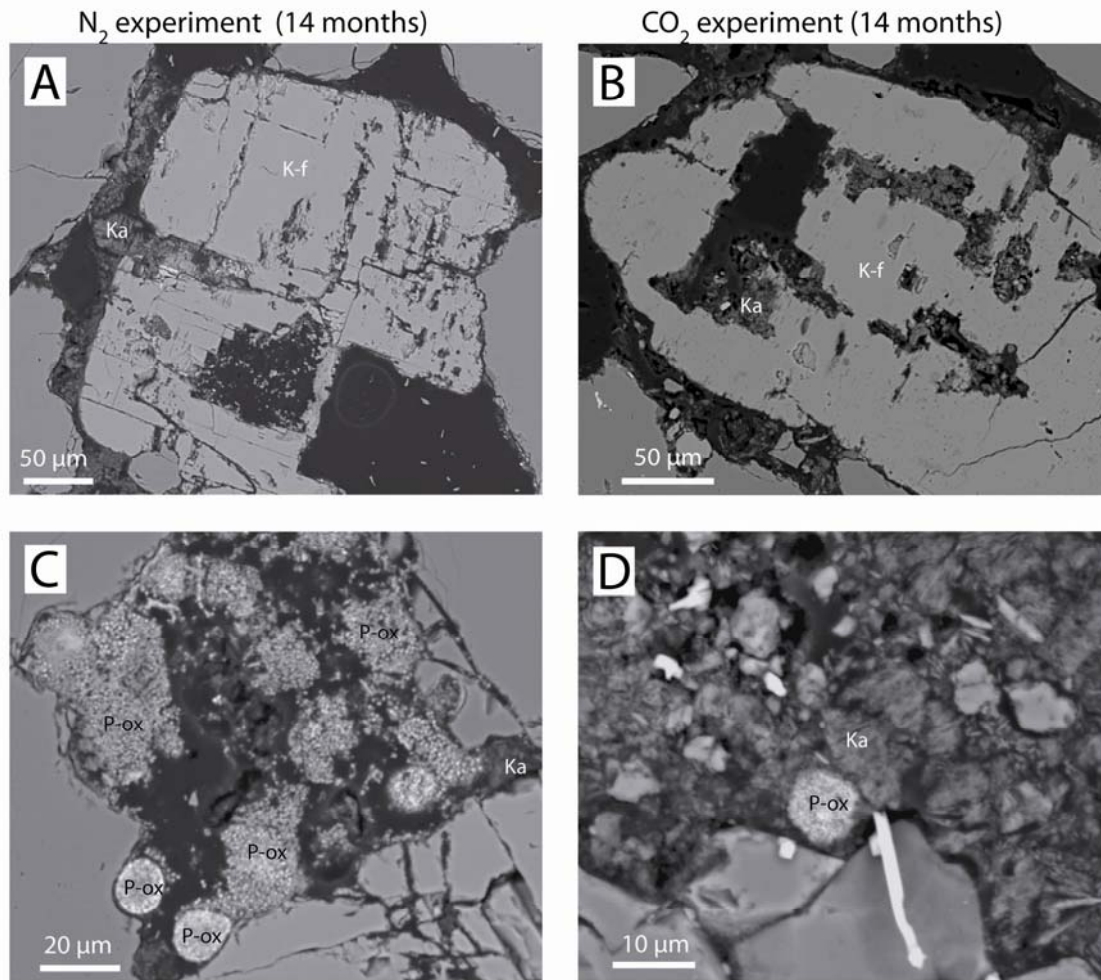


Fig. 20. Haldager Sand Formation in the Vedsted-1 well (depth 1155.5m), BSE images. A. Partly dissolved K-feldspar (K-f) with kaolin (Ka) intragranular and in pore space, after N_2 experiment (14 months). B. Partly dissolved K-feldspar grain (K-f) with intragranular kaolin (Ka) precipitation after CO_2 experiment (14 months). C. Group of oxidised pyrite framboids (P-ox) next to kaolin (Ka,) after N_2 experiment (14 months). D. Oxidised pyrite (P-ox) next to kaolin (Ka) after CO_2 experiment (14 months).

Fjerritslev Formation in the Stenlille-1 well

Experiment	CO ₂ (7 months)	N ₂ (7 months)	CO ₂ (14 months)	N ₂ (14 months)
Method	XRD (Rietveld)	XRD (Rietveld)	SEM / BSC	SEM / BSC
Depth (m)				
Sample ID			1319C	1320N
MINERALOGY				
Quartz	39.5	39.7		
Microcline	4.0	2.4		
Albite (low)				
Calcite	2.9	4.9	Possible dissolution features	Possible dissolution features
Dolomite	1.8	2.0	Possible dissolution features	Possible dissolution features
Siderite	10.9	9.2	Some dissolution features	Some dissolution features
Pyrite				
Anatase				
Montmorillonite	0.4	0.4		
Illitic (2M1)	20.5	20.2		
Clinocllore (11b-2)	2.3	2.9		
Kaolin	17.7	18.3		
TOTAL	100.00	100.00		
(Halite)		Present (0.9 % of sample)		

Illustration of the observed alterations on Fig. 21.

Fjerritslev Formation in the Stenlille-1 well

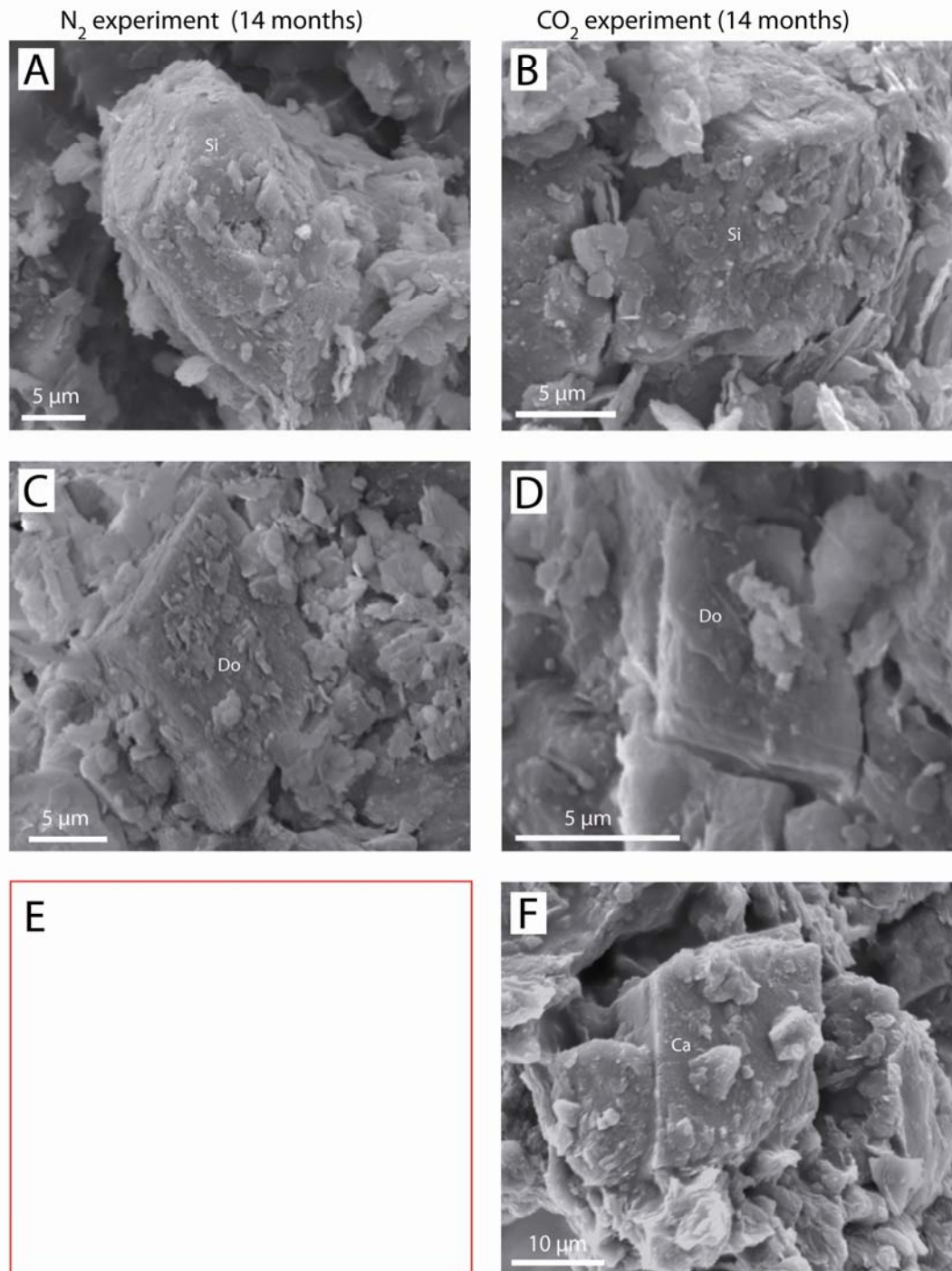


Fig. 21. Fjerritslev Formation in the Stenlille-1 well, depth 1501m, SEM images. A. Siderite (Si) crystal showing some degree of dissolution after N₂ experiment (14 months). B. Siderite (Si) crystal showing some degree of dissolution after CO₂ experiment (14 months). C. Dolomite crystals showing no clear signs of partly dissolution after N₂ experiment (14 months). D. Dolomite crystals showing no clear signs of partly dissolution after CO₂ experiment (14 months). E. No observation. F. Calcite rhomb showing weak sign of dissolution after CO₂ experiment (14 months).

Børglum Formation in the Haldager-1 well

Experiment	CO ₂ (7 months)	N ₂ (7 months)	CO ₂ (7 mths)	N ₂ (7 mths)	CO ₂ (14 mths)	N ₂ (14 mths)
Method	XRD (Rietveld)	XRD (Rietveld)	SEM / BSC	SEM / BSC	SEM / BSC	SEM / BSC
Depth (m)						
Porosity (%)						
Permeability (mD)						
Grain density						
Sample ID			1317C	1318N		
MINERALOGY						
Quartz	28.3	27.6				
Microcline	5.2	4.3				
Albite (low)	3.9	4.5				
Calcite						
Dolomite	2.1	1.9	Partly dissolution		Dissolution features	
Siderite						
Pyrite	1.8	1.8	Partly dissolution or oxidation			
Anatase						
Montmorillonite	4.8	0.4				
Illitic (2M1)	18.3	28.4				
Clinochlore (Ilb-2)	5.8	7.7				
Kaolin	30.0	23.6				
TOTAL	100.0	100.00				
(Halite)	Present (0.42% of sample)					

Illustration of the observed alterations on Figs 22 and 23.

Børglum Formation in the Haldager-1 well

Prior to experiment

CO₂ experiment (7 months)

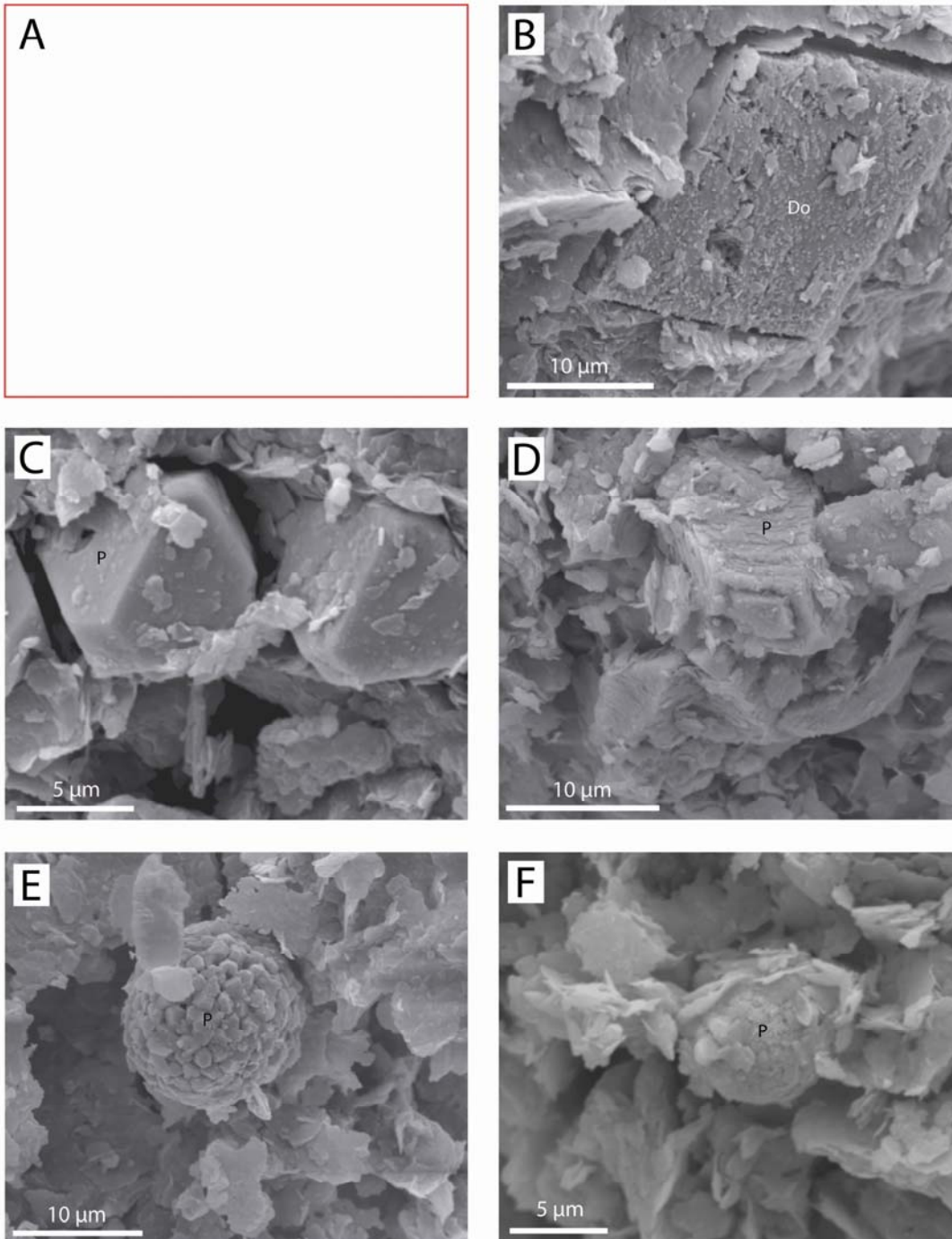


Fig. 22. *Børglum Formation in the Haldager-1 well, depth 1041.2m, SEM images. A. No observation. B. Etched surfaces of dolomite (Do) rhomb after CO₂ experiment (7 months). C. Pyrite crystals (P) prior to experiment. D. Pyrite (P) crystals with etched crystal faces after CO₂ experiment (7 months). E. Framboid of pyrite prior to experiment. F. Framboids of pyrite with etched or oxidised surfaces after CO₂ experiment (7 months).*

Børglum Formation in the Haldager-1 well

N₂ experiment (14 months)

CO₂ experiment (14 months)

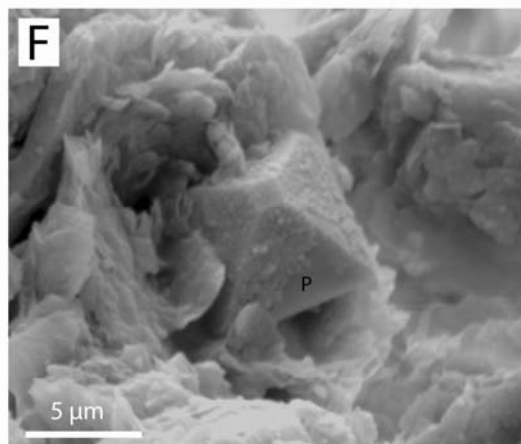
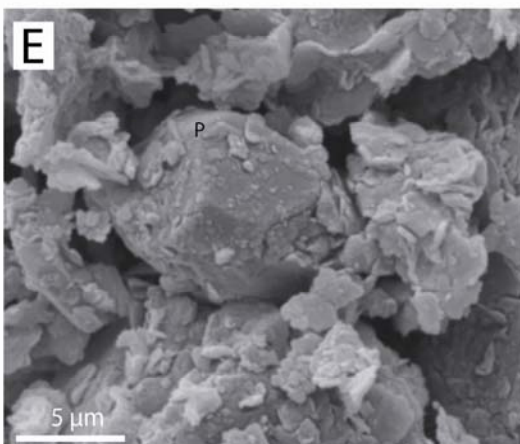
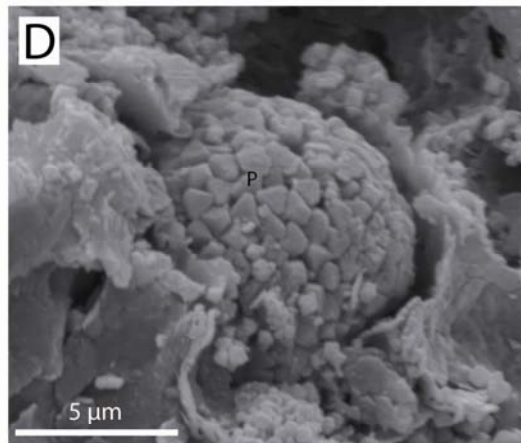
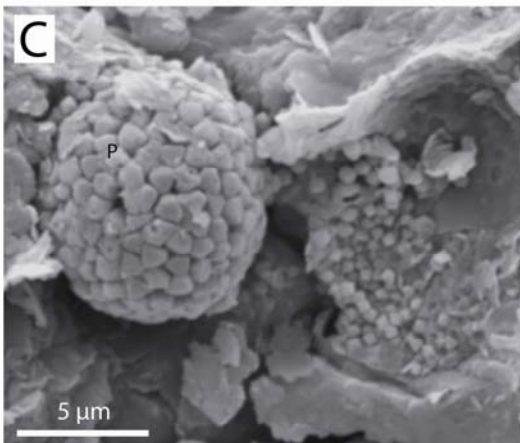
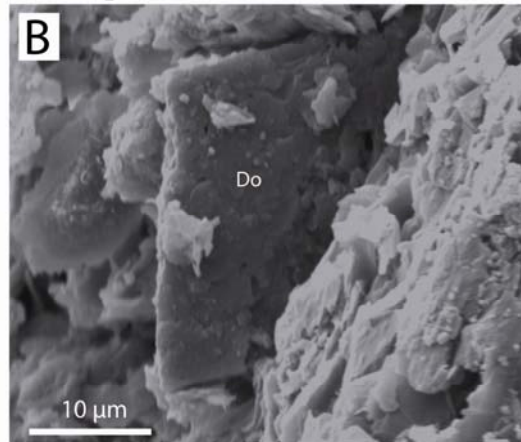
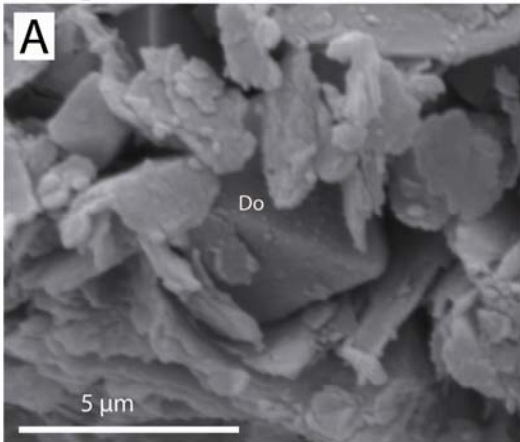


Fig. 23. Børglum Formation in the Haldager-1 well, depth 1041.2m, SEM images. A. Dolomite rhomb (Do) unaffected, after N₂ experiment (14 months). B. Dolomite rhomb (Do) with dissolution features, after CO₂ experiment (14 months). C. Pyrite framboids (P) unaffected after N₂ experiment (14 months). D. Pyrite framboids (P) crystals unaffected after CO₂ experiment (14 months). E. Euhedral pyrite (P) unaffected, only covered by rock dust from preparation, after N₂ experiment (14 months). F. Euhedral pyrite (P) with coating or dissolution features, after CO₂ experiment (14 months).

Appendix 2.

BET and CEC

Specific surface area (BET) and cation exchange capacity (CEC)

Sample No	Sample type	Specific surface area (m²/g)	Cation exchange capacity (meq/100 g)
TØ4-Bu166313	Bulk	3	3.77
TØ4-Bu166317	Clay fraction (< 2 µm)	35	2.07
VE1-Sk206501	Bulk	4	3.07
VE1-Sk206507	Clay fraction (< 2 µm)	12	5.1
ST18-Ga166233	Bulk	2	2.00
ST18-Ga166264	Bulk	2	1.88
ST18-Ga167211	Bulk	2	1.70
ST18-Ga167245	Bulk	2	1.58
ST18-Ga167439	Bulk	4	2.90
ST18-Ga167811	Bulk	3	2.30
ST18-Ga166232	Clay fraction (< 2 µm)	14	8.7
VE1-Ga201010	Bulk	3	6.4
VE1-Ga201016	Bulk	3	2.70
VE1-Ga177566	Bulk	3	2.22
VE1-Ga200777	Bulk	10	5.2
VE1-Ga201013	Clay fraction (< 2 µm)	11	1.39
VE1-Ha115550	Bulk	3	8
VE1-Ha115162	Bulk	4	2.14
FA1-Ha196816	Bulk	4	2.33
FA1-Ha196863	Bulk	3	2.09
FA1-Ha196660	Bulk	3	2.63
HA1-Ha122056	Bulk	5	4.72
HA1-Ha115450	Bulk	6	6.9
ST1-Fj150129	Bulk	15	7.7
VE1-Fj186682	Bulk	43	20
VE1-FJ186740	Bulk	16	5.4
ST1-Fj 1319CO2	After experiment	17	
ST1-Fj 1320N2	After experiment	18	
ST1-Fj 1305C	Clay fraction (< 2 µm) after experiment	56	
ST1-Fj 1304N	Clay fraction (< 2 µm) after experiment	64	
HA1-BØ104120	Bulk	35	3.20
BØ1-BØ098603	Bulk	36	23
HA1-BØ1317CO2	After experiment	28	
HA1-BØ 1318N2	After experiment	35	
Ha1-BØ 1303C	Clay fraction (< 2 µm) after experiment	71	
Ha1-BØ 1306N	Clay fraction (< 2 µm) after experiment	71	

Appendix 3.

XRD results

Sample	Experiments		Months	Lab*	Quartz %	K-feldspar %	Plagioclase %	Ankerite %	Dolomite %	Calcite %	Siderite %	Barite %	Anhydrite %	Analcime %	Pyrite %	Hematite %	Clay minerals %	Kaolinite %	Chlorite %	Illite %	Smectite %	Gypsum %
	Run	Gas																				
TØ4-Bu166328	1307	CO ₂	7	KU	51.0	9.6	20.0			4.7			5.5	2.6					2.3	3.3		
TØ4-Bu166321	1308	N ₂	7	KU	48.3	11.6	21.5			4.7			5.0	4.6					2.1	2.1		
TØ4-Bu166313		alm		AU	54.3	13.4	20.5	1.8		5.3						1.9	2.8					
	1297	CO ₂	14	KU	52.6	12.9	20.9			6.2			0.5	2.2					2.4	2.3		
	1298	N ₂	14	KU	49.9	10.7	19.7			5.9				5.6					2.8	5.5		
VE1-Ha 1309	1309	CO ₂	7	KU	97.1	1.4												1.6				
VE1-Ha115083	1310	N ₂	7	KU	93.9	4.2												2.0				
VE1-Ha115550		alm		AU	83.2	12.3		0.6			1.4						2.5					
	1301	CO ₂	14	KU	91.4	6.6												2.0				
	1302	N ₂	14	KU	91.9	5.8												2.3				
VE1-Sk206498	1311	CO ₂	7	KU	79.1	0.9	14.2	3.5										2.2				
VE1-Sk206487	1312	N ₂	7	KU	81.2	0.7	10.3	6.6										1.2				
VE1-Sk 206501		alm		AU	66.6	4.1	14.9	7.0									7.4					
	1299	CO ₂	14	KU	73.5	2.0	16.2	5.4										2.8				
	1300	N ₂	14	KU	73.2	2.2	13.7	7.1										3.8				
ST18-166244	1313	CO ₂	7	KU	95.9	1.3	0.9			1.0					0.1			0.7				
ST18-166240	1314	N ₂	7	KU	96.2	1.7	0.4			1.3					0.1			0.3				
ST18-Ga166233		alm		AU	89.0	2.7	1.4			1.9	1.7	0.6			0.8		2.0					
	1293	CO ₂	14	KU	96.5	1.0				0.9								1.6				
	1294	N ₂	14	KU	96.2	1.2				1.3								1.3				
VE1-Ga201012	1315	CO ₂	7	KU	86.9	2.5	5.4				2.1							2.4		0.8		
VE1-Ga201009	1316	N ₂	7	KU	81.6	4.8	9.2				0.8							3.8				
VE1-Ga201010		alm		AU	74.9	3.7	10.9	1.9			6.3						2.4					
	1295	CO ₂	14	KU	80.0	4.5	9.0				0.3							5.1		1.0		
	1296	N ₂	14	KU	80.3	4.1	10.4				0.1							3.9		1.2		

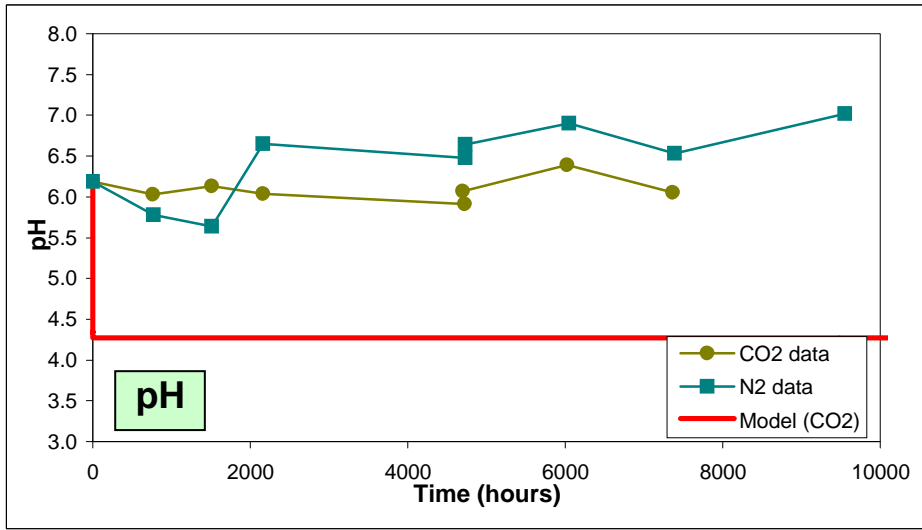
Sample	Experiments		Months	Lab*	Quartz	K-feldspar	Plagioclase	Ankerite	Dolomite	Calcite	Siderite	Barite	Anhydrite	Analcime	Pyrite	Hematite	Clay minerals	Kaolinite	Chlorite	Illite	Smectite	Gypsum
	Run	Gas			%	%	%	%	%	%	%	%	%	%	%	%	%	%	%	%	%	%
HA1-Bø104124	1317	CO ₂	7	KU	28.2	5.2	3.9		2.1						1.8			30.0	5.8	18.3	4.8	
HA1-Bø104125	1318	N ₂	7	KU	27.6	4.3	4.5		1.9						1.8			23.6	7.7	28.4	0.4	
HA1-Bø104120		alm		AU	17.0	3.8	2.4			2.9	3.0	1.0			1.8		68.1					
HA1-Bø104122	1303	CO ₂	14	KU	30.2	3.0	4.6		1.8									30.8	0.3	26.7	0.4	0.6
HA1-Bø104121	1306	N ₂	14	KU	26.4	3.7	5.8		1.5						1.9			29.2	0.8	30.6	0.1	
ST1-Fj150109	1319	CO ₂	7	KU	39.5	4.0			1.8	2.9	10.9							17.7	2.3	20.5	0.4	
ST1-Fj150132	1320	N ₂	7	KU	39.7	2.4			2.0	4.9	9.2							18.3	3.0	20.2	0.4	
ST1-Fj150129		alm		AU	6.5					3.2	77.2*	1.1			0.3		11.8					
ST1-Fj150105	1305	CO ₂	14	KU	29.3	1.4	1.1		2.6	2.6	7.6							16.3		39.0		
ST1-Fj150102	1304	N ₂	14	KU	31.3	2.9	3.8		2.4	4.5	7.4							17.6		30.3		

* Two different methods of quantifying the XRD results have been attempted. Samples analysed at University of Aarhus (AU) has been semi-quantified by application of corrections factors determined for the applied diffractometer. Samples analysed at University of Copenhagen (KU) has been quantified by use of Rietveld refinement. The differences between the two quantifying methods are in particular noteworthy in the Fjerritslev Formation, where siderite is the major constituent according to the quantification by corrections factors, whereas the Rietveld method shows that though siderite is abundant it is not the dominating phase, which is clay. The result from the Rietveld method is supported by the SEM investigations. The quantification method using corrections numbers it a relatively fast semi-quantitative method, but has its drawback when large amounts of poorly crystalline phases are present.

Appendix 4.

Selected results of chemical analysis and forward modelling

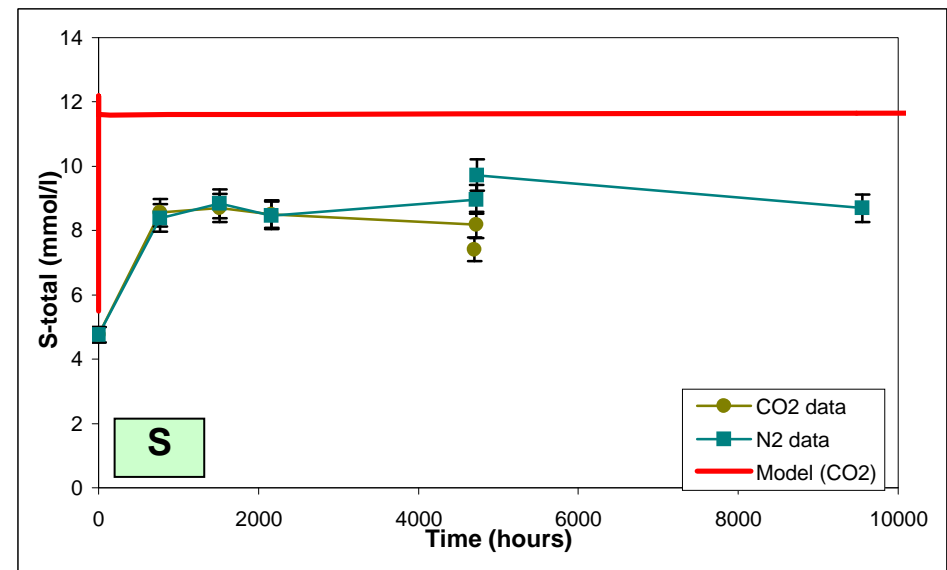
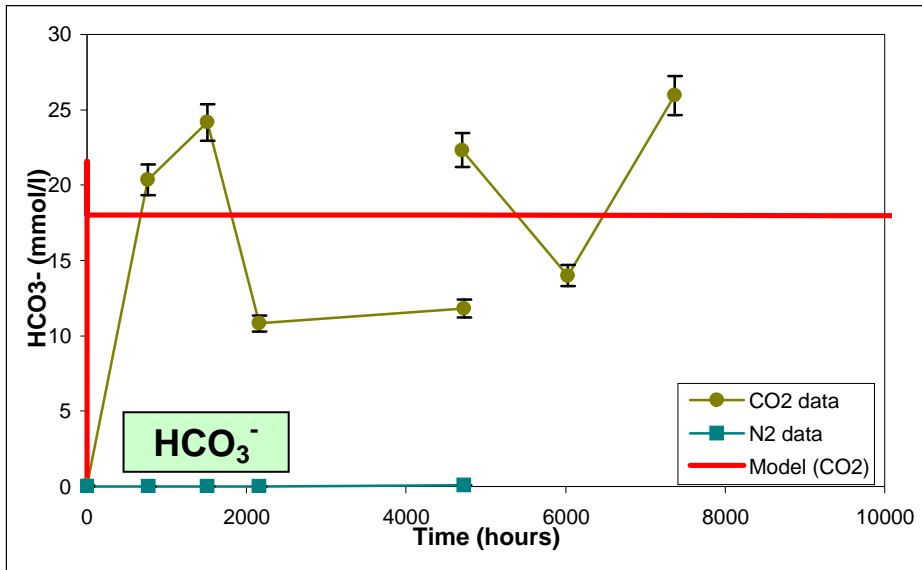
Bunter Formation (Tønder 4 well)



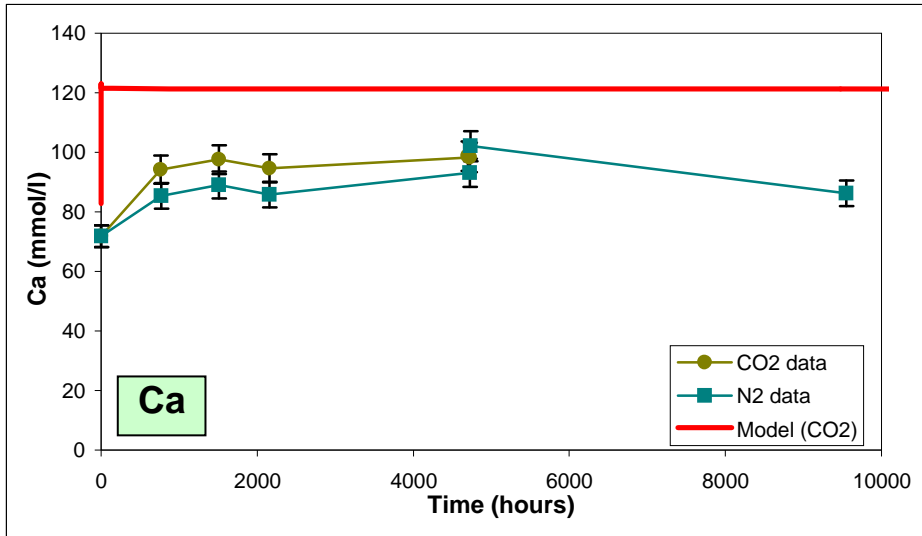
AQUA-DK, Forward model of laboratory experiments (1/3)

Model input:

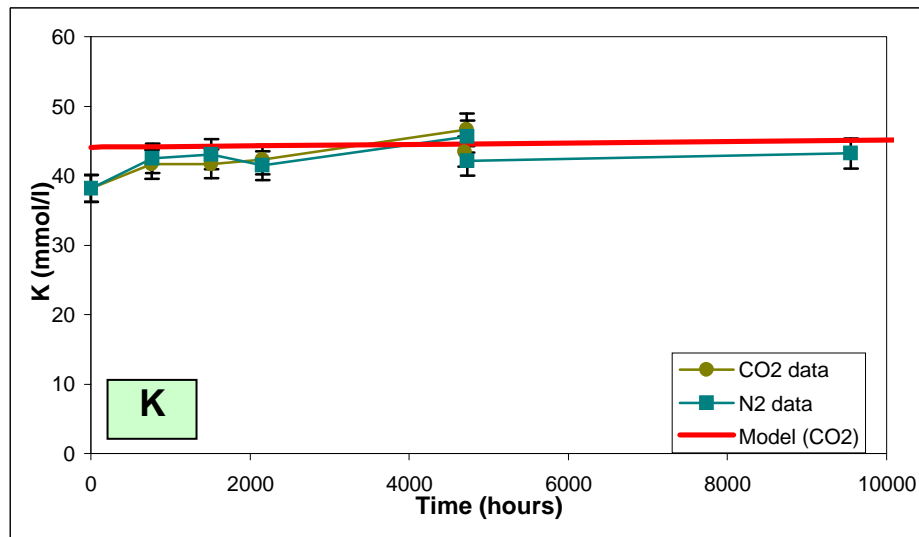
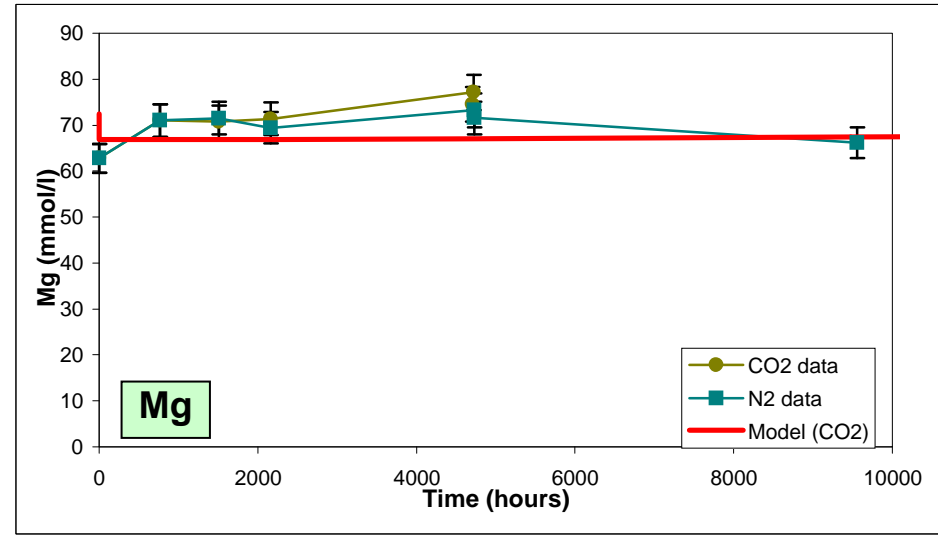
Mineral	SSA (m ² /g)	PHREEQC (vol %)
Chalcedony	0.03	37.8
K-feldspar	0.18	22.8
Albite	0.1	10.6
K-mica	0.05	7.4
Calcite	0.035	1.4
Illite	3.3	4.4
Anhydrite	0.1	1.8
Fluorite	0.1	2.6
Goethite	0.1	10.8
Kaolinite	2.6	0.4



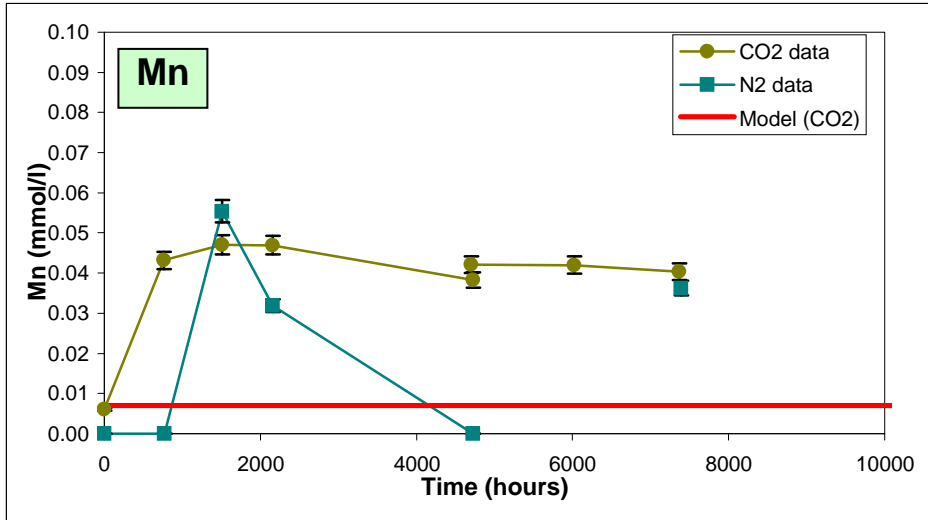
Bunter Formation (Tønder 4 well)



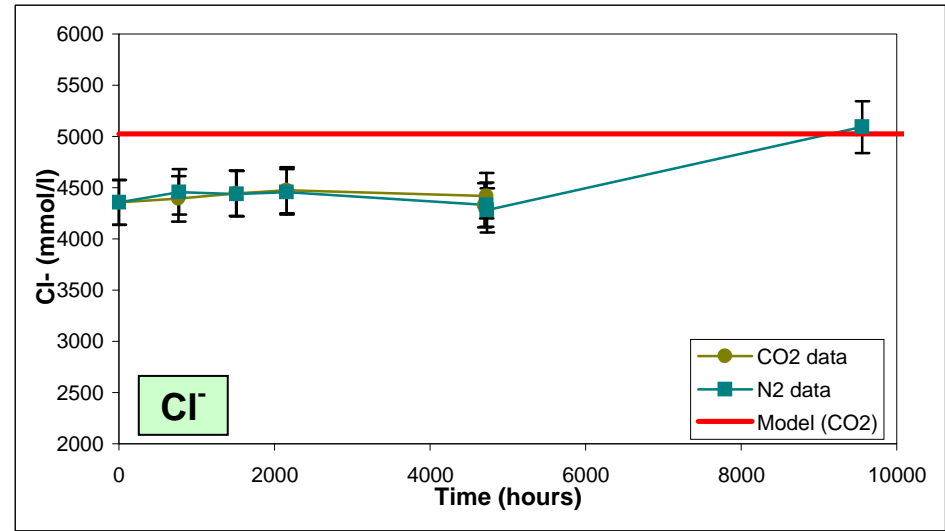
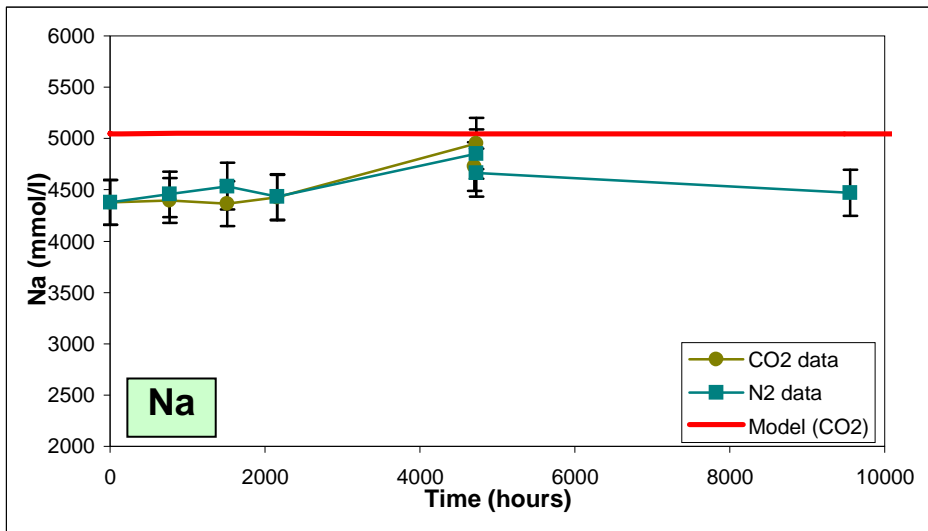
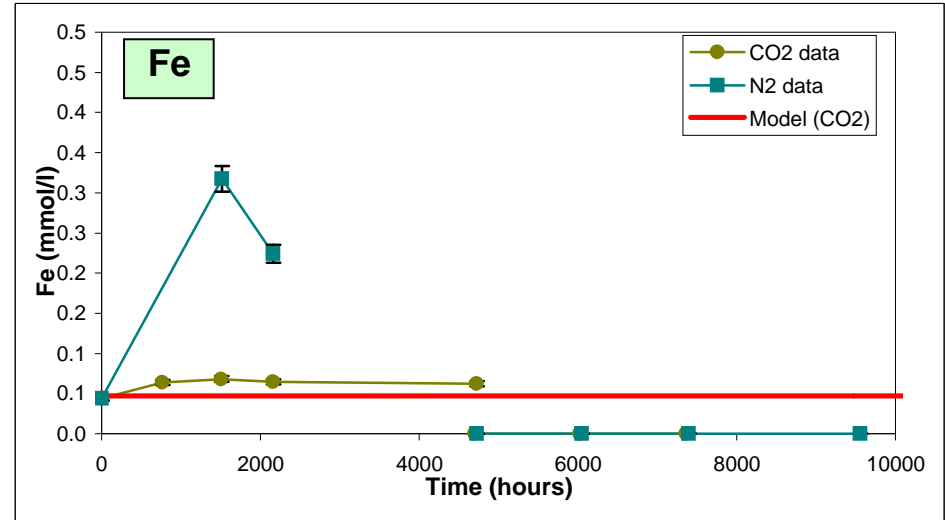
AQUA-DK, Forward model of laboratory experiments (2/3)



Bunter Formation (Tønder 4 well)

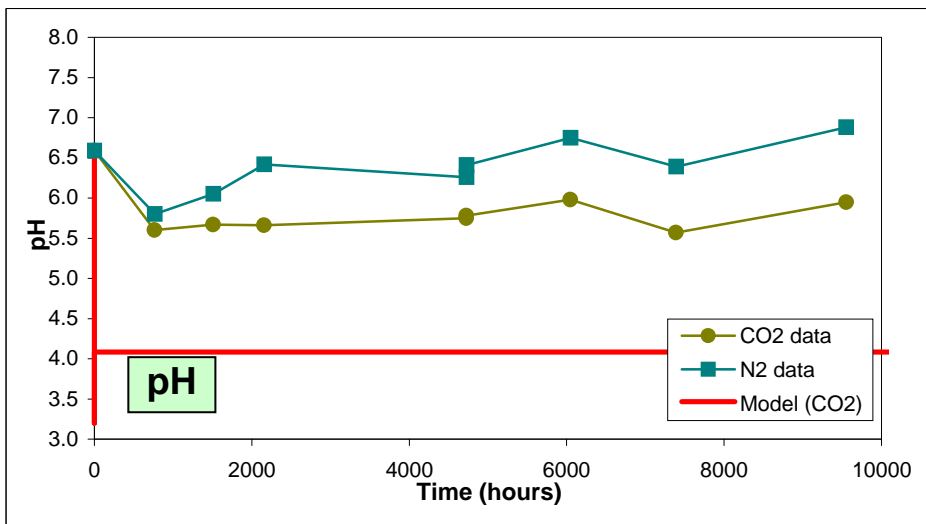


AQUA-DK, Forward model of laboratory experiments (3/3)



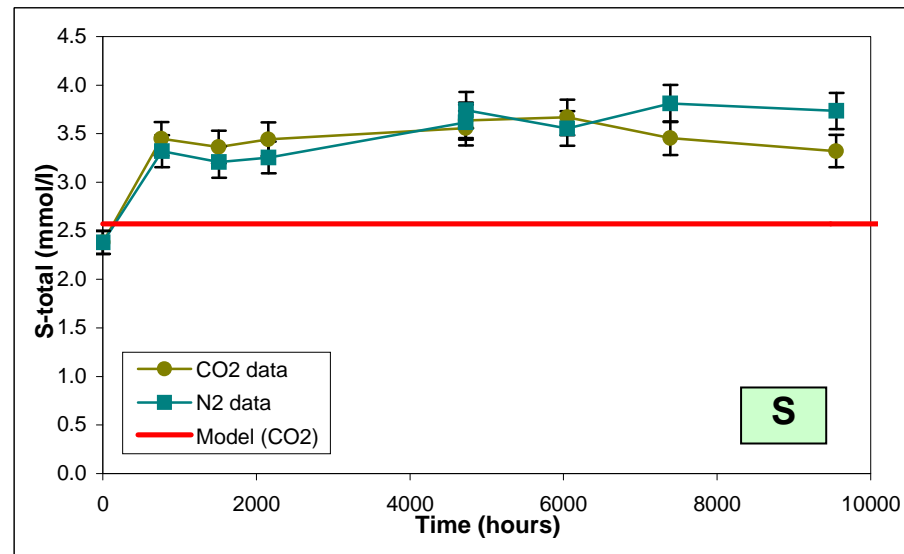
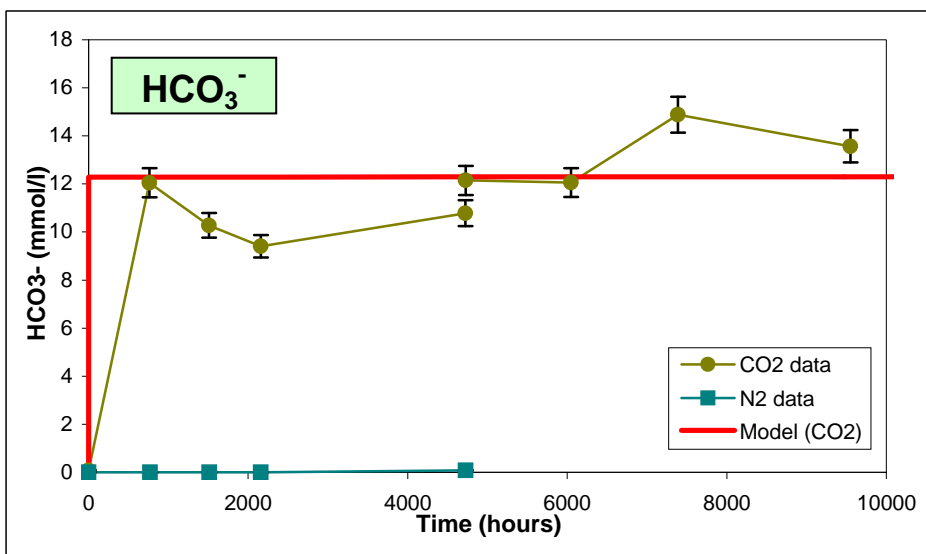
Skagerrak Formation (Vedsted 1 well)

AQUA-DK, Forward model of laboratory experiments (1/3)

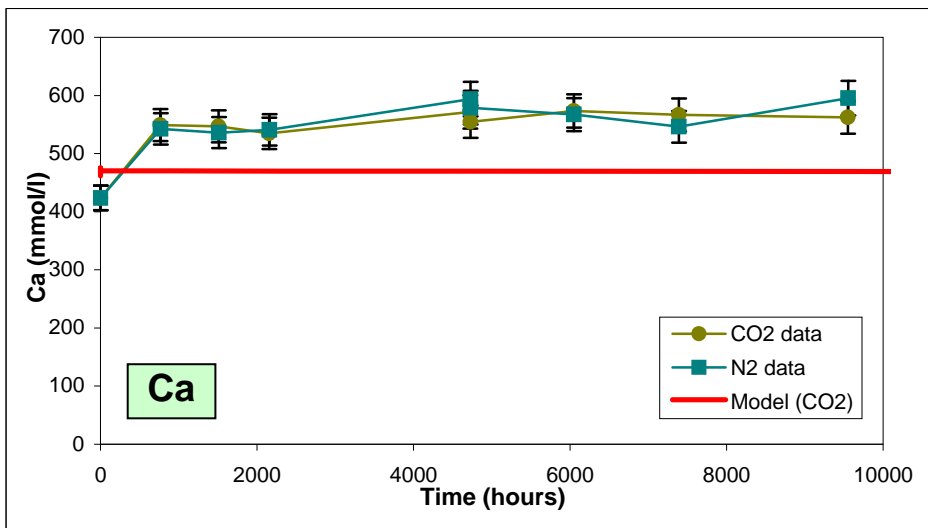


Model input:

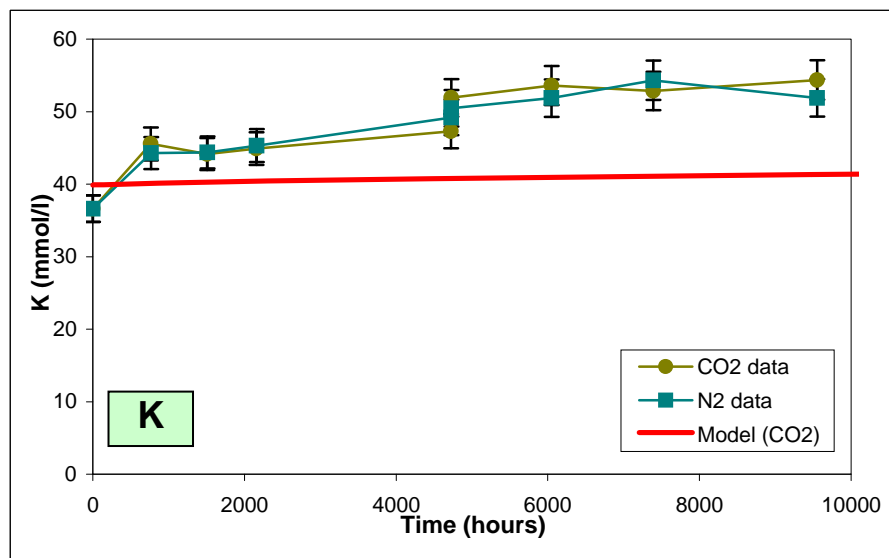
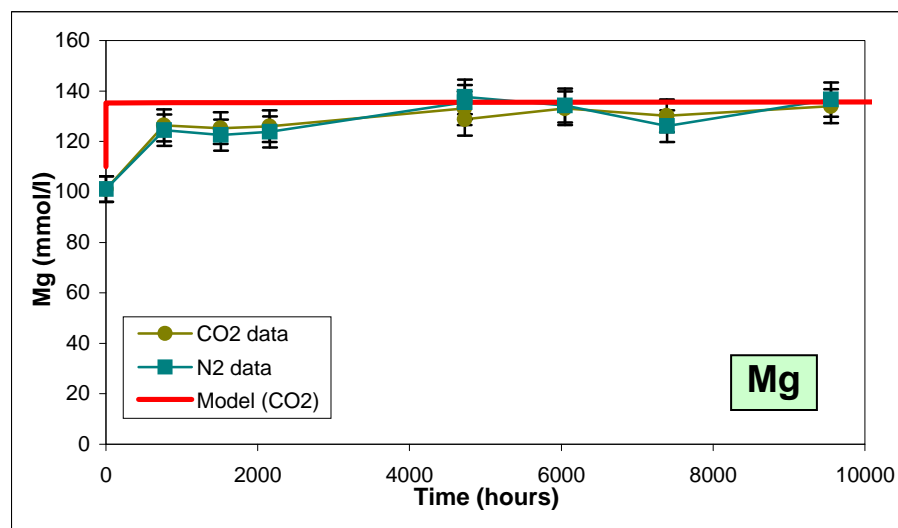
Mineral	SSA (m ² /g)	PHREEQC (vol %)
Chalcedony	0.03	73.4
K-feldspar	0.18	8.9
Albite	0.1	6.1
K-mica	0.05	0.4
Calcite	0.035	0
Dolomite	0.05	1.6
Ankerite	0.05	1.6
Illite	3.3	1.8
Kaolinite	2.6	6.2



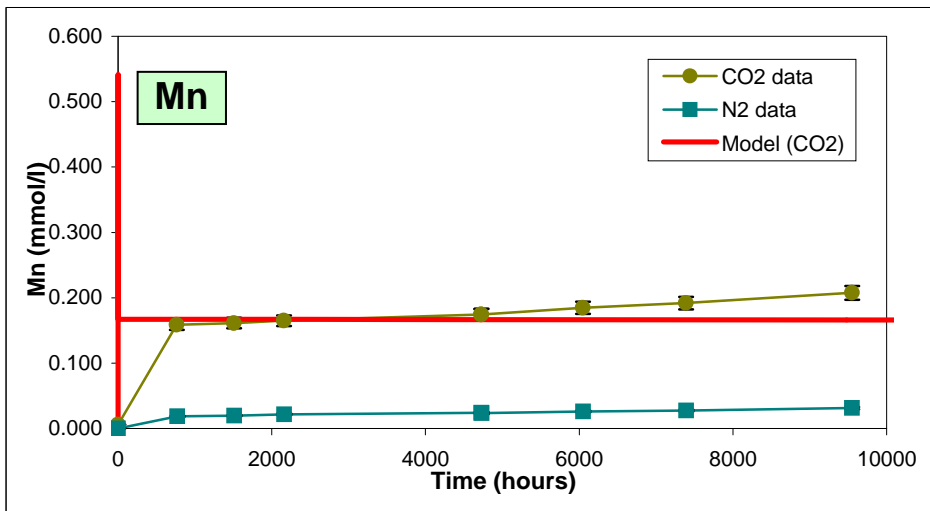
Skagerrak Formation (Vedsted 1 well)



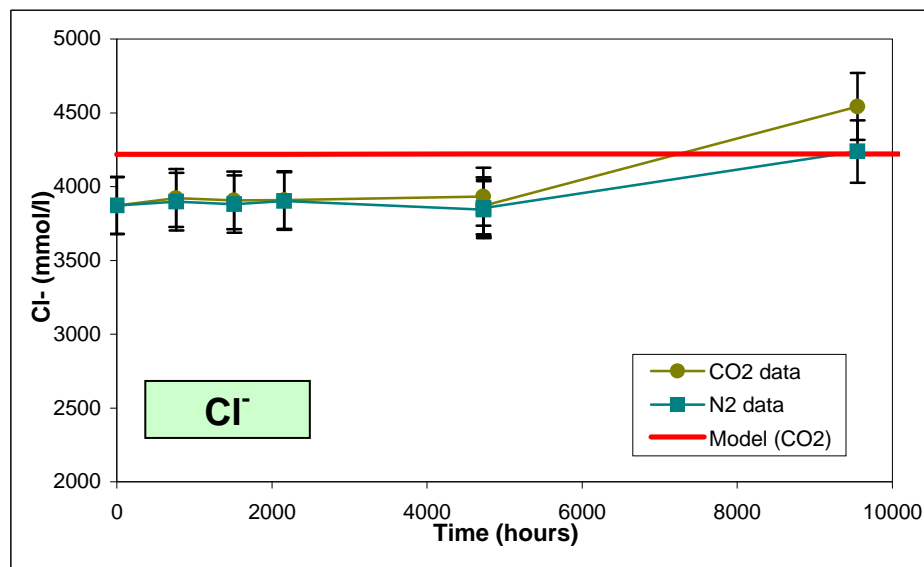
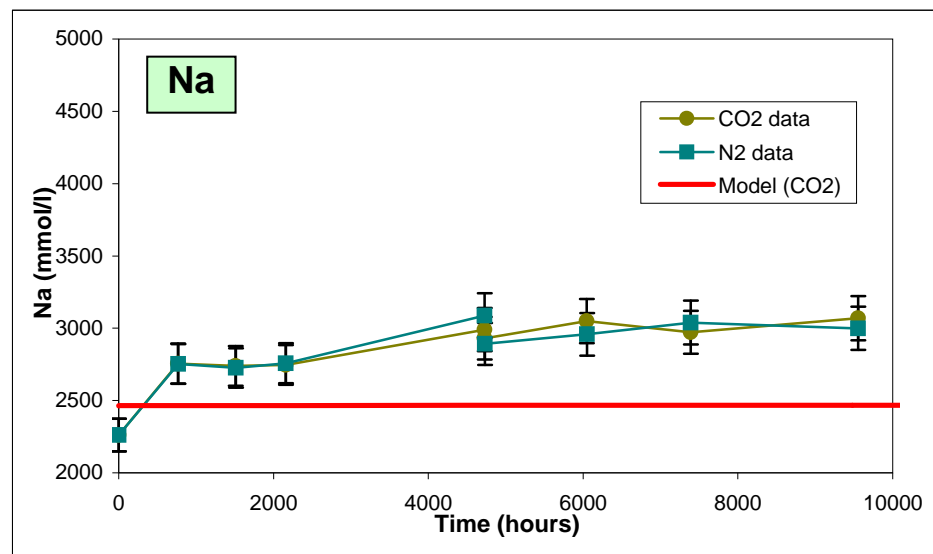
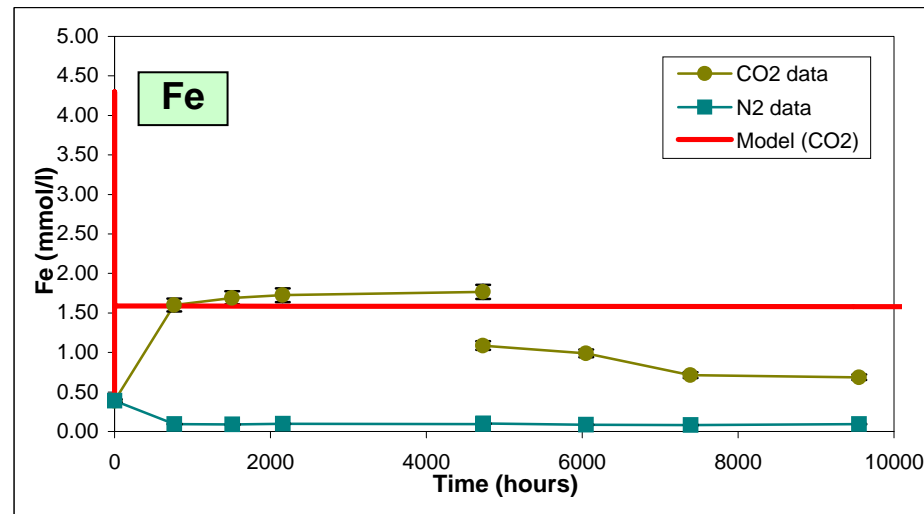
AQUA-DK, Forward model of laboratory experiments (2/3)



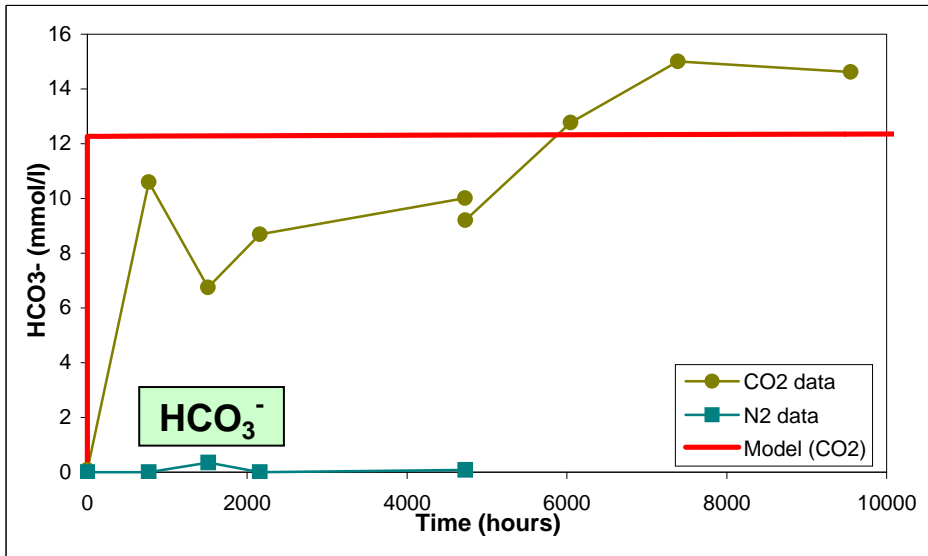
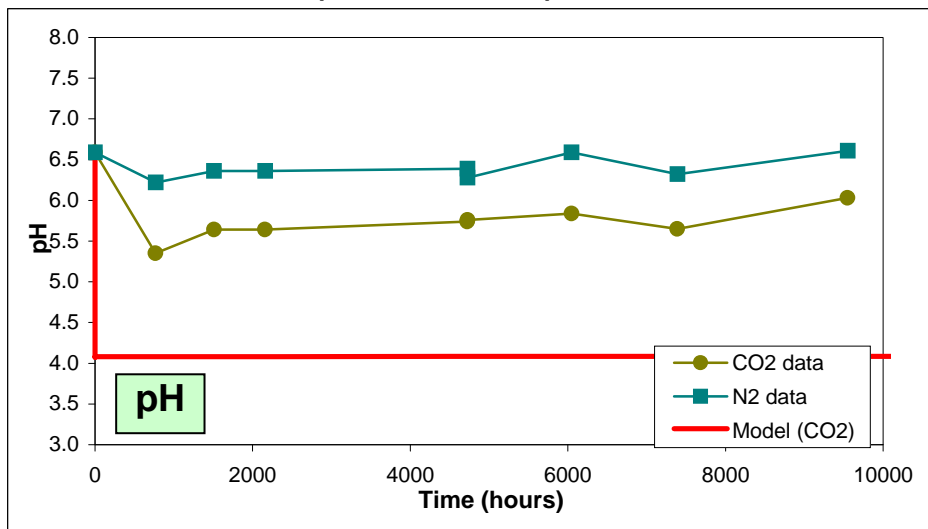
Skagerrak Formation (Vedsted 1 well)



AQUA-DK, Forward model of laboratory experiments (3/3)



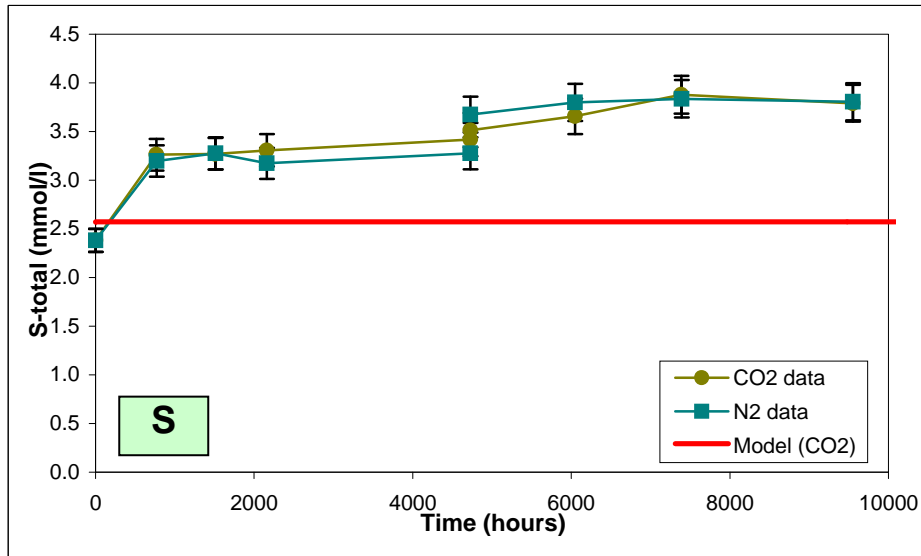
Gassum Formation (Vedsted 1 well)



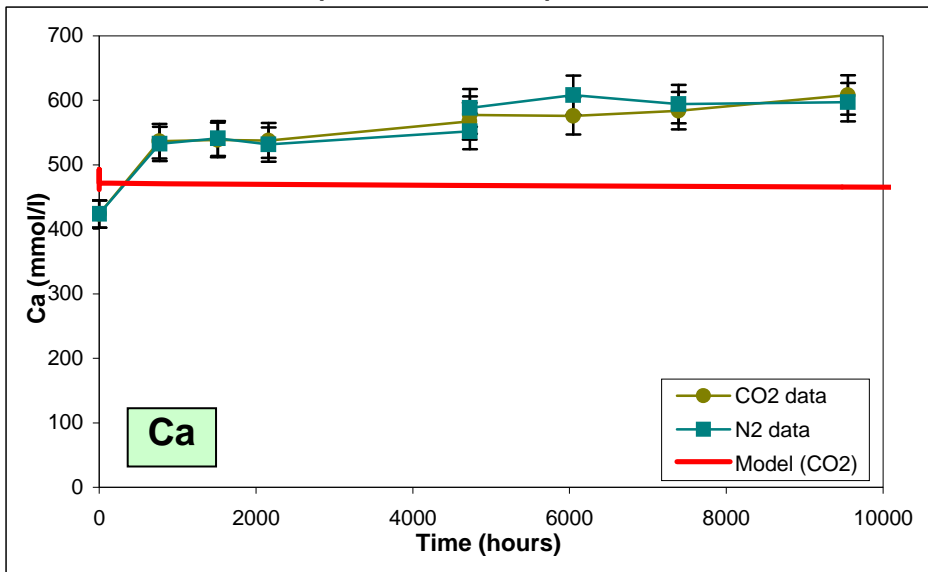
AQUA-DK, Forward model of laboratory experiments (1/3)

Model input:

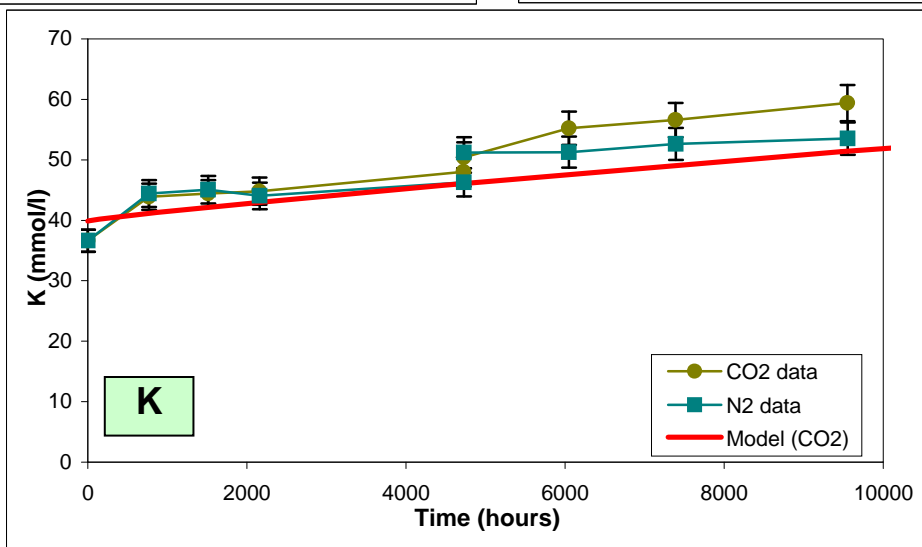
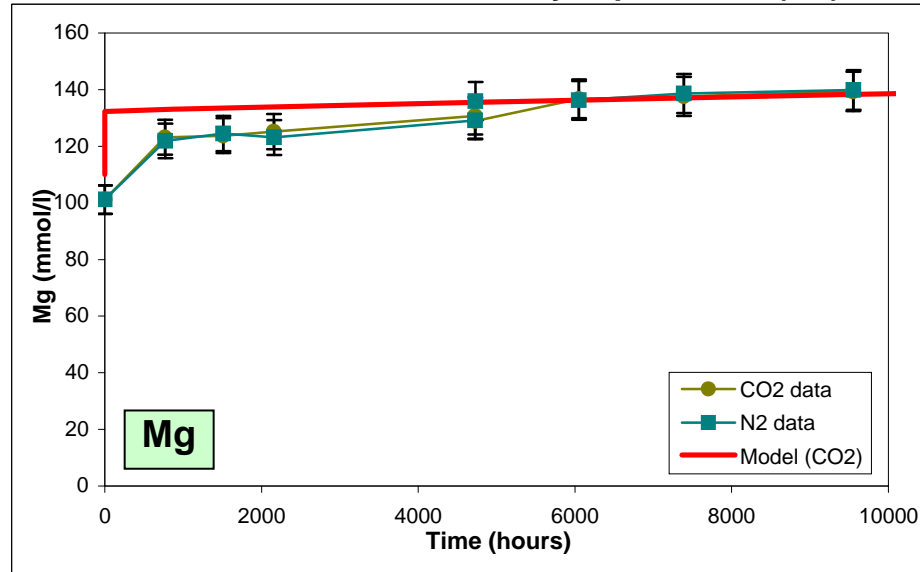
Mineral	SSA (m ² /g)	PHREEQC (vol %)
Chalcedony	0.03	63.2
K-feldspar	0.018	6.8
Albite	0.1	10.6
K-mica	0.005	1.4
Calcite	0.035	2
Dolomite	0.1	1.4
Siderite	0.1	0.4
Ankerite	0.1	1.2
Illite	33	7
Kaolinite	2.6	6



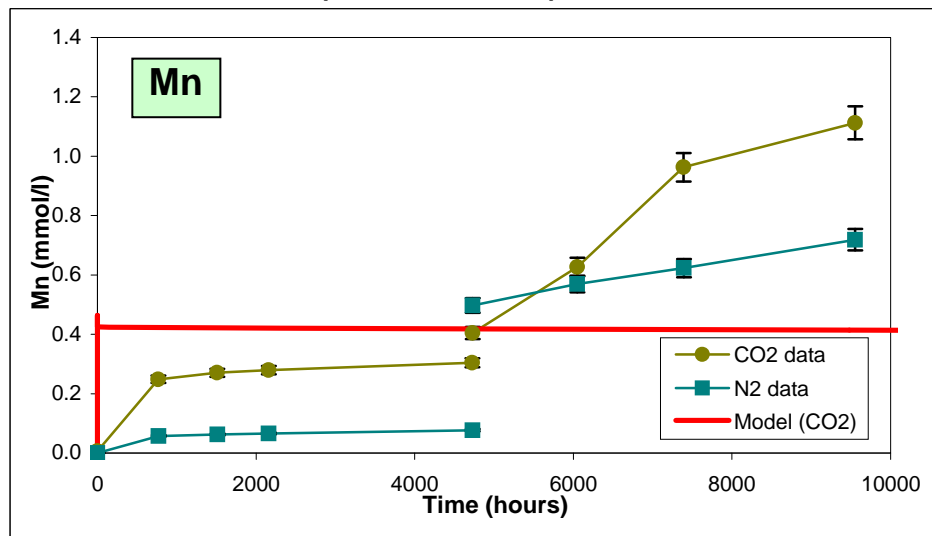
Gassum Formation (Vedsted 1 well)



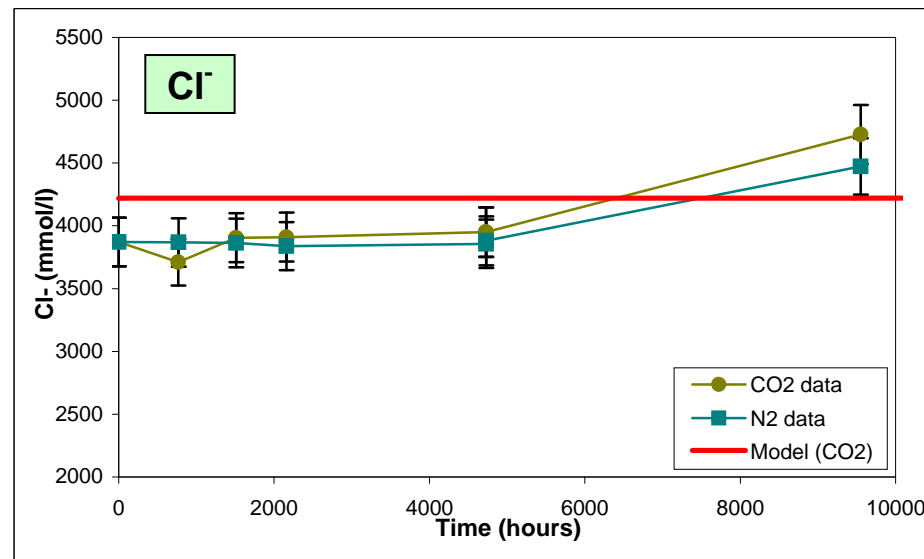
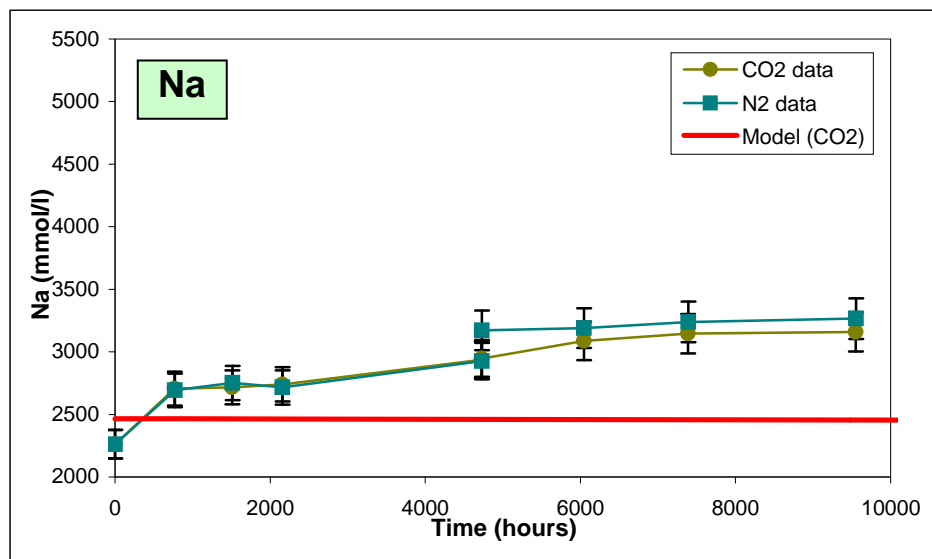
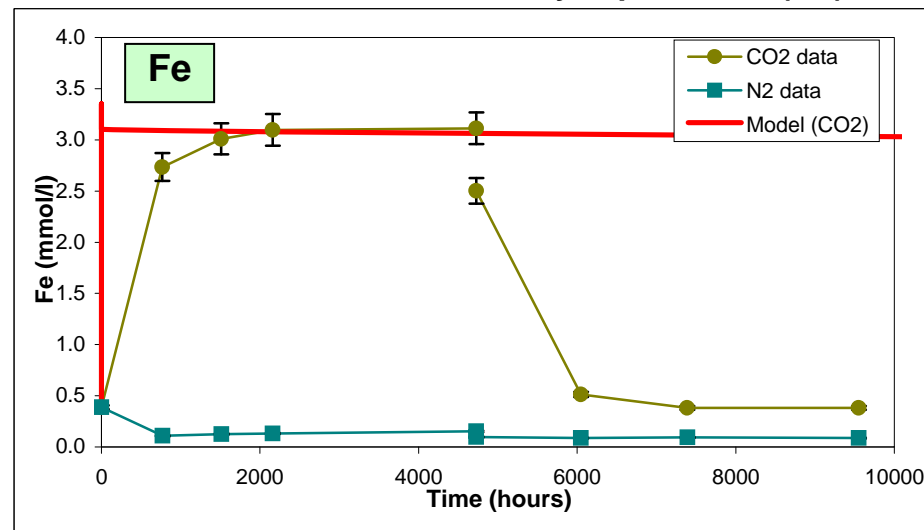
AQUA-DK, Forward model of laboratory experiments (2/3)



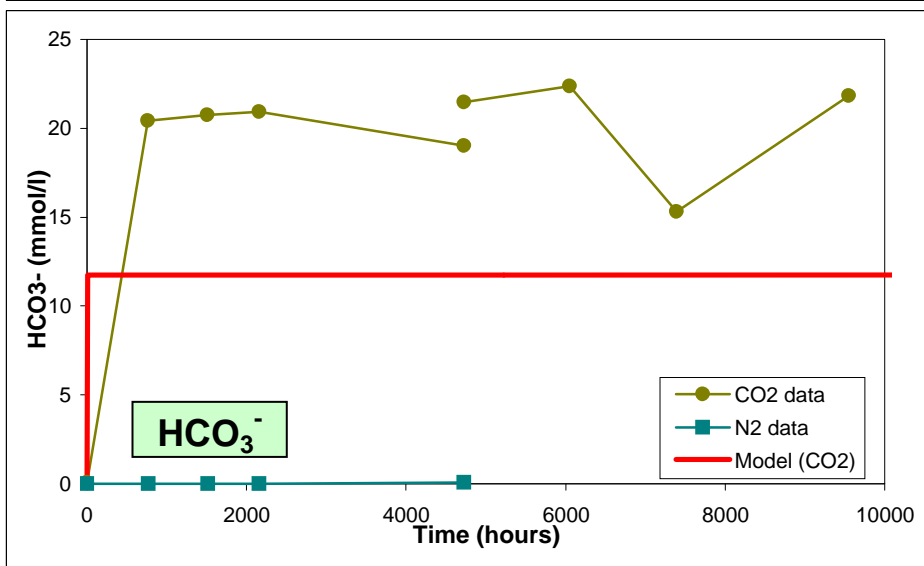
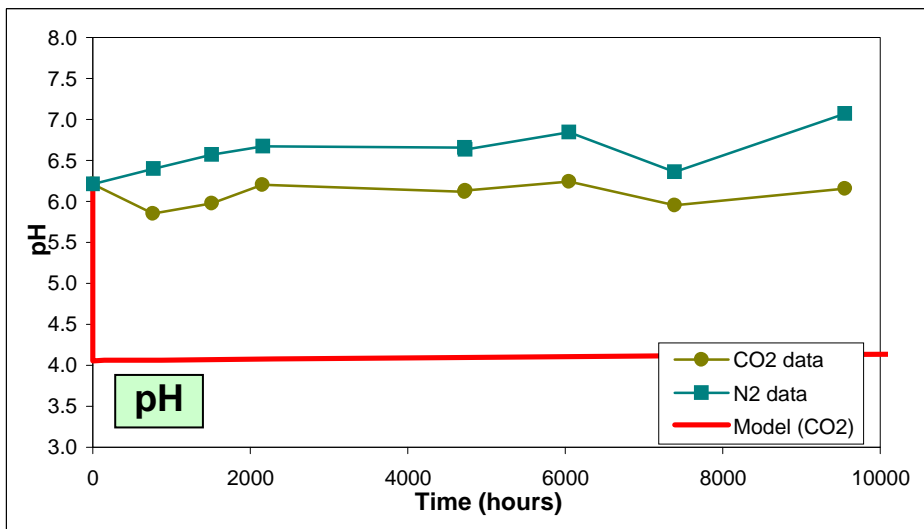
Gassum Formation (Vedsted 1 well)



AQUA-DK, Forward model of laboratory experiments (3/3)



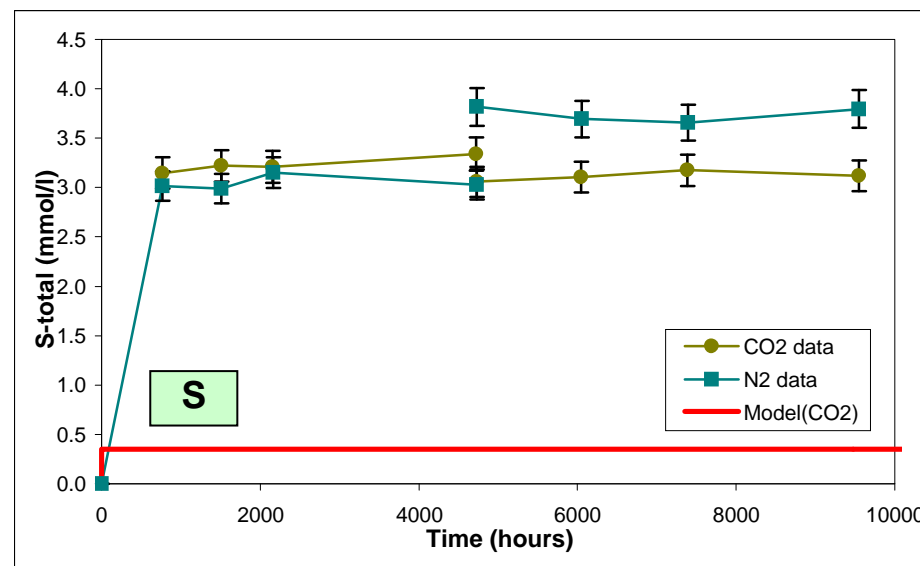
Gassum Formation (Stenlille 18 well)



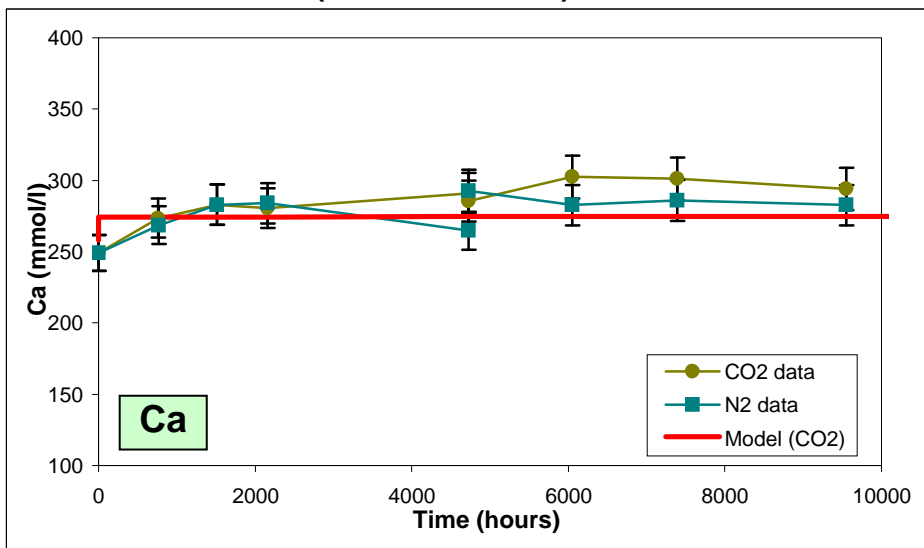
AQUA-DK, Forward model of laboratory experiments (1/3)

Model input:

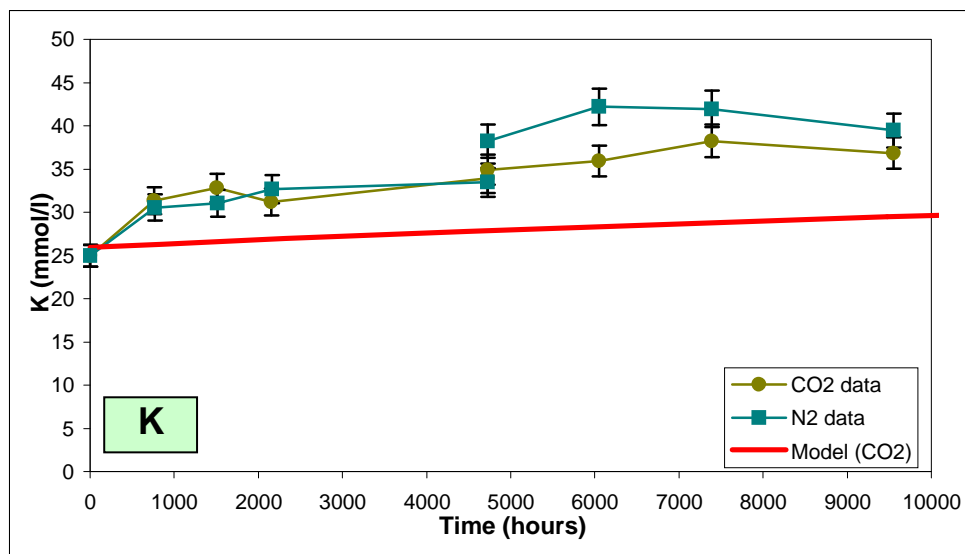
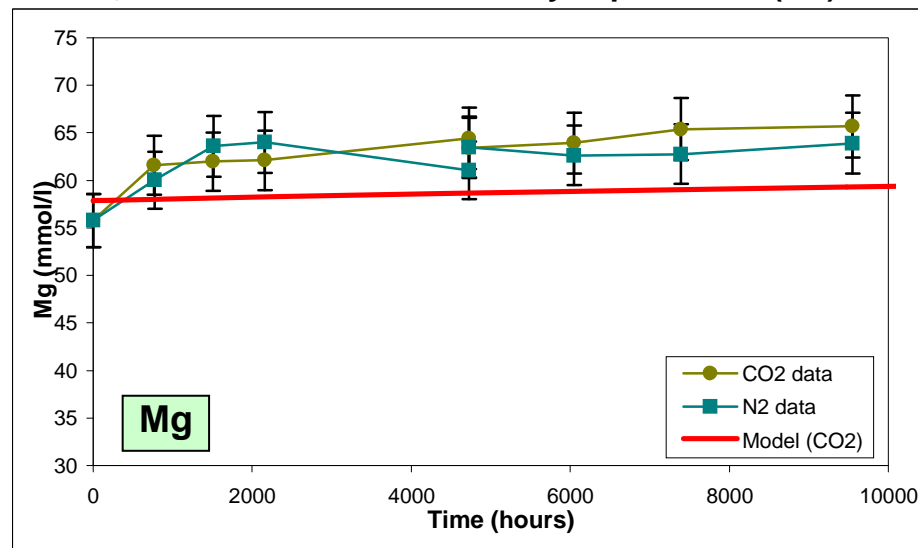
Mineral	SSA (m ² /g)	PHREEQC (vol %)
Chalcedony	0.03	90.2
K-feldspar	0.18	0.6
Albite	0.1	0.8
K-mica	0.05	0
Calcite	0.035	0.6
Illite	13	2.2
Kaolinite	2.6	5.6



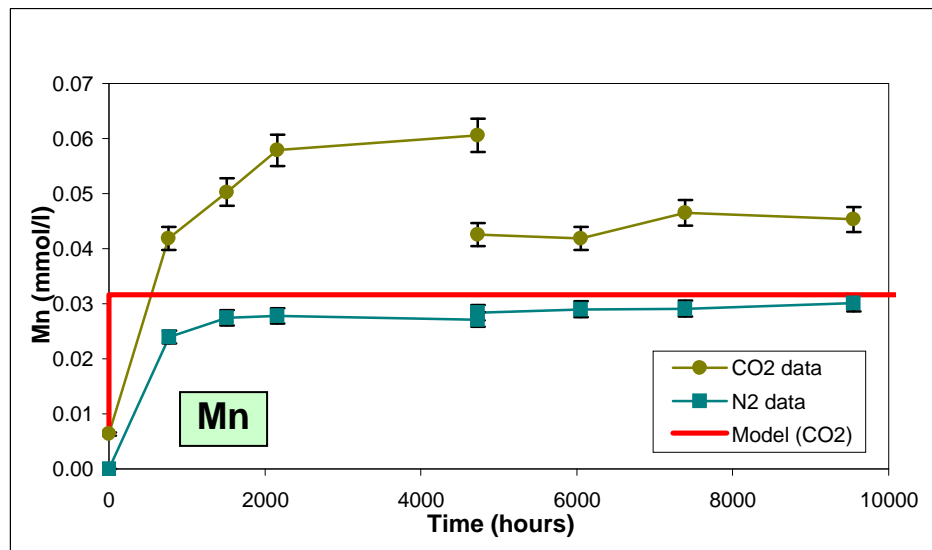
Gassum Formation (Stenlille 18 well)



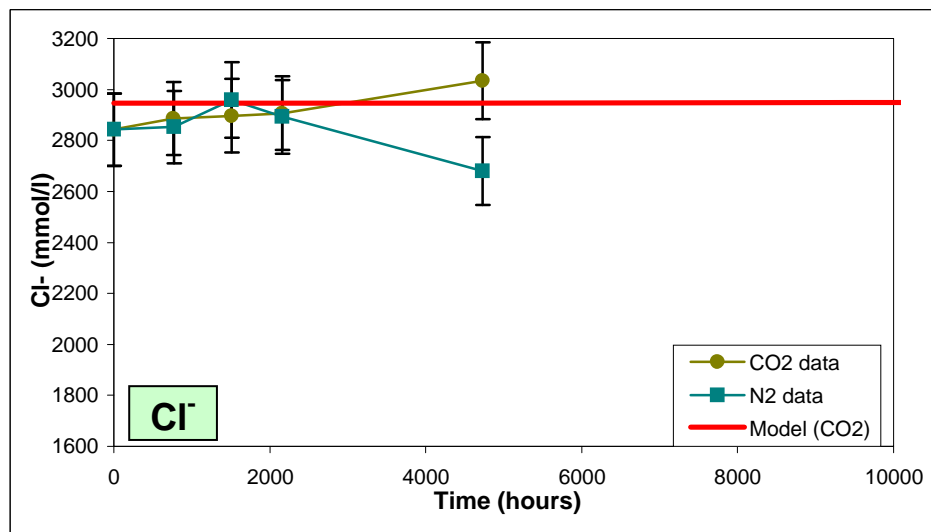
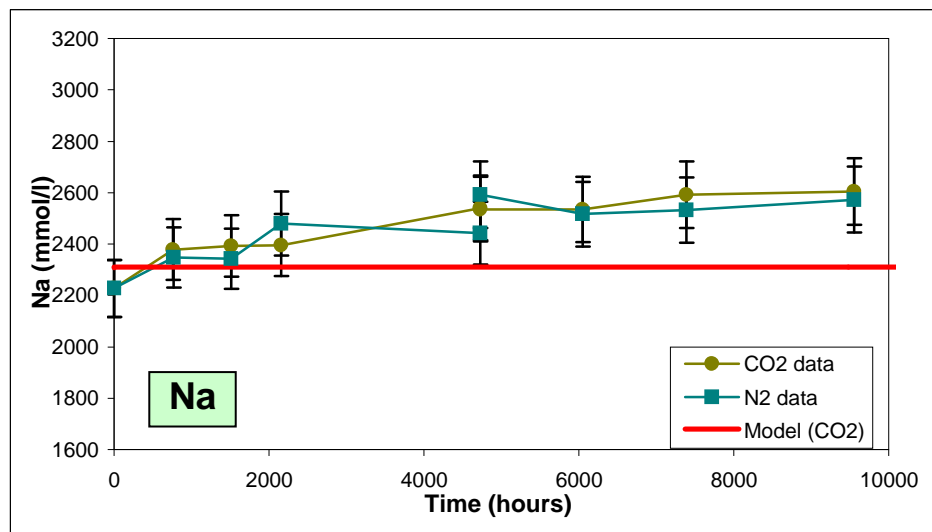
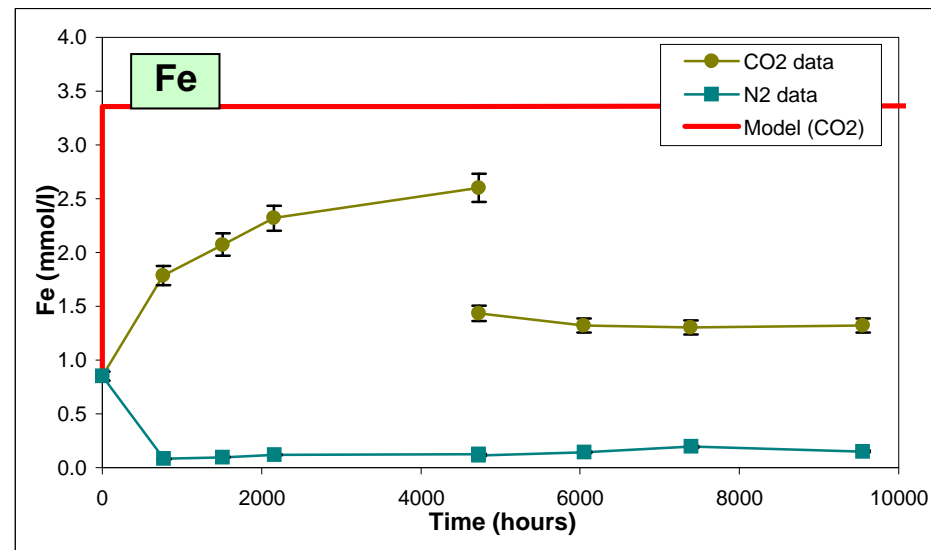
AQUA-DK, Forward model of laboratory experiments (2/3)



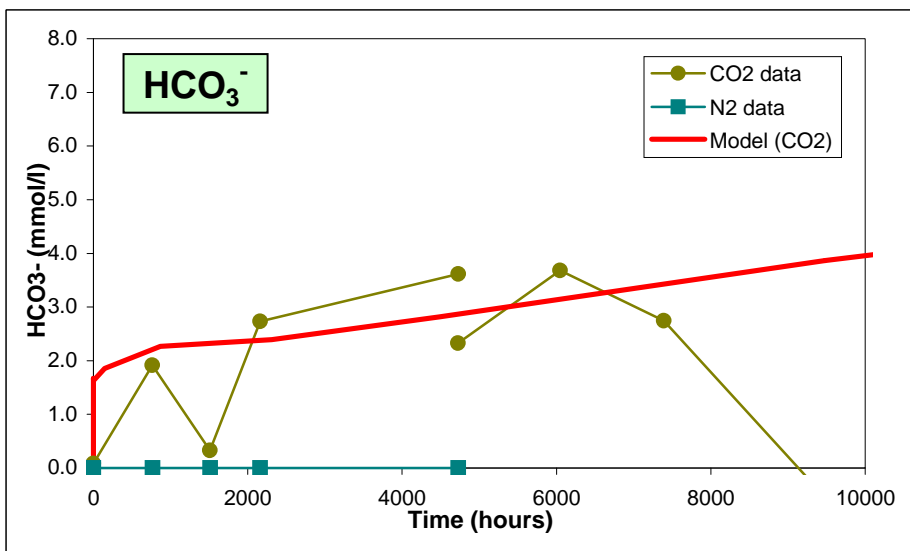
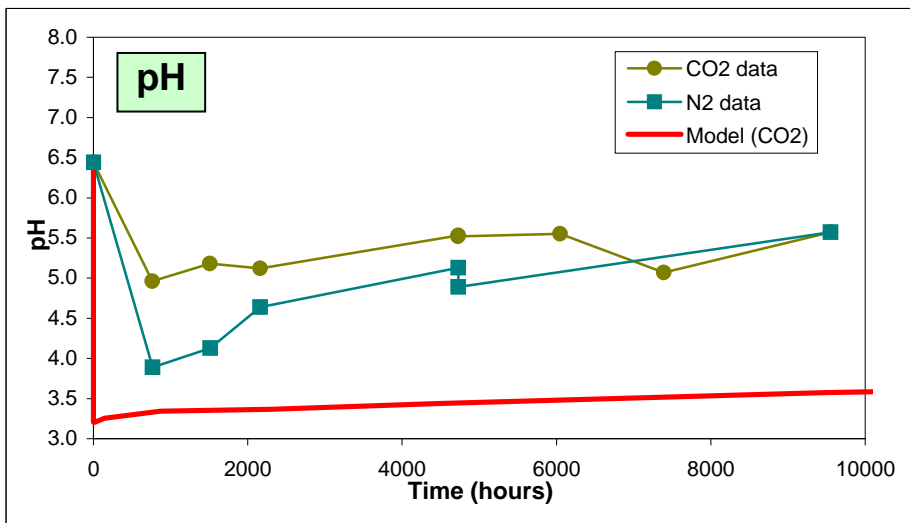
Gassum Formation (Stenlille 18 well)



AQUA-DK, Forward model of laboratory experiments (3/3)



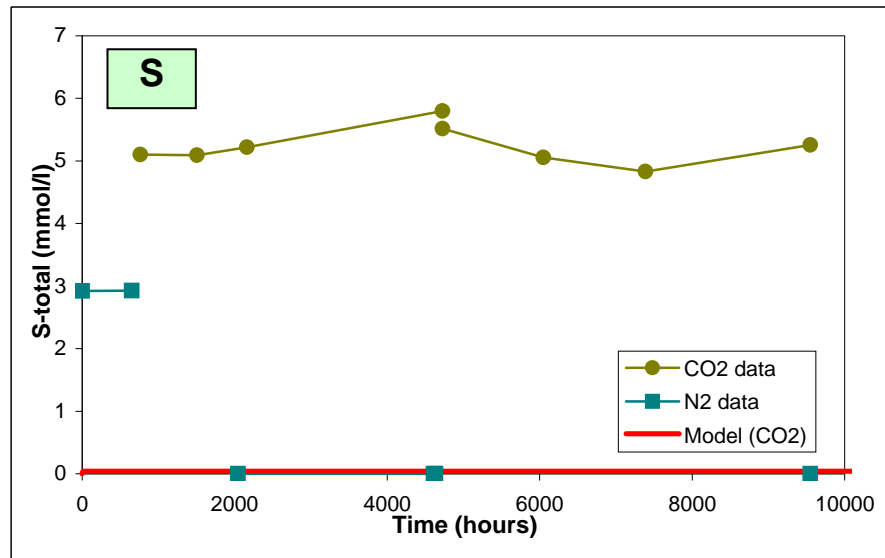
Haldager Formation (Vedsted 1 well)



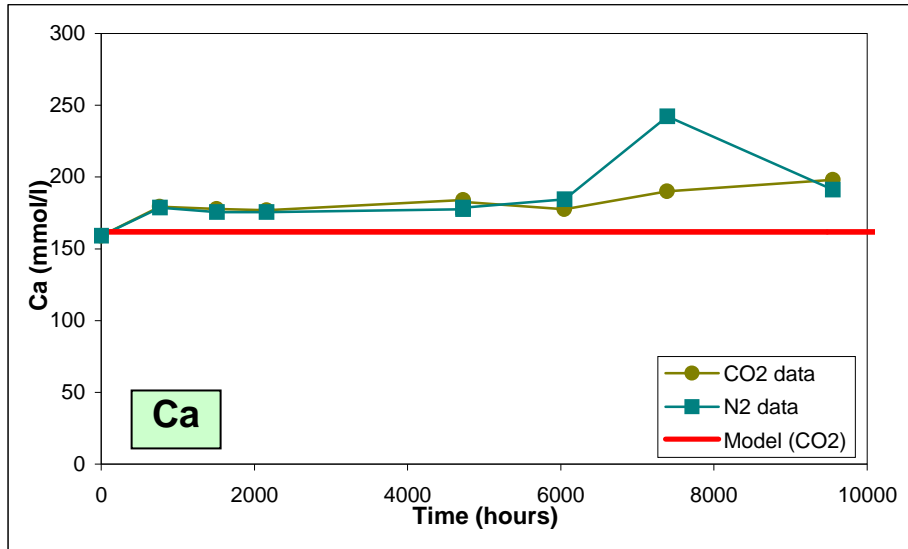
AQUA-DK, Forward model of laboratory experiments (1/3)

Model input:

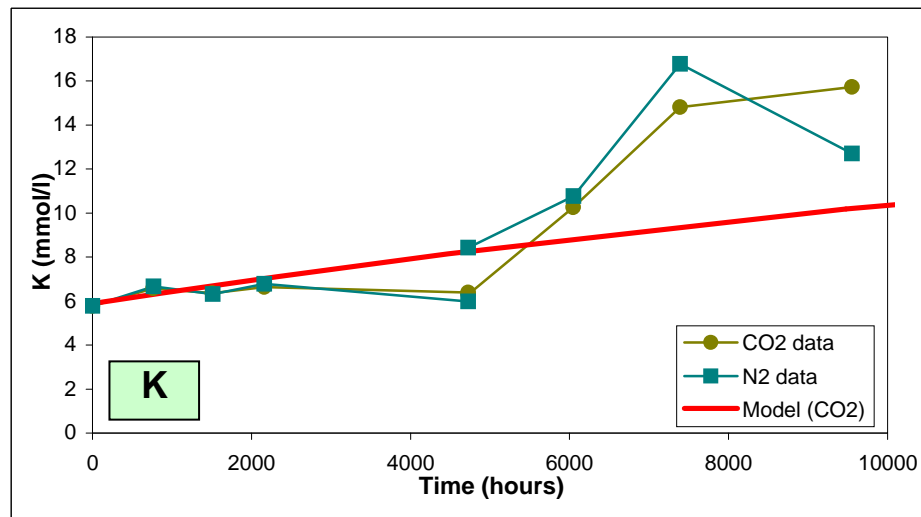
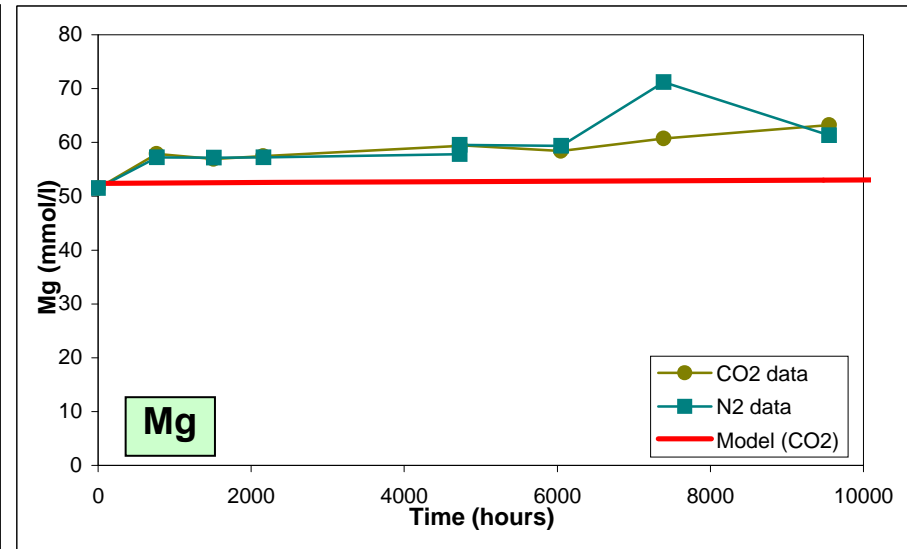
Mineral	SSA (m ² /g)	PHREEQC (vol %)
Chalcedony	0.03	85.4
K-feldspar	0.18	8
Albite	0.1	0.6
K-mica	0.05	0.6
Illite	3.3	2.4
Pyrite	0.1	0.2
Kaolinite	2.6	2.8



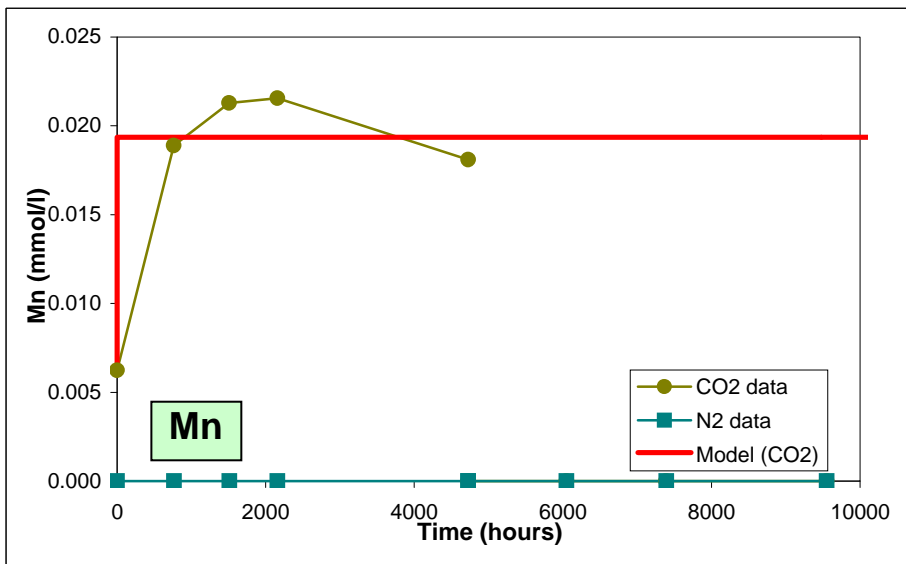
Haldager Formation (Vedsted 1 well)



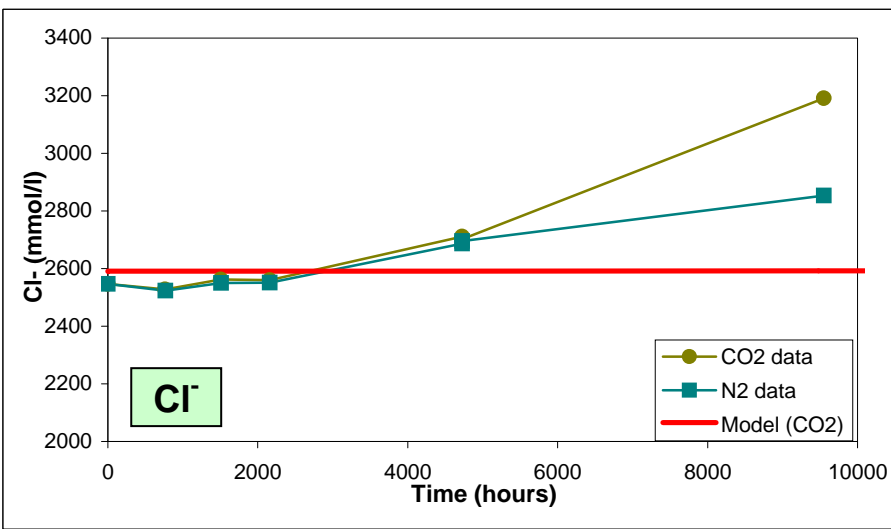
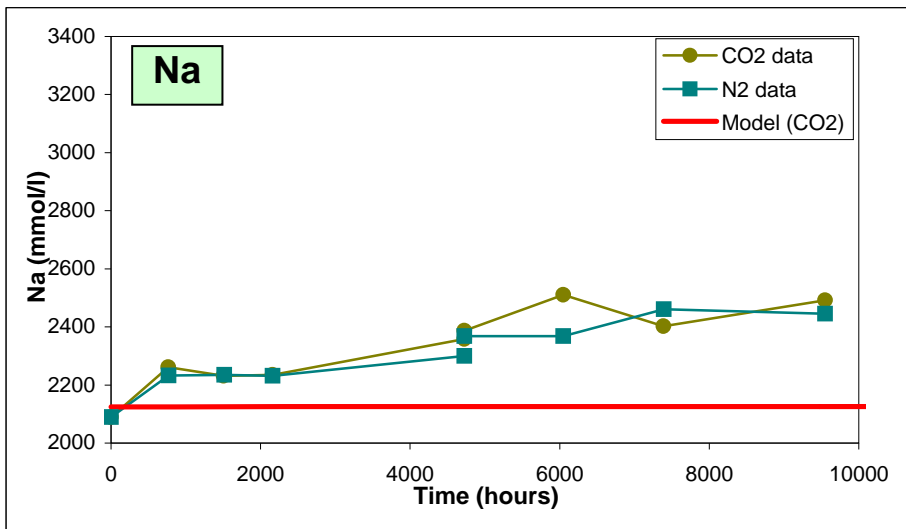
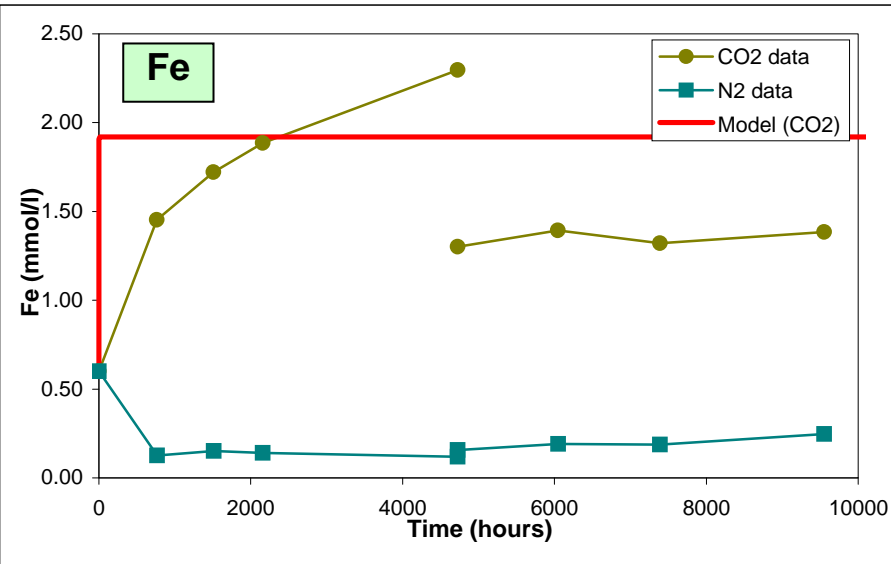
AQUA-DK, Forward model of laboratory experiments (2/3)



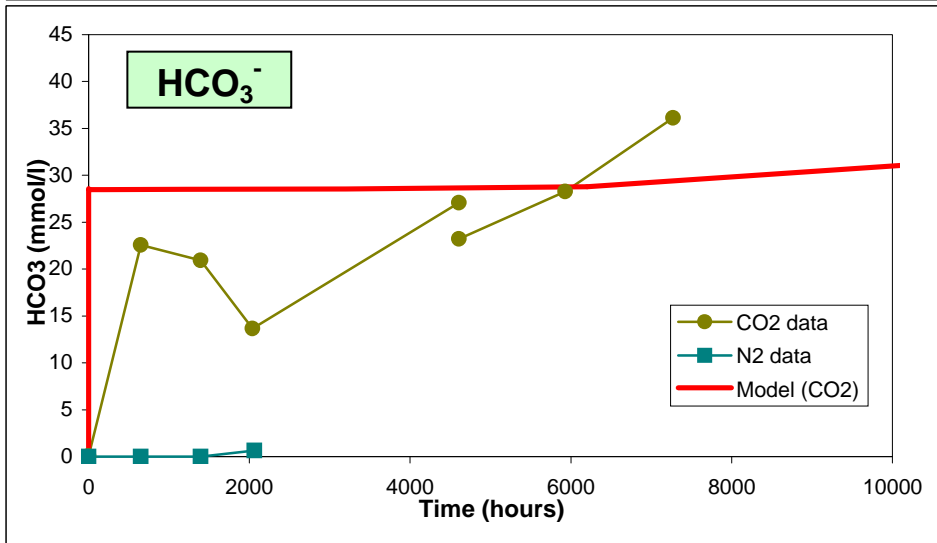
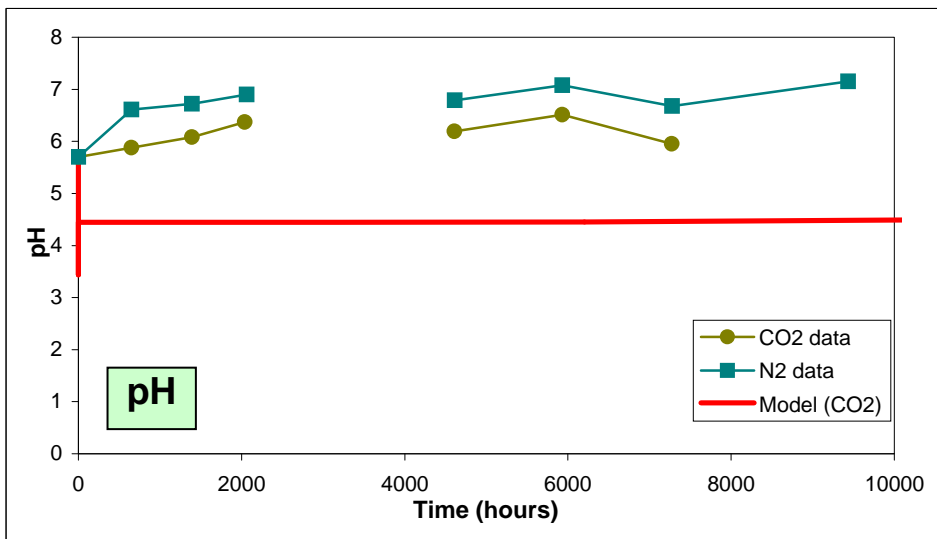
Haldager Formation (Vedsted 1 well)



AQUA-DK, Forward model of laboratory experiments (3/3)



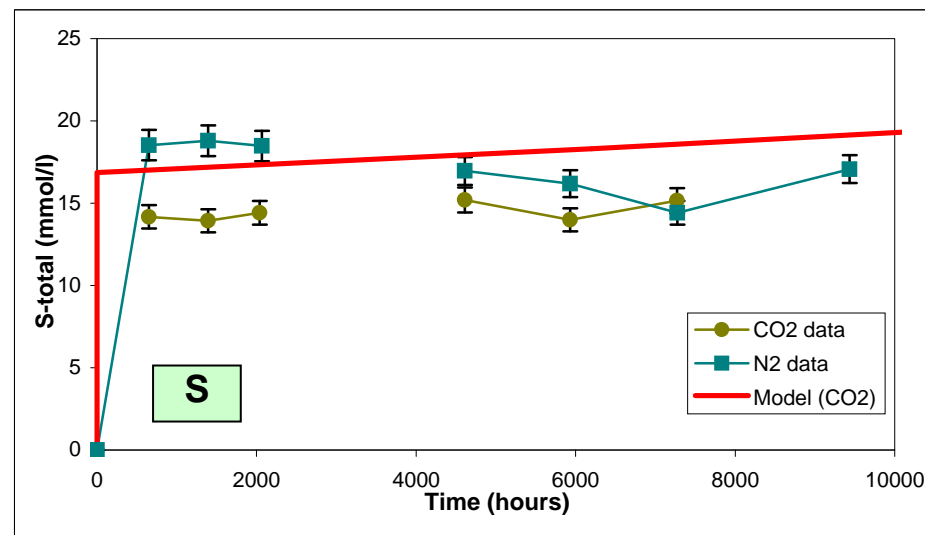
Børglum Formation (Haldager 1 well)



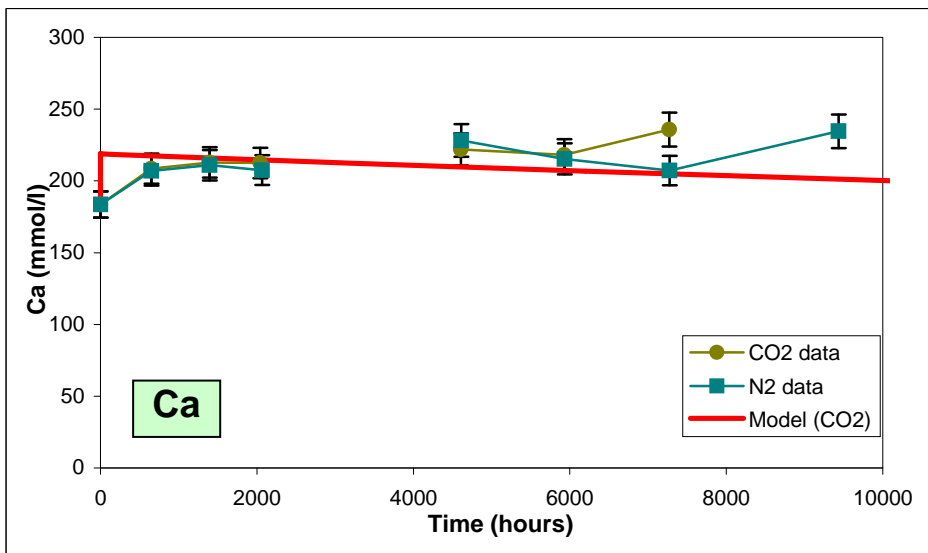
AQUA-DK, Forward model of laboratory experiments (1/3)

Model input:

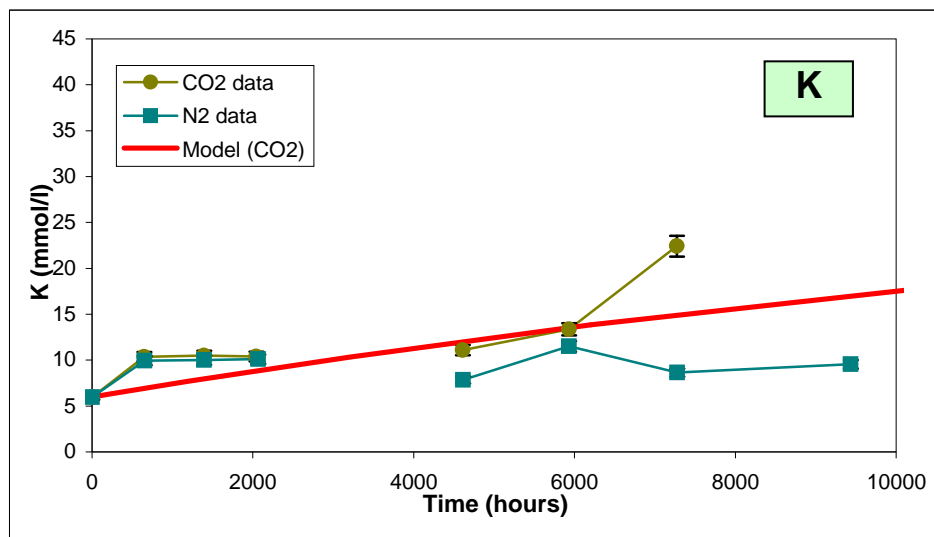
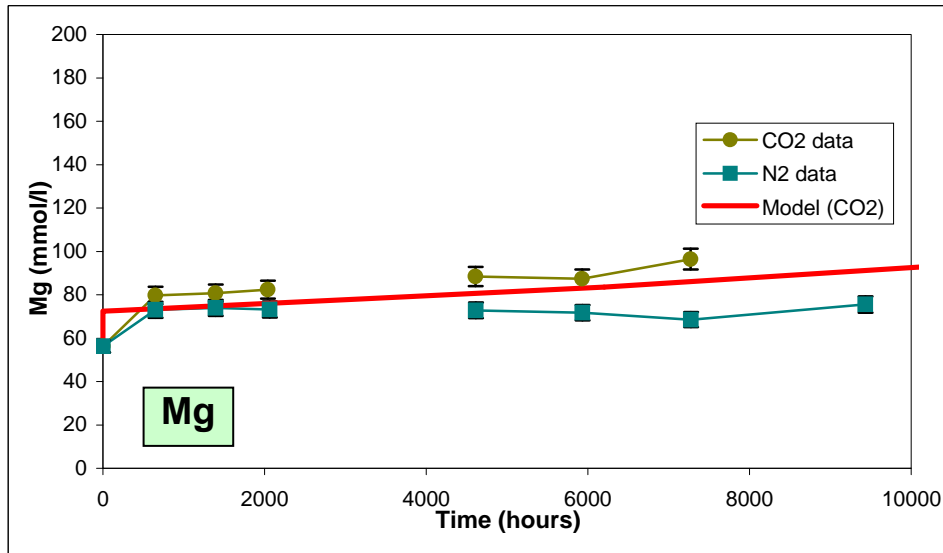
Mineral	SSA (m ² /g)	PHREEQC (vol %)
Chalcedony	0.03	28.2
K-feldspar	0.18	5.2
Albite	0.1	3.9
Dolomite	0.1	2.1
Illite	8.2	18.3
Ca-mont.	3	4.8
Chlorite	0.4	5.8
Kaolinite	2.6	31.7



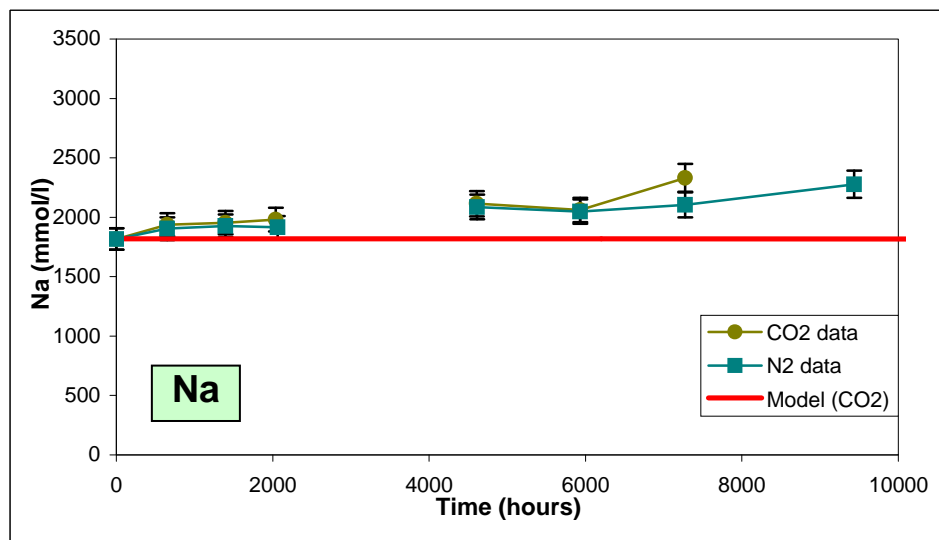
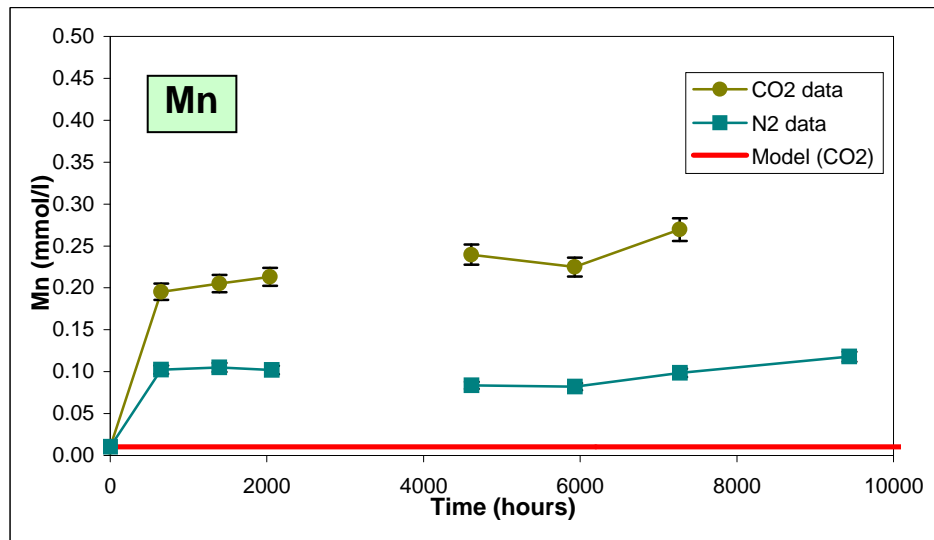
Børglum Formation (Haldager 1 well)



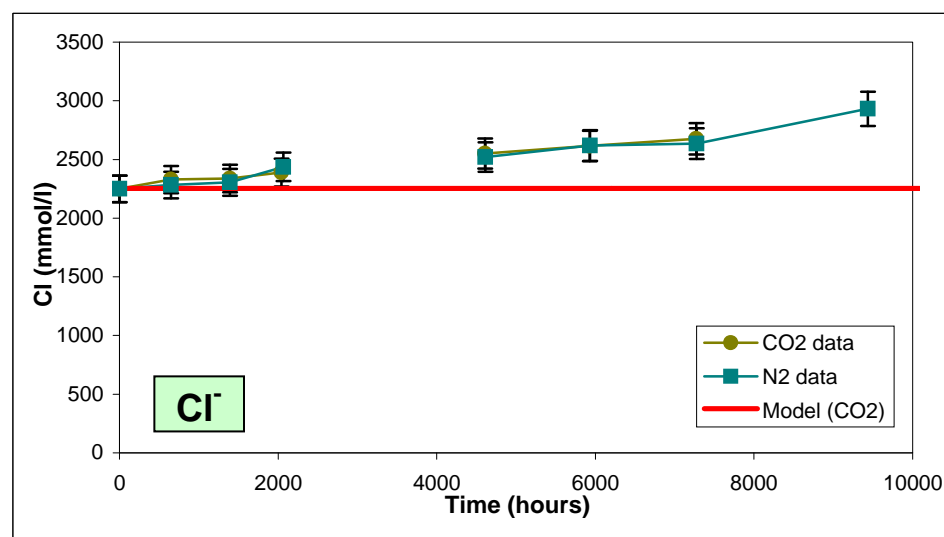
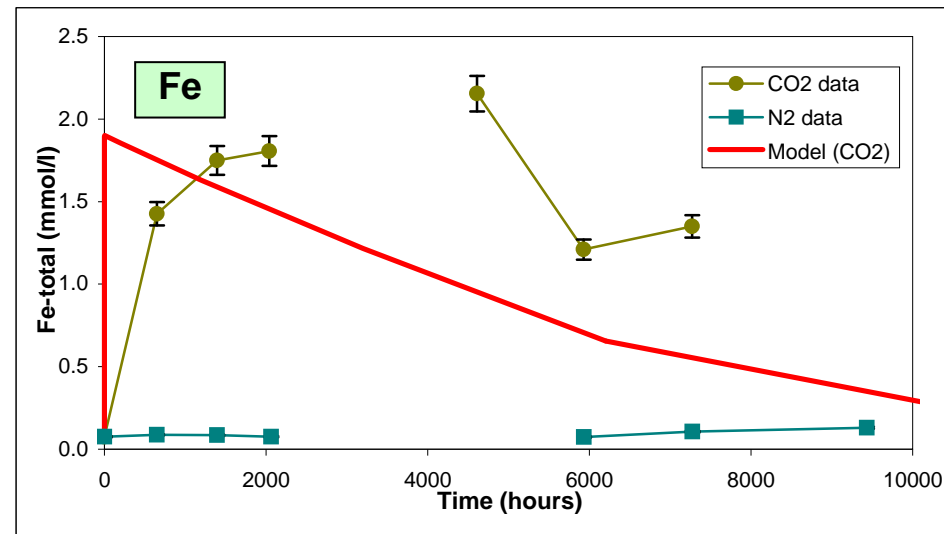
AQUA-DK, Forward model of laboratory experiments (2/3)



Børglum Formation (Haldager 1 well)

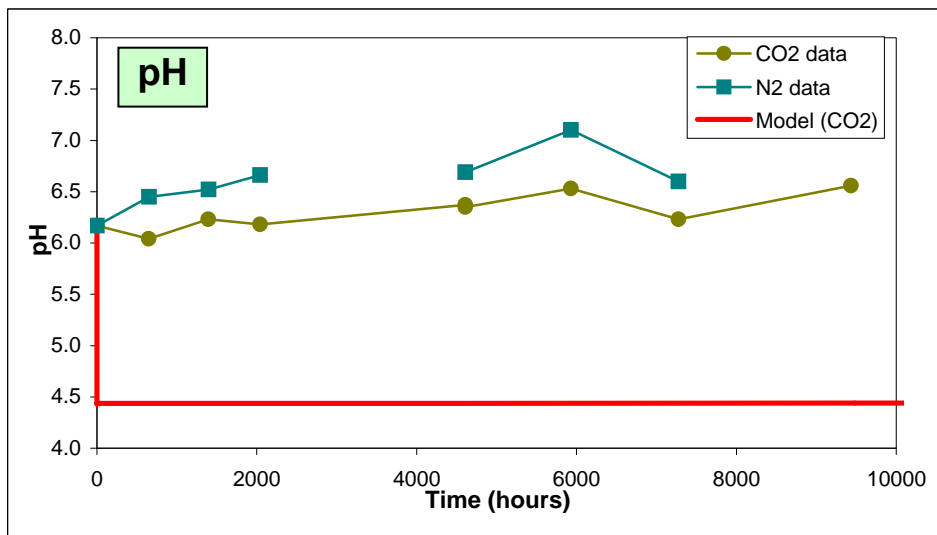


AQUA-DK, Forward model of laboratory experiments (3/3)



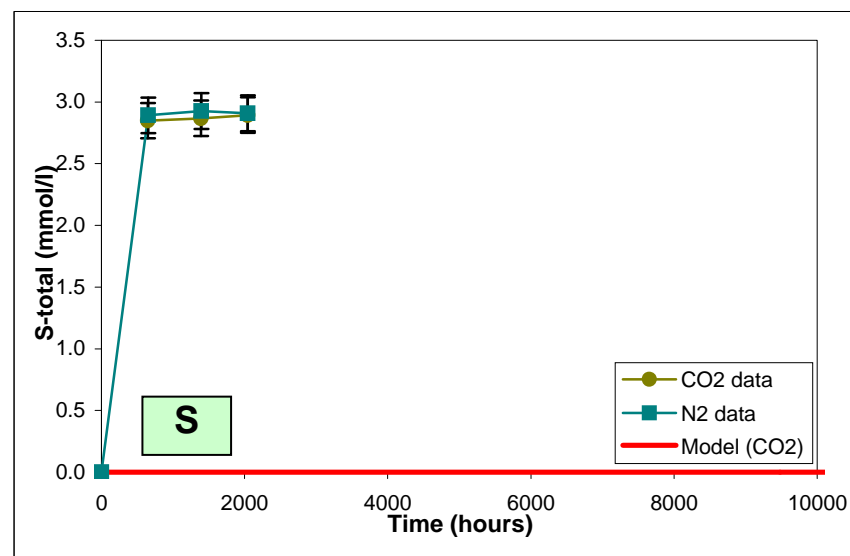
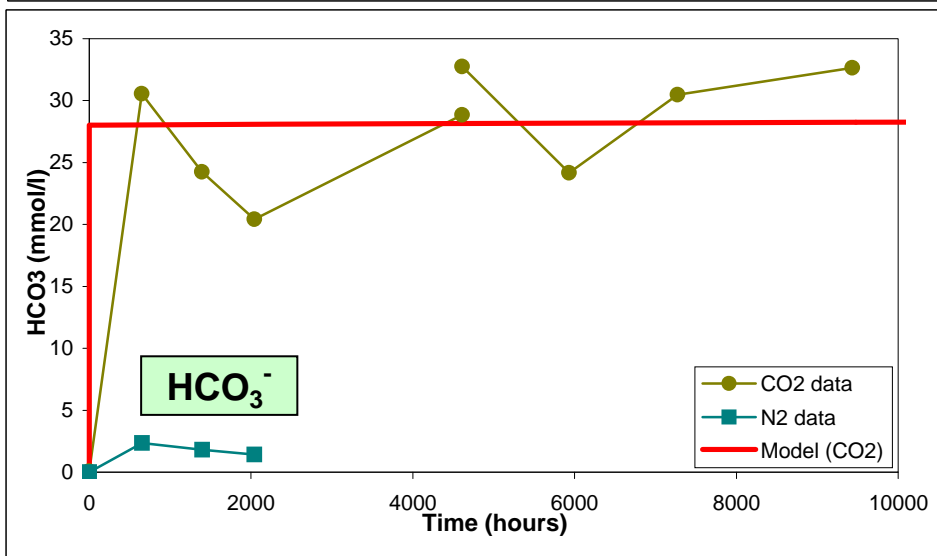
Fjerritslev Formation (Stenlille 1 well)

AQUA-DK, Forward model of laboratory experiments (1/3)

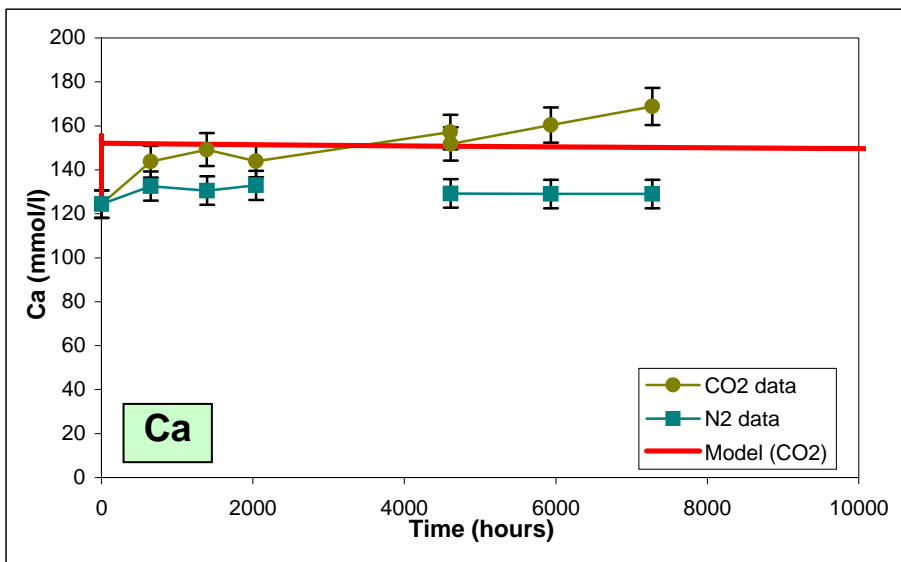


Model input:

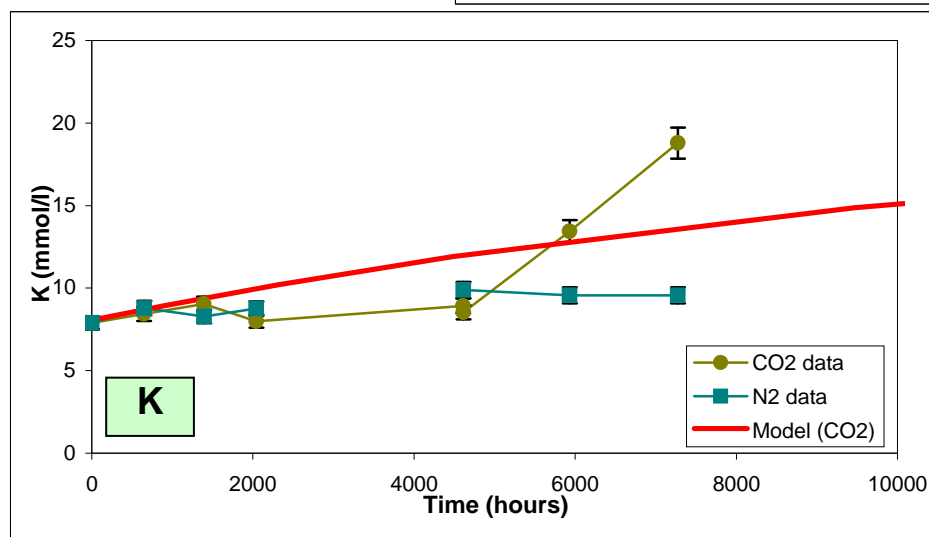
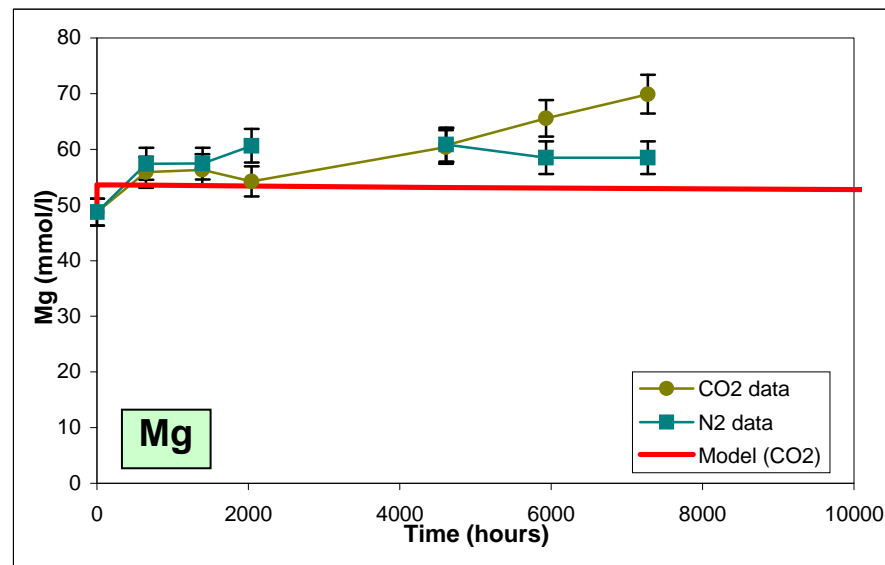
Mineral	SSA (m ² /g)	PHREEQC (vol %)
Chalcedony	0.03	39.5
K-feldspar	0.18	4
Calcite	0.035	2.9
Dolomite	0.1	1.8
Siderite	0.1	10.9
Illite	3.3	20.5
Ca-mont.	3	0.4
Chlorite	0.1	2.3
Kaolinite	2.6	17.7



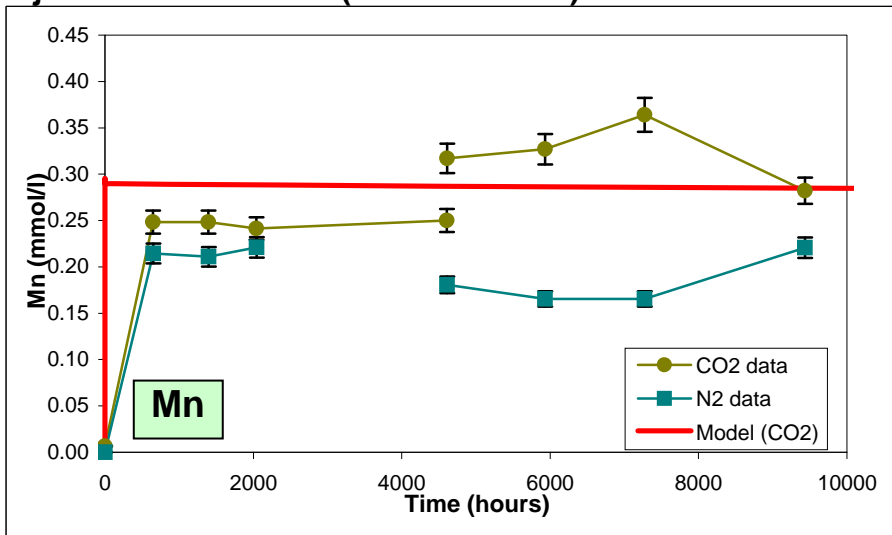
Fjerritslev Formation (Stenlille 1 well)



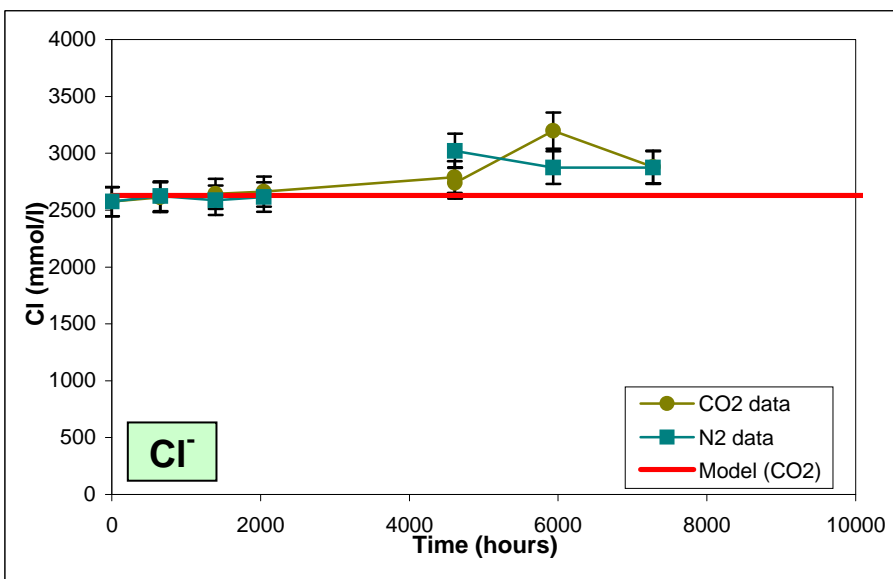
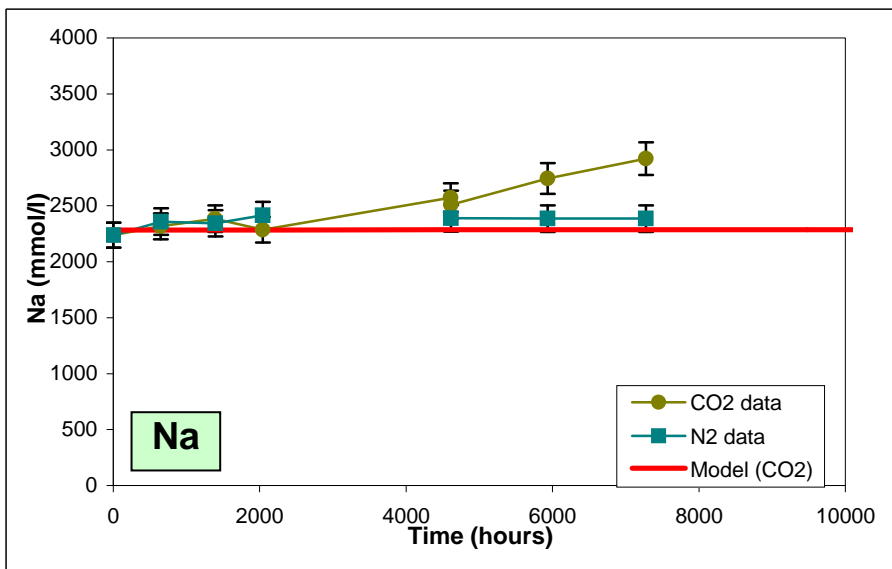
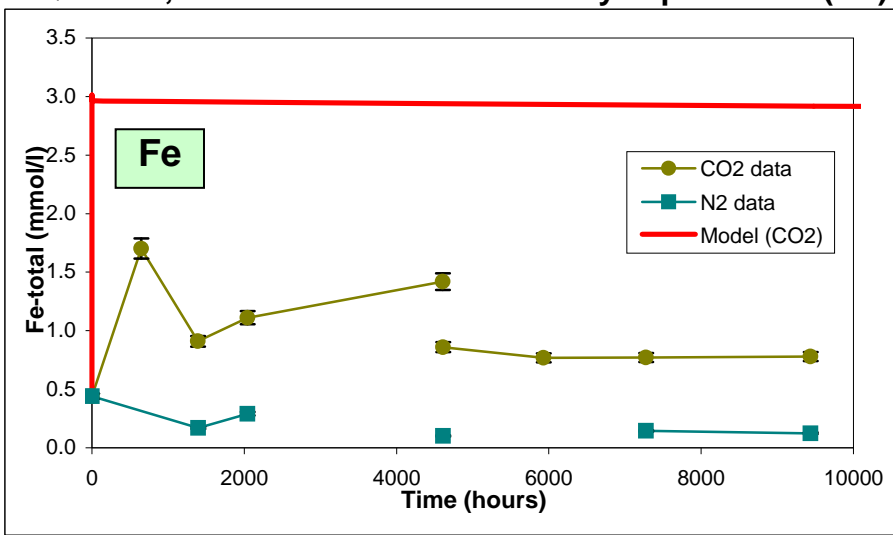
AQUA-DK, Forward model of laboratory experiments (2/3)



Fjerritslev Formation (Stenlille 1 well)



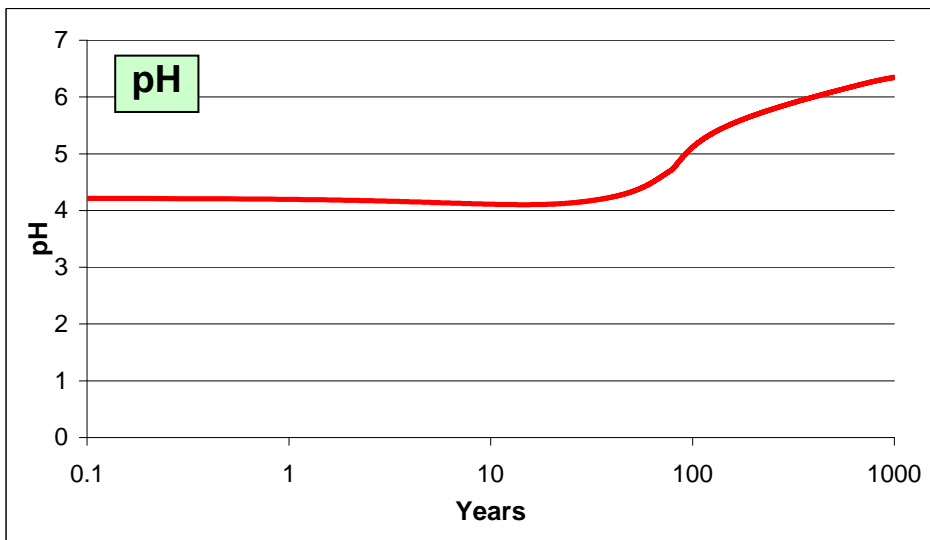
AQUA-DK, Forward model of laboratory experiments (3/3)



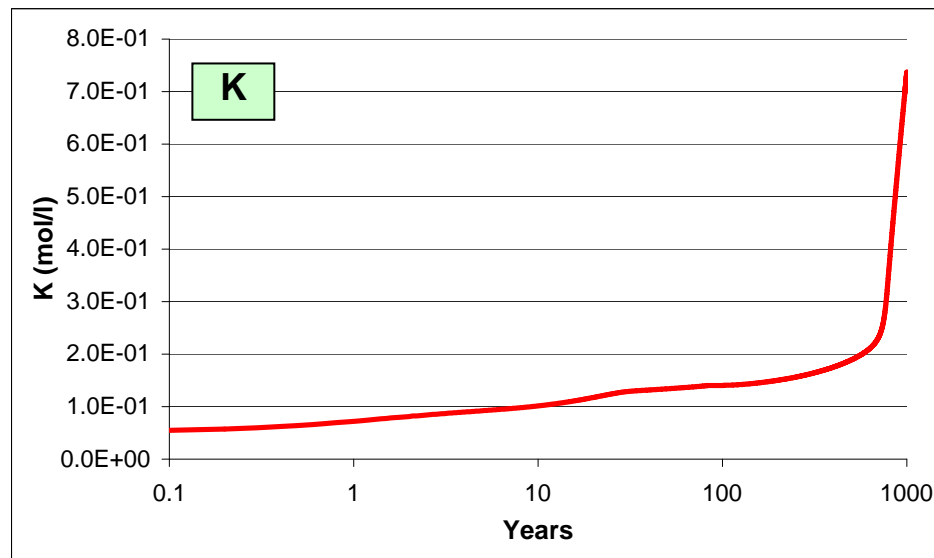
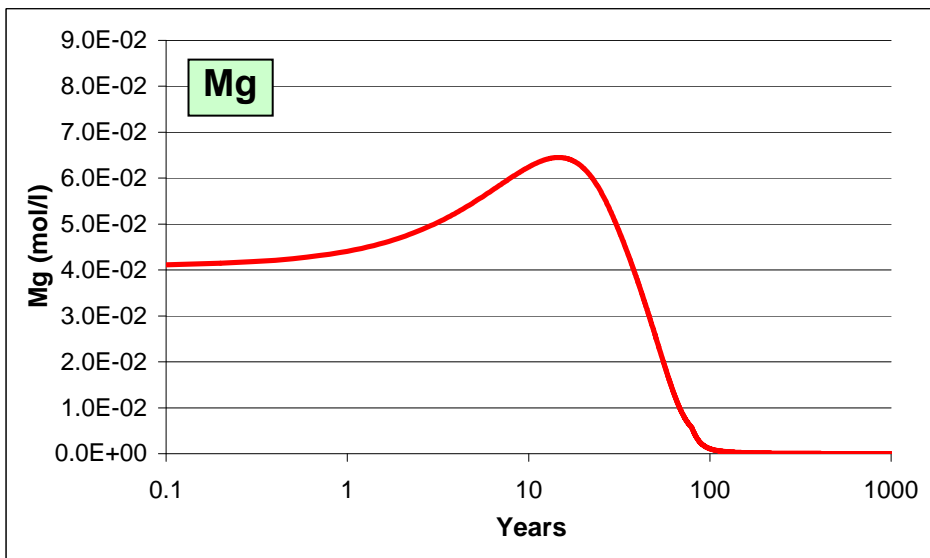
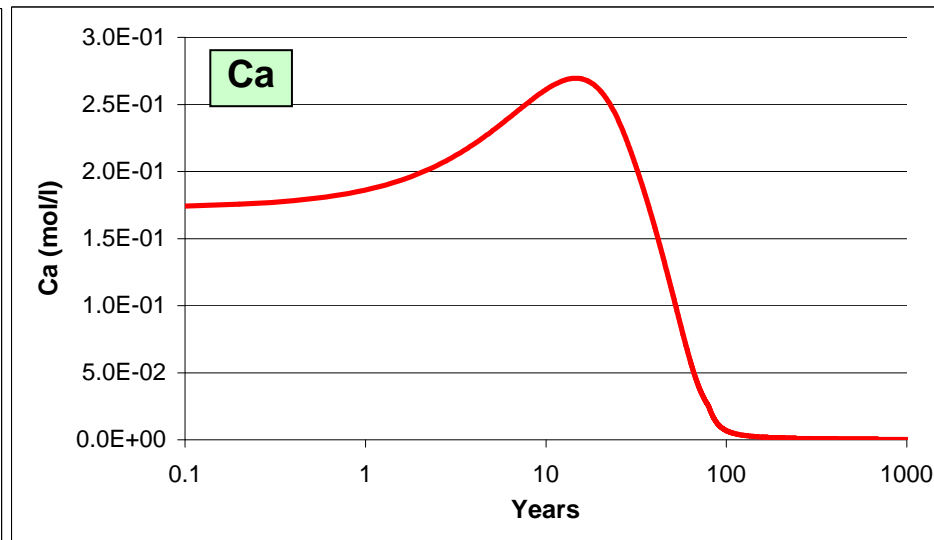
Appendix 5.

Selected results of 1000 years of predictive modelling

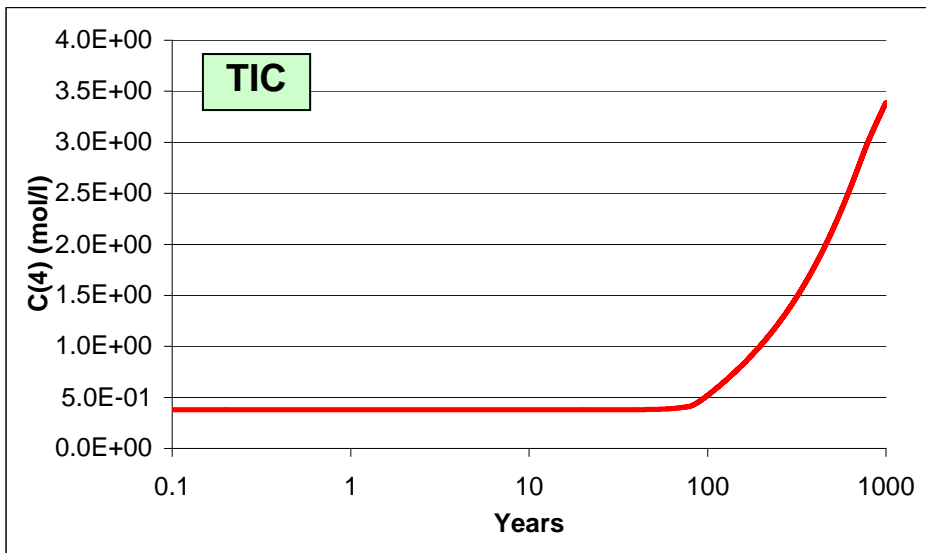
Bunter Formation (Tønder 4 well)



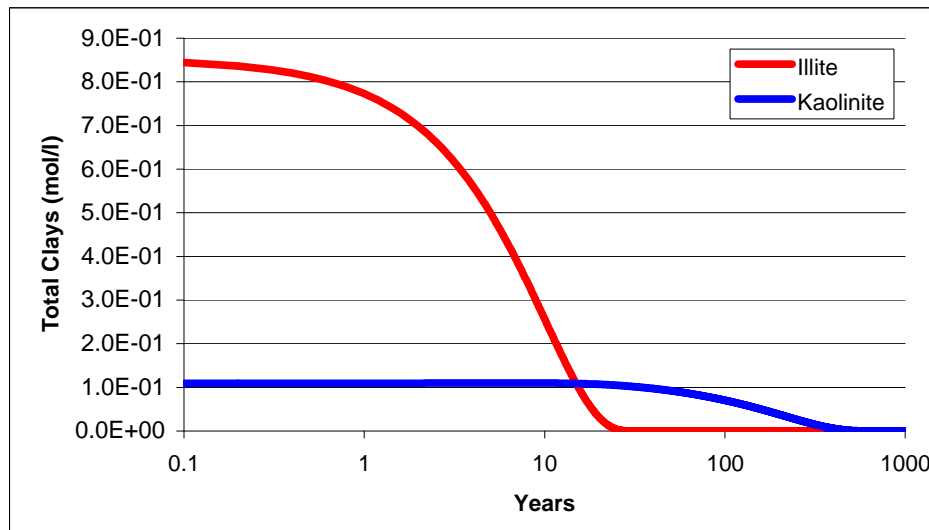
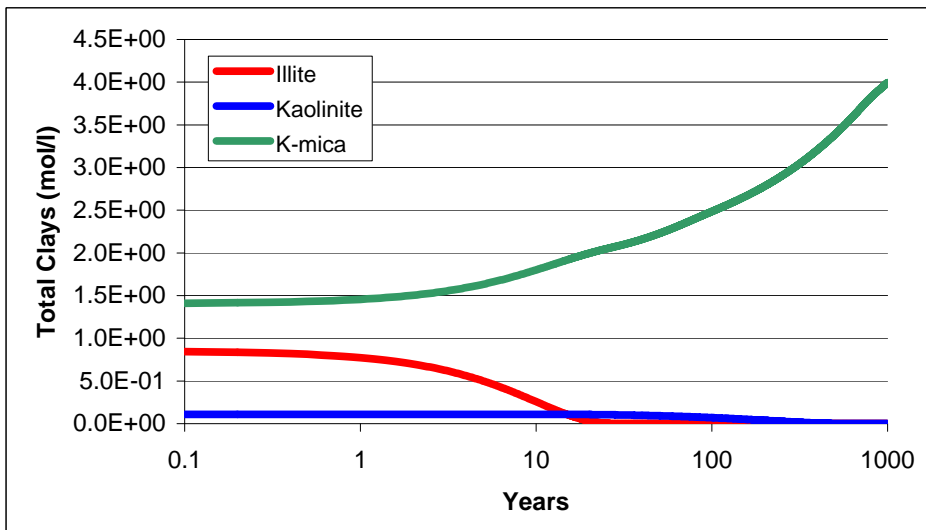
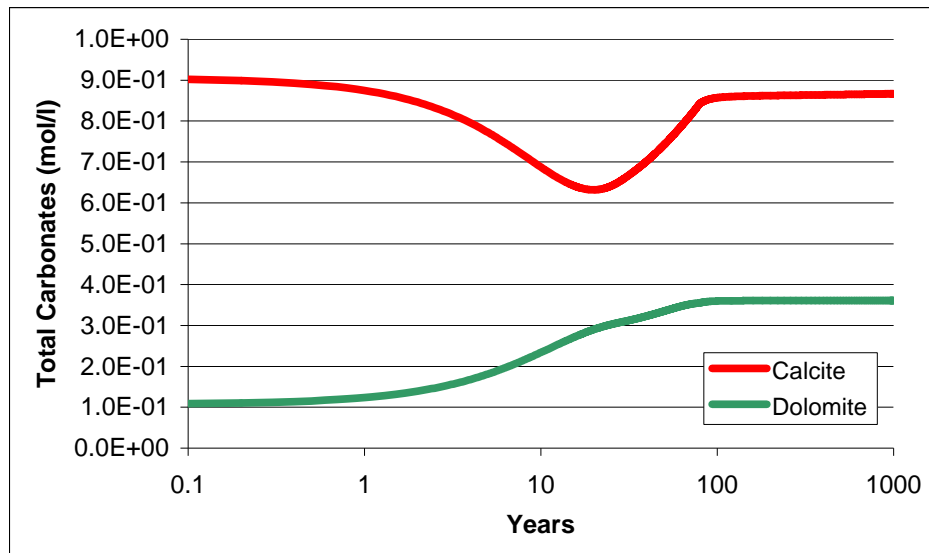
AQUA-DK, Selected results of predictive modelling (1/3)



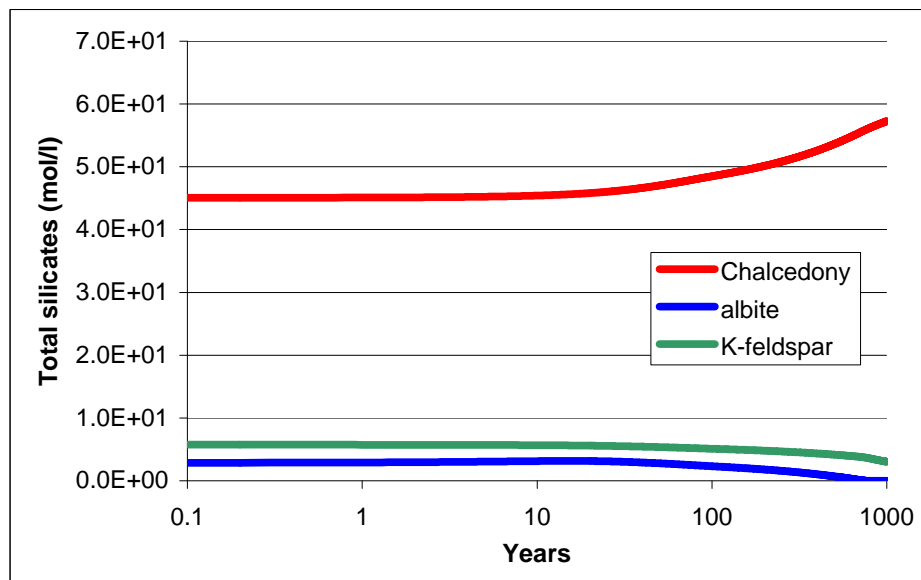
Bunter Formation (Tønder 4 well)



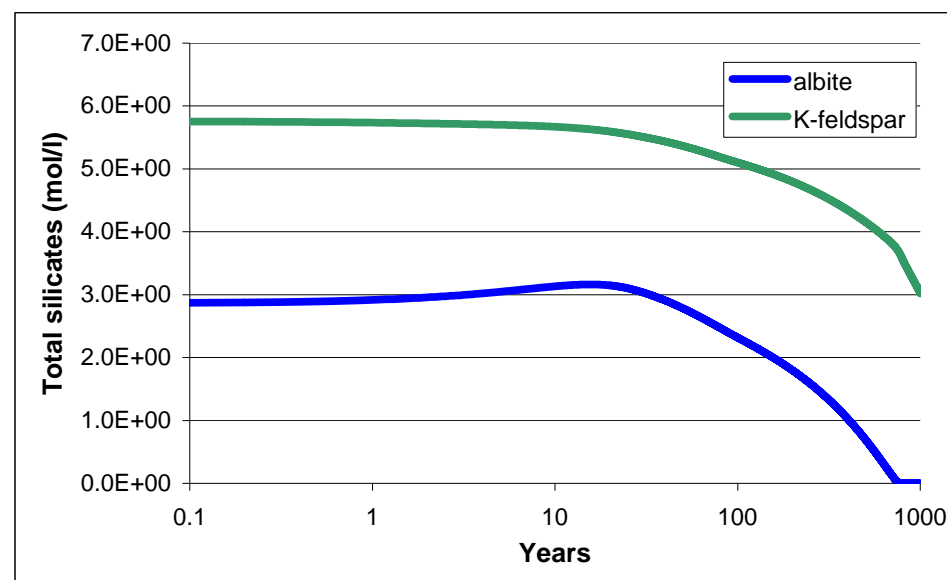
AQUA-DK, Selected results of predictive modelling (2/3)



Bunter Formation (Tønder 4 well)



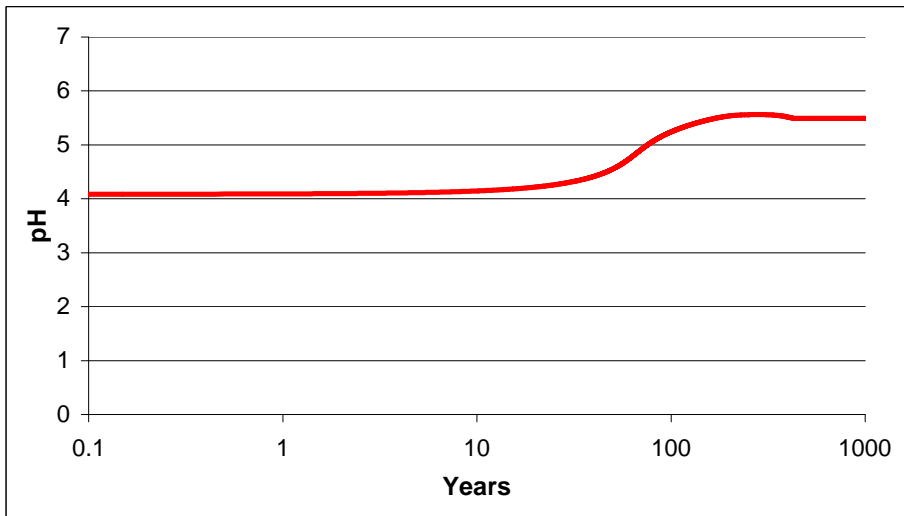
AQUA-DK, Selected results of predictive modelling (3/3)



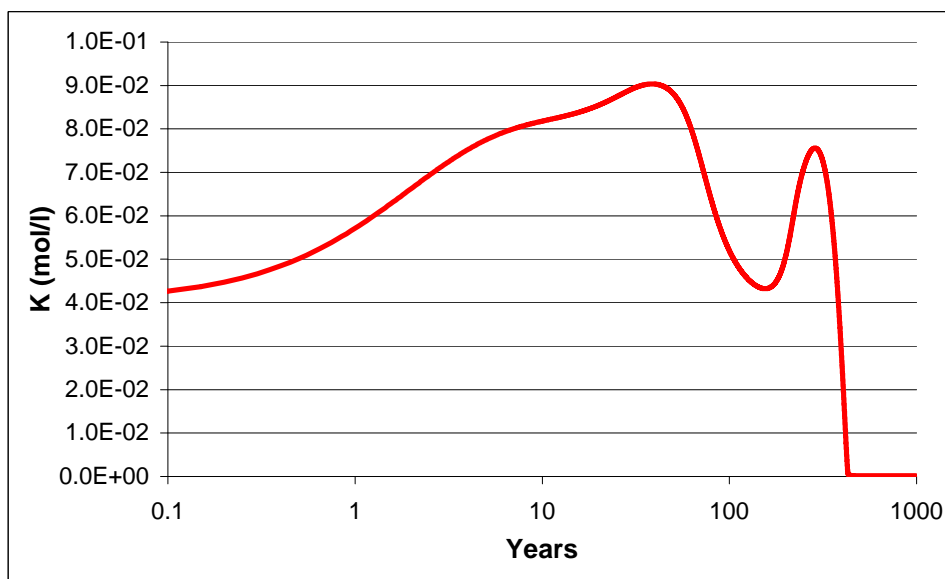
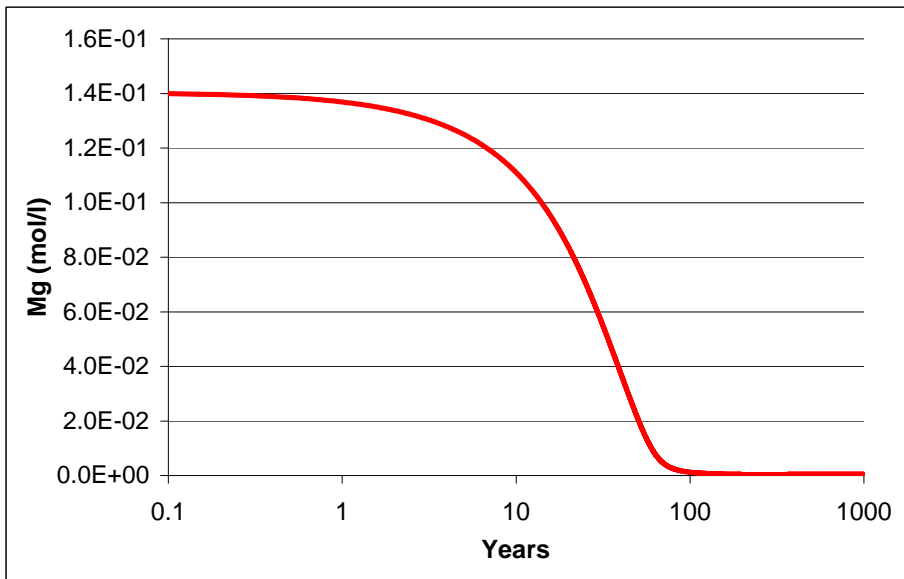
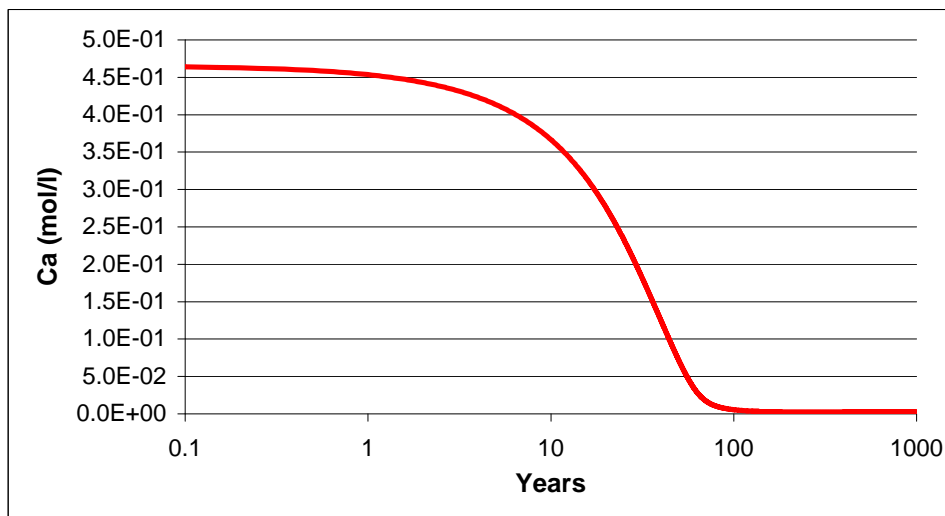
Result summary:

Mineral	Final conc. [mol/L]	Mineral change [mol/(L*1000 years)]	Contrib. to poro. change -
Calcite	8.7E-01	-3.5E-02	0.000
Dolomite	3.6E-01	2.5E-01	-0.005
Illite	0.0E+00	-8.4E-01	0.035
Kaolinite	0.0E+00	-1.1E-01	0.003
K-mica	4.0E+00	2.6E+00	-0.110
Albite	0.0E+00	-2.9E+00	0.086
K-feldspar	3.0E+00	-2.7E+00	0.087
Chalcedony	5.7E+01	1.2E+01	-0.083

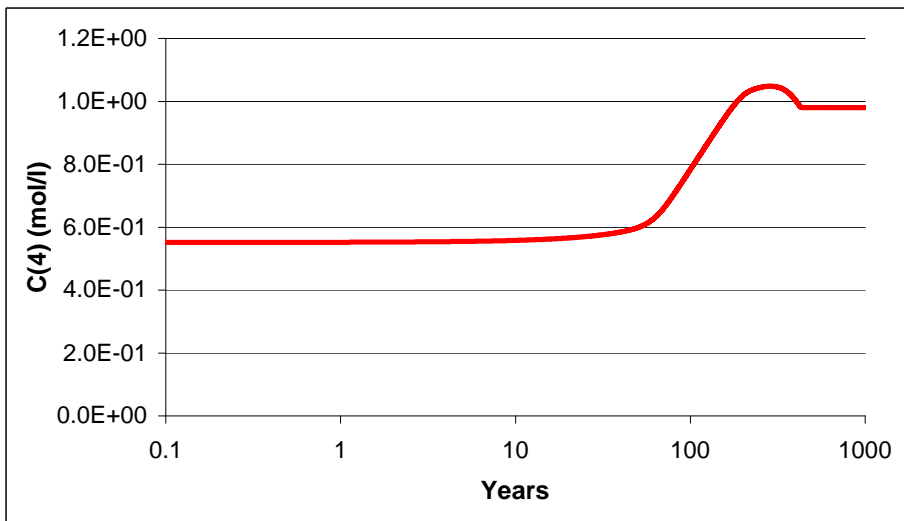
Skagerrak Formation (Vedsted 1 well)



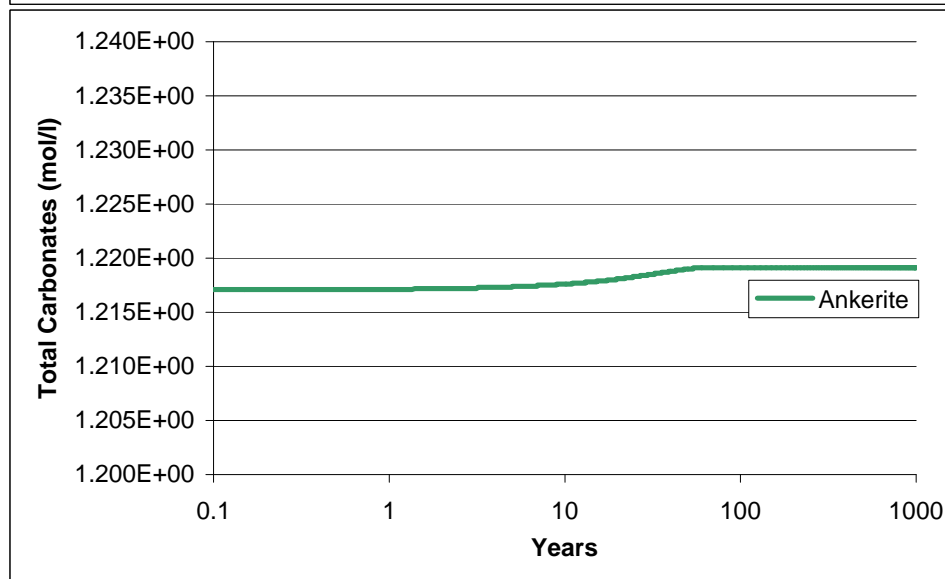
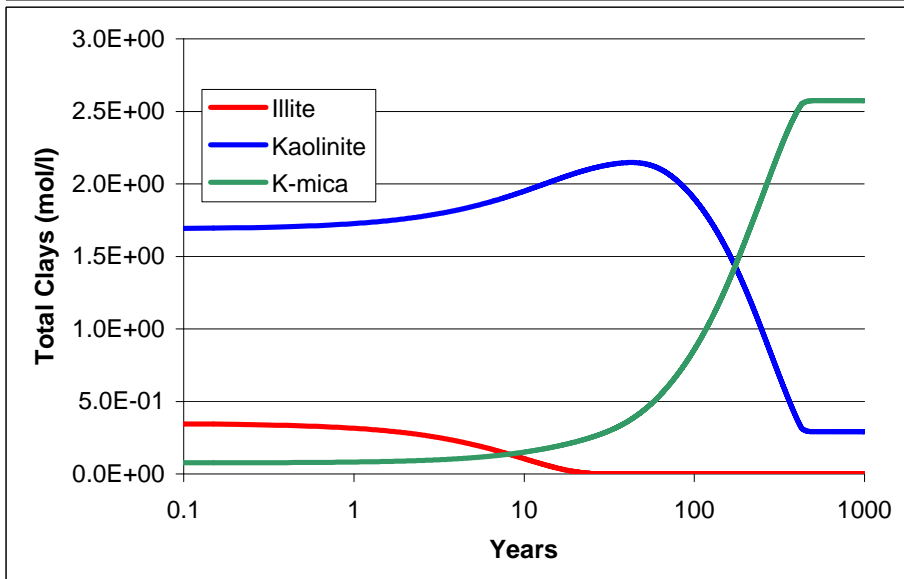
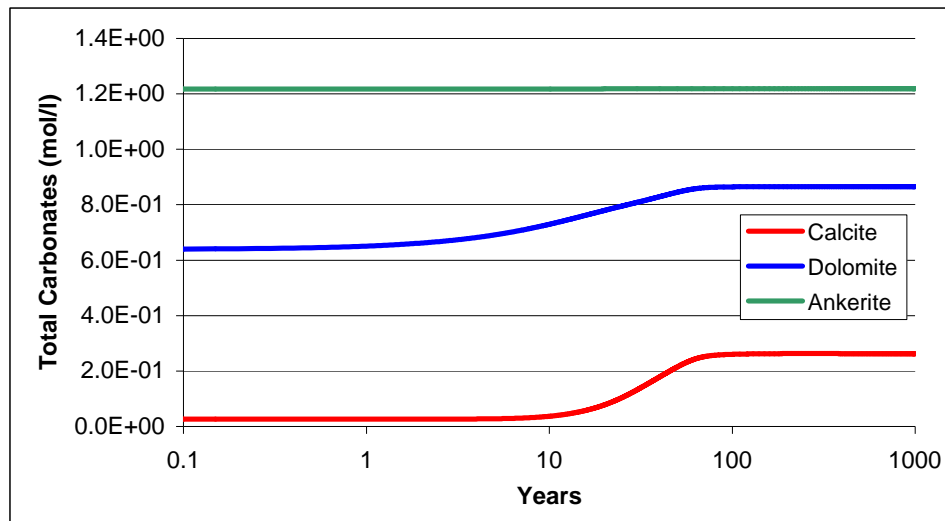
AQUA-DK, Selected results of predictive modelling (1/3)



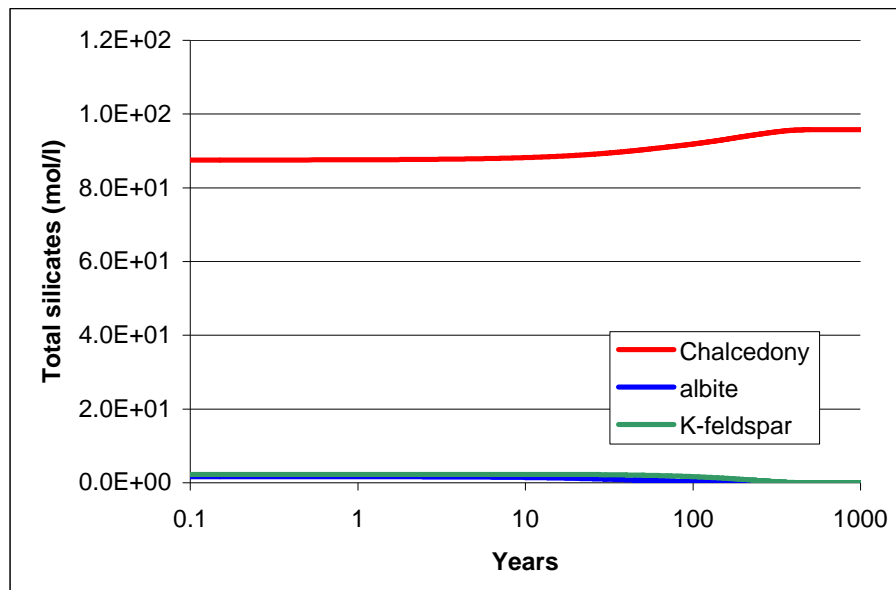
Skagerrak Formation (Vedsted 1 well)



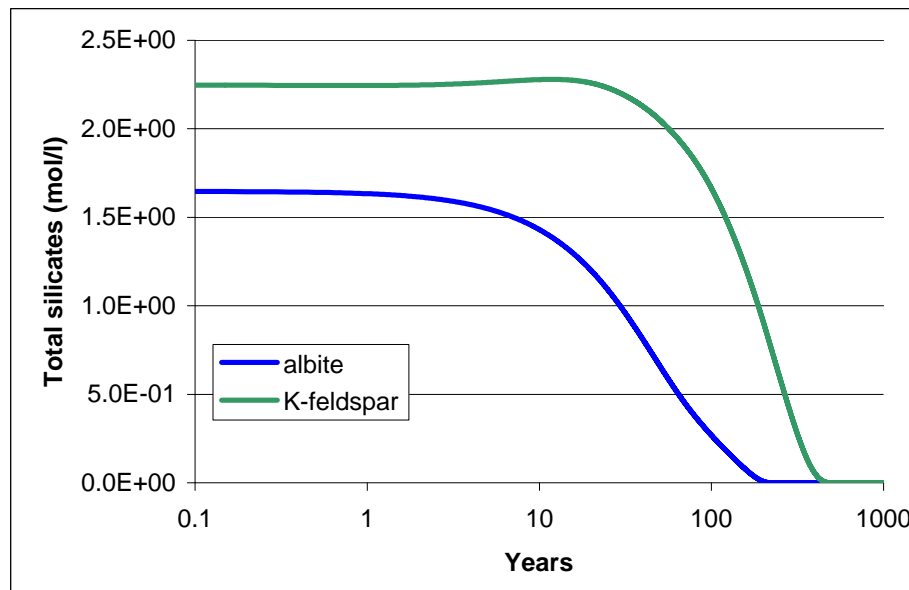
AQUA-DK, Selected results of predictive modelling (2/3)



Skagerrak Formation (Vedsted 1 well)



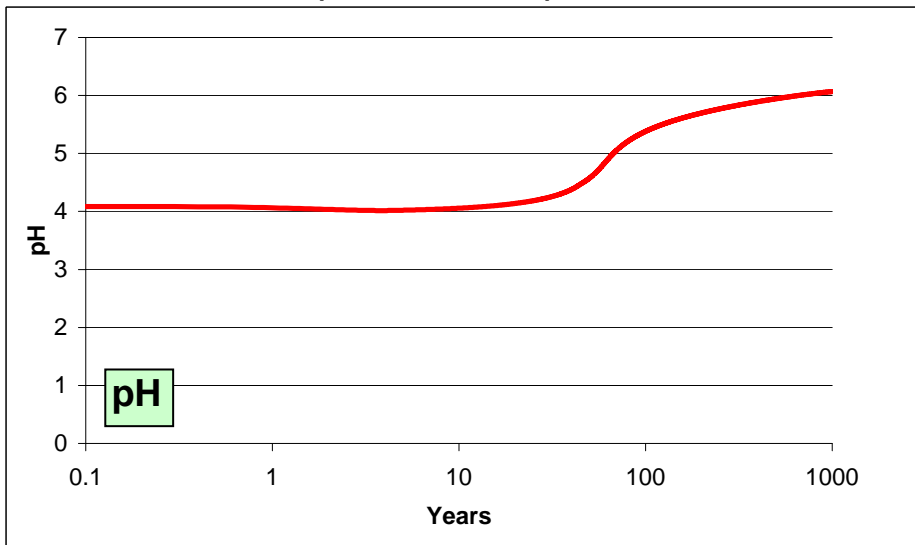
AQUA-DK, Selected results of predictive modelling (3/3)



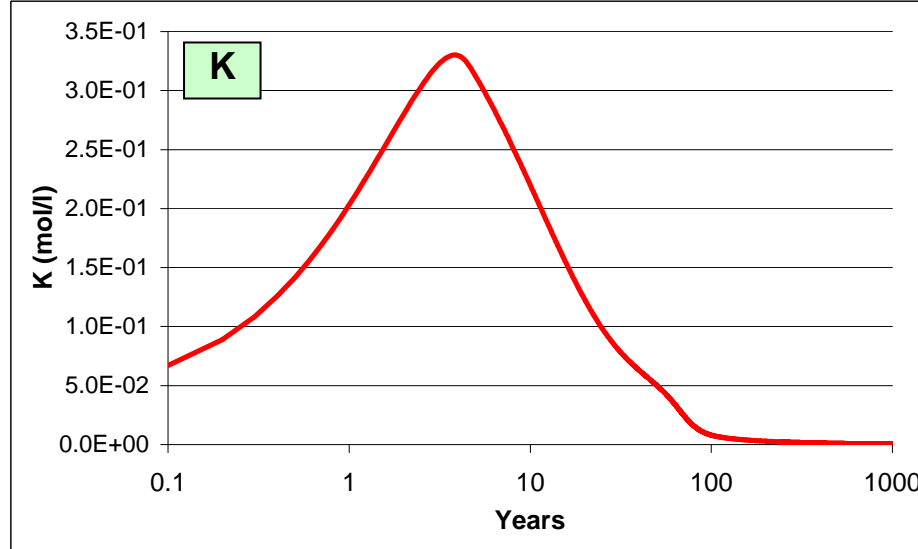
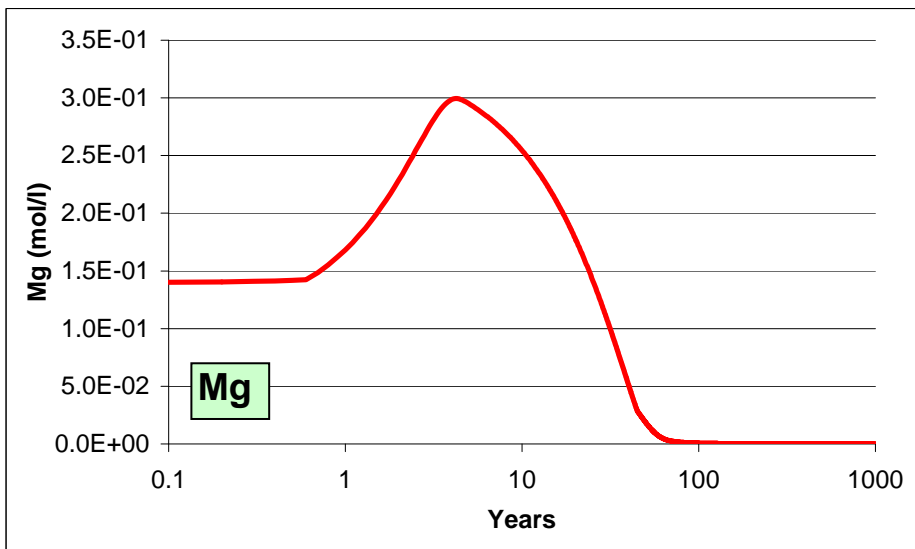
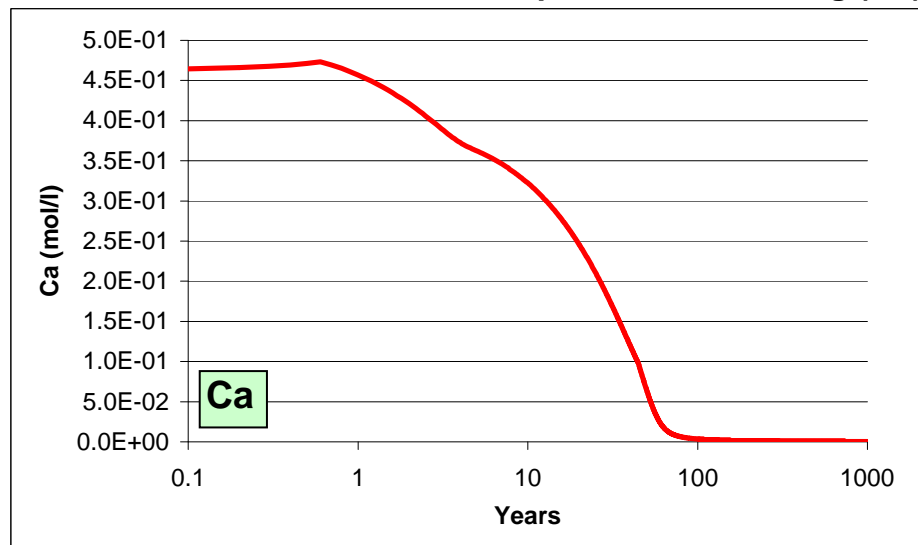
Result summary:

Mineral	Final conc. [mol/L]	Mineral change [mol/(L*1000 years)]	Contrib. to poro. change -
Calcite	2.6E-01	2.4E-01	-0.003
Dolomite	8.7E-01	2.3E-01	-0.004
Ankerite	1.2E+00	2.0E-03	0.000
Illite	0.0E+00	-3.5E-01	0.015
Kaolinite	2.9E-01	-1.4E+00	0.042
K-mica	2.6E+00	2.5E+00	-0.107
Albite	0.0E+00	-1.6E+00	0.049
K-feldspar	0.0E+00	-2.2E+00	0.072
Chalcedony	9.6E+01	8.2E+00	-0.056

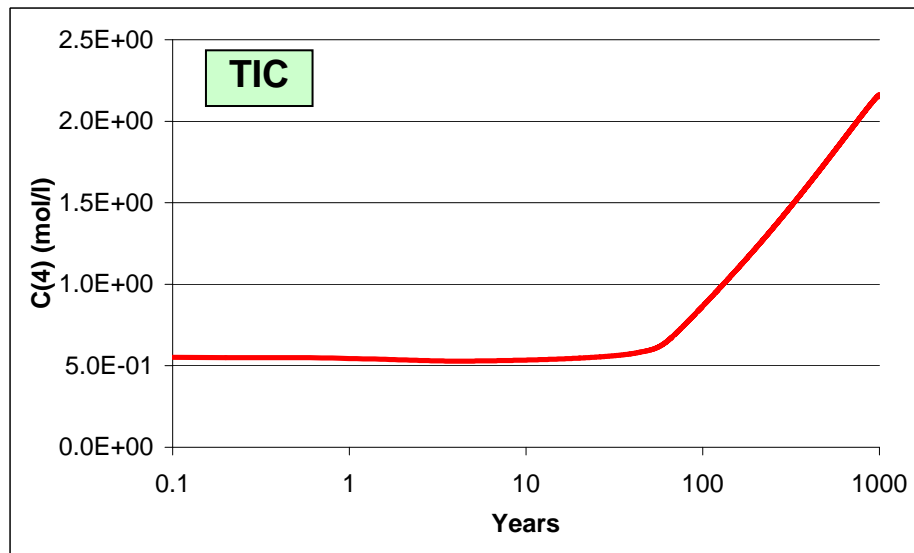
Gassum Formation (Vedsted 1 well)



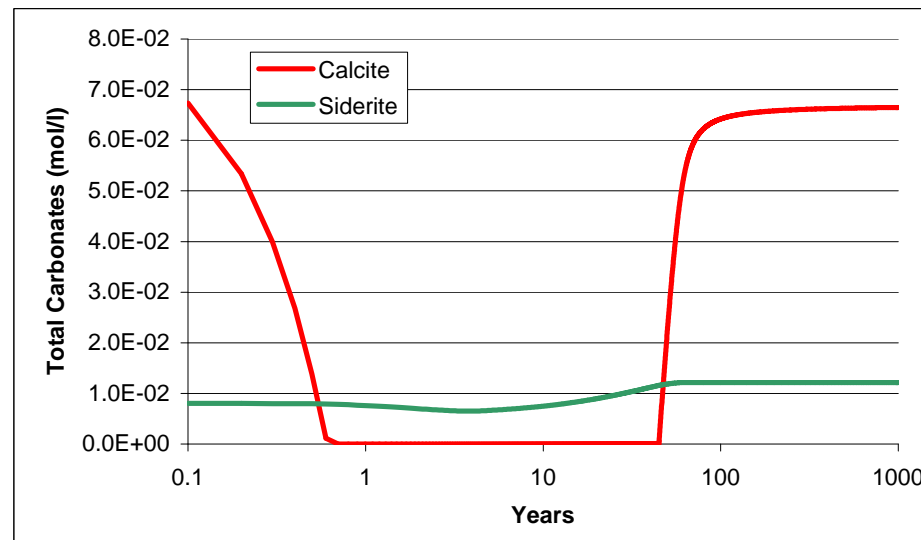
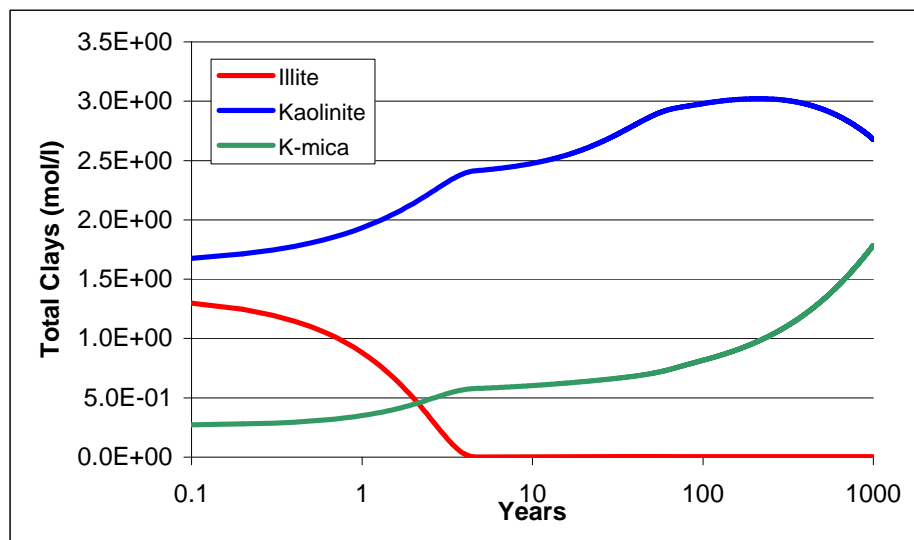
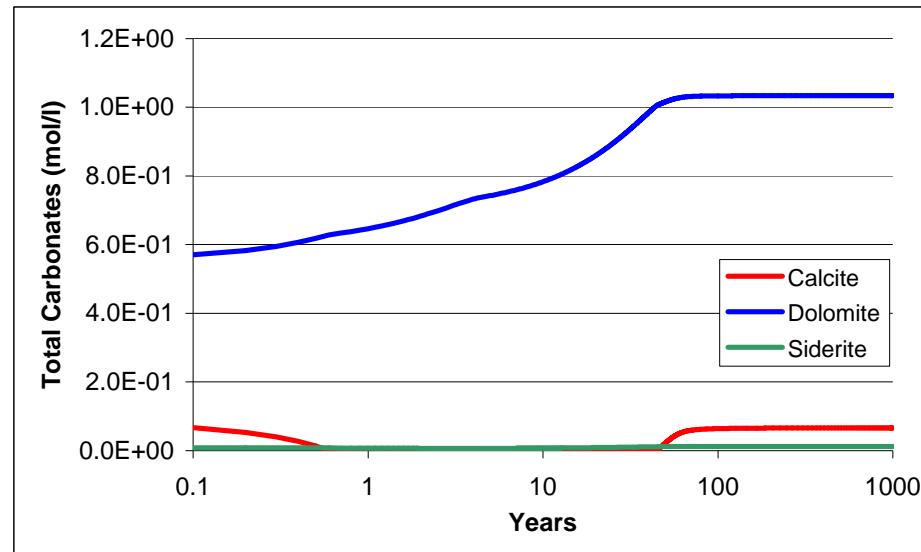
AQUA-DK, Selected results of predictive modelling (1/3)



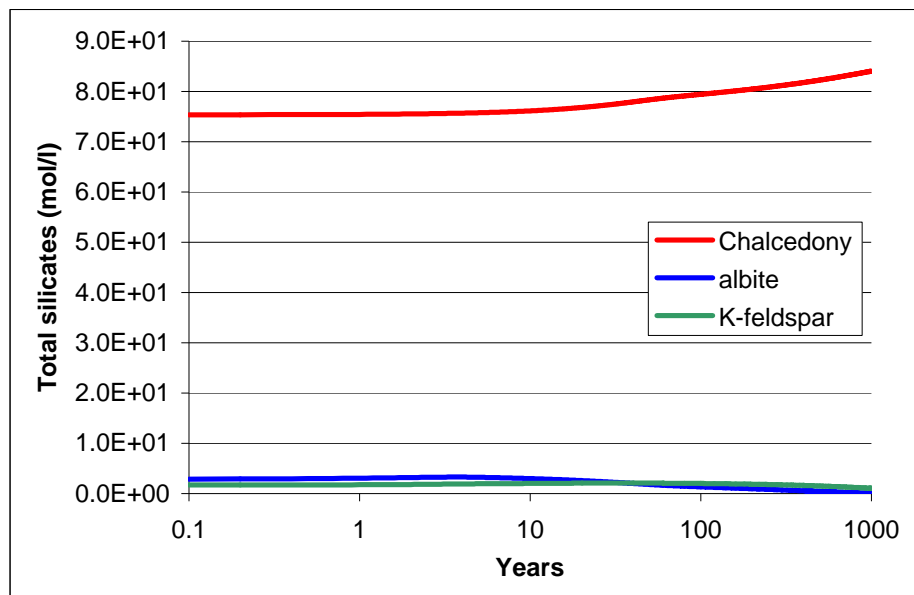
Gassum Formation (Vedsted 1 well)



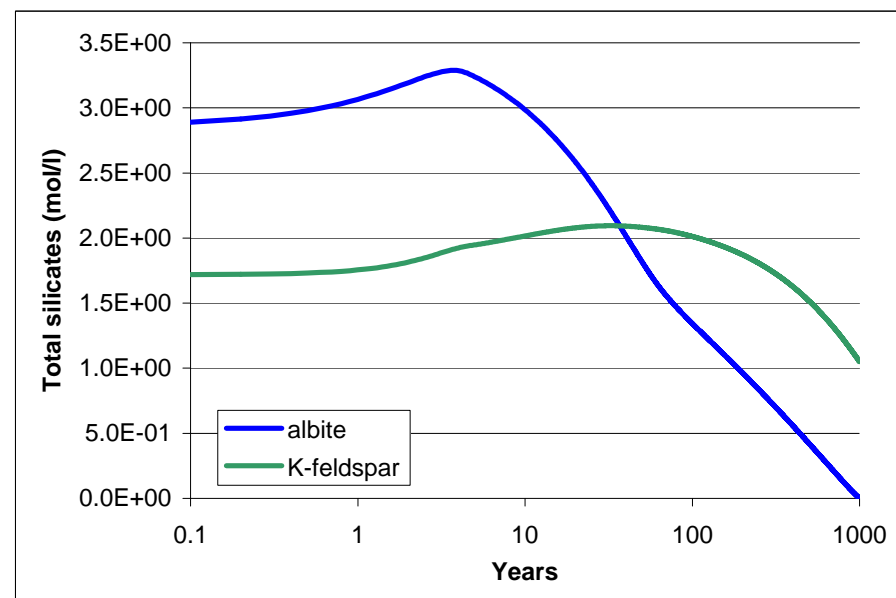
AQUA-DK, Selected results of predictive modelling (2/3)



Gassum Formation (Vedsted 1 well)



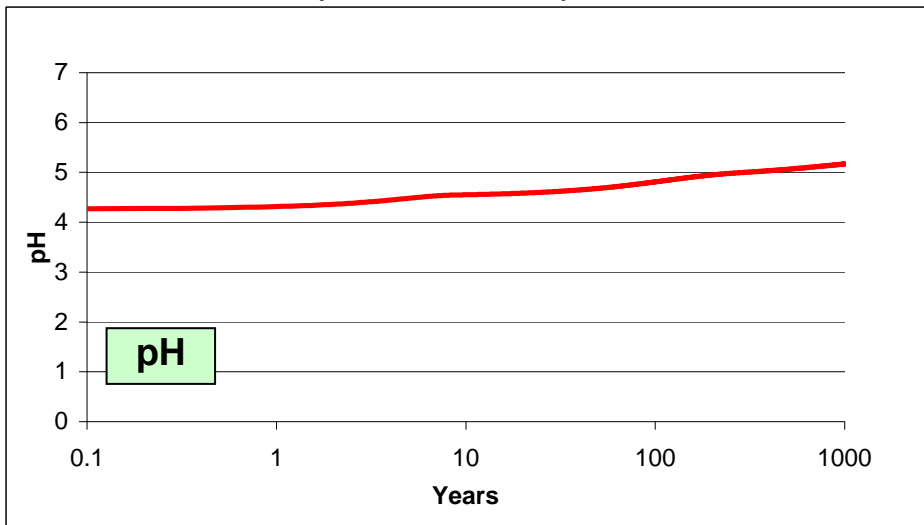
AQUA-DK, Selected results of predictive modelling (3/3)



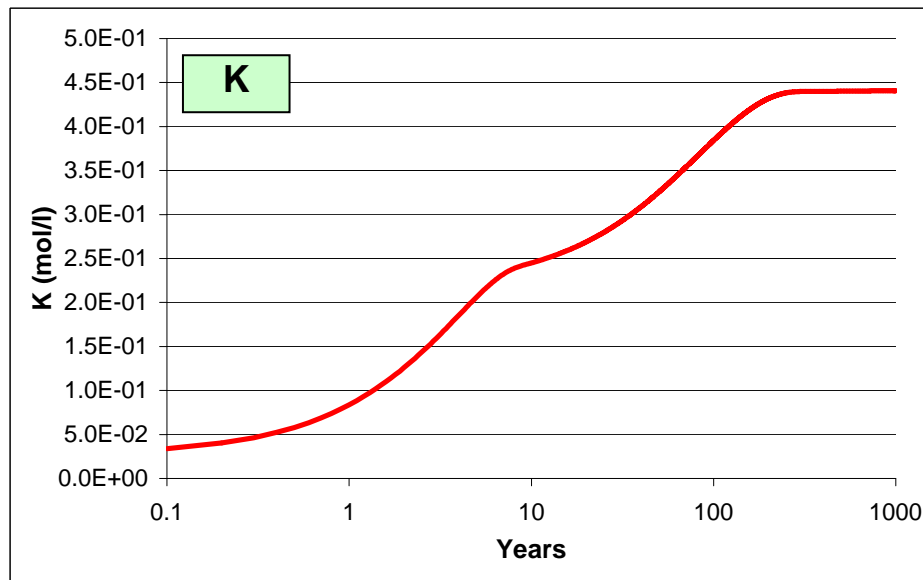
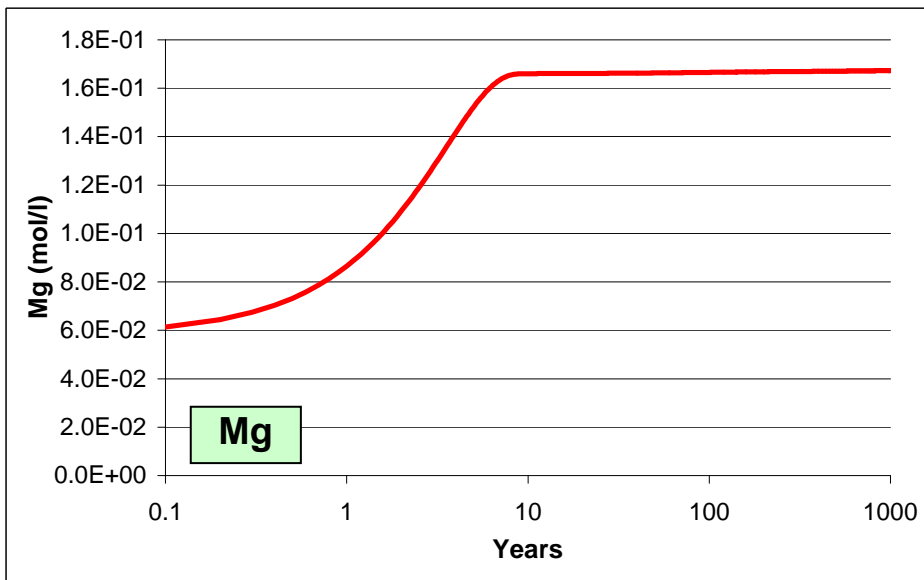
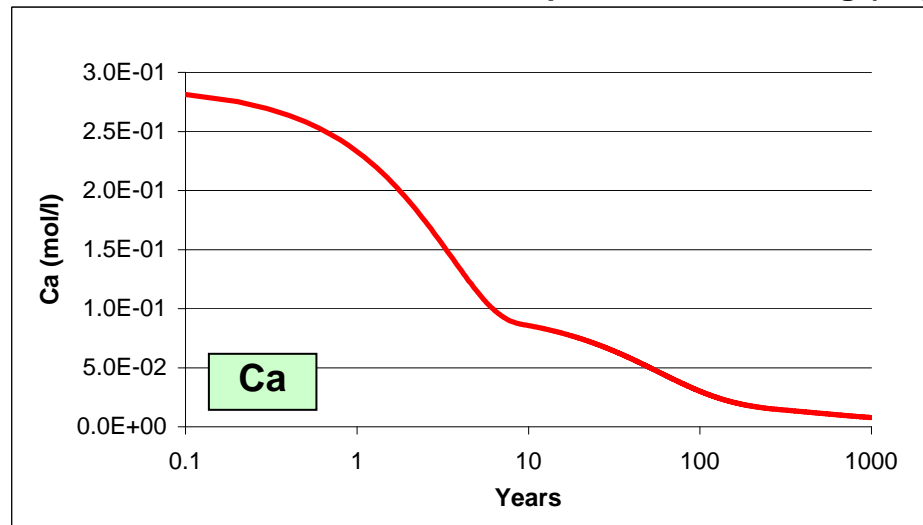
Result summary:

Mineral	Final conc. [mol/L]	Mineral change [mol/(L*1000 years)]	Contrib. to poro. change -
Calcite	6.6E-02	-8.4E-04	0.000
Dolomite	1.0E+00	4.6E-01	-0.009
Siderite	1.2E-02	4.1E-03	0.000
Illite	0.0E+00	-1.3E+00	0.054
Kaolinite	2.7E+00	1.0E+00	-0.030
K-mica	1.8E+00	1.5E+00	-0.065
Albite	4.4E-03	-2.9E+00	0.087
K-feldspar	1.1E+00	-6.7E-01	0.021
Chalcedony	8.4E+01	8.7E+00	-0.059

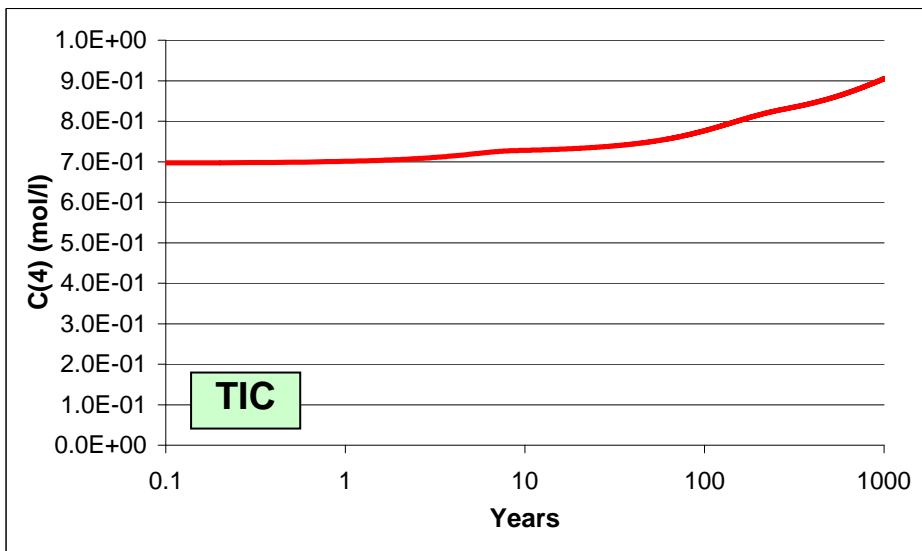
Gassum Formation (Stenlille 18 well)



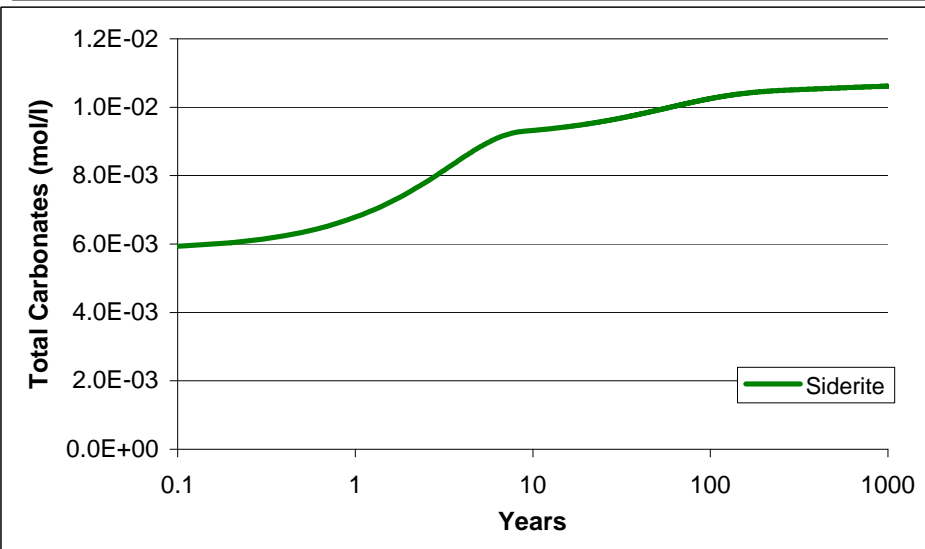
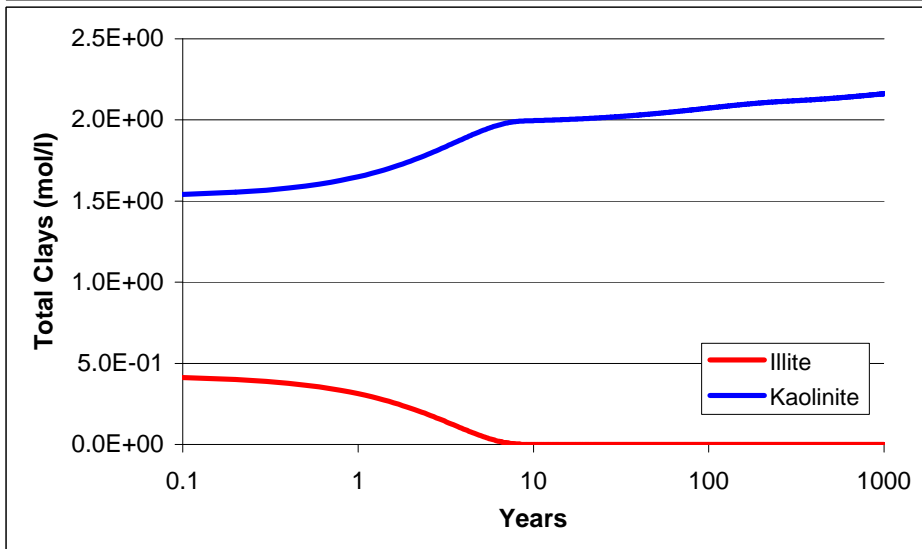
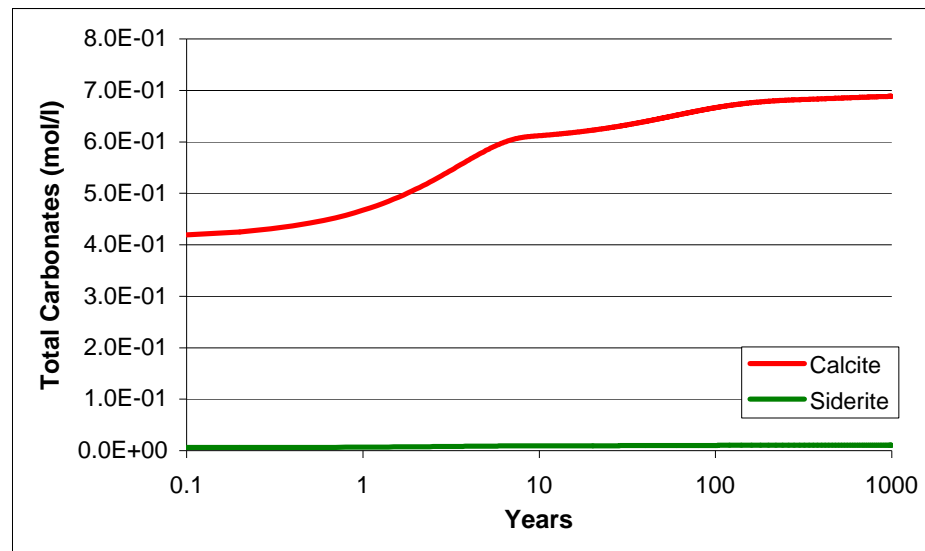
AQUA-DK, Selected results of predictive modelling (1/3)



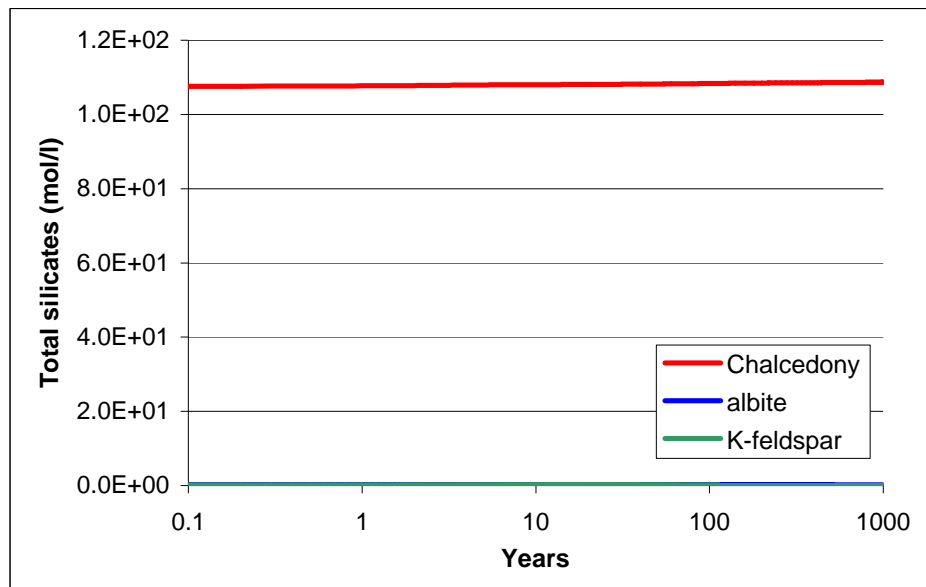
Gassum Formation (Stenlille 18 well)



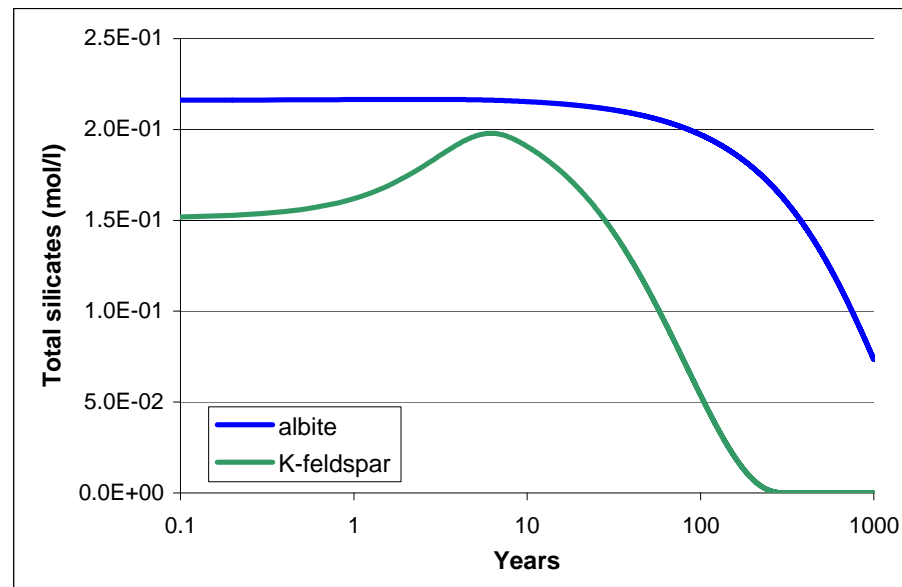
AQUA-DK, Selected results of predictive modelling (2/3)



Gassum Formation (Stenlille 18 well)



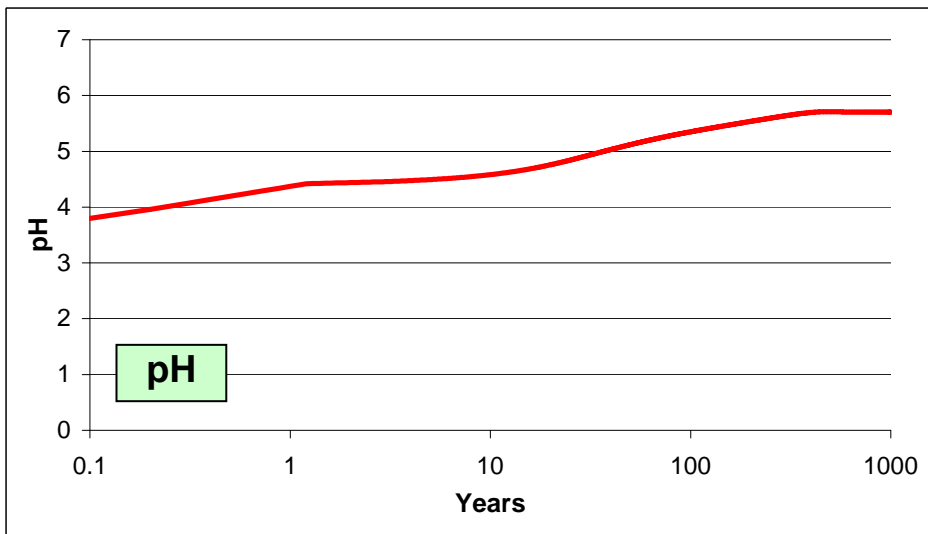
AQUA-DK, Selected results of predictive modelling (3/3)



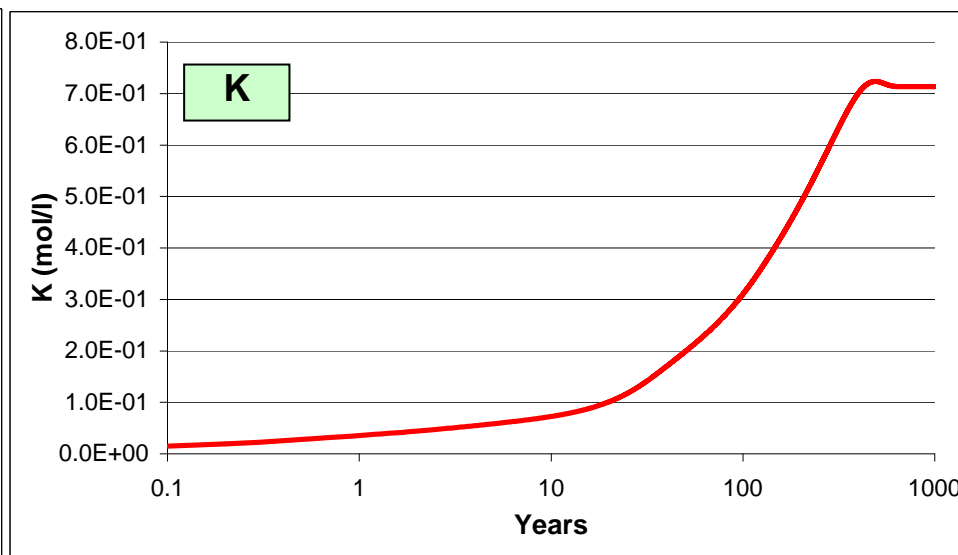
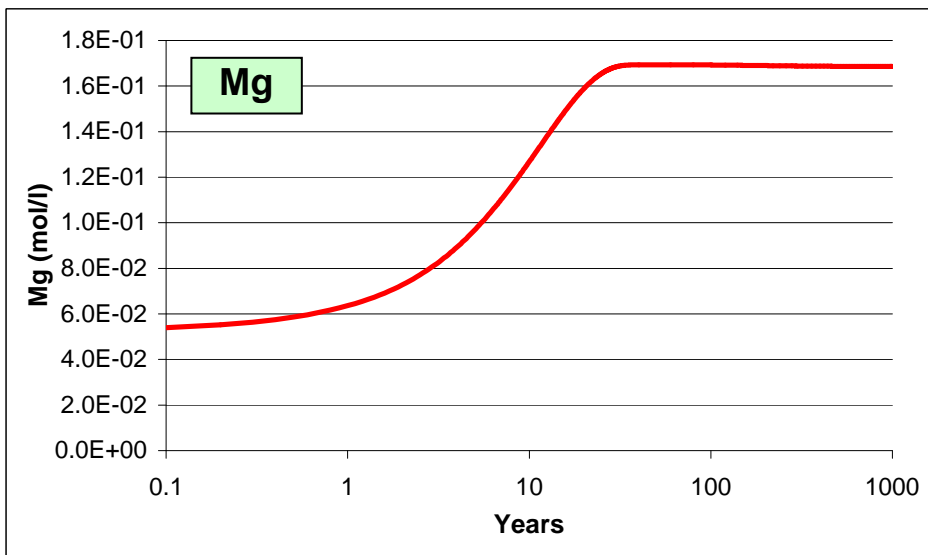
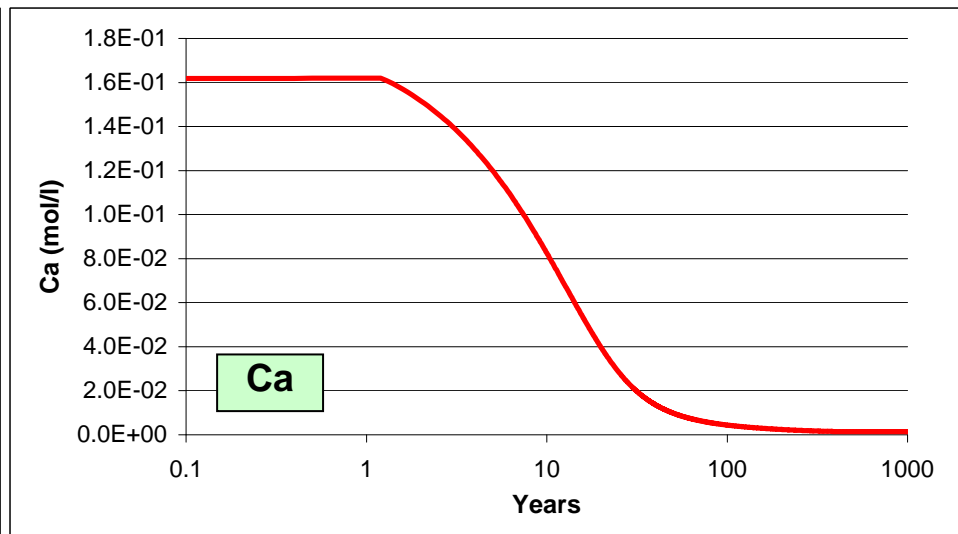
Result summary:

Mineral	Final conc. [mol/L]	Mineral change [mol/(L*1000 years)]	Contrib. to poro. change -
Calcite	6.9E-01	2.7E-01	-0.003
Siderite	1.1E-02	4.7E-03	0.000
Illite	0.0E+00	-4.1E-01	0.017
Kaolinite	2.2E+00	6.2E-01	-0.019
Albite	7.4E-02	-1.4E-01	0.004
K-feldspar	0.0E+00	-1.5E-01	0.005
Chalcedony	1.1E+02	1.1E+00	-0.007

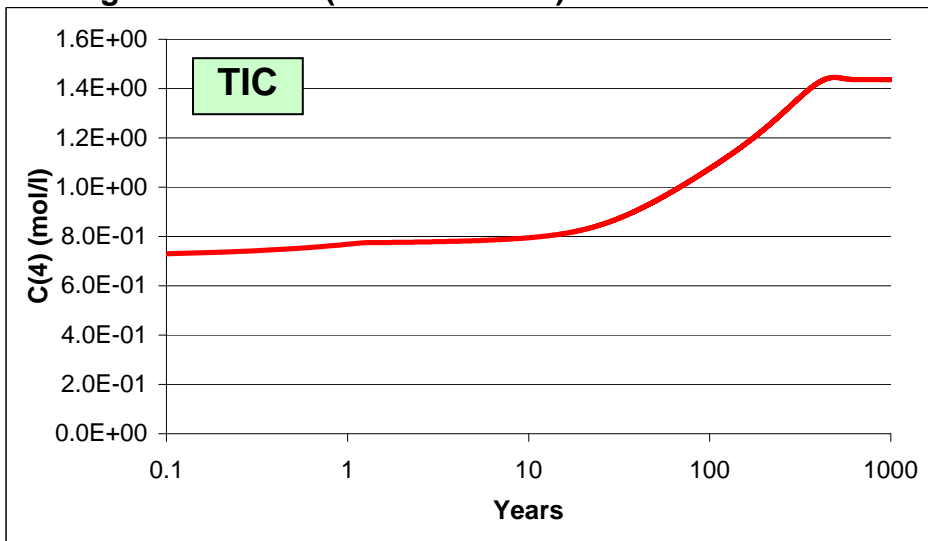
Haldager Formation (Vedsted 1 well)



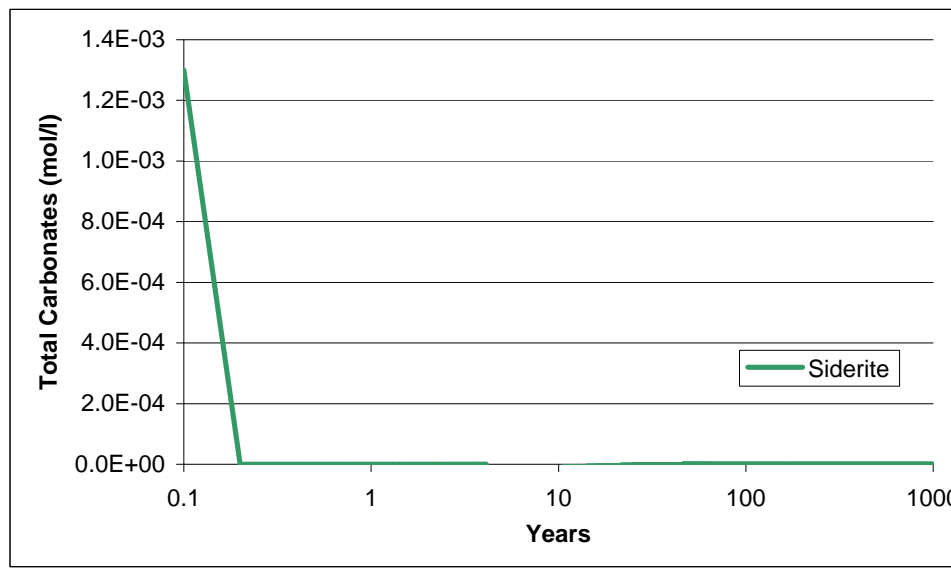
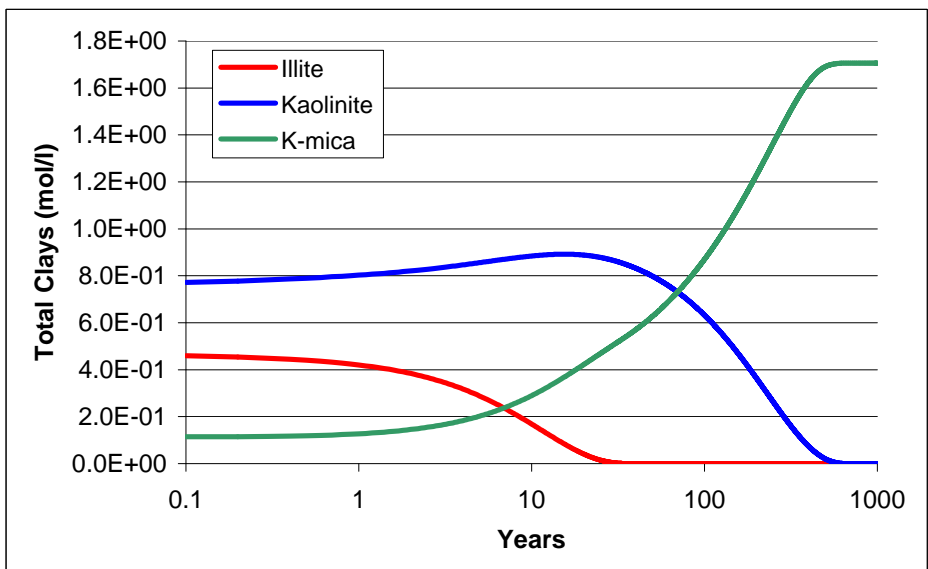
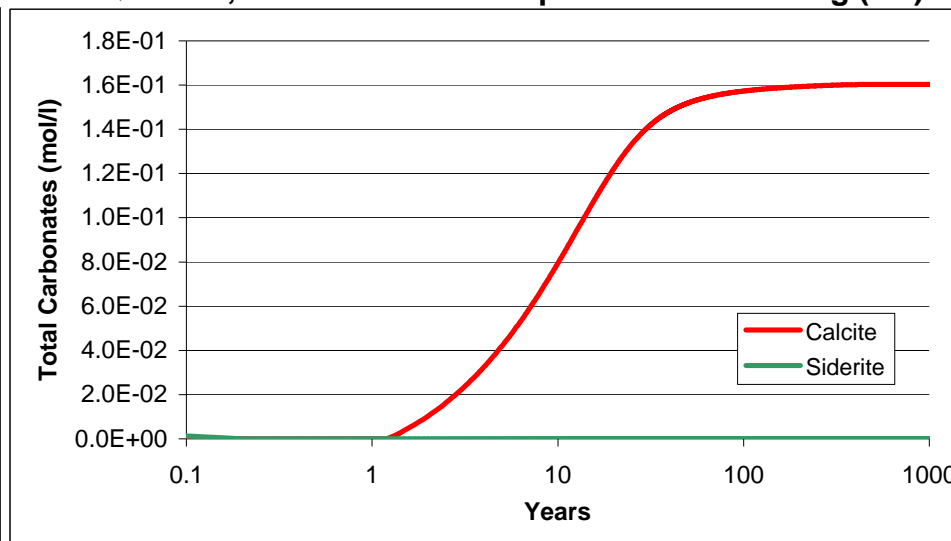
AQUA-DK, Selected results of predictive modelling (1/3)



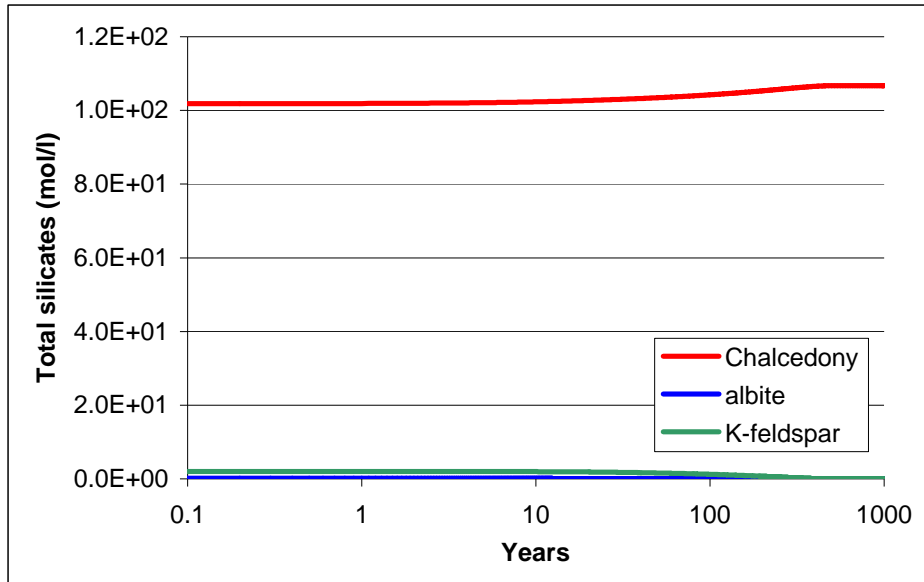
Haldager Formation (Vedsted 1 well)



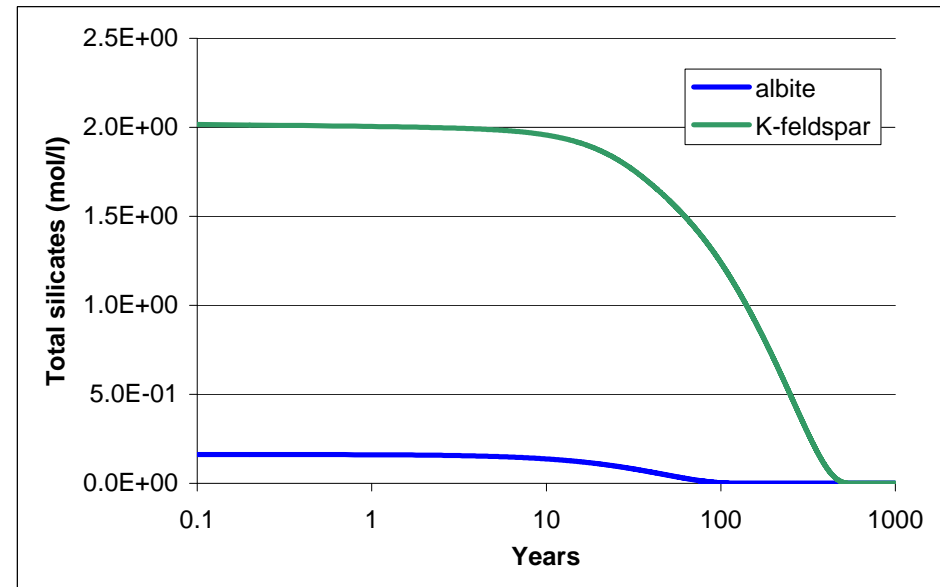
AQUA-DK, Selected results of predictive modelling (2/3)



Haldager Formation (Vedsted 1 well)



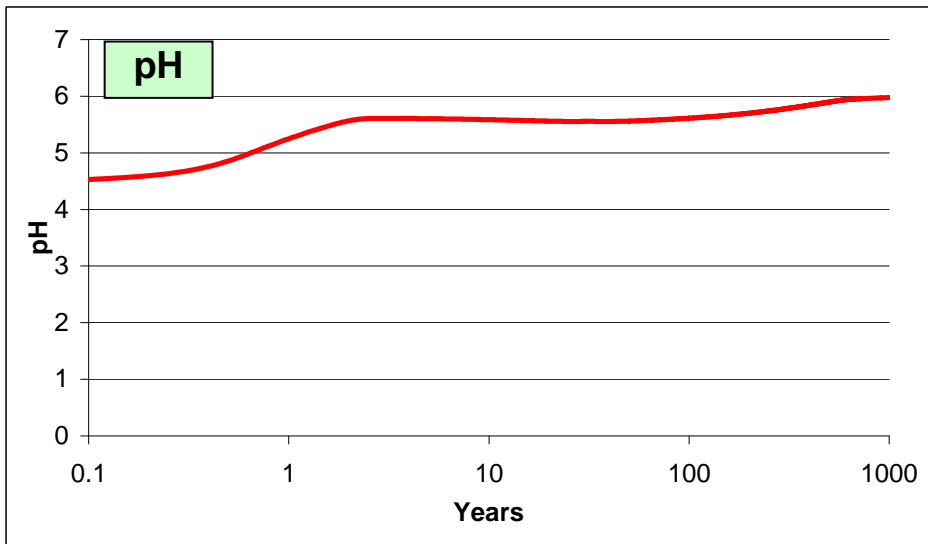
AQUA-DK, Selected results of predictive modelling (3/3)



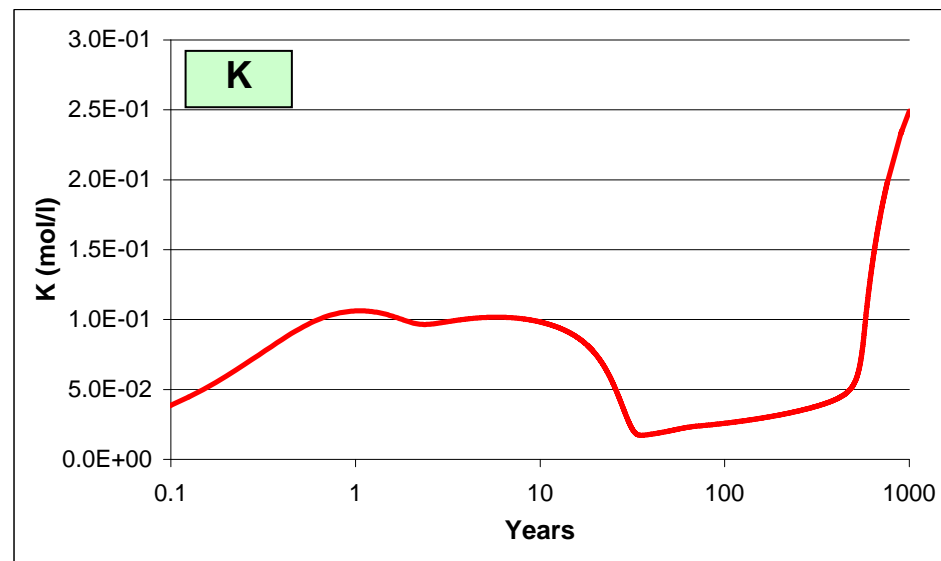
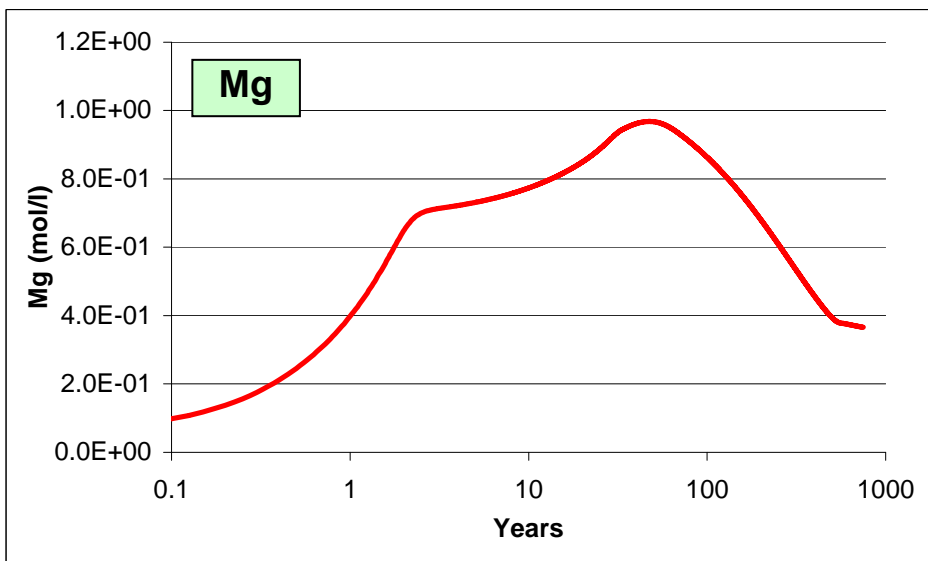
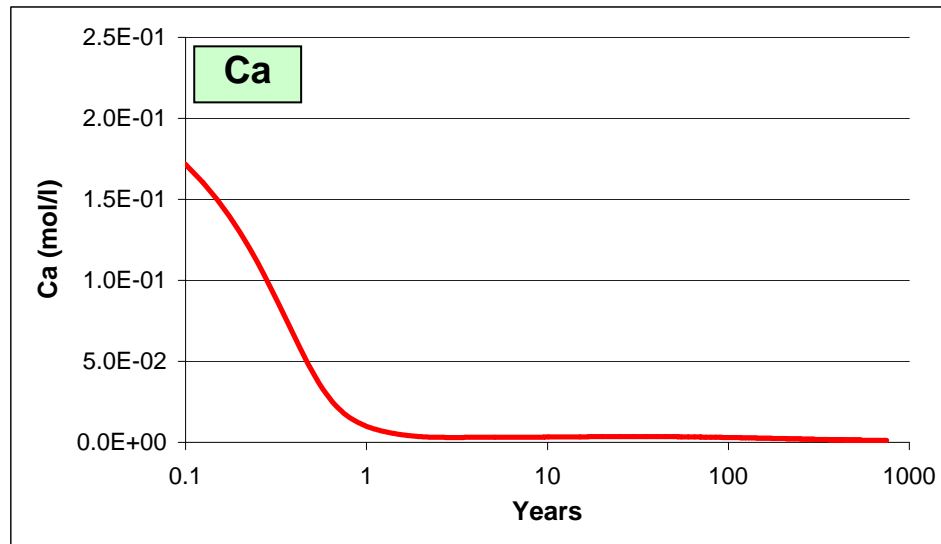
Result summary:

Mineral	Final conc. [mol/L]	Mineral change [mol/(L*1000 years)]	Contrib. to poro. change -
Calcite	1.6E-01	1.6E-01	-0.002
Siderite	1.9E-03	1.9E-03	0.000
Illite	0.0E+00	-4.6E-01	0.019
Kaolinite	0.0E+00	-7.7E-01	0.023
K-mica	1.7E+00	1.6E+00	-0.068
Albite	0.0E+00	-1.6E-01	0.005
K-feldspar	0.0E+00	-2.0E+00	0.065
Chalcedony	1.1E+02	4.9E+00	-0.033

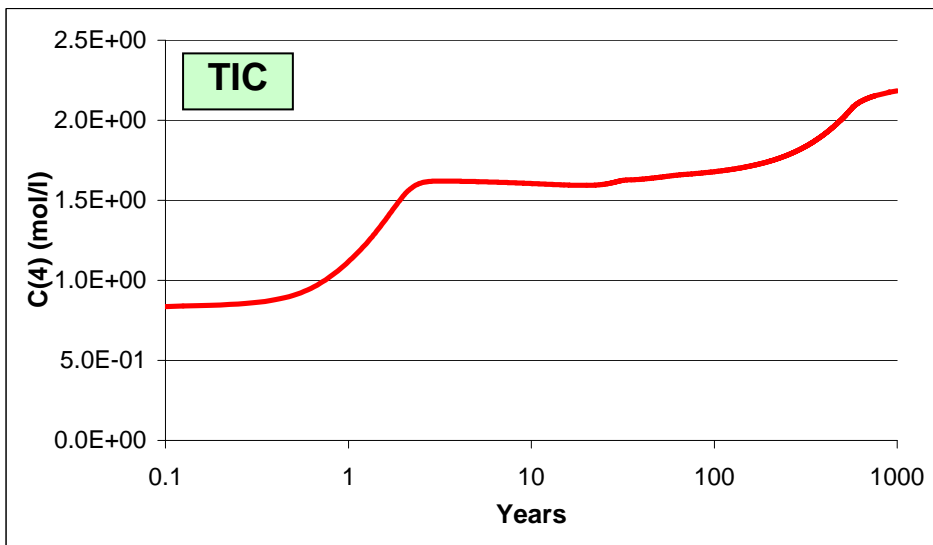
Børglum Formation (Haldager 1 well)



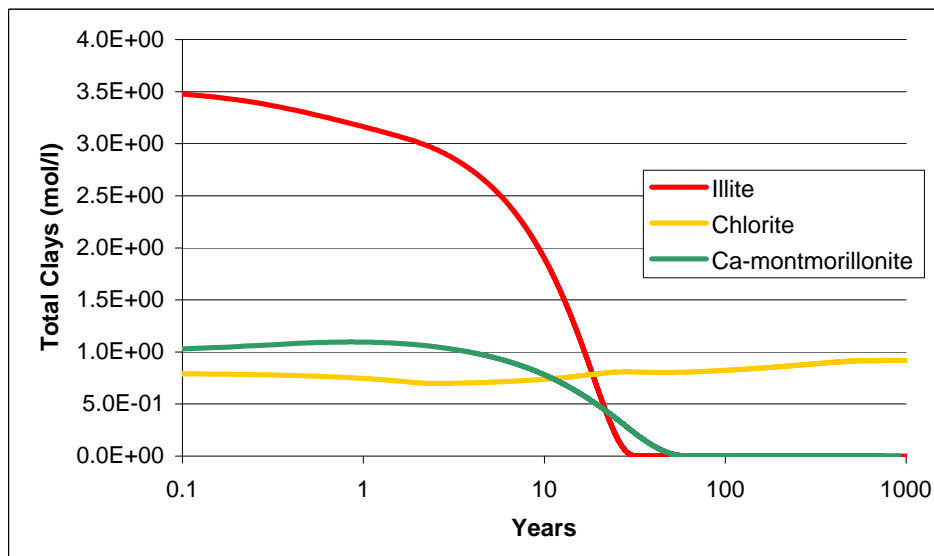
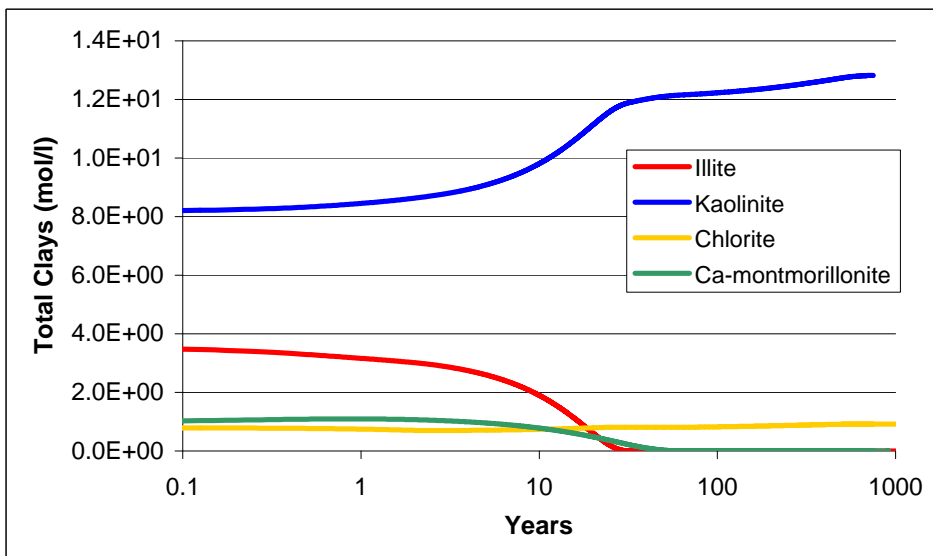
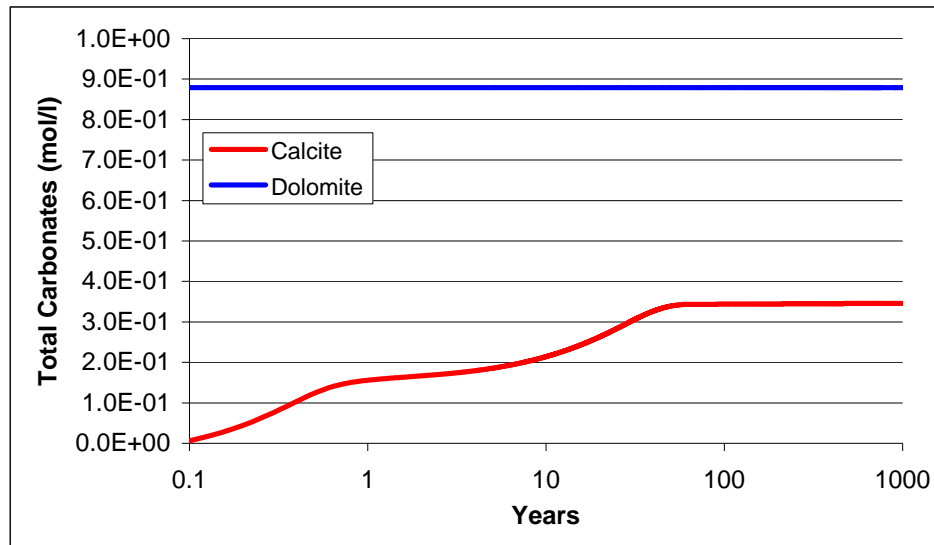
AQUA-DK, Selected results of predictive modelling (1/3)



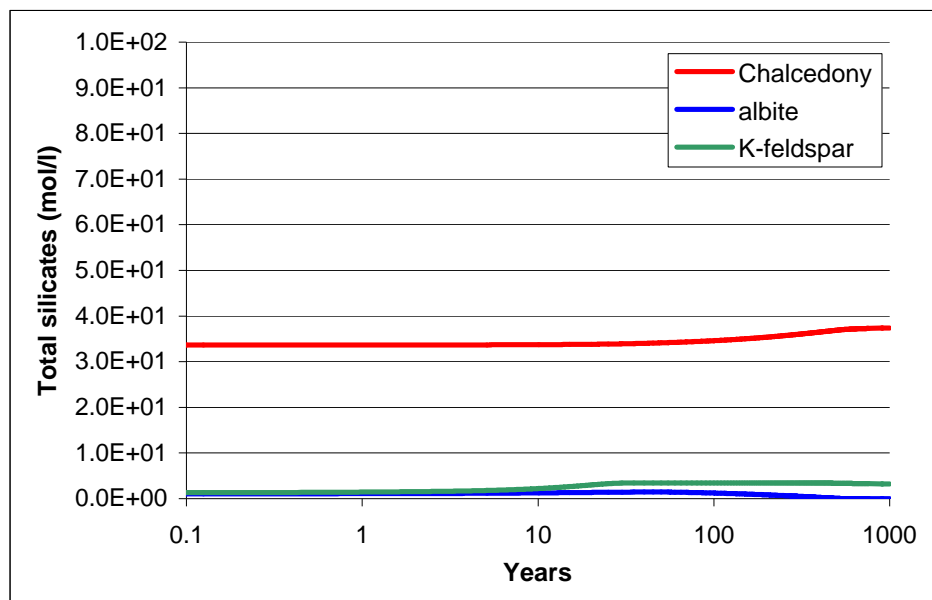
Børglum Formation (Haldager 1 well)



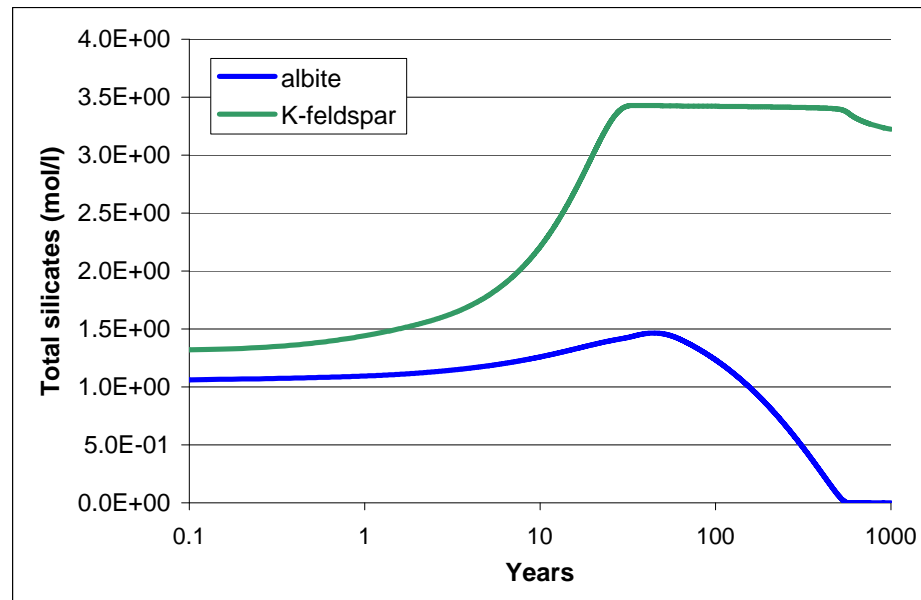
AQUA-DK, Selected results of predictive modelling (2/3)



Børglum Formation (Haldager 1 well)



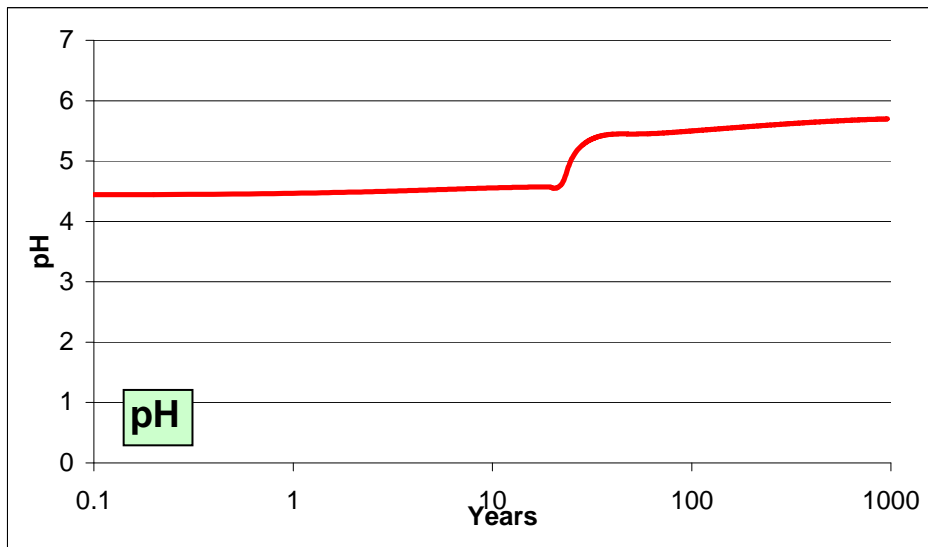
AQUA-DK, Selected results of predictive modelling (3/3)



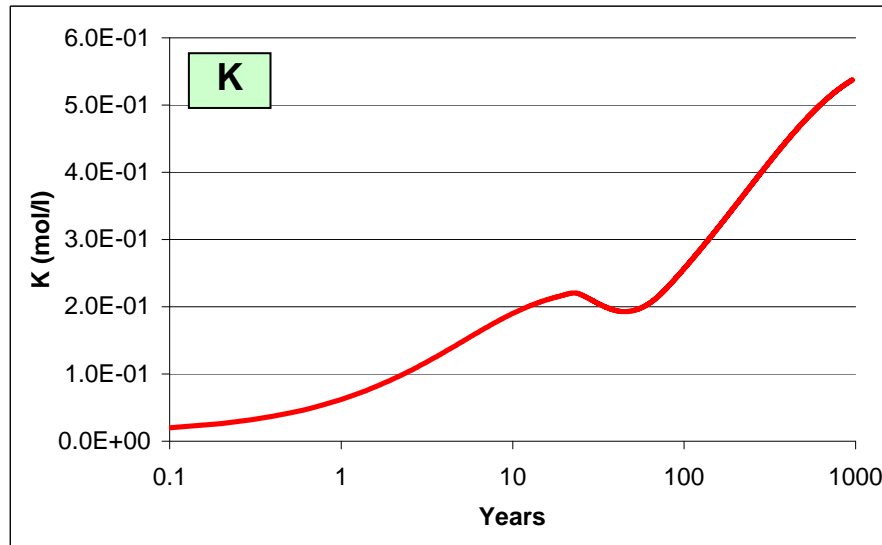
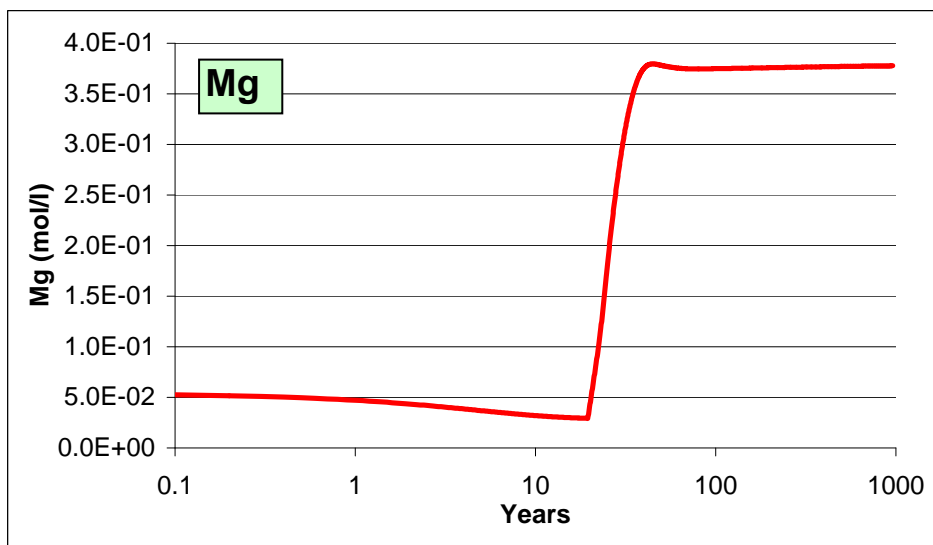
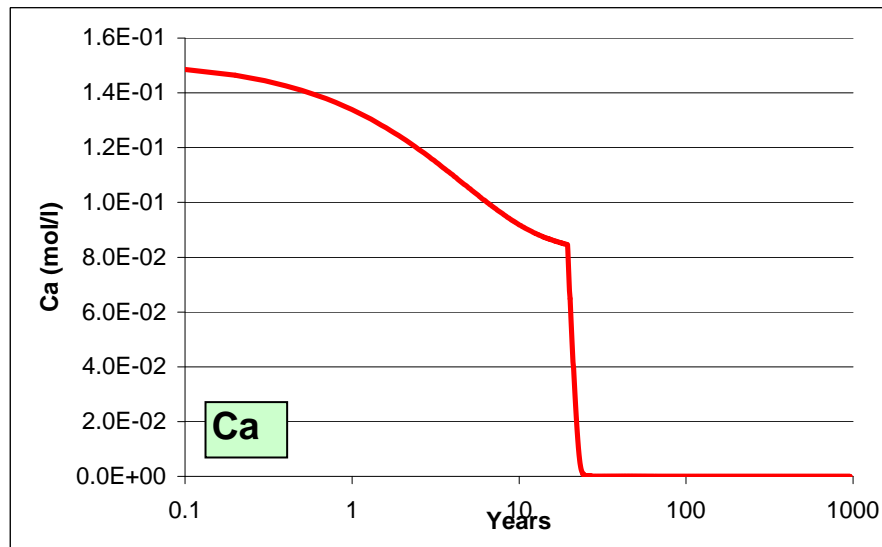
Result summary:

Mineral	Final conc. [mol/L]	Mineral change [mol/(L*1000 years)]	Contrib. to poro. change -
Calcite	3.5E-01	3.5E-01	-0.004
Dolomite	8.8E-01	1.1E-02	0.000
Illite	0.0E+00	-3.5E+00	0.148
Ca-mont.	0.0E+00	-1.0E+00	0.039
Kaolinite	1.3E+01	4.7E+00	-0.139
Chlorite	9.2E-01	1.3E-01	-0.007
Albite	0.0E+00	-1.1E+00	0.032
K-feldspar	3.2E+00	1.9E+00	-0.061
Chalcedony	3.7E+01	3.7E+00	-0.025

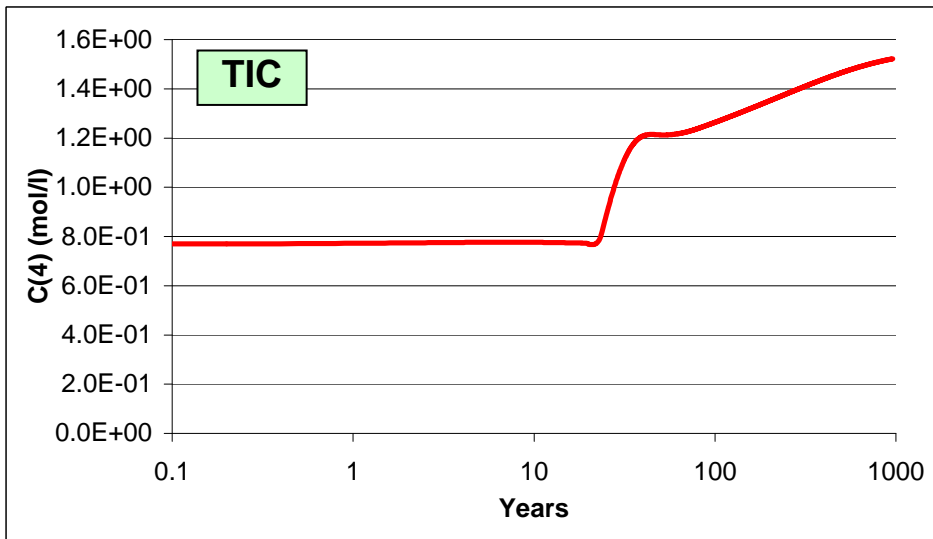
Fjerritslev Formation (Stenlille 1 well)



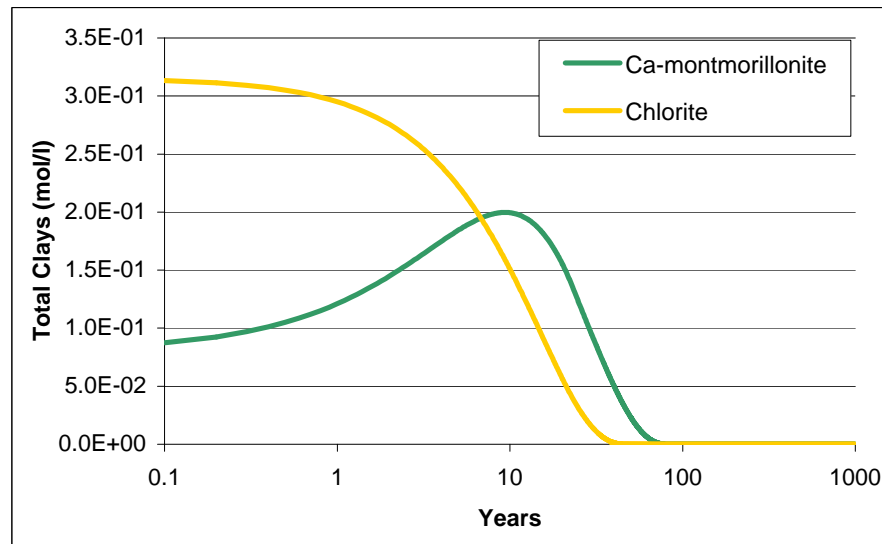
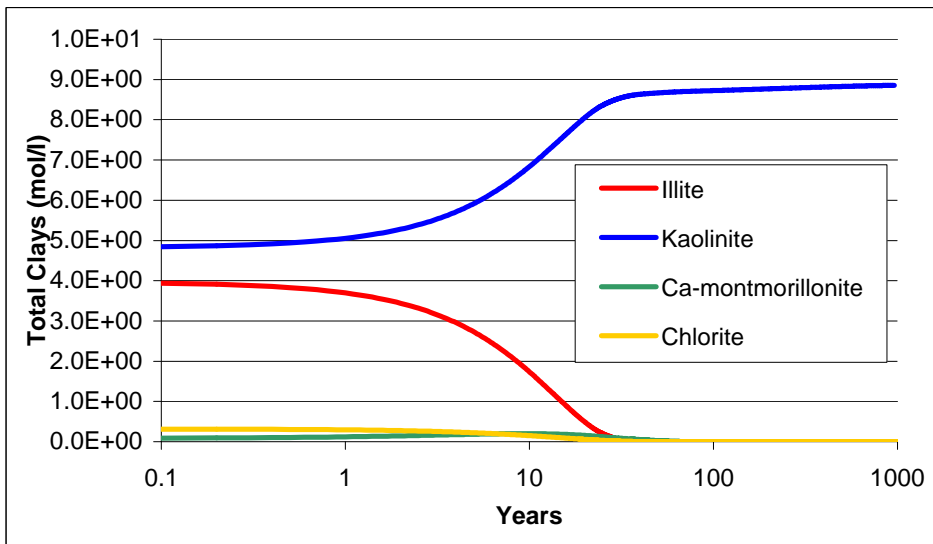
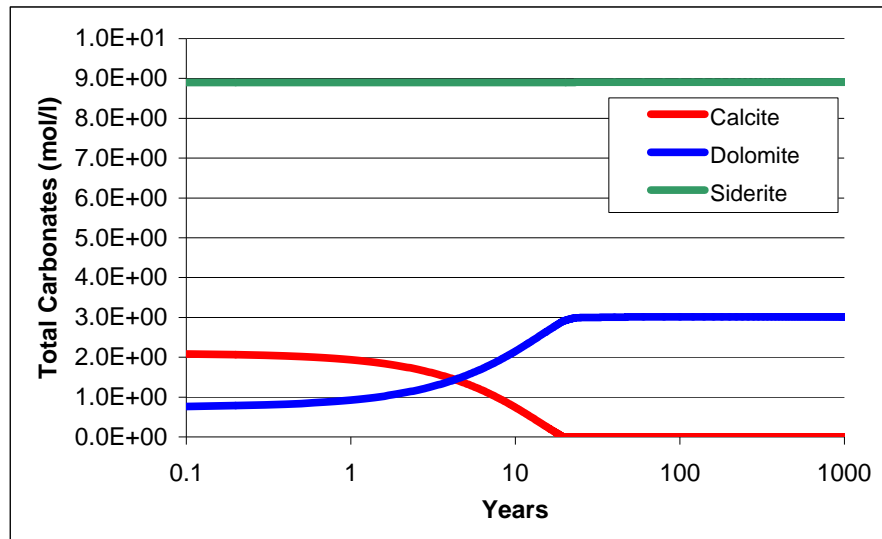
AQUA-DK, Selected results of predictive modelling (1/3)



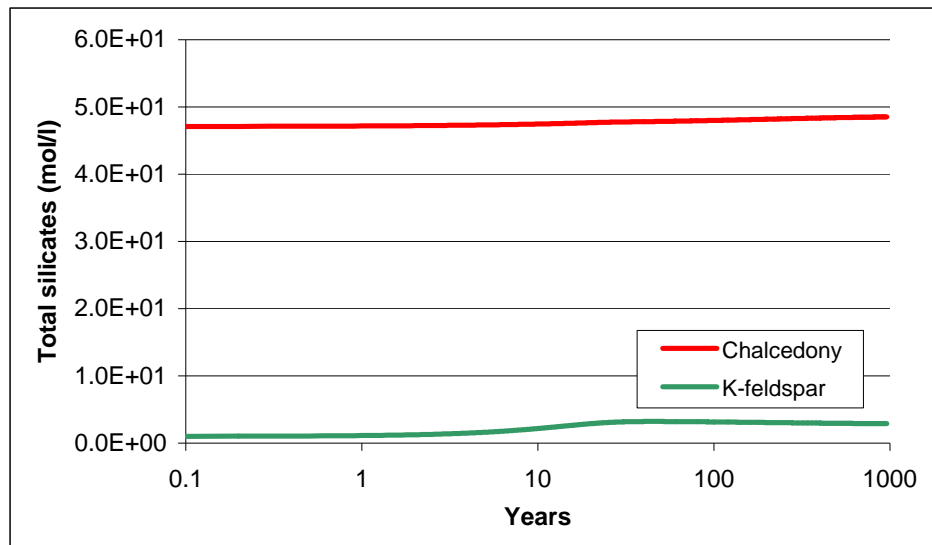
Fjerritslev Formation (Stenlille 1 well)



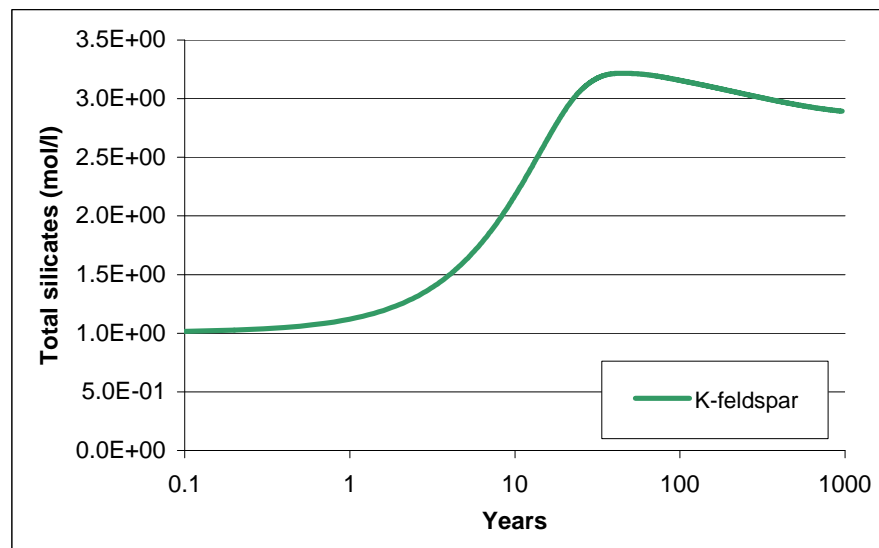
AQUA-DK, Selected results of predictive modelling (2/3)



Fjerritslev Formation (Stenlille 1 well)



AQUA-DK, Selected results of predictive modelling (3/3)



Result summary:

Mineral	Final conc. [mol/L]	Mineral change [mol/(L*1000 years)]	Contrib. to poro. change -
Calcite	0.0E+00	-2.1E+00	0.023
Dolomite	3.0E+00	2.2E+00	-0.044
Siderite	8.9E+00	2.2E-03	0.000
Illite	0.0E+00	-3.9E+00	0.165
Ca-mont.	0.0E+00	-8.7E-02	0.003
Kaolinite	8.9E+00	4.0E+00	-0.120
Chlorite	0.0E+00	-3.1E-01	0.019
K-feldspar	2.9E+00	1.9E+00	-0.060
Chalcedony	4.9E+01	1.4E+00	-0.010